Oncogenic RAS Signalling Promotes Tumour Immunoresistance by Stabilising *PD-L1* mRNA

Matthew Albert Coelho

University College London

and

The Francis Crick Institute

PhD Supervisor: Professor Julian Downward

A thesis submitted for the degree of

Doctor of Philosophy

University College London

September 2016

Declaration

I, Matthew Albert Coelho, confirm that the work presented in this thesis is my own. Where information has been derived from other sources, I confirm that this has been indicated in the thesis.

Abstract

The immunosuppressive molecule PD-L1 is upregulated in many cancers and contributes to evasion of the host immune system. Recent clinical trials of immunotherapies in cancer using antibodies targeting PD-L1 and its receptor PD-1 have led to promising responses in a subset of patients. These results emphasise the pressing need for biomarkers of patient response and means to increase the number of patients that benefit from these immunotherapies. One potential biomarker is PD-L1 on tumour cells, although the relative importance of the tumour microenvironment and cell-intrinsic signalling in the regulation of PD-L1 expression remains unclear. The use of physiological, genetically engineered mouse models (GEMMs) of human cancer may accelerate the preclinical development of immunotherapies targeting complex cancer-host interactions and improve our understanding of the regulation of PD-L1 in cancer.

Here, we discover that widely used, autochthonous GEMMs of Ras-driven lung cancer are poorly immunogenic and refractory to immunotherapies, questioning their disease-relevance and suitability for the preclinical study of immunotherapies in their current form. In addition, we investigate the molecular basis of tumour cell PD-L1 expression in lung cancer. We report that oncogenic RAS signalling is sufficient to upregulate tumour cell PD-L1 expression. Mechanistically, RAS signalling increases *PD-L1* mRNA stability by modulating the AU-rich element-binding protein tristetraprolin (TTP). TTP negatively regulates PD-L1 expression through AU-rich elements in the 3'UTR of *PD-L1* mRNA. In human and mouse lung cancer, TTP expression is reduced and its restoration in tumour cells enhances anti-tumour immunity. Our findings have implications for the interpretation of tumour PD-L1 expression as a biomarker for patient response to immunotherapies, and suggest a role for oncogenic RAS signalling in immune evasion.

Acknowledgements

Foremost, I thank Professor Julian Downward for his guidance and support. I consider myself extremely fortunate to have been given the opportunity to carry out research in his laboratory and under his expert supervision.
Secondly, I thank all the members of the Oncogene Biology Laboratory, past and present. I have learnt a lot from you all, and appreciate all of your help over the last four years; it has been a real pleasure to work alongside friends. I would like to give special thanks to Miriam and Dave, who have always provided valuable advice and a plethora of useful reagents throughout my PhD, Chris, who has been a great help with any *in vivo* experiments reported in this thesis, and Sophie for designing bioinformatics experiments and for many valuable discussions.

I thank the excellent core technology facilities at The Francis Crick Institute Lincoln's Inn Fields Laboratories including FACS, Cell Services, *In vivo* Imaging, Equipment Park, Protein Analysis and Proteomics (especially Bram Snijders and Karin Barnouin) Experimental Histopathology (especially Bradley Spencer-Dene and Emma Nye) Bioinformatics and Biostatistics (especially Phil East) and the Biological Resources Unit (especially Julie Bee).

I thank the funding bodies that have made this work possible, including Cancer Research UK and the European Research Council advanced grant "RASTARGET" from the European Union.
I am also extremely grateful to Professor Charles Swanton and Professor Caetano Reis e Sousa for their helpful guidance and discussion.

Finally, for almost everything else, I thank Mum, Dad and James, and all of my family and Faye Rodgers PhD, who have given me their unwavering support.

Table of Contents

1 Chapter 1. Introduction 21

1.1 Overview 21

1.2 Immune checkpoints 22

1.2.1 Co-signalling 22

1.2.2 PD-1 biology 25

1.2.3 PD-L1 biology 26

1.3 RAS signalling pathway 29

1.3.1 RAS biology and cancer 29

1.3.2 RAS and p38 signalling 31

1.4 Lung cancer and mouse models of the disease 33

1.5 Cancer immunology 36

1.5.1 An overview of cancer immunology 36

1.5.2 Genetically engineered mouse models in cancer immunology 37

1.5.3 Immunogenic cell death 41

1.6 Cancer immunotherapy 43

1.6.1 Clinical data for immune checkpoint blockade 43

1.6.2 Correlates of cancer immunotherapy response 46

1.6.3 PD-L1 expression as a biomarker for sensitivity to PD-1/PD-L1 immune checkpoint blockade 48

1.7 PD-L1 regulation and function in cancer 52

1.7.1 Cell-extrinsic regulation of PD-L1 expression 52

1.7.2 Cell-intrinsic regulation of PD-L1 expression by oncogenes 53

1.8 AU-rich element mediated mRNA decay and tristetraprolin 58

1.8.1 AU-rich element-mediated decay 58

1.8.2 Tristetraprolin biology 60

1.8.3 Decay-independent roles of tristetraprolin 63

1.8.4 Tristetraprolin in cancer 64

1.9 Conclusions 65

2 Chapter 2. Materials and Methods 67

2.1 Cloning, plasmids and stable cell lines 67

2.2 Transfections 68

2.2.1 siRNA 68

2.2.2 Transfections with expression vectors 68
2.3 Luciferase assays 69
2.4 Preparation of lentiviral particles 69
2.5 Flow cytometry 70
2.5.1 In vivo 70
2.5.2 In vitro 71
2.6 Cell sorting and *ex vivo* IFN-γ ELISA 72
2.7 EL4 TCR stimulation 72
2.8 Quantitative real-time PCR (qPCR) 72
2.9 RNA-immunoprecipitation 73
2.10 Immunoprecipitation 73
2.11 *In vivo* studies 74
2.11.1 *KP* mice 74
2.11.2 Tumour transplant models 75
2.11.3 CD4 and CD8 T cell depletion 75
2.11.4 *In vivo* imaging: micro computerised tomography (μCT) 76
2.12 CRISPR/Cas 76
2.13 Histopathology 77
2.13.1 Immunohistochemistry 77
2.13.2 RNAscope 77
2.14 Bioinformatics 77
2.15 Mass Spectrometry 78
2.16 Cell culture 79
2.17 Western blotting 81
2.18 Statistics 84

3 Chapter 3. Results 1. Tumour immunogenicity in genetically engineered mouse models of cancer 85
3.1 Introduction 85
3.2 Results 86
3.2.1 Steady-state and therapy-induced immune contexture of *Kras G12D LSL/+; Trp53 F/F* mouse tumours 86
3.2.2 KrasLSL/+; Trp53 F/F mouse tumours are resistant to immune checkpoint blockade 97

3.2.3 *KrasLSL-G12D/+; Trp53 F/F* mouse tumours are poorly immunogenic 103
3.2.4 Suppression of mismatch repair to increase tumour immunogenicity 117
3.3 Conclusions 123

4 Chapter 4. Results 2. Regulation of PD-L1 by RAS and TTP *in vitro* 125
4.1 Introduction 125
4.2 Results 126
4.2.1 Cell-intrinsic Upregulation of PD-L1 through Oncogenic RAS Signalling 126
4.2.2 RAS Signalling Increases *PD-L1* mRNA Stability through AU-rich Elements in the 3'UTR 136
4.2.3 AU-rich element Binding Proteins TTP and KSRP are Negative Regulators of PD-L1 Expression 140
4.2.4 RAS Regulates *PD-L1* Expression through TTP 145
4.2.5 RAS-ROS-p38 Signalling Controls TTP Activity 153
4.3 Conclusions 162

5 Chapter 5. Results 3. Regulation of PD-L1 by RAS and TTP *in vivo* 164
5.1 Introduction 164
5.2 Results 164
5.2.1 RAS Pathway Activation is Associated with PD-L1 Upregulation in Human Lung Cancer 164
5.2.2 Restoration of Tumour Cell TTP Expression Enhances Anti-tumour Immunity 174
5.3 Conclusions 183

6 Chapter 6. Discussion 186
6.1 Immunogenicity of autochthonous GEMMs 186
6.2 Regulation of PD-L1 expression by TTP and RAS 191
6.3 Concluding remarks 200

7 References 202

List of Figures

Figure 1.1 Co-signalling in T cell activation 24
Figure 1.2 Attenuation of anti-tumour T cell effector function through PD-1 signalling 28
Figure 1.3 A model for the activation of p38 signalling by ROS 33
Figure 1.4 Tumour PD-L1 expression as a biomarker for immunotherapy response 51
Figure 1.5 The control of PD-L1 expression in cancer cells 57
Table 1. AU-rich element binding proteins 59
Figure 1.6 Shematic of mouse TTP protein 63
Table 2. shRNA sequences 70
Table 3. Cell lines and growth conditions 80
Table 4. Antibodies 82
Figure 3.1 Drug selection for the efficient induction of immunogenic cancer cell death 88
Figure 3.2 Paclitaxel induces tetraploidy in lung cancer cells 90
Figure 3.3 Induction of tumour cell apoptosis by chemotherapies and targeted therapies *in vivo* 90
Figure 3.4 Stable immune cell populations following therapy in the lung in *KP* mice 92
Figure 3.5 Therapy-induced changes in the immune contexture of the lung in *KP* mice 94
Figure 3.6 Long-term suppression of CD11c+ cells in tumour-bearing lungs by chemotherapy 95
Figure 3.7 Lack of adaptive immune infiltrate following chemotherapy in tumour-bearing lungs 97
Figure 3.8 Anti-PD-L1 antibody effectively binds to the target lung tissue *in vivo* 98
Figure 3.9 Anti-PD-L1 immune checkpoint blockade is not effective in *KP* mice 100

Figure 3.10 *KrasLSL-G12D/+; Trp53 F/F* mouse tumours are refractory to anti-PD-L1 + anti-CTLA4 combination immunotherapy 102
Figure 3.11 Strategy for the depletion of CD4 and CD8 T cells *in vivo*..... 104
Figure 3.12 Characterisation of *KrasLSL-G12D/+; Trp53 F/F; Rag2 KO* mice 105
Figure 3.13 Adaptive immunity does not restain tumour progression or tumour initiation in *KrasLSL-G12D/+; Trp53 F/F* mice..... 106
Figure 3.14 No significant contribution of adaptive immunity to therapy response in *KP* mouse lung cancer 108
Figure 3.15 Examination of tumour immunoediting in *KrasLSL-G12D/+; Trp53 F/F* mice..... 110
Figure 3.16 *KPRag1-/-* c lung cancer cell line is immunogenic..... 111
Figure 3.17 Immunological memory and rejection of the *KPRag1-/-* c lung cancer cell line 112
Figure 3.18 Kras-driven murine lung tumours express high levels of PD-L1 independently of adaptive immunity 115
Figure 3.19 CD8 T cells from tumour-bearing *KP* mice do not express IFN-γ when presented with autologous lung tumour cells *in vitro* 117
Figure 3.20 Generation of a plentiCre-shRNA contruct for *in vivo* silencing of mismatch repair machinery 120
Figure 3.21 plenti Cre-shMsh2 initiates *KP* mouse lung tumourigenesis but fails to silence tumour Msh2 expression *in vivo* 121
Figure 3.22 *MSH2* expression is increased in human lung tumours..... 122
Figure 4.1 Oncogenic RAS signalling is sufficient to drive PD-L1 expression in breast epithelail cells 126
Figure 4.2 Oncogenic RAS signalling is sufficient to drive PD-L1 expression in lung cells..... 128
Figure 4.3 Oncogenic RAS signalling drives PD-L1 expression through MEK and PI3K pathways..... 129
Figure 4.4 Parental MCF10A and type II pneumocyte cells do not respond to 4-OHT 130

Figure 4.5 Oncogenic stress through forced MYC overexpression does not drive *PD-L1* expression 131
Figure 4.6 PD-L1 induction by RAS *in vitro* is not mediated by an autocrine-loop 132
Figure 4.7 MEK and PI3K inhibition reduces RAS-driven PD-L1 expression 134
Figure 4.8 T cell receptor-dependent induction of PD-L1 is dependent on MEK activity 135
Figure 4.9 RAS-MEK signalling controls *PD-L1* mRNA stability 137
Figure 4.10 *PD-L1 3'UTR* contains multiple conserved AU-rich elements . 138
Figure 4.11 AU-rich elements control the expression of *PD-L1* mRNA downstream of RAS 140
Figure 4.12 A selective siRNA-mediated screen of AU-rich element binding proteins reveals TTP and KSRP as novel negative regulators of *PD-L1* expression 141
Figure 4.13 Knock-down of TTP family members BRF-1 and BRF-2 does not increase *PD-L1* expression 142
Figure 4.14 Overexpression of TTP and KSRP decreases *PD-L1* expression 143
Figure 4.15 TTP and KSRP impart their negative control of *PD-L1* mRNA through the 3'UTR, but do not cooperate 144
Figure 4.16 PD-L1 mRNA is stabilised in TTP KO MEFs 145
Figure 4.17 TTP and KSRP bind to *PD-L1* mRNA, but their occupancy is not affected by MEK activity 147
Figure 4.18 TTP binds to *PD-L1* mRNA..... 147
Figure 4.19 Regulation of PD-L1 by MEK is TTP-dependent 149
Figure 4.20 TTP is controlled by phosphorylation downstream of MEK 153
Table 5. Mass spectrometry analysis reveals MEK-dependent TTP phosphorylation events..... 154
Figure 4.21 S52 and S178 of mouse TTP are phosphorylated in response to MEK signalling..... 154

Figure 4.22 ROS accumulation is critical for RAS-induced PD-L1 upregulation 156
Figure 4.23 Long-term RAS activation leads to augmented PD-L1 expression 156
Figure 4.24 p38 signalling is sufficient to drive PD-L1 induction downstream of ROS 157
Figure 4.25 MK2 activity is required for optimal PD-L1 induction by RAS .. 158
Figure 4.26 p38 inhibitor SB203580 paradoxically increases PD-L1 expression 159
Figure 4.27 CRISPR/Cas-mediated disruption of *Zfp36* 160
Figure 4.28 RAS-induced p38 activity decreases TTP activity 162
Figure 5.1 Clustering of TCGA LUAD samples into high and low RAS pathway activity using GSEA 167
Figure 5.2 High RAS pathway activity in human lung tumours is associated with high PD-L1 expression 168
Figure 5.3 TTP is reduced in murine, Kras-driven lung cancer 169
Figure 5.4 PD-L1 protein expression is upregulated on Kras-driven lung tumour cells *in vivo* 170
Figure 5.5 TTP is reduced in human lung cancer and breast cancer 172
Figure 5.6 Low TTP tumour expression is associated with shorter time to progression in human lung cancer 172
Figure 5.7 Localised RAS activity is assocaited with regions of high *PD-L1* mRNA expression in human lung tumours 174
Figure 5.8 Surveying immunogenicity and PD-L1-dependence of syngeneic tumour models 177
Figure 5.9 Optimisation of the experimental modulation of TTP expression 178
Figure 5.10 3'UTR-dependent suppression of PD-L1 by TTP transgene induction 179
Figure 5.11 The endogenous 3'UTR of PD-L1 decreases expression of a PD-L1 transgene 180

Figure 5.12 TTP transgene induction reduces *PD-L1* mRNA stability but does not reduce cell proliferation *in vitro* 181
Figure 5.13 Restoration of tumour cell TTP enhances anti-tumour immunity 183
Figure 6.1 Regulation of *PD-L1* mRNA stability through RAS and TTP signaling networks 193
Figure 6.2 Post-translational regulation of TTP activity in cancer 198

List of Tables

Table 1. AU-rich element binding proteins 59
Table 2. shRNA sequences 70
Table 3. Cell lines and growth conditions 80
Table 4. Antibodies 82
Table 5. Mass spectrometry analysis reveals MEK-dependent TTP phosphorylation events 154

Abbreviations

4-OHT – 4-Hydoxytamoxifen

ACT – Adoptive cell therapy

ALK – Anaplastic lymphoma kinase

APC – Antigen presenting cell

ARE – AU-rich element

ARE-BP – AU-rich element binding protein

BCR – B cell receptor

Btz – Bortezomib

ChIP – Chromatin immunoprecipitation

CRISPR – Clustered regularly interspaced short palindromic repeats

CRT – Calreticulin

CT – X-ray computed tomography

CTLA-4 - Cytotoxic T-lymphocyte-associated protein 4

DAPI – 4',6-diamidino-2-phenylindole

DC – Dendritic cell

EGFR – Epidermal growth factor receptor

ELISA – Enzyme-linked immunosorbent assay

ER – Oestrogen receptor

ERK – Extracellular signal-regulated kinase

FACS – Fluorescence-activated cell sorting

FDR – False discovery rate

Floxed – Flanked by loxP sites

GAP – GTPase activating protein

GEF – Guanine nucleotide exchange factor

GEMM – Genetically engineered mouse model

H & E – Hematoxylin and eosin

ICB – Immune checkpoint blockade

ICD – Immunogenic cell death

IFN-γ – Interferon γ

iGEMM – Immunogenic genetically engineered mouse model

ITIM – Immunoreceptor tyrosine-based inhibitory motif

KO – Knock-out

KP – Kras LSL/+; Trp53 F/F

KSRP – KH-type splicing regulatory protein

LCMV – Lymphocytic choriomeningitis virus

LSL – loxP-STOP-loxP

MEF – Mouse embryonic fibroblast

MEK – Mitogen-activated protein kinase kinase

MHC – Major histocompatibility complex

miRNA – MicroRNA

MK2 – or MAPKAPK2, mitogen activated protein kinase-activated protein kinase 2

MMR – Mismatch repair

MSH2 –MutS protein homologue 2

NAC – N-acetyl-L-cysteine

NGS – Next-generation sequencing

NK cell – Natural killer cells

NSCLC – Non-small cell lung cancer

OVA – Ovalbumin

PBS – Phosphate-buffered saline

PD-1 – Programmed death-1

PD-L1 – Programmed death-1 ligand 1

PI3K – Phosphatidylinositol-4,5-bisphosphate 3-kinase

PMA – Phorbol 12-myristate 13-acetate

qPCR – Quantitative real-time polymerase chain reaction

Rag – Recombination activating gene

RNAi – RNA interference

ROS – Reactive Oxygen Species

SCLC – Small cell lung cancer

SD – Standard deviation

SEM – Standard error of the mean

shRNA – Short hairpin RNA

siRNA – Small interfering RNA

Taxol – Paclitaxel

TCGA – The Cancer Genome Atlas

TCR – T cell receptor

TTP – Tristetraprolin

TUNEL – Terminal deoxynuceotidyl transferase dUTP Nick-End Labelling

UTR – Untranslated region

WT – Wild type

ZFP36 – Zinc finger protein 36

1 Chapter 1. Introduction

1.1 Overview

An emerging hallmark of cancer is successful evasion of the host immune system (Hanahan and Weinberg, 2011). Fundamentally, cancer immunology is defined by our understanding of the process of cancer immunosurveillance; the detection and elimination of malignant cells by the immune system. This concept was first proposed in the 1950s (Burnet, 1957)(Thomas, 1959). Historically, the concept of host immunity as an extrinsic tumour suppressor has been controversial. We now have overwhelming evidence that cancer immunosurveillance occurs in mice and humans, but is inevitably countered by a fraction of tumour cells through innate and evolved subversion strategies, resulting in cancer.

At this time, there is a renewed interest in the field of cancer immunology and a collective realisation that there is considerable therapeutic potential in re-establishing anti-tumour immunity. Genetically engineered mouse models (GEMMs) have been instrumental in the renaissance of the cancer immunosurveillance hypothesis and are an invaluable tool for studying reciprocal interactions between the host and cancer cells (Dunn et al., 2002). Studies in genetically engineered mice have elaborated the function of several immune checkpoint molecules, the general function of which is to maintain homeostasis and prevent autoimmunity following stimulation of an immune response. However, these immune system checkpoints are often dysregulated and exploited in cancer to avoid immune destruction. Recently, there has been an emphasis on targeting these molecules with antibodies in cancer to block inhibitory signalling from immune checkpoint pathways. Such immunotherapy approaches are often referred to as immune checkpoint blockade (ICB).

An important value of stimulating an anti-tumour immune response is that the immune system can co-evolve with the tumour, and the resulting regressions can be durable, giving immunotherapies a unique advantage over chemotherapies and targeted therapies. Indeed, there have been striking anti-tumour responses reported from clinical trials of immune checkpoint blockade in multiple tumour types, including in some of the most difficult to treat and deadly cancers such as non-small cell lung cancer (NSCLC) and metastatic melanoma. Currently, only a small fraction of cancer patients respond to these immunotherapies, making patient stratification using reliable biomarkers crucial.

Programmed death-1 ligand-1 (PD-L1, also known as B7-H1 or CD274) is a notable immune checkpoint molecule that has been successfully targeted in the clinic, and will be the major focus of this thesis. Although PD-L1 is known to be upregulated in many cancers, the regulation of the expression of this molecule remains poorly defined. Currently, there is increasing interest in PD-L1 as a biomarker for response to immunotherapies and so the need to further understand the regulation of this molecule is greater than ever.

1.2 Immune checkpoints

1.2.1 Co-signalling

An adaptive immune response requires antigen-specific T cell receptor (TCR) or B cell receptor (BCR) engagement by their cognate antigens. However, this alone is not sufficient to stimulate lymphocyte effector function. Co-signalling in parallel with TCR or BCR signalling adds an extra-level of control to the adaptive immune response, making the decision to react context-dependent. Co-signalling is not antigen specific and can activate, or inhibit, lymphocyte activity; so-called co-stimulation or co-inhibition, respectively. Collectively, this relates to the two-signal model that was first proposed by

Bretscher and Cohn in 1970. Here, signal one refers to the antigen-specific activation through the TCR or BCR, and signal two refers to input derived from co-stimulatory molecules. Given the dual dependence on context and cognate antigen, the two-signal system can prevent chronic and self-destructive activation of adaptive immunity. This is especially important in regulating the response to antigens that persist for long periods of time. Hence, co-stimulation or co-inhibition is implicated in disease situations such as chronic infection, auto-immunity and cancer. Since cancer cells do not express co-stimulatory molecules and thus cannot provide co-stimulation themselves (with the possible exception of some lymphomas), anti-tumour adaptive immune responses first require priming by antigen-presenting cells (APCs). This occurs through a process called cross-presentation, whereby APCs present antigens not expressed by the APC itself, but acquired through phagocytosis or endocytosis. The immunological synapse between the T cell and APC represents the interface between the innate and adaptive immune system (Figure 1.1).

Formal proof of the two-signal model came from work by Jenkins and others demonstrating that TCR stimulation alone led to T cell unresponsiveness, but stimulation with an anti-CD28 antibody could lead to T cell activation, even in the absence of accessory cells (Jenkins et al., 1988; Jenkins et al., 1991). Presently, co-signalling through CD28 is the most extensively studied example of co-stimulation. CD28 on T cells can interact with CD80 (B7.1) or CD86 (B7.2) on APCs (Figure 1.1). Only MHC-antigen engagement with the TCR in combination with CD28 co-signalling will initiate T cell activation.

One mechanism of terminating or dampening the resulting immune response against a specific antigen operates through the immunosuppressive molecule cytotoxic T-lymphocyte-associated protein-4 (CTLA-4). CTLA-4 was the first described example of a co-inhibitory molecule. CTLA-4 exerts its negative functions on T cell activity by competing with CD28 for binding to CD80/CD86 (Walunas et al., 1994). In addition, CTLA-4 engagement appears to reverse

TCR and CD28-mediated T cell activation through the recruitment of phosphatases including PP2A and possibly SHP-2 (Chuang et al., 2000; Marengere, 1997). Importantly, the "off" signal from CTLA-4 appears to be dominant, as CTLA-4's binding affinity for CD80 is much higher than that of the activating ligand, CD28 (Linsley, 1995; vanderMerwe et al., 1997). Indeed, the powerful inhibitory effect of CTLA-4 function was functionally demonstrated in *Ctla-4* KO mice. Within 3-4 weeks from birth, *Ctla-4*-deficient mice die from a severe inflammatory disorder related to excessive lymphoproliferation (Tivol et al., 1995; Waterhouse et al., 1995).

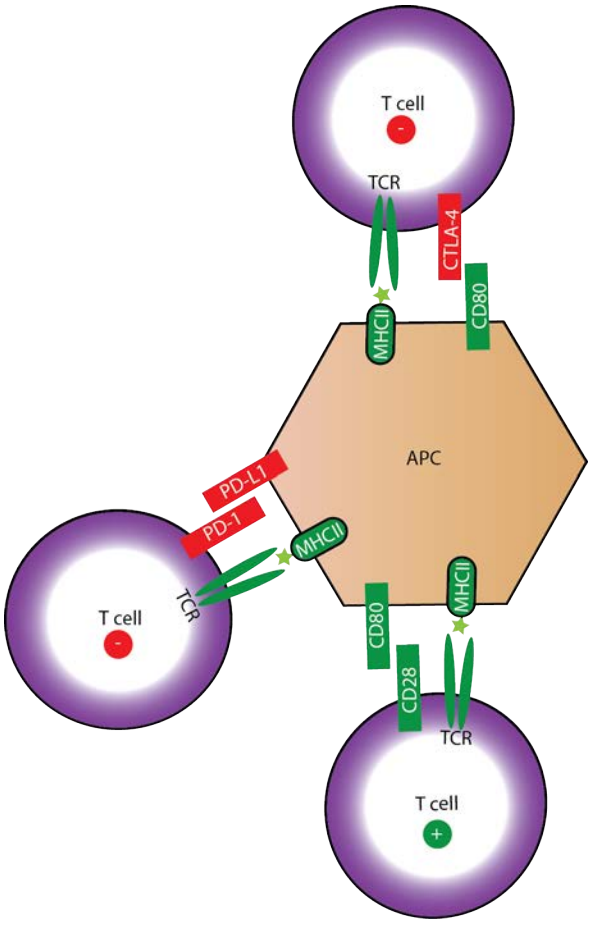

Figure 1.1 Co-signalling in T cell activation

Common co-stimulatory and co-inhibitory signals in the regulation of a T cell response. Co-stimulatory molecules are in green and co-inhibitory molecules are in red. The APC presents a processed antigen peptide via MHC class II. In all situations depicted, signal one is present, but the presence or absence of signal two ultimately determines T cell activity. The PD-1/PD-L1 interaction is also functional in tumour cells, as the tumour cell can present antigens via

MHC class I. Only in the CD80-CD28 engagement situation presented does productive T cell activation take place. In the case of CTLA-4, CD28 is outcompeted by CTLA-4 for CD80 or CD86 binding.
APC, antigen presenting cell. MHCII, major histocompatibility complex class II. TCR, T cell receptor.

1.2.2 PD-1 biology

After the initial discovery of CTLA-4 as an immune checkpoint molecule, the search began for related co-inhibitory molecules within the immunoglobulin superfamily. The Honjo group first identified programmed death-1 (PD-1) in 1992 in a T cell hybridoma undergoing cell death induced by acute stimulation with PMA and ionomycin (Ishida et al., 1992). PD-1 is a membrane-bound receptor of the CD28 superfamily and harbours an internal immunoreceptor tyrosine inhibitory motif (ITIM) and an immunoreceptor tyrosine switch motif (ITSM). Reminiscent of CTLA-4, PD-1 engagement by its ligand PD-L1, has an immunosuppressive effect on T cell activity (Freeman et al., 2000). In an analogous fashion, PD-1 is upregulated on T cells following activation and thus serves to inhibit excessive or inappropriate activation of the immune system. Mechanistically, PD-1 receptor engagement leads to activation of the phosphatase SHP-2, which binds to the ITSM of PD-1 and suppresses the activation of Akt downstream of CD28 and PI3K signalling (Chemnitz et al., 2004; Parry et al., 2005) (Figure 1.2). This culminates in reduced T cell proliferation, reduced cytokine synthesis and changes in T cell metabolism involving reductions in glycolytic capacity. Surprisingly, PD-1 expression has recently been described on a minor subset of melanoma cells in mice and human tumours (Kleffel et al., 2015). Here, PD-1 expression was found to promote tumorigenesis even in the absence of adaptive immunity, apparently involving cell-intrinsic stimulation of the mTOR pathway and upregulation of S6 phosphorylation following PD-L1 engagement. The starkly opposing effects of PD-1 activation on cell proliferation in melanoma cells and T cells warrants further investigation, but may involve tissue-specific differences in the role of SHP-2.

1.2.3 PD-L1 biology

The primary ligand for PD-1, programmed death-1 ligand-1 (PD-L1) was discovered in 2000 (Freeman et al., 2000). PD-L1 is a member of the B7 superfamily of proteins, and was first identified as a PD-1 ligand by database searching for B7-related proteins, due to the structural similarities between CTLA-4 and PD-1. However, unlike CD80, CD86 and CD28, PD-L1 is expressed on non-lymphoid tissues as well as haematopoietic cells. Specifically, PD-L1 is expressed on T and B cells, APCs such as dendritic cells and macrophages, as well as heart, pancreas (β cells), lung, kidney, vascular endothelium, corneal endothelium and placental tissues, and in a multitude of cancers (Keir et al., 2008). Crucially, PD-L1 expression on non-lymphoid tissues allows for peripheral control of T cell activity, preventing autoimmune mediated tissue damage. This is a key difference to the checkpoint mediated by CTLA-4, which exercises control at the earlier stage of T cell priming. In support of this, *Pd-1*-deficient mice have a milder phenotype and live significantly longer than *Ctla-4*-deficient mice (Nishimura et al., 1998; Nishimura et al., 1999). However, there are reports that PD-1 signalling can also determine the initial fate decisions of CD8 T cells in some contexts (Goldberg et al., 2007), but is unlikely to be as critical as CTLA-4 at this early stage.

Since the discovery of PD-L1 in 2000, a second ligand for PD-1 has been identified, PD-L2 (Latchman et al., 2001), which has a more restricted tissue expression than PD-L1 as it is predominantly expressed by dendritic cells. Although IFN-γ induces expression of both PD-1 ligands, PD-L2 is more potently induced in response to IL-4 and GM-CSF, indicating significant differences in regulation of gene expression (Topalian et al., 2015). Presently, the function of PD-L2 is poorly understood. However, not dissimilar to PD-L1, PD-L2 seems to be directly involved in inhibiting T cell activation through ligation of PD-1 (Latchman et al., 2001). Although PD-L2 is

upregulated in several cancers (notably B cell lymphomas), these tend to be cases where there have been amplifications or genetic rearrangements of the genetic locus encoding both PD-L1 and PD-L2, as these genes are in very close proximity. Indeed, they are likely to have arisen from a gene duplication event. Therefore, it is difficult to conclude whether PD-L2 alone plays a significant role in cancer progression.

The generation of the first PD-L1 knock-out (KO) mice by Arlene Sharpe and colleagues provided definitive insights into the function of PD-L1 *in vivo* (Latchman et al., 2004). PD-L1-deficient mice displayed more robust CD4 and CD8 T cell responses, indicating that PD-L1 served as a negative regulator of the adaptive immune response. This evidence was consistent with the phenotype of PD-1 KO mice, which have enhanced CD8 T cell autoreactivity (Keir et al., 2007). Moreover, expression of PD-1 and PD-L1 on T and B cells is closely linked to stimulation. Thus, activation-induced expression allows the PD-1 pathway to function as a rapid homeostatic mechanism for limiting autoimmunity. Testing the potential therapeutic value of reversing PD-1 signalling was not initially performed in the context of cancer, but in chronic infection. Pivotal experiments from Rafi Ahmed and colleagues revealed that administration of anti-PD-L1 antibodies to mice suffering from chronic lymphocytic choriomeningitis virus (LCMV) infections significantly reduced viral load by re-stimulating the exhausted anti-viral T cell population (Barber et al., 2006).

Surprisingly, in addition to its conventional role of signalling through PD-1, PD-L1 has been shown to signal internally into the cell expressing PD-L1. This unconventional, reverse signalling through PD-L1 requires PD-L1 binding to CD80 (Butte et al., 2007). Sophisticated genetic experiments revealed that T cells deficient for CD28 and CTLA-4 were still functionally inhibited by CD80, whereas CD28, CTLA-4, PD-L1 triple-deficient T cells were unaffected. The molecular nature of the resulting signal remains

unclear, as the short cytoplasmic tail of PD-L1 does not contain known motifs for downstream signal transduction.

Crucially, PD-L1 expression on the surface of tumour cells can prevent anti-tumour immunity by decreasing T cell effector function and T cell proliferation (Blank et al., 2004; Freeman et al., 2000), as well as promoting anti-tumour T cell apoptosis (Dong et al., 2002), at least partly through reduced expression of the anti-apoptotic protein Bcl-xL (Parry et al., 2005)(Figure 1.2). Interestingly, PD-1 has apparently opposing effects on regulatory T cells (T regs). PD-1 activation promotes the development or induction of Tregs, which seems to depend on the downregulation of the PI3K-AKT-mTOR pathway by PD-1 (Francisco et al., 2009) (Figure 1.2). This is consistent with the high level of PD-L1 expression commonly found on Treg populations.

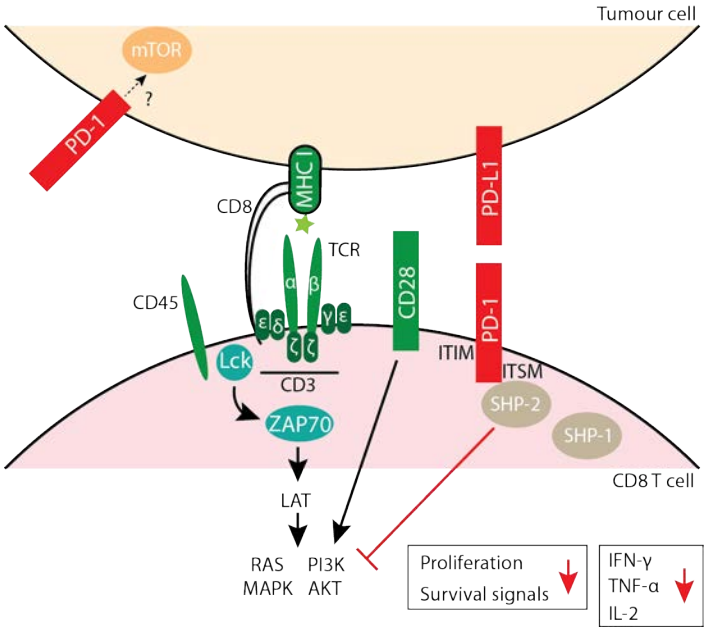

Figure 1.2 Attenuation of anti-tumour T cell effector function through PD-1 signalling

Engagement of the TCR by the MHC in complex with cognate antigen stimulates the tyrosine kinase Lck. This process also requires dephosphorylation of Lck at inhibitory sites by CD45 at the cell membrane. Activated Lck phosphorylates tyrosines on CD3 chains. Phosphorylated CD3 ζ serve as docking sites for the tyrosine kinase ZAP70. Once activated, ZAP70 phosphorylates the transmembrane signalling scaffold protein LAT.

LAT subsequently recruits several downstream adaptor proteins and promotes RAS activation and PI3K activation. PI3K signalling is also activated by co-stimulatory signals emanating from CD28. PD-1 signalling is activated via interaction with PD-L1 expressed on tumour cells. PD-1 signalling counters PI3K and thus AKT signalling stimulated by TCR engagement. Mechanistically, this operates through phosphatase SHP-2 (and possibly SHP-1), which binds to the cytoplasmic tail of PD-1 in the ITSM. Overall, this contributes to the reduction in the synthesis of effector cytokines by CD8 T cells such as IFN-γ, and reductions in T cell survival signals (Bcl-xL expression is downregulated), T cell proliferation and glucose metabolism. In contrast, rare melanoma cells expressing PD-1 may have enhanced tumorigenic potential through increased activation of mTOR activity through PD-1 signalling.

1.3 RAS signalling pathway

1.3.1 RAS biology and cancer

RAS proteins are a superfamily of GTP-binding proteins that are central to the molecular control of cell proliferation and survival. RAS protein activity governs cellular responses to extracellular signals such as growth factors. Approximately 20 % of all cancers have mutations in RAS proteins (HRAS, NRAS or KRAS), and many more dysregulate RAS signalling through mutations in signalling proteins upstream or downstream of RAS (Downward, 2003). The discovery of Ras proteins arose from work on viruses able to initiate cancer in rodents. Thus, the name *Ras* originates from *ra*t *s*arcoma virus (Malumbres and Barbacid, 2003). RAS is a GTPase; it cycles from its biologically active GTP-bound state to the inactive GDP-bound form. Since the intrinsic GTPase activity of RAS is low, GTPase activating proteins (GAPs) accelerate the catalytic hydrolysis of GTP to GDP by RAS, such as neurofibromin 1 (NF1) (Trahey and Mccormick, 1987). Conversely, RAS guanine nucleotide exchange factors (GEFs) promote the timely release of GDP and exchange for GTP, such as son of sevenless (SOS) (Downward et al., 1990b; Wolfman and Macara, 1990). Oncogenic RAS mutant proteins (with point mutations invariably occurring in codons 12, 13 and 61) have

compromised GTPase activity and thus are unable to normally revert to the inactive GDP-bound form. Therefore, oncogenic RAS mutants are considered to be constitutively active. A corollary is that cells harbouring mutant RAS no longer depend on growth factor stimulation for RAS activity, promoting uncontrolled and inappropriate cell proliferation and cancer.

Activated RAS binds to effector proteins at the plasma membrane including RAF proteins (Moodie et al., 1993; Vojtek et al., 1993; Warne et al., 1993), Ral-GEF proteins and the p110 catalytic subunits of phosphatidylinositol-kinases (PI3Ks) (Downward, 2003; Rodriguezviciana et al., 1994), with the notable exception of the p110β isoform of PI3K (Fritsch et al., 2013). The association with the plasma membrane is required for activity of downstream kinases such as RAF (Leevers et al., 1994). Once activated, these kinases can amplify the initial signal from RAS by activating many substrates and therefore facilitate the control of complex cellular processes such as cell division and growth. Specifically, downstream of A, B and C-RAF are mitogen-activated kinase/ERK kinase 1 (MEK1) and MEK2, which can in turn phosphorylate the serine/threonine kinases extracellular-regulated kinase 1 (ERK1) and ERK2. This evolutionarily conserved, three-tier mitogen-activated protein kinase (MAPK) cascade eventually leads to the phosphorylation and activation of transcription factors and cell cycle regulators. In parallel, RAS directly regulates the enzymatic activity of PI3Ks, which are lipid kinases (Vanhaesebroeck et al., 2010). Through conversion of the substrate phosphatidylinositol-4,5-bisphosphate (PIP2) to phosphatidylinositol-3,4,5-trisphosphate (PIP3) by phosphorylation, PI3Ks are able to recruit and activate several effector proteins that bind PIP3 through their pleckstrin homology domains, including the kinase AKT (Downward, 2003).

Pharmacological inhibitors of mutant RAS would have obvious therapeutic value in many cancers, however attempts to find effective RAS inhibitors has proved difficult. For example, farnesyltransferase inhibitors prevent

farnesylation of the C-terminus of RAS, and in doing so; prevent the proper localisation of RAS to the plasma membrane (Kohl et al., 1995). Also of note are recently developed small molecules able to react with the cysteine residue in RAS^{G12C} mutant proteins can inhibit oncogenic RAS signalling and have shown promising selectivity for mutant RAS (Ostrem et al., 2013); however, both of these classes of agents are yet to prove their worth in a clinical setting. On the other hand, there has been a very productive campaign to develop potent small molecule inhibitors of RAS effector proteins (generally kinases), including MEK, ERK and AKT. Inhibitors of MEK1/2 and PI3K will be used extensively in the work presented in this thesis. In addition, upstream growth factor receptor tyrosine kinases, such as epidermal growth factor receptor (EGFR), are amenable to small molecule inhibition or antibody-mediated inhibition, as they are cell membrane proteins.

1.3.2 RAS and p38 signalling

Another class of related MAPKs are the stress-activated kinases including c-Jun N-terminal kinases (JNKs) and p38. In normal cells, the p38 pathway is involved in mediating cellular responses to cellular stresses, cytokines and inflammatory cues such as lipopolysaccharide (LPS). In an analogous manner to the RAS/MEK/ERK signalling module, p38 MAPK is activated through phosphorylation by protein kinases MEKK3 and MEKK6. In mammals, four isoforms of p38 exist: p38α, p38β, p38γ and p38δ.

In the context of transformation, the p38 pathway has been shown to have tumour suppressive properties (Dolado et al., 2007). For example p38α deletion sensitised mice to KRAS-driven lung cancer (Ventura et al., 2007). p38 is activated by oncogenic RAS signalling, eventually leading to oncogene-induced senescence (Xu et al., 2014b). It seems that p38α, p38γ and p38δ (but not p38β) are critical for this process, (Kwong et al., 2013; Kwong et al., 2009). Oncogene-induced senescence is dependent on

MEKK3/6, which is activated downstream of MEK/ERK signalling (Wang et al., 2002). In parallel, p38δ is activated transcriptionally by AP-1 and Ets transcription factors following activation of oncogenic RAS (Kwong et al., 2013). Although the exact nature of the signal downstream of oncogenic RAS/MEK/ERK that leads to p38 activation remains unclear, it is likely that MEK/ERK-induced accumulation of reactive oxygen species (ROS) and/or DNA damage play a key role (Dolado et al., 2007; Nicke et al., 2005). Although the accumulation of ROS and DNA damage are often linked, they both seem capable of independently activating p38 signalling (Xu et al., 2014b). Using an RNA-interference approach to identify novel regulators of RAS-induced growth arrest, Nicke and colleagues identified MINK to be a crucial component in the signalling network activating the senescence program (Nicke et al., 2005). Activation of p38 by MINK appeared to be dependent on ROS accumulation, which was associated with oncogenic levels of MEK activity. ROS can also activate p38 signalling through apoptosis signal-regulating kinase 1 (ASK1), in a mechanism involving the dissociation of thioredoxin from ASK1 under oxidative conditions (Saitoh et al., 1998) (Figure 1.3). Indeed, ROS-mediated ASK1 activation appears to be critical in TLR4-mediated responses to LPS in APCs, which depends on p38. These data suggest a significant functional role for this pathway in the biology of non-transformed cells (Matsuzawa et al., 2005). Interestingly, TNF can also engage the p38 pathway in a mechanism involving the induction of ROS and homo-oligomerisation of ASK1.

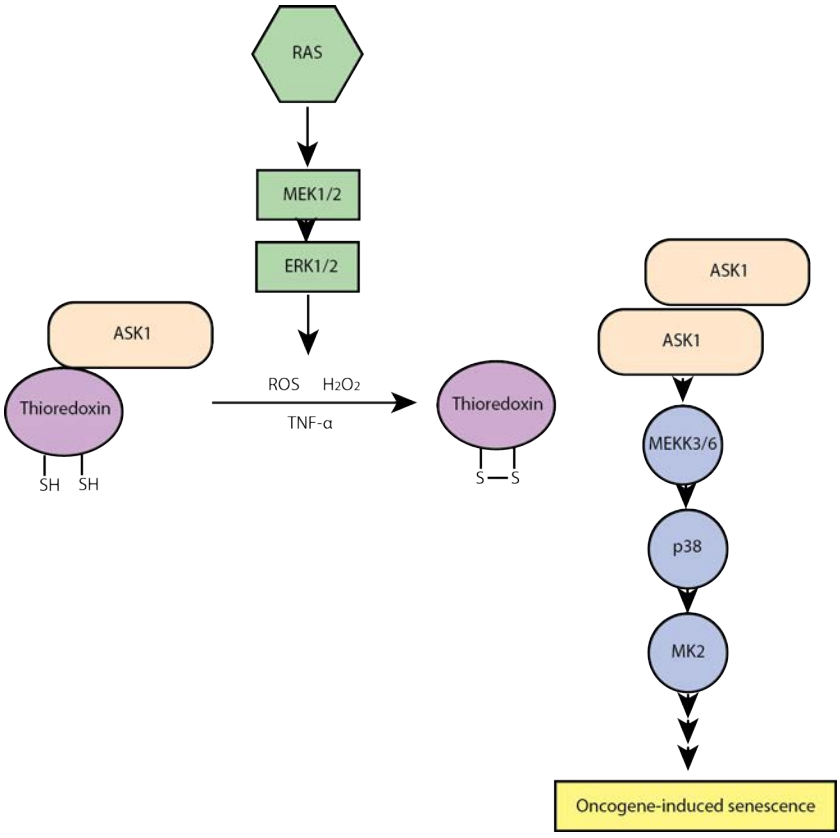

Figure 1.3 A model for the activation of p38 signalling by ROS

Activation of oncogenic RAS signalling leads to increased levels of intracellular reactive oxygen species (ROS) and DNA damage. The resulting oxidative state may be reversed with NADPH reserves in the cell (not shown). ROS accumulation can also be stimulated in normal antigen presenting cells through exposure to TNF-α. Through a redox-sensitive, N-terminal interaction with ASK1, the reduced form of thioredoxin inhibits ASK1 activity. Once oxidised by oxygen radicals, thioredoxin releases ASK1, which can then homo-oligomerise and activate downstream kinases MEKK3/6 and the p38 pathway. Collectively, this process is known to contribute to oncogene-induced senescence (Xu et al., 2014b).

1.4 Lung cancer and mouse models of the disease

The major focus of this thesis is the molecular biology of lung cancer. Lung cancer is the largest cause of cancer related death in the UK and worldwide (Swanton and Govindan, 2016). There are two broad histological subtypes of lung cancer, non-small cell lung cancer (NSCLC) and small-cell lung cancer (SCLC). NSCLC makes up the majority of lung cancer cases (around 85 % of

cases), and is further subdivided into adenocarcinoma and squamous-cell carcinoma (Herbst *et al.* 2008). The most significant environmental risk factor is tobacco smoking, relating to 85-90% of all lung cancer cases (Meuwissen and Berns, 2005; Swanton and Govindan, 2016). Smoking is especially associated with a high frequency of mutations in *KRAS* (20-30 % of lung adenocarcinomas) (Slebos et al., 1990). Mutations in *RAS* in lung cancer often result from G-T transversions, which is a hallmark of mutagenesis caused by carcinogens found in tobacco smoke. Also contributing to lung cancer progression is the frequent loss of the tumour suppressor *TP53*, which is mutated in about 40-50 % of all NSCLCs and 91 % or 92 % of lung squamous-cell or small-cell carcinomas, respectively (Swanton and Govindan, 2016).

Mouse models of human cancer have been used to understand the basic biology of cancer and cancer therapy, and therefore have potential to help discover improved cancer treatment, improved biomarkers and diagnosis and prevention of cancer and understand drug resistance mechanisms (Frese and Tuveson, 2007). Early models of lung cancer relied on carcinogen-induced models (Balmain and Pragnell, 1983). For example, experiments by Balmain and Pragnell in 1983 showed that DNA from mouse skin carcinomas was able to transform 3T3 fibroblasts; crucially, the transforming DNA was found to contain the *H-Ras* oncogene. More controlled genetically engineered mouse models of cancer followed. Notably, the development of the latent *KrasG12D* allele mouse (or *Kras LA* mouse) was the first demonstration that spontaneous recombination of oncogenic *Kras* could lead to early onset lung cancer in mice (Johnson et al., 2001). Tumorigenesis was accelerated when the *KrasLA* mice were crossed onto a strain deficient in the tumour suppressor *Trp53*. Subsequently, significant advances in mouse genetics, notably from the Tyler Jacks laboratory, led to the development of more sophisticated models of RAS-driven lung cancer, where the expression of the oncogene can be controlled in a temporal and spatial (tissue-specific) manner; so called conditional mouse models. By nasal instillation of

adenoviral Cre recombinase, tissue-specific recombination of the *Kras LoxP-Stop-LoxP-G12D* (or, *Kras LSL-G12D*) allele was achieved in the lung epithelium, leading to pre-neoplastic lesions (Tuveson et al., 2004). In this system, the bacteriophage LoxP sites flank the genetic element that will be excised after the expression of the LoxP-specific bacterial recombinase Cre. However, in cases where the LoxP sequences are running in opposite orientations, rather than deletion of the intervening sequence, there is an inversion event. Oncogenes can be expressed after the removal of transcriptional and translational stop sequences flanked by LoxP sites (LSL cassette), or an essential exon or entire gene can be removed when flanked by LoxP sites (flanked by LoxP; "floxed"). The Cre-LoxP system is now used extensively in cancer and many other areas of biology involving genetic manipulation of model systems. A major advantage of conditional mouse models is the ability to activate or inactivate genes in adult mice, which would have resulted in embryonic lethality or severe developmental defects if initiated constitutively. Using this system, tissue-specific recombination was used to concomitantly activate oncogenic RAS signalling and delete *Trp53* in the lung epithelium with adenoviral Cre in *KrasLSL-G12D/+; Trp53 flox/flox* mice (DuPage et al., 2009a). This mouse model of lung cancer, referred to as the *KP* mouse, recapitulates many histopathological features of the human disease, including the adenoma to adenocarcinoma histological transition and, although rare in this model, metastasis to lymph nodes (DuPage et al., 2009a). Adenoviral or lentiviral delivery of Cre allows for the tissue-specific and sporadic initiation of lung cancer in this model without detailed knowledge of the cell-of origin for the disease. Furthermore, the viral delivery component allows for the incorporation of other genetic elements into the tumour-initiating cells such as short hairpin RNAs (shRNAs) or cDNAs. This system is rarely "leaky" (i.e. unwanted expression of the transgene) unlike models using inducible Cre recombinases, as gene expression is tightly controlled by viral infection. Finally, another advantage of this conditional model is that *Kras* is expressed from its endogenous locus and therefore at

physiological levels. However, infection of other non-epithelial tissues in the lung is likely to occur, with as yet unknown effects on tumour progression.

1.5 Cancer immunology

1.5.1 An overview of cancer immunology

It is well accepted that tumours initiated by viruses are less common in immunocompetent individuals. In the context of cancer without viral aetiology, the existence of cancer immunosurveillance has remained contentious. However, a substantial body of clinical evidence has accumulated in favour of this concept. For example, patients who undergo immunosuppressive therapy as part of organ transplantation have developed melanoma clonally derived from the donor organ, suggesting occult cancer cells are kept in check by the immune system until transplanted into an immunosuppressed recipient (Strauss and Thomas, 2010). Secondly, paraneoplastic syndrome is an autoimmune condition associated with the aberrant recognition of normal tissues as tumour by the immune system, owing to the expression of common targeted antigens (Albert and Darnell, 2004). Moreover, there have been reports of spontaneous tumour regressions. Rare spontaneous melanoma regressions have been linked with concomitant incidence of vitiligo (loss of skin pigment, which can be caused by autoimmune destruction of melanocytes), implying immune system involvement (Smith and Stehlin, 1965). In line with this, there is consensus that lymphocyte infiltration in diverse tumour types is linked with improved prognosis (Denkert, 2010; Halama et al., 2011; Hiraoka et al., 2006). In a landmark paper, the density of tumour-infiltrating lymphocytes in colorectal cancer was shown to be a powerful prognostic factor and even outperformed classical histological grading (Galon et al., 2006). Quantitative analysis of the immune contexture of the tumour microenvironment for prognosis is now commonly referred to as the tumour “immunoscore”.

The recent explosion in the number of reported clinical successes of cancer immunotherapies has finally silenced critics of the cancer immunosurveillance hypothesis, and will be discussed in detail in later sections.

1.5.2 Genetically engineered mouse models in cancer immunology

Despite clinical indications, the cancer immunosurveillance hypothesis fell out of favour within the scientific community due to the lack of direct experimental evidence from animal models. For example, there was little difference in carcinogen-induced tumorigenesis in *nu*/*nu* athymic mice compared with immunocompetent mice (Stutman, 1974). A caveat to these experiments is that Stutman used a strain background that was exceptionally prone to carcinogen-induced tumorigenesis, perhaps masking small differences in tumour incidence. More importantly, it developed that nude mice still posses some functional $\alpha\beta$ T cells and a repertoire of extrathymically derived lymphocytes such as NK and $\gamma\delta$ T cells (Dunn et al., 2002). Mice mutant for the recombination activating genes 1 and 2 (*Rag1*-/- and *Rag2*-/-, respectively) necessary for V(D)J rearrangement, allowed for complete elimination of NKT, B and T cells (Shinkai et al., 1992). The use of the more profoundly immunocompromised *Rag*-deficient mice was instrumental in re-establishing the immunosurveillence hypothesis (Shankaran et al., 2001), and is still invaluable today in modelling cancer in the absence of adaptive immunity. *Rag*-null mice were revealed to be more susceptible to carcinogen-induced and spontaneous tumours. It has since emerged that innate immunity can generate independent anti-tumour responses (Beatty et al., 2011) and pro-tumorigenic roles (Lujambio et al., 2013), revealing added layers of complexity that cannot be fully explored in such models.

Robert Schreiber's lab has made extensive use of the *Rag*-deficient and other immunodeficient mouse models to demonstrate that there is selection against immunogenic cancer clones; a phenomenon dubbed "cancer immunoediting" (Shankaran et al., 2001). In a landmark study, they observed that tumours arising in *Rag2*-/- hosts could be rejected when transplanted into syngeneic immune competent mice, whereas tumours transplanted from wild-type mice grew comparably, suggesting that tumours from *Rag 2*-/- hosts are more immunogenic (or "un-edited) (Shankaran et al., 2001). Finally, they demonstrated that tumour rejection was CD4+ and CD8+ T cell-dependent, showing that these lymphocytes not only protect against immunogenic tumours *in situ*, but also sculpt the immunogenicity of these tumours by selection. Collectively, Schreiber's work provided a model for dynamic tumour-host interactions and immunoediting processes dubbed the "three Es"; that is, tumour elimination, equilibrium and escape (Dunn et al., 2002).

11 years later, Schreiber and colleagues asked which antigens trigger tumour rejection. Using a similar system of transplanting mutationally complex tumours induced by the carcinogen methylcholanthrene, they carried out exon capture and deep sequencing of cDNA from immunogenic clones generated in *Rag 2*-/- hosts to identify antigens necessary and sufficient for tumour rejection (Matsushita et al., 2012). Computational prediction algorithms for strong MHC class I binders identified a mutant form of spectrin-β2 as a candidate neo-antigen strongly represented on the tumour cell surface. Its antigenicity was later confirmed by conventional expression cloning techniques. This study provides a rationale for personalized immunotherapies, where prominent neo-antigens are identified and may be re-targeted by vaccination strategies, especially in tumour types with high mutational load such as smoking-related lung cancer (Matsushita et al., 2012). However, there is a possibility that immunogenic passenger mutations may be easily lost by selection. In related work, Willimsky and Blankenstein asked whether such selection exists when the driving oncogene is the major

tumour antigen (Willimsky and Blankenstein, 2005). Making use of a mouse model of spontaneously arising cancer driven by randomly activated expression of SV40 Large T antigen, they found that immunoediting did not occur in this context, as there is an absolute requirement to retain the oncogene for tumour maintenance. Rather, tumours arising in immune competent hosts initially triggered a T cell and humoral immune response, but this was eventually overcome by induced T cell tolerance, associated with TGFβ-induced cytotoxic T lymphocyte anergy.

Tyler Jacks and colleagues recently addressed a similar question using a GEMM of oncogenic *Kras*-driven sarcomagenesis (DuPage et al., 2012). They investigated whether immunoediting of potent neo-antigens occurred in the context of spontaneously arising tumours. The neo-antigens were not required to maintain tumourigenesis in this case. To this end, they utilised lentiviral delivery of Cre recombinase ("Lenti-x" vector) to initiate oncogenic *Kras* activation and concomitant deletion of *Trp53*, or lentiviral particles expressing both Cre and luciferase linked to three distinct model immunogenic peptides ("Lenti-LucOS"). They could follow neo-antigen expression *in vivo* by detecting luciferase activity. Interestingly, they observed increased latency in the progression of Lenti-x tumours in the immunocompetent hosts compared to *Rag2*-/- hosts. This immune-related tumour suppression was not apparent in the context of transplantation of fully developed Lenti-x tumours, which were established with similar efficiencies in wild-type and *Rag2*-/- recipients. As expected, growth of immunogenic Lenti-LucOS tumours was initially inhibited in wild-type mice relative to Lenti-x tumours. Interestingly, the authors found that the engineered neo-antigens were eventually silenced in progressively growing sarcomas. The immunoediting process was dependent on T cells and/or the reduced presentation of tumour antigens by surviving tumour cells.

In further work, DuPage *et al* demonstrated that a similar experiment performed in the lung epithelium gives quite different results, revealing key

tissue specific differences (DuPage et al., 2011). In a *Kras*-driven, *Trp53*-null NSCLC mouse model (DuPage et al., 2009b), immunogenic ("Lenti-LucOS") tumours again grew slower in wild-type hosts than *Rag2*-/- hosts, but this time retained antigen expression (as determined by luciferase expression). Instead, they observed immune tolerance associated with tumour-specific CD8+ T cell PD-1 expression, influx of regulatory T cells and an anergic phenotype in anti-tumour CD8+ T cell population, characterised by downregulation of IFN-γ and TNF-α. These tissue-dependent differences may reflect the different levels of immune regulation in muscle and lung parenchyma, potentially caused by their disparate exposures to environmental pathogens, microbiota and debris. This raises an interesting point; what mechanisms of immune suppression are at play at metastatic sites? How the resident immune-compartment influences where tumour cells seed, and how the mechanisms of tumour immune escape are adapted for the new microenvironment are intriguing questions to be addressed.

Experiments in mouse models using potent, model tumour neo-antigens universally expressed by every cell does not reliably mimic the heterogeneous and clonal nature of cancer (de Bruin et al., 2014; Gerlinger et al., 2012). Accurately modelling polyclonal cancer immune responses in GEMMs of lung cancer requires intrinsically high somatic mutation rates similar to those found in humans. Comprehensive sequencing efforts have addressed the mutational burden of tumours derived from different mouse models of lung cancer. Tyler Jacks and colleagues found a very low somatic point mutation rate in tumours derived from a mouse model of small-cell lung cancer driven by the loss of *Rb* and *Trp53* tumour suppressors (McFadden et al., 2014a). Concordantly, in the *Kras*-driven mouse model of NSCLC, a comparably low point mutation rate was found in lung tumours in the absence of tobacco carcinogens (6 non-synonymous mutations on average), but this was considerably higher in tumours initiated with the carcinogens urethane or methyl-nitrosourea (MNU) (192 non-synonymous mutations on average in MNU-initiated tumours) (Westcott et al., 2015b). These data highlight

important discrepancies in predicted neo-antigen burden between GEMM and human tumours. However, GEMMs have key advantages over classical syngeneic transplantation models in the study of cancer-immune interactions: (1) GEMM tumours arise more slowly, allowing for co-evolution of the host immune system and tumour, (2) GEMM tumours arise at the orthotopic site, allowing accurate modelling of the microenvironment, whereas tumour transplants are often subcutaneous, (3) some transplanted tumour cells inevitably undergo cell death during the process of injection, which might act as an anti-tumour vaccine and have a significant impact on anti-tumour immunity.

1.5.3 Immunogenic cell death

An important question related to the broad effects of anticancer drugs is the contribution of the immune system to the anti-tumour response. Seminal work from the Zitvogel and Kroemer labs have revealed that certain anticancer drugs can lead to an immunogenic cell death (ICD) programme, which requires at least three molecular characteristics: (1) cell surface exposure of calreticulin (Obeid et al., 2007), (2) active release of ATP (Michaud et al., 2011), and (3) passive release of high-mobility group protein 1 (HMGB1) (Galluzzi et al., 2012). These damage-associated molecular patterns have been shown to be necessary for the induction of adaptive immunity against cancer cells in mouse tumour transplantation experiments (Apetoh et al., 2007; Michaud et al., 2011; Obeid et al., 2007). However, ICD-inducing drugs are mechanistically and structurally diverse, leading to confusion as to the precise signalling mechanisms driving these processes. However, it is now clear that endoplasmic reticulum (ER) stress and the accumulation of reactive oxygen species are important factors (Garg et al., 2012). For example, chemotherapies inducing hyperploidy have been shown to induce ER-stress and promote calreticulin exposure at the cell membrane (Senovilla et al., 2012). This process underlies immune selection against polyploid cancer cell clones in mouse models. It seems that the activation of

dendritic cells and subsequent instigation of adaptive immune memory against the tumour is better achieved by inducing ICD than the release of intracellular antigens from dying tumour cells alone. This process has been called *in situ* vaccination (Galluzzi et al., 2012).

For example, in syngeneic tumour transplant experiments, immunogenic anthracycline chemotherapy treatment of tumour-bearing mice stimulates the ATP-dependent recruitment of CD11c+CD11b+Ly6Chigh cells to the tumour-bed, which are able to engulf dying tumour cell debris and contribute to the anti-tumour T cell response (Ma et al., 2013). Furthermore, in a GEMM of lung adenocarcinoma, oxaliplatin and cyclophosphamide treatment sensitised ICB-refractory tumours to PD-1 and CTLA-4 combination blockade through a mechanism involving drug-induced innate immune responses depending on TLR4, and infiltration of CD8+ T cells into lung tumours (Pfirschke et al., 2016).

Although the characteristics of ICD were initially identified in the unnatural context of tumour cell transplantation, patients carrying defective alleles of receptors for extracellular ATP or HMGB1 have been found to be poor responders to some ICD-inducing chemotherapies, suggesting these findings have clinical relevance (Apetoh et al., 2007; Ghiringhelli et al., 2009). In contrast to the above observations, a study from de Visser and colleagues using the ICD-inducers doxorubicin and oxaliplatin to treat breast cancer in an autochthonous GEMM, showed that survival in treated *Rag 2*+/- mice was not significantly different from *Rag 2*-/- mice (Ciampricotti et al., 2012; Zitvogel and Kroemer, 2012a). These findings highlight the controversies in this field of research and further illustrate important differences between GEMMs and tumour transplantation models. It is possible that results from de Visser and colleagues could indicate profound tumour-mediated immune suppression. Whether combining chemotherapy with immune checkpoint blockade would significantly change the outcome in this context remains to be tested.

Targeted therapies and chemotherapies are commonly derived from a cell autonomous perspective, and how they impinge on the tumour microenvironment is often overlooked. What is clear is that the chronic selection pressure exerted by such agents will lead to Darwinian selection for resistant clones, resulting in acquired resistance. Conversely, the concept of *in situ* vaccination by cytotoxic agents in conjunction with immunomodulatory drugs is an attractive alternative for several reasons. The growing class of ICD inducers only need to be used in short bursts for anti-tumour vaccination, making both acquired resistance and long-term dose-related toxicity less likely. It can be envisaged that serial *in situ* vaccination by ICD-inducers will re-prime the adaptive immune system against immunoedited subclones. An improved understanding of how targeted therapies and chemotherapies affect the reciprocal signalling between the immune system and tumour in clinically relevant GEMMs, and how to combat adaptive mechanisms of tumour-mediated immune suppression may present opportunities for durable therapeutic responses in cancer (Galluzzi et al., 2015).

1.6 Cancer immunotherapy

1.6.1 Clinical data for immune checkpoint blockade

Perhaps the first recorded clinical use of cancer immunotherapy was by the New York surgeon William Coley in the late 19th century. He noted that *Streptococcus pyrogenes* skin infections occurred in sarcoma patients with unexpected tumour regression, and subsequently treated patients with an inactivated bacterial concoction (“Coley’s toxins”), with some success (Nauts et al., 1953). In an analogous manner, administration of Bacillus Calmette-Guerin (BCG) is still used as a component of standard therapy for bladder cancer (Herr et al., 1995).

Intriguingly, several clinical case studies lend support for the idea that the immune system can contribute to the efficacy of classical cancer treatments such as radiotherapy. Patients receiving radiotherapy very occasionally experience spontaneous regressions of distant, non-radiated lesions; this rare phenomenon is called the abscopal effect. Presently, there is mounting evidence that the abscopal effect is in fact mediated by a systemic immune response. For example, a patient presenting with metastatic melanoma experienced tumour regression at distant sites after receiving radiotherapy and anti-CTLA-4 immunotherapy (Postow et al., 2012). The anti-tumour response clearly correlated with markers of increased systemic immune reactivity to the melanoma tumour-associated antigen NY-ESO-1.

Steven Rosenberg pioneered some of the first successful, controlled cancer immunotherapy trials in human patients (Rosenberg, 2014). In 1985, a fraction of patients with metastatic disease responded durably to high-dose recombinant IL-2 therapy, a cytokine involved in promoting T cell proliferation (Rosenberg et al., 1985). These were among the trial results that eventually led to the FDA-approval of IL-2 for patients with metastatic renal cancer in 1992. However, severe adverse effects and treatment related deaths were observed, often relating to capillary leak syndrome and excessive fluid retention in visceral organs. Nonetheless, these reports provided some of the first clinical evidence supporting immune modulation for anti-cancer therapy in humans.

The discovery of IL-2 and its ability to promote the long-term survival of T cells in culture simultaneously ignited interest in the related field of adoptive cell therapies (ACT). Early ACT for cancer treatment involved re-infusion of expanded anti-tumour T cells. However, the discouragingly poor success rates of these approaches in early trails meant that ACT technologies did not really progress until relatively recently. The clinical approval of a novel cancer immunotherapy Sipuleucel-T reinvigorated research into ACT for cancer. Sipuleucel-T therapy involves the re-infusion of autologous APCs incubated

with prostate-specific antigen and GM-CSF *ex vivo*. Clinical trials revealed a significant but modest mean overall survival benefit of about four months for men with metastatic, castration-resistant, prostate cancer receiving Sipuleucel-T over placebo (Kantoff et al., 2010). Presently, there is growing enthusiasm over treatments based on infusion of cancer patients with genetically engineered T cells with chimeric antigen receptors (CAR-T cells) that can specifically identify and eliminate haematological cancers, and more recently, solid cancers (Rosenberg and Restifo, 2015).

Seminal preclinical work by Allison and colleagues validated the immune checkpoint molecule CTLA-4 as a viable therapeutic target. Administration of anti-CTLA-4 antibodies caused regressions of established subcutaneous tumours (Leach et al., 1996). Some antibody-treated mice remained tumour-free for long periods of time, and moreover, were more resistant to tumour re-challenge, implying induction of immunological memory. These preclinical data were followed by major successes in early clinical trials with ipilimumab, the human anti-CTLA-4 antibody from Bristol-Myers Squibb (Hodi et al., 2010; Phan et al., 2003; Yang et al., 2007). Remarkably, a subset of melanoma patients treated with ipilimumab experienced complete regressions and have remained disease-free for over 10 years (Sharma and Allison, 2015).

Topalian and colleagues grasped the attention of the cancer research community with a landmark phase I clinical study demonstrating durable and profound tumour regressions in multiple human cancers using an anti-PD-1 antibody (Topalian et al., 2012). Notably, NSCLC was among the malignancies that showed promising responses to anti PD-1 ICB, a cancer that has hitherto been considered poorly immunogenic. The distinct biology of the PD-1 and CTLA-4 checkpoints in regulating T cell function, and the clinical successes of these ICB agents as monotherapies, provided sufficient rationale for their combination. As expected, the first trial of nivolumab (anti-PD-1) and ipilimumab (anti-CTLA-4) in combination revealed increased

toxicity compared with either monotherapy, but the combination also achieved greater overall survival benefit in patients with previously untreated melanoma over single agent therapy (Larkin et al., 2015b; Postow et al., 2015). Notably, as a single agent nivolumab is clearly superior to ipilimumab, even in cases were tumours were classified as PD-L1 negative.

1.6.2 Correlates of cancer immunotherapy response

The mechanistic understanding of how cancer immunotherapies work is currently lagging behind the clinical progress. Next-generation sequencing (NGS) of tumour specimens has suggested that the tumour mutational load is the best molecular correlate for immunotherapy success, but its value as a biomarker for response is perhaps limited. Melanoma response to anti-CTLA-4 therapy with ipilimumab significantly correlated with mutational burden (Snyder et al., 2014), and similar findings have been reported for lung adenocarcinoma (Rizvi et al., 2015b). Using whole-exome sequencing and bioinformatics analyses in NSCLC patients treated with pembrolizumab, the authors demonstrated sensitivity to PD-1 blockade was significantly correlated with non-synonymous mutational burden and the corresponding predicted neo-antigen burden. More support for this link came from evidence that patients with mismatch repair-deficient colorectal tumours (and thus higher somatic mutation rate) had a significantly higher response rate to pembrolizumab than mismatch repair-proficient colorectal tumours (Le et al., 2015). Further work in this field has revealed that lung tumours with lower clonal heterogeneity tend to respond better to PD-1 ICB than tumours with a more complex and branched sub-clonal architecture (McGranahan et al., 2016). Interestingly, the authors revealed a tendency for tumours with low clonal neo-antigen complexity to express higher levels of *PD-L1* mRNA, perhaps reflecting increased targeting by anti-tumour T cells. However, precisely why tumours with lower tumour heterogeneity respond better to PD-1 ICB remains unclear. Until recently, most of the cancer immunotherapy field has been focussed on anti-tumour CD8 T cell responses, but tumour-

specific CD4+ T cells have now been described in human melanoma, and their therapeutic efficacy in adoptive cell transfer for treatment of epithelial cancers has been vindicated (Linnemann et al., 2015; Tran et al., 2014).

Finally, two reports using similar approaches to determine tumour-rejection antigens revealed that tailored peptide vaccines can induce significant anti-tumour activity (Gubin et al., 2014; Yadav et al., 2014). Both studies used a combination of RNA sequencing and MHC binding prediction algorithms to predict mutant antigens likely to be presented by MHC class I on tumour cells. Peptide vaccines based on validated tumour neo-antigens were effective when co-administered with immunostimulatory adjuvants in both studies, using distinct syngeneic tumour models. Gubin *et al* went on to show that anti-PD-1 and anti-CTLA-4 therapy is associated with phenotypic changes in tumour-antigen-specific CD8+ T cells in mice. Specifically, following ICB, antigen-specific CD8+ T cells expressed more effector cytokines and granzyme B (especially after anti-CTLA-4 therapy), and showed decreased expression of immunosuppressive molecules such as lymphocyte-activation gene 3 (LAG-3) and T cell immunoglobulin and mucin protein 3 (TIM-3). Collectively, these data highlight the potential therapeutic value of combining peptide vaccines with ICB, and demonstrate that alterations in the phenotype of pre-existing anti-tumour immune cells contribute to the anti-tumour effects of ICB.

Collectively, these results imply that genomic instability, a hallmark of cancer, could be a potential weakness for cancer cells, ultimately compromising immune evasion (Hanahan and Weinberg, 2011). From the perspective of cancer immunology, rather than mutations in driving oncogenes, passenger mutations in innocuous proteins may in fact be cancer's therapeutic vulnerability. Increasingly personalised medicine involving comprehensive NGS and profiling of active immune checkpoints will clearly be required to adopt the most effective immunotherapy combinations. These results also raise the following question: can some forms of chemotherapy increase the

number of tumour mutations and thus, with careful scheduling, work synergistically in combination with ICB?

1.6.3 PD-L1 expression as a biomarker for sensitivity to PD-1/PD-L1 immune checkpoint blockade

Only a fraction of patients currently respond to immune checkpoint blockade, presenting a major clinical challenge. Reliable biomarkers of patient response are urgently needed to maximise the number of patients that can benefit form these therapies and simultaneously reduce the huge cost of clinical failure with these expensive antibody therapeutics. To date, no conclusive evidence has been put forward for a molecular target to serve as an appropriate biomarker. In stark contrast to targeted therapies, knowledge of the driving oncogene does not seem to provide much prognostic value in this context.

However, tumour PD-L1 expression and tumour-proximal stromal/immune cell PD-L1 expression have been shown to correlate with response to ICB targeting the PD-1 pathway, but remains contentious. In an early study of the response to PD-1 ICB in NSCLC, melanoma, renal cell carcinoma, colorectal cancer and prostate cancer response, PD-L1 positive tumours had a significantly better response rate than PD-L1 negative tumours; objective responses were 9/25 for PD-L1 positive and 0/17 for PD-L1 negative tumours (Topalian et al., 2012). These data are concordant with a recent phase I study of pembrolizumab in NSCLC patients, where PD-L1 expression in over 50 % of tumour-cells was significantly correlated with improved drug efficacy (Garon et al., 2015). In contrast, large-scale clinical trials of nivolumab in NSCLC have revealed that tumour PD-L1 expression on tumour cells is correlated with therapy response in non-squamous, but not the squamous subtype of NSCLC (Borghaei et al., 2015; Brahmer et al., 2015). Crucially, the Brahmer and Borghaei studies both used the same PD-L1 detection antibody and scoring criteria to determine tumour PD-L1 positivity,

suggesting that their results may reflect genuine biological differences between these histological tumour types, rather than trivial technical differences. Interestingly, Borghaei *et al* demonstrated that patients with tumours harbouring mutations in *KRAS* responded better on nivolumab than *KRAS* wild-type patients. One speculative explanation for increased efficacy of PD-1 pathway ICB in *KRAS* mutant tumours is that *KRAS* mutations are more prevalent in smokers, which are known to have a higher tumour mutational burden. However, there is evidence that *KRAS* and *EGFR* mutant (but not *ALK* mutant) NSCLCs have a significantly higher frequency of tumour PD-L1 positivity when compared with triple-negative cases (*EGFR P* < 0.001, *KRAS P* = 0.02, *ALK P* = 0.06) (D'Incecco et al., 2015). These data are supported by the observation that a higher proportion of patients with *KRAS* mutant NSCLC had >50 % PD-L1 expressing tumour-cells when compared with *KRAS* wild-type tumours (Garon et al., 2015). That is, 42.2 % of patients with *KRAS* mutations and 26.8 % of patients deemed *KRAS* wild-type had tumours with at least 50 % of tumour-cells expressing PD-L1. In contrast, no clear distinction was seen for mutations in other common drivers such as *EGFR* and *ALK*.

Recently, five independent reports published in the same issue of *Nature* comprehensively profiled the mechanisms governing responses to PD-1 and CTLA-4 ICB in humans and mice. Herbst and colleagues performed a phase I clinical trial with the Genentech anti-PD-L1 monoclonal antibody MPDL3280A for the treatment of multiple malignancies (Herbst et al., 2014). Notably, 21 % of NSCLC patients responded to this therapy, with a higher proportion of responders being smokers than never-smokers. Significantly, the presence of PD-L1-positive tumour infiltrating immune cells was a strong positive predictor of response, whereas tumour-cell PD-L1 expression was not. Tumours undergoing treatment-related regressions appeared to have large increases in tumour immune infiltrates and increased PD-L1 expression on tumour cells and infiltrating immune cells, possibly reflecting high levels of IFN-γ in the tumour bed. Genentech also trialled their PD-L1 antibody in

patients with urothelial bladder cancer, and had comparable results; high PD-L1 expression on tumour-infiltrating immune cells was the clearest positive predictor of therapy response (Powles et al., 2014). The authors also noted that the promising responses they obtained with PD-L1 ICB in this cancer might reflect its high mutation rate. In melanoma, response to the anti-PD-1 antibody pembrolizumab (Merck) was associated with the presence of PD-1-postive immune cells at the tumour margin (Tumeh et al., 2014).

Interestingly, anti-tumour responses following pembrolizumab dosing were associated with tumour-proximal T cell clonal expansion and increased clonality, which was determined by NGS of TCRs expressed by tumour-infiltrating lymphocytes (Gubin et al., 2014). This effect might reflect the expansion of anti-tumour T cell clones. Remarkably, using responder characteristics from their discovery patient cohort (including the IHC-based assessment of tumour-proximal CD8, PD-1 and PD-L1 expression and T cell density and distribution), Ribas and colleagues successfully predicted response to pembolizumab in 13/15 melanoma patients, emphasising the clinical significance of their findings. Taken together, these reports demonstrate that the efficacy of ICB depends on whether there is a significant pre-existing anti-tumour T cell response, and whether the given checkpoint is currently functional in the tumour.

Differences in the interpretation of PD-L1 expression on tumour cells or tumour-infiltrating immune cells as a biomarker for PD-1 pathway blockade likely arise from several factors including: (1) different antibodies used to detect PD-L1, (2) different quantification methods and thresholds between studies to define a “PD-L1 positive” tumour, (3) tumour PD-L1 expression is likely to be heterogeneous and not reliably represented by single region biopsies, (4) PD-L1 expression is highly dynamic, so precisely when the biopsy is taken is critical, and (5) PD-L1 expression can be determined by cell-intrinsic signalling, which may be independent of tumour cell immunogenicity. In summary, this field would benefit from standardising

methods to detect and interpret tumour PD-L1 expression in patients.

Examples of these confounding factors are depicted in Figure 1.4.

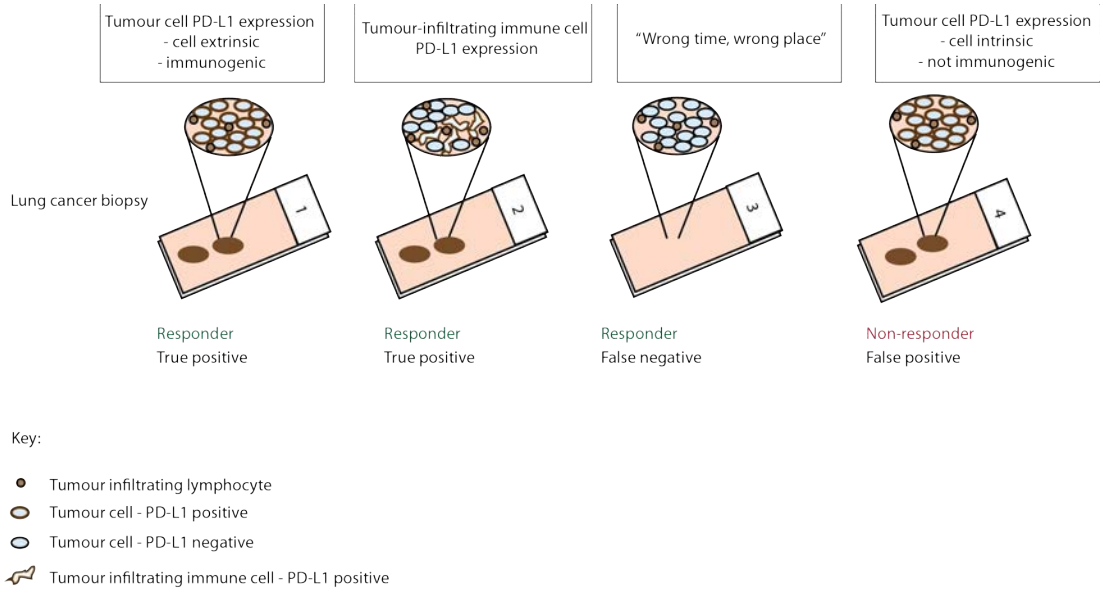

Figure 1.4 Tumour PD-L1 expression as a biomarker for immunotherapy response

Clinically demonstrated associations between tumour PD-L1 expression and response to PD-1/PD-L1 pathway blockade in NSCLC. (1) Tumour cell PD-L1 expression, governed by cell-extrinsic cues such as inflammation in the tumour-microenvironment and thus likely reflects the immunogenicity of the tumour (Borghaei et al., 2015; Garon et al., 2015; Topalian et al., 2012). (2) Tumour-infiltrating immune cell or stromal cell PD-L1 expression has been shown to be predictive of PD-L1 response, although the mechanism is unclear (Herbst et al., 2014). (3) PD-L1 expression is highly dynamic and heterogeneous so failure to obtain representative multi-region biopsies, or biopsy of the tumour at an unrepresentative point in time may lead to spurious assumptions. (4) Here, tumour cell PD-L1 positivity is predominantly due to cell-intrinsic signalling and not reflective of the immunogenicity of the tumour. Other possible confounding factors including technical issues concerning IHC methods and interpretation and are not shown.

1.7 PD-L1 regulation and function in cancer

1.7.1 Cell-extrinsic regulation of PD-L1 expression

Presently, the best-defined activator of PD-L1 expression is IFN-γ. Following exposure to IFN-γ, the transcription factor interferon regulatory factor-1 (IRF-1) binds to the *PD-L1* promoter and initiates transcription, although IRF-1 is also important for constitutive PD-L1 expression (Lee et al., 2006). In addition, the induction of PD-L1 expression downstream of IFN-γ appears to be dependent on JAK/STAT signalling in A549 lung cancer cells (Lee et al., 2006). Indeed, STAT3 binds to the *PD-L1* promoter in APCs, with STAT1 seemingly playing a relatively minor role (Wolfle et al., 2011). In addition, the *PD-L1* promoter also contains a binding site for NF-κB, which is transiently activated following IFN-γ stimulation by the associated ERK and PI3K activity (Lee et al., 2005). However, whether NF-κB activity is necessary for IFN-γ-driven PD-L1 expression remains unclear and may be tissue-specific (Lee et al., 2006; Lee et al., 2005). Similarly, TLR stimulation of multiple myeloma plasma cells led to increased PD-L1 expression through a mechanism involving the activation of MEK (Liu et al., 2007). Finally, hypoxia in the tumour microenvironment may have a direct impact on tumour cell and stromal cell PD-L1 expression, as a functional hypoxia-response element in the proximal *PD-L1* promoter has recently been described (Noman et al., 2014). ChIP experiments verified HIF1-α binding to the *PD-L1* promoter under hypoxic conditions, implying that tumour-associated hypoxia may contribute to upregulation of PD-L1 in cancer.

1.7.2 Cell-intrinsic regulation of PD-L1 expression by oncogenes

PD-L1 expression is elevated in many cancers (Dong et al., 2002), although there appears to be very few unifying principles of aberrant genetic or epigenetic regulation. Genetic mechanisms for directly increasing PD-L1 expression include structural rearrangements of the promoter region, gene amplification, and loss of the 3'UTR. Using RNA-sequencing of B-cell lymphomas, recurrent translocation events in the major histocompatibility class II transactivator (*CIITA*) resulted in highly transcriptionally active gene fusions with *PD-L1* and *PD*-L2, correlating with elevated expression of these PD-1 ligands (Steidl et al., 2011). Moreover, amplification of 9p24.1, a genetic region containing the proximal genes *PD-L1*, *PD-L2* and *JAK2*, is found in some cases of Hodgkin lymphoma, and is invariably associated with increased PD-1 ligand transcription (Green et al., 2010). The combined increase in gene dosage and transcription mediated by elevated JAK2 activity may concertedly drive high levels of PD-L1 and PD-L2 expression.

Loss or shortening of 3'UTRs has been associated with overexpression of many genes involved in tumour progression (Mayr and Bartel, 2009). Recently, structural variations in the 3'UTR of *PD-L1* were found in multiple cancers at a low frequency, with the highest prevalence in stomach adenocarcinoma (2%), B-cell lymphoma (8%) and adult T-cell leukaemia/lymphoma (27%) (Kataoka et al., 2016). Structural disruption of the *PD-L1* 3'UTR was found to be cell-intrinsic, or directly induced by viral integrations following infection (e.g. Esptein-Barr virus in stomach adenocarcinoma). Loss of the *PD-L1* 3'UTR was associated with increased *PD-L1* mRNA expression in human cancers and increased PD-L1 expression in mouse cancer cell lines with genetically engineered deletion of the 3'UTR. Although the mechanism for this genetic regulation remains unclear, the authors speculate that miRNAs and a putative AU-rich element in the long *PD-L1* 3'UTR might have a role.

PD-L1 levels are also directly governed by cell-intrinsic signalling. In cancer, this is becoming increasingly evident, as several oncogenes have been implicated in controlling tumour cell PD-L1 expression and thus anti-tumour immunity (Pardoll, 2012). A simplified overview of the molecular control of PD-L1 expression is shown in Figure 1.5.

The first report linking an oncogenic pathway to PD-L1 regulation and immune evasion reported that loss of the tumour suppressor PTEN in glioma could cause upregulation of *PD-L1* mRNA translation, dependent on mTOR activity (Parsa et al., 2007). How this mechanism operates for the *PD-L1* transcript specifically remains unclear, as the 5'UTR does not contain canonical elements such as 5' terminal oligopyrimidine tract (TOP) sequences that are known to be responsive to S6K1 activity. Since, mTOR has also been described as a driver of PD-L1 expression through upregulating PD-L1 translation in lung cancer (Lastwika et al., 2016). Using mouse models of Ras-driven lung cancer the authors were able to demonstrate that chronic rapamycin treatment reduces tumour PD-L1 protein expression *in vivo*. Moreover, rapamycin treatment appeared to combine well with anti-PD-1 therapy to reduce lung tumour burden. Considering the well-known immunosuppressive effects of rapamycin, it is difficult to conclude whether the observed decrease in tumour PD-L1 expression *in vivo* is at least partly due to rapamycin-induced changes in tumour-associated leukocytes.

Interestingly, a recently developed mouse model of lung squamous cell carcinoma driven by the loss of *Pten* and *Lkb1* was found to harbour a subpopulation of tumour-propagating cells that expressed high levels of PD-L1, suggesting that this cell population may be exceptionally immunoresistant (Xu et al., 2014a). Following on from this work, the authors found that *LKB1* loss in human and mouse Ras-driven lung cancer was associated with lower levels of PD-L1 (Koyama et al., 2016). These results imply that the loss of

Pten may be the dominant genetic determinant driving immune resistance in their mouse model of lung squamous cell carcinoma.

MEK inhibition was found to be effective in reducing PD-L1 expression in acute myeloid leukaemia (Berthon et al., 2010). In support of this finding, melanoma cells that develop resistance to the BRAF inhibitor vemurafenib were found to elevate MEK activity and, in parallel, elevate expression of PD-L1 (Jiang et al., 2013). Crucially, MEK inhibition significantly reduced tumour cell PD-L1 levels in BRAF inhibitor-resistant melanoma cells, as did siRNA-mediated knock-down of the transcription factor *c-jun*. Based on these data, the authors predict the functional involvement of an upstream AP-1-dependent enhancer at the *PD-L1* locus. BRAF inhibition has been shown to decrease PD-L1 expression in some BRAF V600E positive cell lines, however, work from the Ribas laboratory has revealed that inhibitors of BRAF, MEK and PI3K result in variable effects on PD-L1 expression across an extensive panel of melanoma cell lines; in some cases decreasing PD-L1 expression and occasionally even modestly increasing levels of PD-L1 (Atefi et al., 2014). These results imply that PD-L1 expression responses to such pathway inhibitors are nuanced, even in the same tissue type, and highlight the lack of molecular detail linking these pathways to PD-L1 gene expression.

Using a GEMM of *EGFR*-mutant NSCLC, PD-L1 levels were shown to be strikingly elevated on lung tumour cells, suggesting the development of an intrinsic immunosuppressive phenotype (Akbay et al., 2013). Moreover, EGFR inhibitors successfully reduced PD-L1 expression in several NSCLC cell lines, implying that EGFR TKIs may be of use in combination with immunotherapy treatments. Notably, lung tumours from the mouse model of NSCLC driven by a mutant, human EGFR transgene were responsive to PD-1 blockade. Conversely, a mouse model of NSCLC driven by oncogenic *Kras* and the loss of *Trp53* was refractory to anti-PD-1 therapy. These data imply disparate immunosuppressive programmes at play in these mouse models.

Alternatively, their data might reflect the increased immunogenicity of EGFR+ cancer cells, as the EGFR transgene is a highly expressed cell surface protein of human origin.

Oncogenic ALK-fusion proteins have been implicated in promoting PD-L1 expression through different mechanisms. In T cell lymphoma, the nucleophosmin-anaplastic lymphoma kinase (NPM-ALK) fusion protein induces activation of PD-L1 expression through STAT3 (Marzec et al., 2008), whereas in lung cancer, PD-L1 level upregulation by echinoderm microtubule-associated protein-like 4 (EML4)-ALK seems dependent on MEK and PI3K signalling rather than STAT3 (Ota et al., 2015). Nonetheless, inhibitors of ALK were effective in reducing PD-L1 expression in both scenarios.

The proto-oncogene transcription factor MYC has recently been implicated in promoting PD-L1 expression in mouse T cell lymphoblastic leukaemia (Casey et al., 2016a). Oncogenic levels of MYC facilitated occupancy of the PD-L1 promoter, suggesting direct transcriptional regulation. In addition, another transcription factor, FoxA1, has been implicated in promoting PD-L1 expression in an atypical Treg subset (FOXP3- FoxA1+ Tregs) involved in reducing autoimmune inflammation in the central nervous system (Liu et al., 2014). When overexpressed, FoxA1 bound to the *PD-L1* promoter in ChIP experiments, and modestly increased expression of a luciferase reporter bearing the *PD-L1* promoter region. Furthermore, FoxA1+ Tregs express high levels of PD-L1 and their immunosuppressive function seems to be dependent on PD-L1 expression. Finally, PD-L1 may be a p53 target gene, as enforced expression of p53 upregulated PD-L1 expression, and moreover, DNA damage-induced expression of PD-L1 is dependent on p53 (Yoon et al., 2015). However, there is conflicting evidence on this, as p53 has since been shown to upregulate the mircoRNA (miRNA) miR34, which can target *PD-L1* mRNA, indicating that p53 may in fact indirectly reduce PD-L1 expression in cancer (Cortez et al., 2016).

Numerous other studies have implicated miRNAs in the negative regulation of *PD-L1* expression, including miR34, miR200, miR513, miR424 and miR570. Chen *et al* showed that epithelial to mesenchymal transition in lung cancer cells is accompanied by a ZEB1-mediated decrease in miR200, resulting in de-repression of PD-L1 (Chen et al., 2014). In addition, elevated PD-L1 expression was shown to enhance the metastatic capability of lung cancer cells *in vivo*. In humans, somatic mutations within the *PD-L1* 3'UTR binding site for miR-570 can partially disrupt miRNA binding and are associated with higher PD-L1 expression in gastric adenocarcinoma cells *in vitro* and *in vivo* (Wang et al., 2013; Wang et al., 2012). In cholangiocytes, miR-513 is downregulated following IFN-γ-stimulation, contributing to PD-L1 induction by de-repression of *PD-L1* mRNA translation (Gong et al., 2009). Interestingly, Kataoka and colleagues found that cells with *PD-L1* 3'UTR deletions could still respond to IFN-γ, suggesting that transcriptional and post-transcriptional control govern PD-L1 induction by IFN-γ (Kataoka et al., 2016).

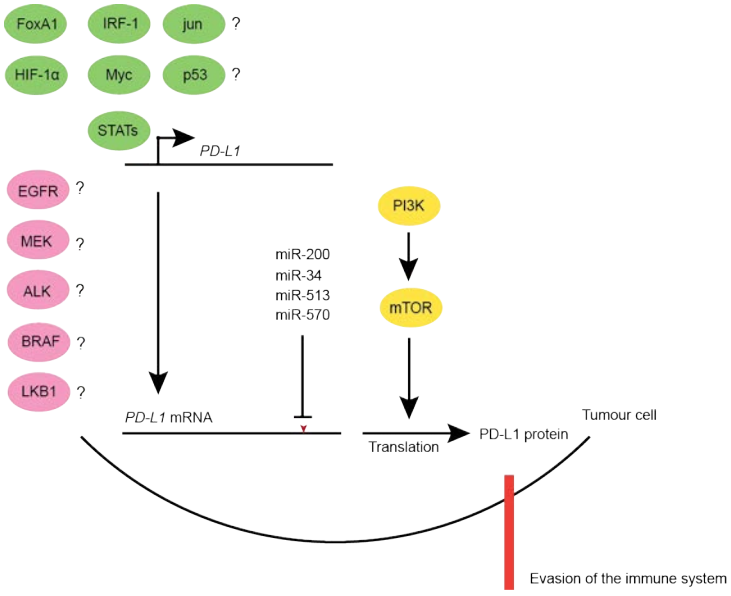

Figure 1.5 The control of PD-L1 expression in cancer cells

Schematic overview of the points of regulation governing PD-L1 expression in cancer. The regulatory pathways highlighted here mostly correspond to

experiments performed in cancer cells, but may also apply in non-malignant contexts. Question marks indicate that a functional link has been made with the regulation of PD-L1 expression but the mechanistic detail remains unclear.

1.8 AU-rich element mediated mRNA decay and tristetraprolin

1.8.1 AU-rich element-mediated decay

Post-transcriptional control of gene expression in mammals can generally be subdivided into the regulation of mRNA translation, and mRNA degradation. Common genetic elements controlling mRNA stability include miRNAs and adenosine and uridine (AU)-rich elements (AREs). AREs are AUUUA sequences in the 3'UTR of mRNAs that confer instability. AREs were first described in 1986, when strikingly conserved AU-rich sequences were found in the 3'UTR of TNF mRNA and other mRNAs encoding proteins relating to the regulation of immunity (Caput et al., 1986). Since, AREs have been implicated in many cellular functions and disease. Remarkably, when classified by sequence alone, up to 5-8 % of human genes contain AU-rich elements (Bakheet et al., 2006). Commonly, these are known to be functional mainly in transcripts coding for cytokines, chemokines, immediate early genes and proto-oncogenes that require rapid and dynamic control of gene expression. In functionally validated AREs, the core AUUUA-pentamer motif is usually found within AU-rich context. AREs are classified into class I, II and III based on the core motif and surrounding RNA sequence (Chen and Shyu, 1995). Class I AREs are found in AU-rich context but are non-overlapping, whereas class II AREs contain several overlapping nonamer sequences in AU-rich context (Barreau et al., 2005). Class III AREs are less common and non-canonical as they lack the AUUUA core pentamer sequence and instead contain only uridine-rich sequences (for example *c-jun* mRNA). Although the

functional differences between the ARE classes remains unclear, cytokine mRNAs tend to harbour class II AREs.

Ultimately, AREs recruit AU-rich element binding proteins (ARE-BPs), most of which are destabilising, but some act to stabilise the labile transcript (Table 1). There is evidence to suggest that stabilising AUBPs function by competing with destabilising ARE-BPs for ARE binding (Linker et al., 2005).

ARE-BP	Function
TTP	Destabilising
BRF-1	Destabilising
BRF-2	Destabilising
KSRP	Destabilising
HuR	Stabilising
HuD	Stabilising
AUF1	Destabilising/Stabilising

Table 1. AU-rich element binding proteins

Known ARE-BPs and their effect on ARE-containing mRNAs.

ARE-BPs, such as TTP, are not sufficient to degrade ARE-mRNA in isolation (Lai et al., 2003). Rather, ARE-BPs subsequently recruit the catalytic machinery to the target mRNA for deadenylation (shortening of the poly(A) tail), decapping and degradation. Specifically, ARE-mediated mRNA decay is initiated by mRNA deadenylation by the Ccr4-Caf1-Not complex, Pan2-Pan3 complex or poly A-specific ribonuclease (PARN) complex, which allows for the activity of the exosome 3'-to-5' RNA exonuclease complex. Alternatively, ARE-BPs such as TTP are involved in directing mRNAs to processing bodies (P-bodies), where partially deadenylated mRNAs associate with decapping machinery including Dcp1a, Dcp2 and Hedls, enabling the 5'-to-3' RNA exonuclease activity of Xrn1 (Franks and Lykke-Andersen, 2007).

1.8.2 Tristetraprolin biology

Tristetraprolin (TTP) or zinc-finger protein 36 (ZFP36), is a CCCH-type zinc-finger AU-rich element binding protein involved in destabilising target mRNAs. Perry Blackshear's laboratory first discovered TTP, and subsequently named the protein tristetraprolin due to its three distinctive PPPPG repeats (Lai et al., 1990). However, TTP has several additional names including Nup475, G0S24 and TIS11, due to the fact that several labs cloned the *Zfp36* sequence within a short space of time (Brooks and Blackshear, 2013). Currently, it is arguably the best studied of all ARE-binding proteins.

Using a TTP knock-out mouse, Blackshear and colleagues identified TNF-α as the first mRNA target of TTP (Taylor et al., 1996). TTP KO mice suffered from an autoimmune syndrome involving severe arthritis and weight loss. Strikingly, many aspects of the disease phenotype were almost completely reversed when KO mice were treated with a monoclonal antibody against TNF-α. Shortly after, it was shown that TTP downregulates TNF-α levels following co-induction of both TNF-α and TTP by LPS in macrophages, constituting a mechanism for rapid feedback inhibition (Carballo et al., 1998).

TTP is subject to complex regulation by phosphorylation at many sites. In fact, 49 phosphosites have been documented to date, out of a total of 319 amino acids in the mouse TTP protein (www.phoshphosite.org). Of these, only two phosphosites have been identified that are patently important for regulating the activity of TTP; S52 and S178 of mouse TTP (Figure 1.6). *In vitro* kinase assays initially verified phosphorylation of mouse TTP by MK2 (MAPKAPK2) at S25 and S178 (Chrestensen et al., 2004; Mahtani et al., 2001). Phosphorylation of these residues has been proposed to regulate TTP activity in several ways including: (1) increasing binding to 14-3-3 proteins, (2) changing the sub-cellular localisation of TTP, (3) decreasing target mRNA

binding by TTP, (4) preventing deadenylase recruitment, and (5) stabilising TTP protein.

S52 and S178 weakly conform to the MK2 phosphorylation consensus motif (Hyd-X-R-X-L/N-phS/T-I/V/F/L, where Hyd is a hydrophobic residue), and 14-3-3 binding consensus motif (R-S-X-phS-X-P) (Cargnello and Roux, 2012) (Figure 1.6). Phosphorylation of S52 and S178 has been shown to mediate exclusion from stress granules through a mechanism involving MK2-mediated phosphorylation inducing 14-3-3 binding to TTP (Stoecklin et al., 2004). It has been suggested that TTP binding to ARE-containing mRNAs may be partially inhibited by MK2 activity (Hitti et al., 2006), although the evidence for this remains contentious and there are reports suggesting that TTP's mRNA binding efficiency is not influenced by MK2 (Clement et al., 2011; Marchese et al., 2010).

There are multiple reports suggesting that the hyerphosphorylated form of TTP protein is more stable. Increased TTP protein stability is dependent on MK2-mediated phosphorylation and reduced proteasomal targeting of TTP (Brook et al., 2006; Deleault et al., 2008). Indeed, MK2 knock-out cells have very low basal levels of TTP protein compared to wild-type cells (Hitti et al., 2006). This mechanism may seem counterintuitive at first, but it has been proposed that the accumulation of a pool of inactive, stable, hyperphosphorylated TTP protein primes the cell for rapid TTP function and mRNA downregulation when termination of mRNA expression is required. Consistent with this concept, p38 signalling is co-activated by several stimuli that stimulate the expression of TTP target genes. For example, LPS can acutely induce TNF-α expression, TTP expression, and p38 signalling (Carballo et al., 1998). Hyperphosphorylated TTP is eventually activated by phosphatases resulting in feedback inhibition of TNF-α mRNA gene expression (Brooks and Blackshear, 2013). Recently, PP2A has been identified as the primary phosphatase responsible for activating TTP (Rahman et al., 2015; Sun et al., 2007). PP2A has been shown to physically

interact with TTP, and PP2A inhibition increases 14-3-3 binding to hyperphosphorylated TTP.

The first crystal structure of human TTP bound to CNOT1 provided novel insights into how TTP interacts with the effector complex CCR4-NOT in human cells (Fabian et al., 2013). TTP interacts with CNOT1, an essential component of CCR4-NOT RNA deadenylase complex, through a highly conserved C-terminal region, which the authors named the CNOT1 interaction motif (CIM) (Figure 1.6). Notably, the authors found that phosphorylation of serine residue 323 (within the human TTP CIM) dramatically reduced binding to CNOT1 *in vitro*. Interestingly, Lykke-Andersen's group showed that phosphorylation of TTP at MK2 target sites led to decreased deadenylation recruitment and activity using immunoprecipitation and *in vitro* deadenylation assays (Clement et al., 2011). Although the binding of the deadenylase complex seemed inversely proportional to 14-3-3 binding, the known binding sites for 14-3-3 and CNOT1 are not predicted to significantly overlap (Fabian et al., 2013). Notably, the authors show that TTP also interacts with the Pan2-Pan3 complex (Clement et al., 2011). To our knowledge, the interaction site for Pan2-Pan3 with TTP remains to be identified. In addition, it is possible that TTP binds to the deadenylase PARN, although there is conflicting data on this (Clement et al., 2011; Lai et al., 2003).

In mammals, TTP is a member of a family of four related proteins; the other members are ZFP36L1, ZFP36L2 (also known as butyrate-response factor 1 and 2; BRF-1 and BRF-2) and Zfp36l3, however the latter appears to be mouse or rodent-specific and is only expressed in placenta and yolk sac (Blackshear et al., 2005). TTP, ZFP36L1 and ZFP36L2 are more widely expressed and share target specificity for the AU-rich nonamer consensus motif (Brooks and Blackshear, 2013). One study showed that ZFP36L1 and ZFP36L2 proteins are negatively regulated by RSK downstream of ERK through phosphorylation of two conserved residues in the CIM. RSK was

shown to be capable of increasing phosphorylation of serine 334 of human ZFP36L1 in an *in vitro* kinase assay, decreasing binding to CNOT7. Tantalisingly, these residues are analogous to those proposed by Fabian et al. to be functionally important in regulating TTP itself (Adachi et al., 2014) (see also Figure 1.6). Furthermore, early *in vitro* kinase assays and mass spectrometry analysis by the Blackshear lab revealed TTP phosphorylation at several sites by ERK, although the functional relevance of these ERK target sites are yet to be verified (Cao et al., 2003). However, ERK and p38 have been shown to act synergistically to stabilise TNF-α mRNA and regulate TTP protein stability and localisation (Brook et al., 2006; Deleault et al., 2008).

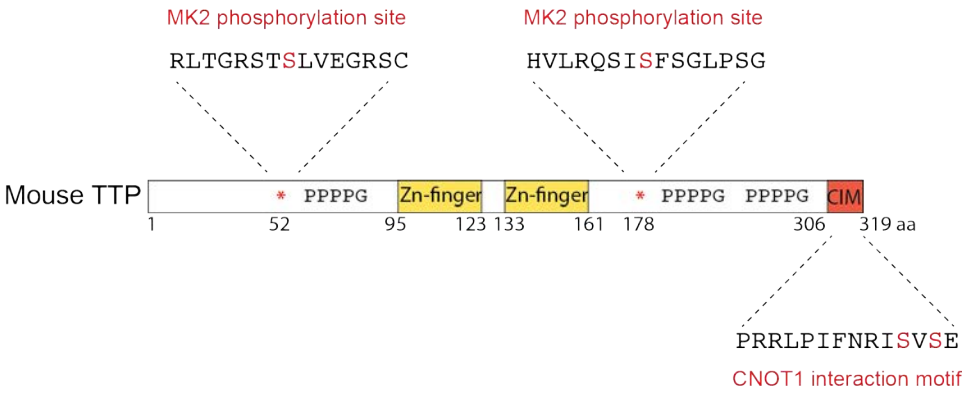

Figure 1.6 Shematic of mouse TTP protein

Functional annotation of mouse TTP protein. PPPPG repeats, zinc-finger domains and CNOT1 interaction motif (CIM) are highlighted. Asterisks correspond to serine residues (highlighted in red) that are known MK2 phosphorylation sites. The CIM also contains known phosphosites, highlighted in red. Numbering corresponds to the amino acid sequence of mouse TTP.

1.8.3 Decay-independent roles of tristetraprolin

TTP has been shown to have mRNA-decay-independent functions, including repression of mRNA translation (Schott et al., 2014). Conserved PPPPG motifs 1 and 2 within TTP mediate the interaction with GYF2 of the EHP2-GYF2 translational repression complex, thus preventing proper eIF4F

complex formation and cap-dependent translation initiation (Fu et al., 2016). This is the first report describing a function for the eponymous PPPPG repeats within TTP (Figure 1.6). Moreover, in some cases TTP appears to associate with polysomes and compete for AREs with the translation-promoting AUBP, HuR (Tiedje et al., 2012).

Furthermore, using an RNA interference screening approach in *Drosophila* cells, TTP was implicated in miRNA-mediated mRNA repression of ARE-containing mRNAs, through association with Ago/eiF2C family members (Jing et al., 2005). miR16 (which is complementary to the ARE) affected the stability of a TNF-α 3'UTR reporter, and this effect was apparently dependent on TTP.

1.8.4 Tristetraprolin in cancer

Although it is rarely mutated in cancer (COSMIC database), TTP expression is dramatically reduced in many cancers (Brennan et al., 2009), and there is mounting evidence that TTP can have multifaceted anti-tumour effects; therefore, *ZFP36* is a putative tumour suppressor gene (Stoecklin et al., 2003). Mechanistically, how TTP expression is reduced in cancer versus normal tissue remains unclear, however there are indications that in tumours with Myc dysregulation, *TTP* transcription may be directly repressed by Myc through binding to *TTP* initiator elements (Rounbehler et al., 2012). The Cleveland and Blackshear laboratories have shown that re-expression of TTP in a Myc-driven B-cell lymphoma model can significantly halt disease progression in mice, which the authors partly attribute to reductions in *cyclin D1* expression (a TTP target ARE-mRNA). However, it is likely that TTP regulates a plethora of ARE-mRNAs, therefore the reprogramming of the expression profile of cancers with low TTP expression or activity will be more complex. Indeed, rescue of cyclin D1 expression alone was not sufficient to re-establish the malignant phenotype once TTP was expressed (Rounbehler et al., 2012). In addition, TTP targets VEGF and COX-2 in colon carcinoma

cell lines and forced TTP transgene expression has therapeutic effects in xenograft mouse models of colon cancer (Cha et al., 2011; Essafi-Benkhadir et al., 2007; Lee et al., 2010). VEGF is well known to promote tumour angiogenesis, whereas tumour cell COX-2 expression has recently been shown to mediate evasion of anti-tumour immunity in melanoma (Zelenay et al., 2015). Intriguingly, VEGF mRNA stability is destabilised by MEK inhibition, and VEGF 3'UTR luciferase reporter assays respond to RAS activity (Essafi-Benkhadir et al., 2007). It seems enforced expression of TTP is able to partially counter-act RAS-ERK driven VEGF expression, but TTP activity is hindered by ERK signalling (Essafi-Benkhadir et al., 2007). The mechanistic detail of this link warrants further investigation.

1.9 Conclusions

Early genetic experiments in mice and syngeneic tumour transplant models have paved the way to the clinic for blockbuster drugs such as ipilimumab and nivolumab. The development of successful ICB therapies has led to substantial remodelling of classical drug discovery, with the sales of ICB expected to be in excess of $1.2 billion by the year 2020 in the US alone (Webster and Mentzer, 2014). Unlike targeted therapies, which have the advantage of traceable target mutations in tumours, the clinical emphasis now resides on identifying biomarkers of response to ICB. Investigating anti-cancer immunity and immune-escape in relevant preclinical models can potentially accelerate our understanding of the clinical determinants of cancer immunotherapy response. In the search for reliable biomarkers, tumour cell or tumour-associated immune cell PD-L1 expression is currently the front-runner. However, many unanswered questions still remain over the molecular regulation of PD-L1 expression in cancer, especially with regard to potential regulation by common oncogenic drivers.

AU-rich element mediated mRNA decay is an important process regulating gene expression in immune cell biology and thus anti-cancer immunity.

These *cis*-acting elements act by recruiting highly regulated ARE-BPs, which often act in a combinatorial and competitive fashion. The most intensively studied ARE-BP is TTP. Given its complex regulation, it has been postulated that TTP acts as a molecular sensor for the ARE RNA degradation machinery. The relative paucity of ARE mutations in human disease may reflect the relative ease of altering ARE-BP function through dyregulation of these pathways. However, how these regulatory pathways are altered in cancer is poorly characterised.

The majority of this thesis focuses on investigations into: (1) the immunogenicity of a RAS-driven mouse model of lung cancer, and the use of this model for the preclinical study of cancer immunology, (2) the regulation of PD-L1 expression in lung cancer by RAS and the ARE-BP TTP, and (3) the functional relevance of the regulation of PD-L1 expression by RAS and TTP *in vivo*.

2 Chapter 2. Materials and Methods

2.1 Cloning, plasmids and stable cell lines

peGFPC1-6XHis-FL-KSRP was a gift from Douglas Black (Addgene plasmid # 23001)(Hall et al., 2004) and the S193A mutant was generated by site-directed mutagenesis (QuikChange II; Agilent).

Full length human TTP was cloned from H358 genomic DNA into pCDNA3-MycX2 generating two N-terminal Myc tags. The S218/228A TTP double mutant was generated by site-directed mutagenesis (QuikChange II; Agilent).

For the luciferase reporter constructs, the full length human *PD-L1* 3'UTR was cloned from H358 genomic DNA into the TOPO-TA vector (Life Technologies). The six most 3' ATTTA pentamers (including the three most highly conserved) were mutated to ATGTA (QuikChange Multi-site; Agilent). Wild type and mutant fragments were subcloned into the Xba1, BamH1 site of pGL3-control (Promega) to generate the reporter constructs.

CT26 cells were transfected with linearised pUNO empty and pUNO-mouse *PD-L1*Δ3'UTR plasmids (InvivoGen) before selection with blasticidin, and for *PD-L1*Δ3'UTR cells, subsequent FACS sorting of PD-L1 high, blasticidin-resistant cells. For the lentiviral pTRIPZ constructs, full-length mouse TTP was cloned from KPB6 genomic DNA into pCDNA3-MycX2 generating two N-terminal Myc tags. MycX2-TTP was subsequently subcloned into the Age1-Mlu1 site of pTRIPZ-empty (GE Healthcare), resulting in the final TTP (tet-ON) construct, without the TurboRFP or shRNAmir-related elements of the parental pTRIPZ plasmid. Lentiviral particles were generated from HEK 293FT cells (see Preparation of lentiviral particles, below) and infected target cells were subsequently selected with puromycin to establish stable cell lines.

For the construction of plenti-Cre *shMsh2*, the Puro-Cre.empty vector from the Tyler Jacks laboratory (Addgene plasmid #17408) was linearised with Xba1 and Not1, thus removing the puromycin resistance cassette. The U6 promoter and downstream shRNA sequence was PCR amplified from shScr or shMsh2.2 p.LKO-1 vectors and the relevant PCR products were inserted into the lentiviral Cre plasmid backbone.

2.2 Transfections

2.2.1 siRNA

For RNA interference, cells were reverse-transfected with a final concentration of 50 nM siGENOME siRNA pools of four siRNAs or the ON-TARGETplus Non-targeting pool ("SiScrambled" control) and DharmaFECT 1 transfection reagent (Dharmacon; GE Healthcare) in 96 well plates. Briefly, 1.25 μl of siRNA was mixed with 3.75 μl HBSS (Gibco) and in a separate tube, 0.15 μl of DharmaFECT 1 was mixed with 14.85 μl HBSS per reaction. After a 5 min incubation, these solutions were mixed together and incubated for a further 15 min. 80 μl of cell suspension in antibiotic-free medium was plated onto 20 μl of siRNA-lipid complex per well of a 96 well plate.

2.2.2 Transfections with expression vectors

For transfection with TTP or KSRP constructs, cells were seeded in a 12 well plate in antibiotic-free medium, and the following day, transfected using Lipofectamine 2000 according to manufacturer's instructions (Life Technologies). Media was changed 7 h post-transfection.

2.3 Luciferase assays

H358 cells or ER-HRAS^{G12V} MCF10A cells were plated in 96 well plates and the following day co-transfected with pRL-TK control and pGL3-*3'UTR PD-L1* luciferase constructs using Lipofectamine 2000 (Life Technologies). 0.25 μl of Lipofectamine 2000, 15 ng of pRL-TK luciferase control and 85 ng of pGL3 luciferase reporter (wild-type or mutant *PD-L1* 3'UTR) were used per well. For H358 cells, 24 h after transfection, PMA (200 nM; Sigma) was added, and 6 h later the Dual-Luciferase Reporter Assay (Promega) was performed. For ER-HRAS^{G12V} MCF10A cells, 24 h after transfection cells were serum-starved overnight, and then treated with 4-OHT (100 nM) for 24 h before the Dual-Luciferase Reporter Assay (Promega) was performed according to manufacturer's instructions.

2.4 Preparation of lentiviral particles

Lentiviral particles for use *in vitro* were produced by co-transfection of HEK 293FT cells with the lentiviral construct, psPAX2 and pMD2.G plasmids. 48 h and 72 h after transfection, viral supernatant was harvested and filtered through a 0.45 μm filter. Filtered viral supernatants were diluted in fresh medium, supplemented with 8 μg/ml polybrene (Millipore) and used to infect target cells.

For generation of high titre lentiviral preparations for *in vivo* application, transfections of 293FT cells were scaled-up for 15 cm dishes and the resulting viral supernatant was concentrated by spinning for 2 h in an ultracentrifuge at 70,000 g. Supernatant was gently removed and the remaining liquid volume further reduced by evaporation at room temperature, before the viral pellets were resuspended in PBS or HBSS and incubated overnight at 4 °C.

pLKO.1 shRNAs were sourced from Dharmacon. Sequences and reference number of shRNAs used in this thesis are listed in Table 2.

Table 2. shRNA sequences

RNAi Reagent	Target Gene	Clone Number	Reference Number	Sequence
shRNA	*TTP* mouse	1	TRCN0000102300	AAGTCGTCATAAATAAAGGGC
		2	TRCN0000102302	AAGCTGATGCTTTGTCGCAGC
		3	TRCN0000102304	TGGCGTAGTCATCAGGATCGG
		4	TRCN0000102303	TTAGGGTCTCTTCGAGTCACA
		5	TRCN0000102301	TTTATGTTCCAAAGTCCTCCG
shRNA	*PD-L1* mouse	1	TRCN0000068002	TTTGGAGCCGTGATAGTAAAC
		2	TRCN0000067998	TTGAGCTTGTATCTTCAACGC
		3	TRCN0000068000	TAGTTCATGCTCAGAAGTGGC
		4	TRCN0000068001	TCGAATTGTGTATCATTTCGG
		5	TRCN0000067999	TTATGCAGCAGTAAACGCCTG
shRNA	*Msh2* mouse	1	TRCN0000042493	AAACTGAGAAAGATTGCCGGG
		2	TRCN0000042494	TTTATCCGTGAAATGATCTCG
		3	TRCN0000042495	AAAGGCACCAATCTTCGTTGC
		4	TRCN0000042496	AACAATGGCGTCTAAGTGAGC
		5	TRCN0000042497	TTAATACCCTGATACAGTCGG

2.5 Flow cytometry

2.5.1 In vivo

Lung tissue was harvested in ice-cold PBS before mincing and then enzymatic digestion in Liberase TM and Liberase TH (both 75 μg/ml final; Roche) with DNaseI (25 μg/ml final; Sigma) in HBSS (Gibco) for 45 min at 37 ºC. After washing in DMEM + 10 % FCS, cells were filtered through 70 μm filters (BD Bioscience) and then washed in FACS buffer (PBS supplemented with 2 mM EDTA and 0.5 % BSA v/v final). Samples were then treated with Red Blood Cell Lysis Buffer (Qiagen), washed in FACS buffer, filtered again and resuspended with FcR blocking reagent (BD Bioscience) before antibody staining in FACS buffer. Samples were washed twice in FACS buffer and

resuspended in DAPI (1 μg/ml final; eBioscience) immediately before analysis.

For immune profiling of mouse lung tissues, the relevant fluorescent minus one (FMO) and single-staining controls were included. The following antibodies were used in these experiments: CD45 (30-F1; eBioscience), CD11b (M1/70; eBioscience), Ly6G (1A8; BD Biosciences), F4/80 (CD: A3-I; BioLegend), CD3 (145-2C11; BD Biosciences), CD19 (1D3; eBioscience), CD11c (HL3; BD Biosciences), CD49b (DX5; eBioscience), CD4 (GK1.5; eBioscience), CD8a (53-6.7; eBioscience).

2.5.2 In vitro

For FACS analysis of cells lines, cells were harvested with trypsin or versene, washed in media and filtered before antibody staining in FACS buffer. Annexin V staining was performed using Annexin V binding buffer (Invitrogen) and following the manufacture's instructions (Invitrogen). After staining, samples were washed twice in FACS buffer and resuspended in DAPI (1 μg/ml final; eBioscience) immediately before analysis on LSRII or LSRFortessa (BD Biosciences) cell analysers.

For detection of intracellular ROS, adherent cells were washed once in PBS before staining in 5 μM H_2DCFDA (Invitrogen) for 20 min at 37 °C. Cells were then harvested and stained for PD-L1 as described before FACS analysis.

Cell cycle analysis was performed as follows: cells were pulsed with BrdU (10 μM, 45 min), harvested with trypsin or versene, washed in PBS, fixed in ice-cold 70 % ethanol. After washing in PBS, cells were resuspended in 2 M HCl at room temperature, incubated for 30 min with mixing, washed in PBS-T before staining with anti-BrdU antibody. Cells were then treated with RNase before staining with PI and FACS analysis.

2.6 Cell sorting and *ex vivo* IFN-γ ELISA

Spleen, lung and lung tumour tissue was harvested and digested as above. For lung and tumour tissue, negative cell sorting by FACS was based on CD31, CD45 and DAPI negativity. For CD8 T cell negative sorting, selection was based on Cd11b, Ly6G, CD11c, F4/80, CD4, CD18, CD49b and DAPI negativity. 5 000 target cells were plated with 10 000 or 100 000 purified, CD8 T cells and incubated in a total of 200 μl of medium. After a 12 h incubation period, an IFN-γ ELISA was performed using 100 μl of conditioned media, according to the manufacturer's instructions (eBioscience). Duplicate technical repeats were performed for each experimental condition.

As a control, EL4 lymphoma cells or EG.7-OVA cells were used as targets and CD8 T effector cells were harvested from naïve mice or mice vaccinated against OVA. Briefly, mice received PBS control or 100 μg OVA protein and 50 μg poly(I:C) (InvivoGen) in PBS by i.v administration, 6-7 days before sacrifice.

2.7 EL4 TCR stimulation

EL4 cells were plated in 24 well plates and the following day, stimulated with the addition of CD3/CD28 Dynabeads (Invitrogen) at a 1:1 cell to bead ratio. Cells were concomitantly treated with DMSO vehicle control or MEK inhibitor (25 nM trametinib GSK1120212). After 24 h, beads were removed with a magnet and by washing and cells were stained with antibodies against PD-L1 and CD69 and prepared for flow cytometry as described.

2.8 Quantitative real-time PCR (qPCR)

RNA was extracted using RNeasy Mini Kit (QIAGEN). Generally, 1 μg of RNA was used to generate cDNA using SuperScript VILO or SuperScript II

Reverse Transcriptase (Life Technologies). qPCR reactions were carried out using QuantiTect Primer Assays (QIAGEN) and SYBR Green reagents (Life Technologies). Gene expression changes relative to the stated housekeeping gene were calculated using the ΔΔCT method.

2.9 RNA-immunoprecipitation

RNA-immunoprecipitation (RNA-IP) reactions were carried out using Magna-RIP RNA-IP Kit (Millipore) with IgG control, anti-TTP or anti-KSRP antibodies according to the manufacturer's instructions, except for the exclusion of EDTA from lysis and wash buffers, as TTP is a zinc-finger protein. Total RNA was isolated and qPCR was carried out using methods specified in the above section, except using the % input method to calculate RNA enrichment.

2.10 Immunoprecipitation

For each immunoprecipitation reaction, 25 μl slurry of Dynabeads (Life Technologies) was coupled to 3 μg of anti-Myc antibody (9E10; in-house). In some experiments, beads were cross-linked using DSS following manufacturer's instructions (ThermoFisher). Beads were washed in Lysis Buffer (20 mM Tris-HCl, pH 7.4, 137.5 mM NaCl, 10 % glycerol, 1 % Triton X-100) and incubated overnight with rotation at 4 ºC with cleared cell lysates prepared in Lysis Buffer supplemented with protease and phosphatase inhibitor cocktails (Calbiochem). Beads were washed three times with IP Wash Buffer (modified Lysis Buffer: 0.1 % Triton X-100, final), before elution with LDS Sample Buffer (Life Technologies).

2.11 *In vivo* studies

All studies were performed under a UK Home Office approved project license and in accordance with institutional welfare guidelines.

2.11.1 *KP* mice

Kras$^{LSL\text{-}G12D/+}$; *Trp53*$^{F/F}$ mice were sourced from the Mouse Models of Human Cancer Consortium and were backcrossed to C57Bl/6 for 6 generations. Lung tumours were initiated as described (DuPage et al., 2009a) using intratracheal intubation of 1x10^6 pfu adenovirus expressing Cre-recombinase (Gene Transfer Vector Core). Lung tumour or normal lung tissue was analysed 12 weeks after infection. *Kras*$^{LSL\text{-}G12D/+}$; *Trp53*$^{F/F}$; *Rag2*$^{+/-}$ mice were generated by crossing *Kras*$^{LSL\text{-}G12D/+}$; *Trp53*$^{F/F}$ mice of mixed strain background with C57B/6 *Rag2*$^{+/-}$ JAX mice (The Jackson Laboratory).

For the anti-PD-L1 therapy study, tumours were initiated as described (DuPage et al., 2009a) using 1x10^6 pfu adenovirus expressing Cre-recombinase (Gene Transfer Vector Core). 12 weeks after infection, animals were randomly assigned treatment groups and were then micro-CT scanned to analyse tumour burden using SkyScan 1176 as described (Castellano et al., 2013). Animals were treated with 10 mg/kg, endotoxin-free, anti-PD-L1 10F.9G2 or isotype control LTF-2 antibody (BioXCell) twice weekly, for two weeks by intraperitoneal injection, resulting in a total of four doses per animal.

For anti-PD-L1 and anti-CTLA-4 combination therapy, we treated *KP* mice with anti-PD-L1 antibody (10F.9G2, 10 mg/kg) and anti-CTLA-4 antibody (9H10, 5 mg/kg) in combination, by concomitant i.p administration. Alternatively, mice received the combination of isotype control antibodies

(LTF-2 and Syrian hamster IgG, respectively). Mice received a total of three doses of combination therapy over a two-week treatment course, with injections on day 0, 4 and 8.

For trametinib MEK inhibitor treatments, mice received 3 mg/kg GSK1120212 by oral gavage daily, for two-weeks periods as indicated (Castellano et al., 2013).

2.11.2 Tumour transplant models

For CT26 tumour studies, 8-10 week old BALB/c or *nu/nu* mice received $1x10^5$ CT26-derivative cells in PBS by subcutaneous injection into the left flank and were then immediately randomly assigned into treatment cohorts. Mice were treated with water or doxycycline by oral gavage (50 mg/kg) on day three after cell injection and then daily, with a two-day break every five days of treatment. Tumours were measured using callipers and volume was estimated using the formula: $width^2$ x length x 0.5, where length is the longest dimension and width is the corresponding perpendicular dimension.

2.11.3 CD4 and CD8 T cell depletion

CD4 GK1 and CD8 2.43 IgG2b rat monoclonal antibodies were diluted in sterile PBS and were injected i.p at a dose of 300 μg to deplete CD4 and CD8 T cells. A rat IgG2b antibody against an irrelevant antigen (large-T antigen) was used as a control. Three days later, CD4 and CD8 T cell populations were quantified by FACS. CD4 antibody clone RM4-5 and CD8 antibody clone 53.6-7 were used as detection antibodies (eBioscience).

2.11.4 *In vivo* imaging: micro computerised tomography (*μ*CT)

Mice were anesthetised by inhalation of isoflurane (Abbott Labs) and CT scanned using SkyScan 1176 (Bruker). Breathing rate and body temperature were measured throughout the scan using in-built physiological monitoring devices. Scanning parameters were as follows: aluminium filter 0.5 mm, 0.7 degrees rotation step over 180 degrees, 60 ms exposure, source current 500 mA, source voltage 50 kV, image isotropic pixel size 35 *μ*m. Lung images were grouped into bins based on the respiratory cycle with RespGate software and images reconstructed using N-Recon. Estimations of lung tumour volumes were generated by highlighting 3D regions of interest in CTAnalyser.

2.12 CRISPR/Cas

The CRISPR/Cas genome editing was performed on CT26 cells using a U6gRNA-Cas9-2A-GFP construct targeting mouse *Zfp36* with gRNA sequence GTCATGGCTCATCGACTGGAGG (Sigma, MM0000323992). Following plasmid transfection, single GFP-positive cells were selected by FACS for expansion in culture. Transfection with Cas9-2A-GFP only, served as a negative control. KO of functional TTP was confirmed by Western blotting and complete *Zfp36* allele disruption was confirmed by TOPO-TA cloning followed by sequencing.

2.13 Histopathology

2.13.1 Immunohistochemistry

Tissue was prepared for histology by incubation in 10 % NBF for 24 h followed by 70 % ethanol for a further 24 h before embedding in paraffin. For CD3 staining, sections were boiled in sodium citrate buffer (pH6) for 15 min and incubated for 1 h in anti-CD3 antibody (ab134096; Abcam), followed by biotinylated secondary antibody and HRP/DAB detection. Tumours from *nu/nu* mice served as a negative control for CD3 staining. Haematoxylin and eosin staining was performed using standard methods.

2.13.2 RNAscope

In situ hybridisation was performed using RNAscope probes and buffers according to manufacturer's instructions (Advanced Cell Diagnostics). Tissues were fixed, embedded in paraffin and sectioned as above. Sections older than 2-3 weeks were not used for mRNA detection due to the potential loss of signal. A positive control probe for *PPIB* and negative control probe that is bacteria-specific were included in all experiments. Probes used for the detection of human and mouse *PD-L1* mRNA are as follows: Probe-Hs-CD274 600861, Probe-Mm-Cd274 420501.

2.14 Bioinformatics

Using two published RAS activation gene expression signatures (Loboda et al., 2010; Sweet-Cordero et al., 2005), we identified high and low RAS activity LUAD TCGA RNASeq samples. We determined high and low RAS activity using GSEA (GeneSetTest, Bioconductor) against genes ranked by

their log2 normalized counts scaled across all tumour samples. Only the upregulated genes from the signatures were used in the GSEA. Samples with a significant GSEA association (FDR < 0.05) of a RAS signature to the upper portion of the rank were assigned as having high RAS activity. Those with a significant association to the lower portion of the rank were assigned as having low RAS activity. Once assigned, we identified RAS-dependent gene expression changes between the high and low RAS activity groups by standard RNASeq analysis methods (DESeq2, FDR < 0.05). A short-list of “T cell Function” related genes was generated from gene ontology annotation based on the nanoString Technologies nCounter Human PanCancer Immune Profiling Panel.

2.15 Mass Spectrometry

Gel bands were excised and subjected to digestion as described (Plaza-Menacho et al., 2014). Tryptic peptides were analysed by LC-MS using Ultimate 3000 uHPLC system connected to a Q-Exactive mass spectrometer (Thermo Fisher Scientific) and acquired in data-dependent mode (DDA) for identification and in targeted SIM/PRM mode for quantification. A SIM isolation list was setup for the following peptides: STSLVEGR (m/z 424.7272, 2+, non phos), STSLVEGR (m/z 464.7104, 2+, phos S52), QSISFSGLPSGR (m/z 618.3276, 2+, non phos) and QSISFSGLPSGR (m/z 658.3057, 2+, phos S178). For SIM/PRM scans, MS1 peaks were acquired at resolution of 70,000 (at m/z 200) and scan time (1x256 ms); MS2 fragment ion resolution was 17,500 (at m/z 200) scan time (64x4 ms); and SIM/PRM cycle time was (1280 ms). For identification and generation of spectral libraries, the resulting DDA data was searched against a mouse Uniprot database containing common contaminants (UniProt_KB2012_08_taxonomy_mouse_10090_canonical_with_contaminants.fasta) as well as a custom database containing the Myc-tagged mouse Zfp36 sequence using the Andromeda search engine and MaxQuant (version 1.3.0.5). For MaxQuant, a false discovery rate of 0.1 % was used to generate

protein, peptide and site identification tables. The DDA data were uploaded into Perseus (MaxQuant) for statistical analyses of phosphosite identifications. The targeted mass spectrometry raw data was uploaded into Skyline (version 3.5.0.9319) for identification, quantification and further statistical analyses.

2.16 Cell culture

Cells were grown in a humidified, 37 °C incubator with a controlled atmosphere of 5 % CO_2 and 95 % air. Specific culture conditions and origin of all the cell lines used in this study are listed in Table 3.

Table 3. Cell lines and growth conditions

Cell line	Source	Normal medium	Starvation medium
H358	ATCC	RPMI + 10 % FCS	N/A
A427	CRUK Cell Services	RPMI + 10 % FCS	N/A
H1792	ATCC	RPMI + 10 % FCS	N/A
KPB6	Sergio Quezada Laboratory	DMEM + 10 % FCS	N/A
Type II pneumocytes	Olivier Pardo, Michael Seckl (Imperial College, London) and (Molina-Arcas et al., 2013b)	DCCM-1 + 10 % FCS	+ 0.5 % FCS for qPCR and FACS + 0 % FCS for mRNA half-life analysis
NL-20	Silvia Carvalho, Yosef Yarden (Weizmann Institute, Rehovot) and (Molina-Arcas et al., 2013b)	F12 + 4%FCS and 5 µg/mL insulin, 10 ng/mL EGF, 500 ng/mL hydrocortisone, 1 µg/mL transferrin, 0.1x non-essential amino acids, 2.7g/L glucose	+ 0.4 % FCS
368T1	Tyler Jacks Laboratory	DMEM + 10 % FCS	N/A
H23	CRUK Cell Services	RPMI + 10 % FCS	N/A
293FT	CRUK Cell Services	DMEM + 10 % FCS	N/A
TTP KO and TTP WT MEFs	Perry Blackshear Laboratory	DMEM + 10 % FCS	+ 0.5 % FCS
MCF10A	(Molina-Arcas et al., 2013b)	F12:DMEM mix (1:1) and 5 % horse serum, 20 ng/ml EGF, 10 μg/ml insulin, 100 ng/ml cholera toxin, 0.5 μg/ml hydrocortisone	+ 5 % horse serum
CT26	CRUK Cell Services	RPMI + 10 % FCS	N/A

N/A, not applicable.

2.17 Western blotting

Protein lysates for Western blotting were prepared by cell harvest in lysis Buffer (20 mM Tris-HCl, pH 7.4, 137.5 mM NaCl, 10 % glycerol, 1 % Triton X-100) supplemented with phosphatase and protease inhibitor cocktails (Calbiochem). Lysates were left on ice for 20 min before clearing at 12 000 rpm on a bench-top centrifuge at 4 °C. Protein concentrations in supernatants were estimated using a Bradford assay (Bio-Rad). Samples were boiled in SDS loading buffer for 5 min before loading onto SDS-polyacrylamide gels. Generally, 25-30 μg of protein was loaded per lane. Primary antibodies used are listed in Table 4. Secondary antibodies were conjugated to horseradish peroxidase (GE Healthcare).

Table 4. Antibodies

Antibody epitope	Application	Concentration	Company	Catalogue number
p-ERK	WB	1:1000	CST	9101
p-AKT (S473)	WB	1:1000	CST	9271
PD-L1 (anti-human)	Flow cytometry	Manufacturer's instructions	eBioscience	12 5983 42
Isotype control	Flow cytometry	Manufacturer's instructions	eBioscience	9012-4714-025
PD-L1 (anti-mouse)	Flow cytometry	Manufacturer's instructions	eBioscience	14-5982-82
Isotype control	Flow cytometry	Manufacturer's instructions	eBioscience	12-4321-41
CD45	Flow cytometry	1:300	eBioscience	11-0451-82
CD31	Flow cytometry	1:100	eBioscience	11-0311-81
TTP	RNA-IP	See Experimental Procedures	Santa Cruz	sc-8458
TTP endogenous	WB	1:1000	Miilipore	ABE285
KSRP	RNA-IP	See Experimental Procedures	Cambridge Bioscience	A302-021A
KSRP	WB	1:1000	CST	5398S
Myc (9E10)	IP/WB/IHC	3 μg/IP, 1:2000 WB	CRUK Cell Services	N/A
ERK	WB	1:1000	CST	9107
p-CREB (S133)	WB	1:1000	CST	9196
AKT	WB	1:1000	CST	2920
p-PXSP	WB	1:1000	CST	2325
p-RXXS/T	WB	1:1000	CST	9611
p-p38 (T180/Y182)	WB	1:1000	CST	9211
CD3	IHC	1:500	Abcam	ab134096
Calreticulin	Flow cytometry	1:100	Abcam	ab2907

CST, Cell Signalling Technologies.

2.18 Statistics

Unless stated otherwise, data were compared using unpaired, two-tailed Student's *t*-tests.

3 Chapter 3. Results 1. Tumour immunogenicity in genetically engineered mouse models of cancer

3.1 Introduction

Since only a subset of cancer patients currently responds to immunotherapies in the clinic, preclinical testing of immunotherapies is required to accelerate the discovery of biomarkers for response, and systematically test rational combination treatment strategies. To date, much of the preclinical work on cancer immunotherapy has relied on syngeneic, subcutaneous transplants of highly mutated and immunogenic cancer cells. More complex GEMMs of cancer have since been developed to model cancer at the orthotopic site with a physiological tumour microenvironment. GEMMs also have the capacity to reflect a more heterogeneous, clonal disease. However, it remains unclear whether these increasingly used GEMMs are suitable for the study of immune checkpoint blockade.

Here, we investigate the immunogenicity of *Kras G12D LSL/+; Trp53 F/F* (*KP*) mouse lung tumours. We provide evidence that (1) immunogenic cell death inducing agents fail to elicit a sustained immune response against these tumours, (2) *KP* tumours are resistant to anti-PD-L1 and anti-CTLA-4 immunotherapy, and (3) *KP* tumour progression is not significantly impeded by the adaptive immune system.

In this chapter, I present images generated from histopathological analyses performed by Bradley Spencer-Dene and Emma Nye on my behalf.

3.2 Results

3.2.1 Steady-state and therapy-induced immune contexture of *Kras G12D LSL/+; Trp53 F/F* mouse tumours

We set out to analyse the potential anti-tumour effects mediated by eliciting immunogenic cell death (ICD) in a GEMM of lung cancer. Specifically, we employed a widely-used mouse model of NSCLC where oncogenic *Kras* expression and concomitant loss of *Trp53* in the lung epithelium can be achieved by intratracheal delivery of adenovirus expressing Cre recombinase (DuPage et al., 2009a). Please note that *Kras G12D LSL/+; Trp53 F/F* mice will be referred to as *KP* mice throughout.

Firstly, we selected a small panel of inhibitors based on their ability to (1) promote lung cancer cell death, and/or (2) elicit characteristics of immunogenic cell death. Firstly, we tested their efficacy *in vitro*.

We selected carboplatin, which has not been shown to induce ICD but is used as standard of care for lung cancer in the clinic. We also chose the microtubule poison paclitaxel, as this chemotherapy or similar agents can be used as first-line treatment for lung cancer patients and has also been shown to induce aneuploidy, ER-stress and traits of ICD (Senovilla et al., 2012). Similarly, we used the anthracycline chemotherapeutic doxorubicin, as this is known to induce ICD (Galluzzi et al., 2015), but is not commonly used for the treatment of NSCLC in the clinic. In addition, we used tunicamycin, which specifically causes ER-stress by inducing the unfolded protein response as a consequence of the inhibition of protein glycosylation. We chose selumetinib (AZD6244), a potent and specific MEK inhibitor that is in clinical testing (now phase III) in NSCLC (Janne et al., 2013) with little known about its impact on traits of ICD. Finally, we selected bortezomib; a clinically approved

proteasome inhibitor used in patients with multiple myeloma, but there are indications that it also has activity in lung cancer (Kumar et al., 2012; Xue et al., 2011), and may stimulate signs of ICD through ER-stress caused by unfolded protein accumulation.

Using this panel of inhibitors, we first calculated inhibitor doses that killed 368T1 *Kras*-mutant mouse lung cancer cells (derived from *KP* mice) to a similar degree. We could therefore control for differences in cell death as much as possible when making comparisons between inhibitor effects on the mode of cell death. To this end, we used crystal violet and Cell Titre Blue assays to analyse cell proliferation and cell survival over a range of drug concentrations. Once a single dose of the inhibitor was selected that killed approximately 70 % of cells after 72 h, we verified this using an independent technique; annexin V and DAPI staining measured by flow cytometry (Figure 3.1A). This analysis is quantified in Figure 3.1B. All drugs started to induce cell death by 24 h to a modest degree, which was substantially higher and comparable at 72 h, with the possible exception of taxol, which caused lower levels of cell death consistent with a predominantly cytostatic effect on this cell line.

Next, we examined the ability of these agents to induce characteristics of immunogenic cell death *in vitro*. One key trait of immunogenic cell death is the exposure of calreticulin (CRT) at the cell membrane (Obeid et al., 2007). We tested the ability of our drug panel to induce CRT exposure by flow cytometry (Figure 3.1C). At 24 h after drug addition we observed significant increases in ecto-CRT following treatment with paclitaxel (taxol), bortezomib and selumetinib (AZD6244), however paclitaxel showed the most striking increase. Surprisingly, doxorubicin did not significantly increase ecto-CRT exposure in our hands, perhaps reflecting differences in sensitivity between cell lines used here and in studies by Kroemer and colleagues.

We tested the specificity and sensitivity of our flow cytometry assay by genetic silencing of CRT expression in 368T1 cells by stably introducing an shRNA against *CRT* as a control (Figure 3.1D). Indeed, we could detect lower levels of ecto-CRT exposure in sh*CRT* cells relative to parental 368T1 cells, verifying the specificity of the primary and secondary antibody detection.

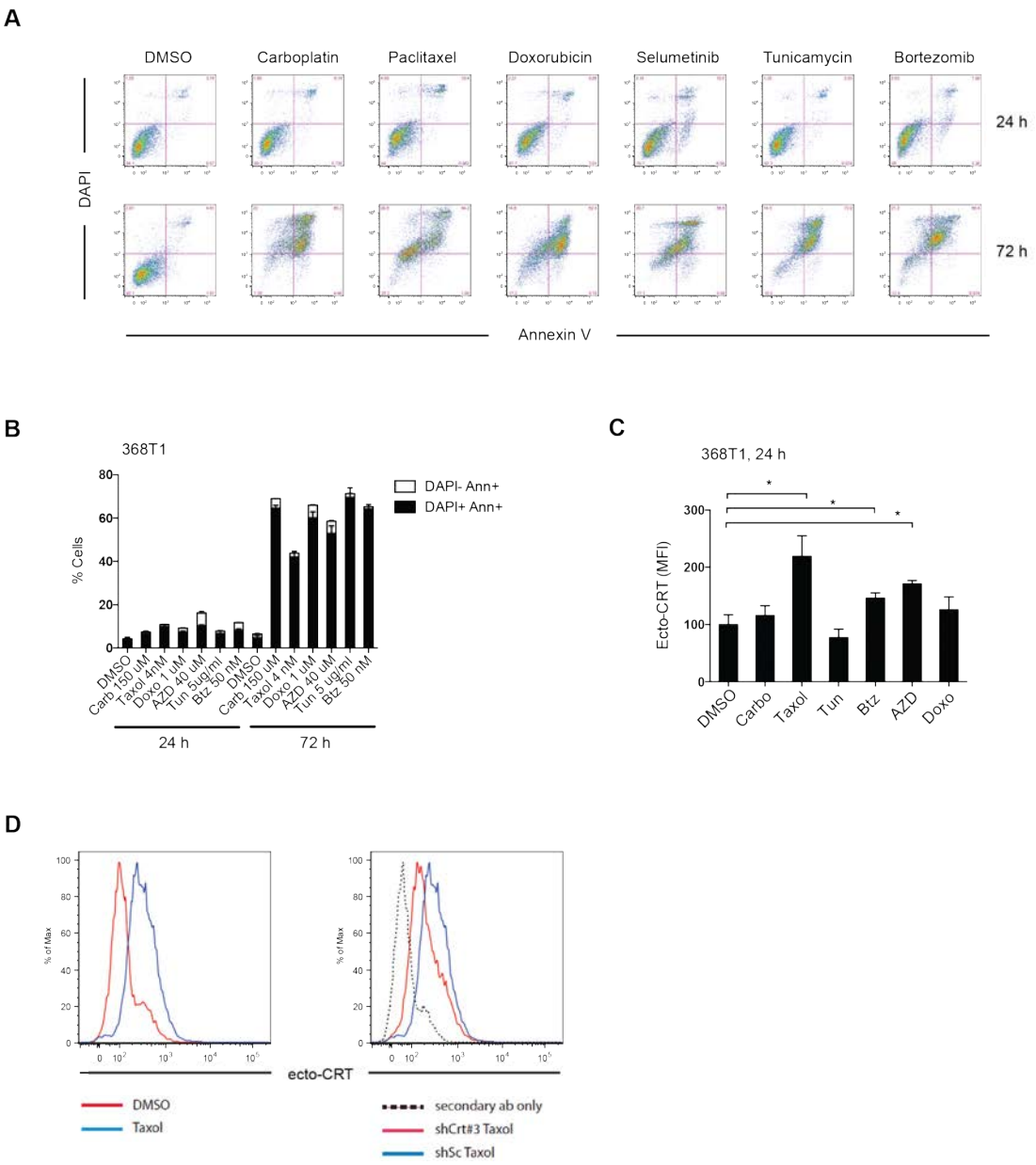

Figure 3.1 Drug selection for the efficient induction of immunogenic cancer cell death

(**A** and **B**) Flow cytometry analysis of cell death as measured by annexin V and DAPI staining in 368T1 lung cancer cells, induced by the indicated cytotoxic agents at 24 h and 72 h, and quantified in (B). Data are mean ± SEM of biological duplicates.
(**C**) Ecto-calreticulin (CRT) as measured by flow cytometry 24 h after the addition of the indicated cytotoxic agents. Data are mean ± SD of biological triplicates. *$P < 0.05$; Unpaired, two-tailed Student's *t*-test; n.s, not significant.
(**D**) Representative histograms from flow cytometry analysis of 368T1 cells treated with taxol or vehicle for 24 h. shRNA-mediated knock-down of CRT was used as a control to verify the specificity of the CRT antibody.
Tun, tunicamycin. Doxo, doxorubicin. Btz, bortezomib. Taxol, paclitaxel. Carbo, carboplatin. AZD, AZD6244, selumetinib. Drug doses used are indicated in (B).

We asked whether taxol might be inducing CRT exposure by inducing aneuploidy, as this has been reported previously (Senovilla et al., 2012). Cell cycle analysis by flow cytometry revealed approximately 17 % of 368T1 cells were tetraploid after 24 h of treatment with taxol (Figure 3.2). The JNK inhibitor SP600125, known to promote aneuploidy by disrupting microtubule dynamics (MacCorkle and Tan, 2004), served as a positive control. Collectively, these results suggest that taxol strongly induces aneuploidy and ecto-CRT in 368T1 lung cancer cells. Whether CRT exposure is completely dependent on aneuploidy in this case still remains unclear. Although hyperploidy has been associated with ER-stress and CRT exposure (Senovilla et al., 2012), we did not observe a clear double population of CRT high and low cells in our flow cytometry analysis of ecto-CRT in taxol-treated cells, as may have been expected given the majority of cells remain diploid at 24 h.

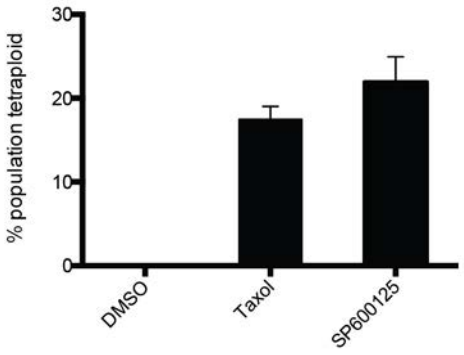

Figure 3.2 Paclitaxel induces tetraploidy in lung cancer cells

Quantification of tetraploid populations in 368T1 lung cancer cells 24 h after treatment with vehicle, paclitaxel (taxol; 4 nM), or the JNK inhibitor SP600125 (45 μM). Cells were pulse labelled with BrdU and then propidium iodide before standard cell cycle analysis by flow cytometry. Data represent the mean ± SD of biological triplicates.

Based on our results, we proceeded to test the efficacy of taxol and carboplatin, or bortezomib and carboplatin *in vivo* in tumour-bearing *KP* mice. We selected taxol and bortezomib due to their ability to induce CRT exposure, and combined them with carboplatin to increase the likelihood of apoptosis induction *in vivo*. Furthermore, the taxol and carboplatin combination reflects a standard of care regimen often used in the clinic for patients with NSCLC, increasing the clinical relevance of our approach. Firstly, to test efficacy *in vivo*, we measured tumour cell apoptosis by TUNEL-staining at the short time-point of 24 h after treatment (Figure 3.3A). A representative image is shown in Figure 3.3B. All drug treatments resulted in a significant induction in tumour cell apoptosis when compared with vehicle control treated animals. However, the absolute numbers of TUNEL-positive cells in each case remained low (Figure 3.3B). We speculate that this may be partly explained by the rapid clearance of apoptotic cells *in vivo*.

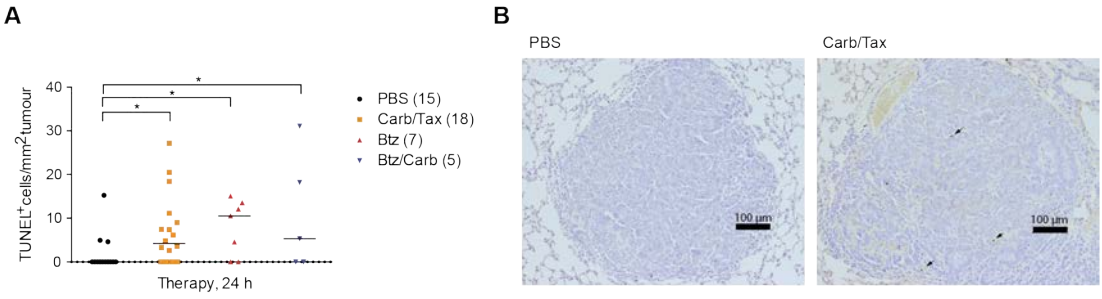

Figure 3.3 Induction of tumour cell apoptosis by chemotherapies and targeted therapies *in vivo*

(**A**) Quantification of TUNEL positive cells in *KP* mouse lung tumours 24 h after treatment with PBS vehicle control, or carboplatin (50 mg/kg i.p) and paclitaxel (10 mg/kg i.p) (Carb/Tax), bortezomib (Btz; 0.5 mg/kg i.p) or

bortezomib and carboplatin (Btz/Carb). n = 3-6 mice per group with 1-8 tumours per mouse quantified. The total number of tumours quantified for each condition is indicated in parenthesis. *$P < 0.05$; Mann-Whitney test. (**B**) Representative histological images of TUNEL staining in *KP* mouse lung tumours treated with PBS vehicle control or Carb/Tax as described in (A).

Given the evident apoptosis and associated CRT exposure *in vitro*, we tested whether our treatment strategies may stimulate anti-tumour immune responses. We analysed the immune contexture of tumour-bearing lungs from *KP* mice 24 h after treatment with vehicle, carboplatin and taxol, bortezomib alone, or bortezomib and carboplatin. In theory, tumour cell apoptosis will be followed by apoptotic debris being cleared and presented by APCs, thereby augmenting anti-tumour immunity by acting as an *in situ* tumour vaccine.

We analysed the composition of whole lungs rather than individual tumours as single tumours were often small, limiting the number of cell populations that can be investigated by FACS. We predominantly focussed on the carboplatin and paclitaxel treatment (Carb/Tax), as the number of *KP* mice was limited, and this combination seemed the most promising from previous results concerning ecto-CRT and *in vivo* tumour cell apoptosis. Populations of, F480+ CD11b+ cells (representing interstitial macrophages), Ly6G+ CD11b high cells (representing neutrophils and monocytes) CD49b+ cells (predominantly NK and NKT cells) and CD3+ cells (representing T lymphocytes and NKT cells) did not change significantly after any of the therapies relative to PBS-treated mice (Figure 3.4).

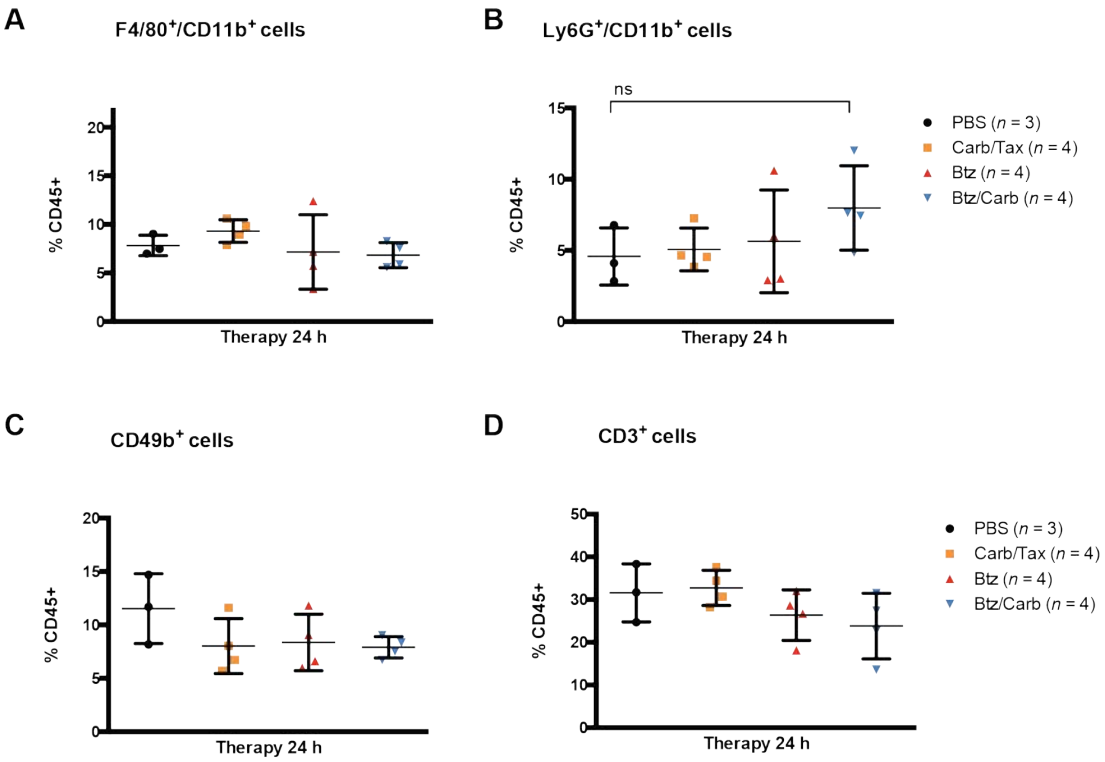

Figure 3.4 Stable immune cell populations following therapy in the lungs of *KP* mice

(**A**) 24 h after therapy with the indicated cytotoxic drugs, F480+ CD11b high cells were quantified by flow cytometry analysis in tumour-bearing lungs from *KP* mice. Carboplatin (50 mg/kg i.p) and paclitaxel (10 mg/kg i.p) (Carb/Tax), bortezomib (Btz; 0.5 mg/kg i.p) or bortezomib and carboplatin (Btz/Carb). Shown are F480+ CD11b high cells representing interstitial macrophages.
(**B**) Quantification of Ly6g+ CD11b high cells as in (A), representing neutrophils and monocytes.
(**C**) Quantification of CD49b+ cells as in (A), representing NK cell populations.
(**D**) Quantification of CD3+ cells as in (A), representing T lymphocytes and NKT cells.
Each data point represents an individual mouse and group numbers are indicated in parenthesis. Unpaired, two-tailed Student's *t*-test; n.s, not significant.

However, we observed a significant increase in the total number of CD11c+ cells in tumour-bearing lungs 24 h after Carb/Tax (Figure 3.5A). In addition, we also observed a significant increase in the frequency of F4/80+CD11b low cells (Figure 3.5B). The CD45+ CD11c+ population predominantly describes APCs including macrophages, monocytes and DCs, whereas CD45+ F4/80+

CD11b low cells represent the alveolar macrophage population in the lung. Therefore, the therapy-induced increases in these cell populations could reflect the recruitment of professional APCs to clear apoptotic debris. It remains unclear at this point whether this increase in frequency is due to local proliferation of these populations, or recruitment from a distant site.

Next, we addressed whether this local increase in APC populations was specific to tumour-bearing mice, or if it was a tumour-independent phenomenon. Interestingly, base-line levels of lung CD11c+ cells were higher in normal mice than in tumour-bearing animals, possibly implying a level of immunosuppression or barrier exclusion; however, we did not observe an increase in this population after therapy in tumour-free control mice (Figure 3.5C). Similarly, F4/80+ CD11b low cells were slightly increased in normal lungs, and there was no increase in frequency following therapy in healthy mice (Figure 3.5D). Rather, we observed a slight decrease in both immune cell populations when expressed as a percentage of the total cells analysed, possibly reflecting the modest decrease in total CD45+ leukocytes in the lung after chemotherapy in healthy mice. Taken together, our data suggest that there is a tumour-specific increase in the population of CD11c+ phagocytes and F4/80+ CD11b low alveolar macrophages after Carb/Tax chemotherapy in *KP* mice.

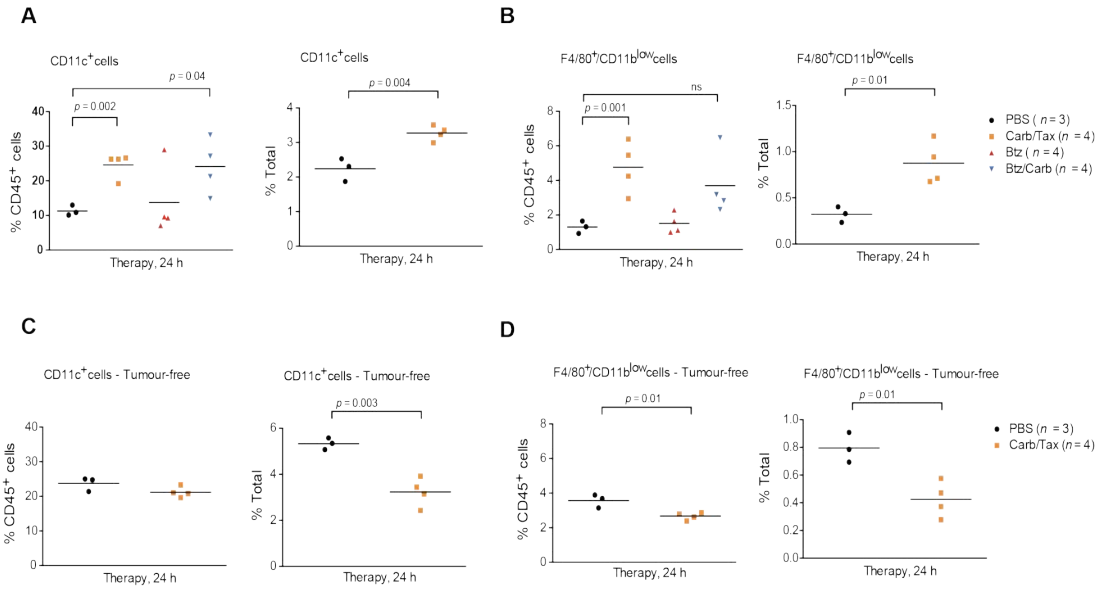

Figure 3.5 Therapy-induced changes in the immune contexture in the lungs of *KP* mice

(**A**) 24 h after therapy with the indicated cytotoxic drugs, CD11c+ cells were quantified by flow cytometry analysis in tumour-bearing lungs from *KP* mice. Carboplatin (50 mg/kg i.p) and paclitaxel (10 mg/kg i.p) (Carb/Tax), bortezomib (Btz; 0.5 mg/kg i.p) or bortezomib and carboplatin (Btz/Carb). Shown are CD11c+ cells representing dendritic-like cells.
(**B**) Quantification of F480+ CD11b low cells as in (A), representing alveolar macrophages.
(**C**) Tumour-free mice were treated with the indicated cytotoxic drugs and CD11c+ cells in lung tissues were quantified.
(**D**) Tumour-free mice were treated with the indicated cytotoxic drugs and F480+ and CD11b low cells in lung tissues were quantified.
Each data point represents an individual mouse and group numbers are indicated in parenthesis. Unpaired, two-tailed Student's *t*-test; n.s, not significant. Percentage total represents the percentage of viable cells.

Since CD11c+ DCs are crucial for mediating anti-tumour immunity (Salmon et al., 2016a), we further investigated the dynamics and phenotype of this cell infiltrate. We further classified the CD11c+ population by including the MHCII marker, which is more specific to the conventional DC subset, and represents DCs that are capable of presenting antigen. We analysed these populations at four days after treatment to see if there was retention of increased APC populations long-term after therapy. However, although the fraction of CD45+ leukocytes was not changed after therapy at four days (Figure 3.6A), we

noted a significant reduction in CD11c+ cells (Figure 3.6B) and CD11c+ MHCII high cells (Figure 3.6C) in mice treated with Carb/Tax. Although this was unexpected, this effect is consistent with myelosuppression as a reported adverse effect in lung cancer patients treated with carboplatin and paclitaxel together (Langer et al., 1995). Also, this myelosuppression was unlikely to have been significant at 24 h post-treatment.

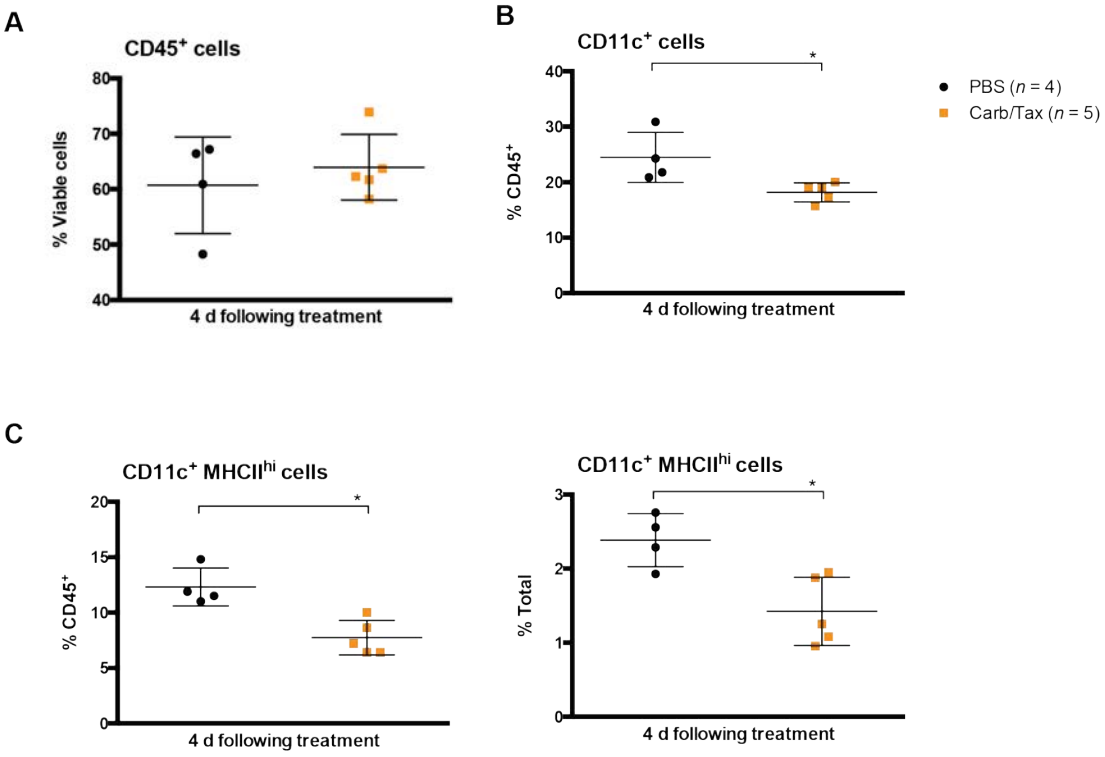

Figure 3.6 Long-term suppression of CD11c+ cells in tumour-bearing lungs by chemotherapy

(**A**) Four days after therapy with the indicated cytotoxic drugs, CD45+ cells were quantified by flow cytometry analysis in tumour-bearing lungs from *KP* mice. Carboplatin (50 mg/kg i.p) and paclitaxel (10 mg/kg i.p).
(**B**) Quantification of CD45+ CD11c+ cells as a percentage of total CD45+ cells.
(**C**) Quantification of CD45+ CD11c+ MHCII high cells as a percentage of total CD45+ cells and as a percentage of total viable cells.
Each data point represents an individual mouse and group numbers are indicated in parenthesis. Unpaired, two-tailed Student's *t*-test; $*P < 0.05$.
Percentage total represents the percentage of viable cells.

Even short-term activity of APCs in the tumour microenvironment following activation of apoptosis could be sufficient to elicit an adaptive immune response against the tumour. Therefore, we checked whether chemotherapy could lead to infiltration of CD4 and CD8 T cells at four days post-Carb/Tax treatment, which is typically enough time to mount an adaptive T cell response following antigen exposure. For example, Rafi Ahmed and Colleagues have shown that antigen-specific CD8 T cell responses to viral infection begin as early as three days, and peak at eight days post-infection (Murali-Krishna et al., 1998). However, we did not observe an increase in the frequency of CD4+ or CD8a+ T lymphocytes in the diseased lung tissue of *KP* mice treated with Carb/Tax chemotherapy (Figure 3.7). We concede that it is difficult to foresee how the dynamics of a T cell viral response compare to an anti-tumour response, where some prior exposure to antigens and a degree of T cell anergy is expected in the latter. However, our results suggest that Carb/Tax chemotherapy is capable of inducing an acute and tumour-specific increase in APCs in the lung, but it is not sufficient to generate a significant subsequent adaptive T cell response. We have shown that the paclitaxel component of this therapy can induce indications of ICD (CRT exposure at the cell membrane), but the chronic signs of myelosupression demonstrated here are a concern, and will most likely have negative implications for mounting an anti-tumour immune response. In further work, it would also be interesting to analyse infiltration at the longer time-point of 7-10 days after therapy.

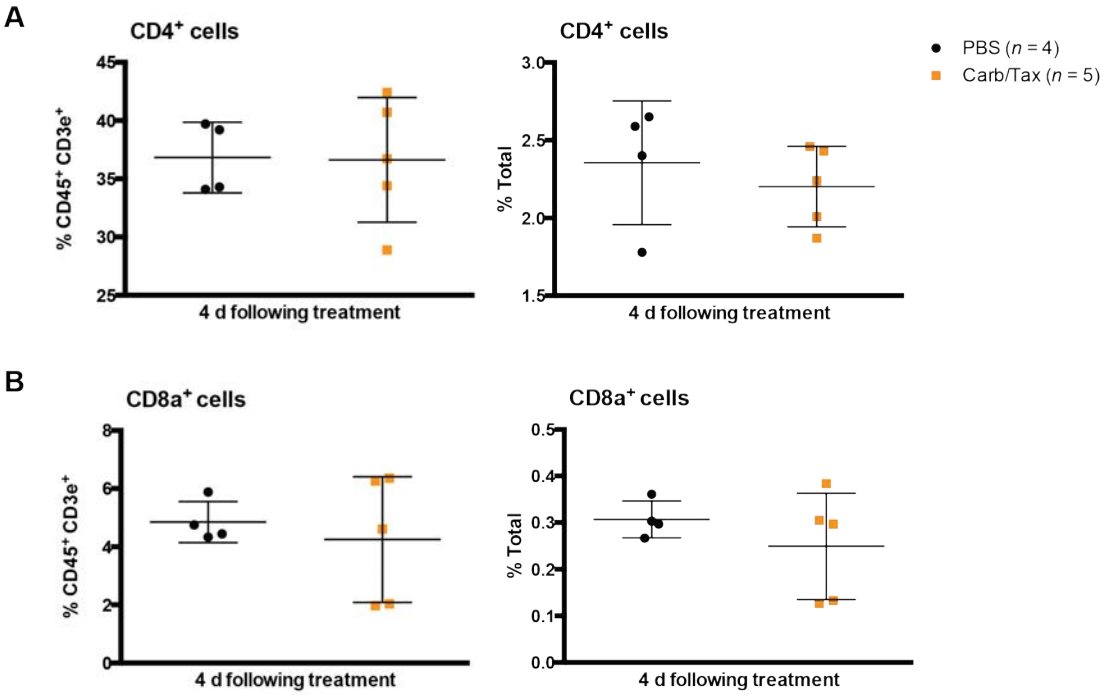

Figure 3.7 Lack of adaptive immune infiltrate following chemotherapy in tumour-bearing lungs

(**A**) Four days after therapy with the indicated cytotoxic drugs, CD45+ CD3e+ CD4+ cells were quantified by flow cytometry analysis in tumour-bearing lungs from *KP* mice. Carboplatin (50 mg/kg i.p) and paclitaxel (10 mg/kg i.p). (**B**) Quantification of CD45+ CD3e+ CD8a+ cells as in (A).
Each data point represents an individual mouse and group numbers are indicated in parenthesis. Percentage total represents the percentage of viable cells.

3.2.2 KrasLSL/+; Trp53 F/F mouse tumours are resistant to immune checkpoint blockade

Our results from previous sections do not exclude the possibility that *KP* tumours are indeed immunogenic, and capable of responding to immunotherapies. The striking clinical successes in the treatment of NSCLC in the clinic (Borghaei et al., 2015) prompted us to test the efficacy of commonly used ICB antibodies in *KP* mice. As a first approach, we tried treatment with anti-PD-L1 antibody monotherapy. We selected the highest dose of antibody that successfully caused NSCLC regressions in humans; 10 mg/kg (Brahmer et al., 2012). Firstly, we confirmed that the antibody was

successfully reaching and binding to the target lung tissue in healthy mice, by secondary detection of the therapeutic rat antibody with an anti-rat APC antibody by flow cytometry (Figure 3.8). 24 h after antibody injection, we observed significant and reproducible binding to lung cells at this dose.

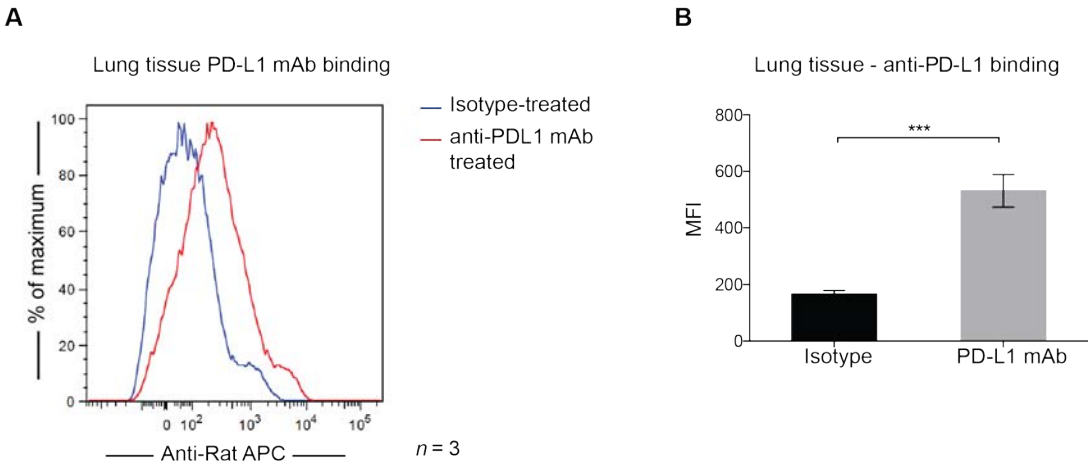

Figure 3.8 Anti-PD-L1 antibody effectively binds to the target lung tissue *in vivo*

(**A**) Representative histograms from flow cytometry analysis of anti-rat secondary antibody binding to lung tissue from wild-type C57Bl/6 mice 24 h after i.p injection with 10 mg/kg rat anti-PD-L1 antibody (clone 10F.9G2) or rat isotype control (LTF-2). Data are representative of three independent mice per group. Single, viable cells were analysed from freshly isolated lung tissue.
(**B**) Quantification of anti-PD-L1 antibody binding efficiency *in vivo* as described in (A) by means of secondary detection with anti-rat antibody. MFI, mean fluorescence intensity. ***$P<0.001$, unpaired, two-tailed Student's t-test.

We also combined PD-L1 blockade with the MEK inhibitor trametinib, since trametinib has shown promising results in NSCLC patients and in our own laboratory in *KP* mice (unpublished data) and does not negatively impact on anti-tumour immunity (Ebert et al., 2016). We monitored tumour progression over time by μCT scanning of the lungs. Interestingly, anti-PD-L1 antibody therapy did not result in detectable anti-tumour activity, even in combination with MEK inhibitor (Figure 3.9A and Figure 3.9B). MEK inhibitor alone led to

significant reductions in tumour volume, suggesting that some cell death is induced by this therapy.

Immunotherapies can have non-standard regression dynamics, with paradoxical increases in tumour size, likely corresponding to immune cell infiltration, which is then followed by clinical regressions (Topalian et al., 2014). These characteristics necessitate longer-term tumour monitoring. However, following these animals over time through survival analysis also revealed no benefit of anti-PD-L1 therapy, and surprisingly, no survival benefit of MEK inhibitor treatment either (Figure 3.9C and Figure 3.9D). As MEK inhibitor was only administered for two weeks, we anticipate that any benefit from tumour regression was masked by long-term recovery of tumour growth off therapy.

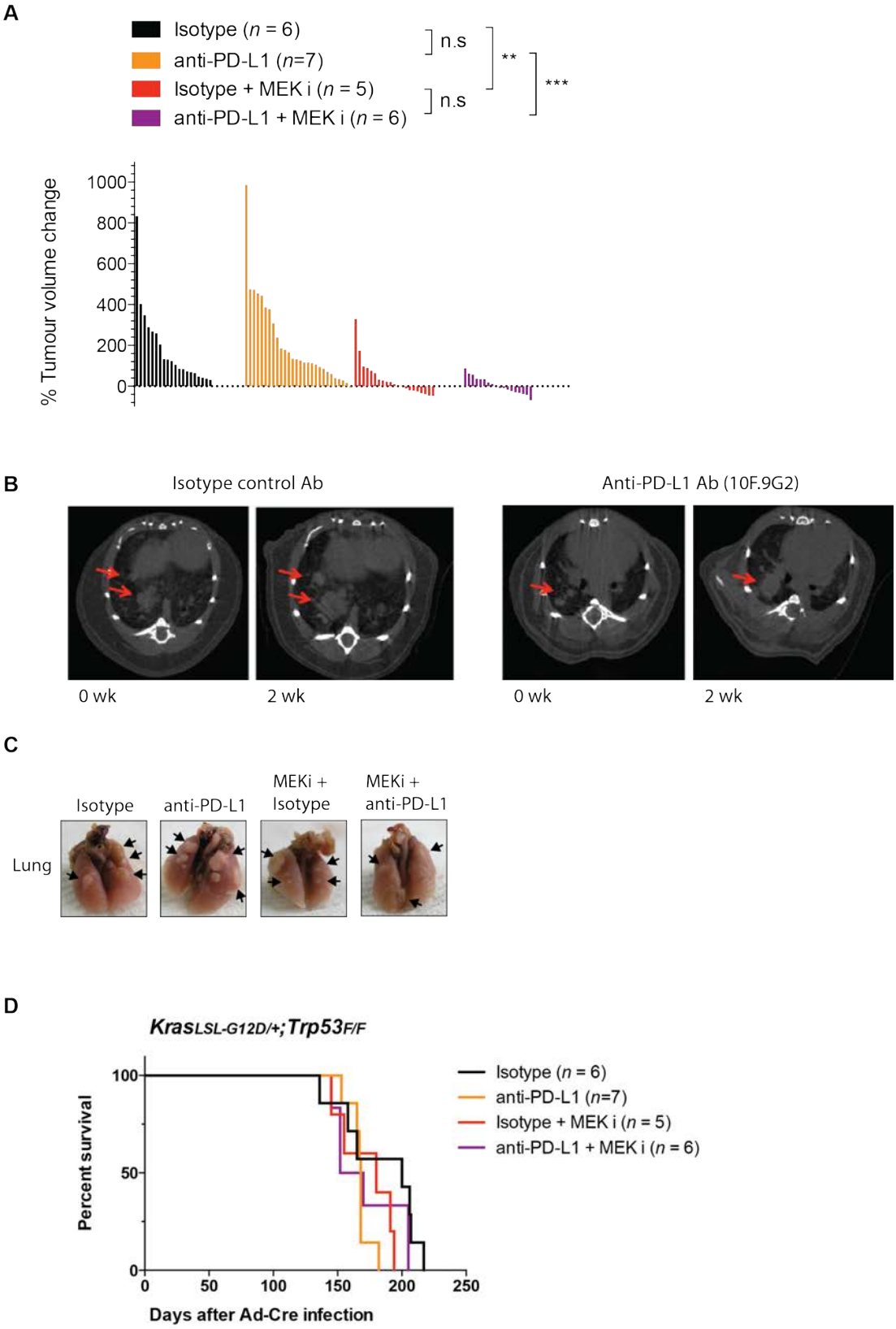

Figure 3.9 Anti-PD-L1 immune checkpoint blockade is not effective in *KP* mice

(**A**) Waterfall plot showing tumour volume change over a two-week treatment period as measured by *μ*CT scanning. Each bar represents volume change of an individual tumour. Tumours were initiated by intratracheal administration of Adeno-Cre to the lung. 16 weeks post-infection mice were treated daily with the MEK inhibitor trametinib (3 mg/kg, o.g) and with anti-PD-L1 antibody 10F.9G2 (10 mg/kg, i.p) twice per week for two weeks in total.
(**B**) Representative images showing tumour progression from *μ*CT scanning from the experiment described in (A).
(**C**) Representative histological images of lungs from mice at sacrifice from the experiment described in (A).
(**D**) Kaplan-Meier survival plot of the experiment described in (A).

Our results suggest that PD-L1 blockade as a monotherapy or in conjunction with the targeted agent trametinib does not show signs of anti-tumour immune activity in the *KP* mouse model of NSCLC. However, we cannot exclude that we have only partially inhibited the immunosuppressive mechanisms at play in these tumours. Recent reports have indicated that anti-PD-1 antibody combined with anti-CTLA-4 antibody has superior efficacy compared to either monotherapy in melanoma (Larkin et al., 2015a). Moreover, Tregs, which are suppressed following CTLA-4 blockade, have been implicated in immunosuppression in a modified *KP* mouse model (Joshi et al., 2015a). Therefore, we examined the anti-tumour effect of anti-PD-L1 and anti-CTLA-4 combination therapy on *KP* lung tumours (Figure 3.10).

Similar to the results from anti-PD-L1 antibody monotherapy, the combination treatment of anti-PD-L1 and anti-CTLA-4 antibody did not result in detectable anti-tumour responses. Short-term *μ*CT analysis over two weeks only revealed significant progression of lesions with a comparable rate to that of isotype-treated mice (Figure 3.10A and Figure 3.10B). Furthermore, following disease progression long-term showed that survival of mice treated with the combination therapy was not significantly different to the isotype control-treated cohort. This lack of anti-tumour activity was also clearly evident by inspection of surface lung tumours at sacrifice (Figure 3.10C and Figure 3.10D).

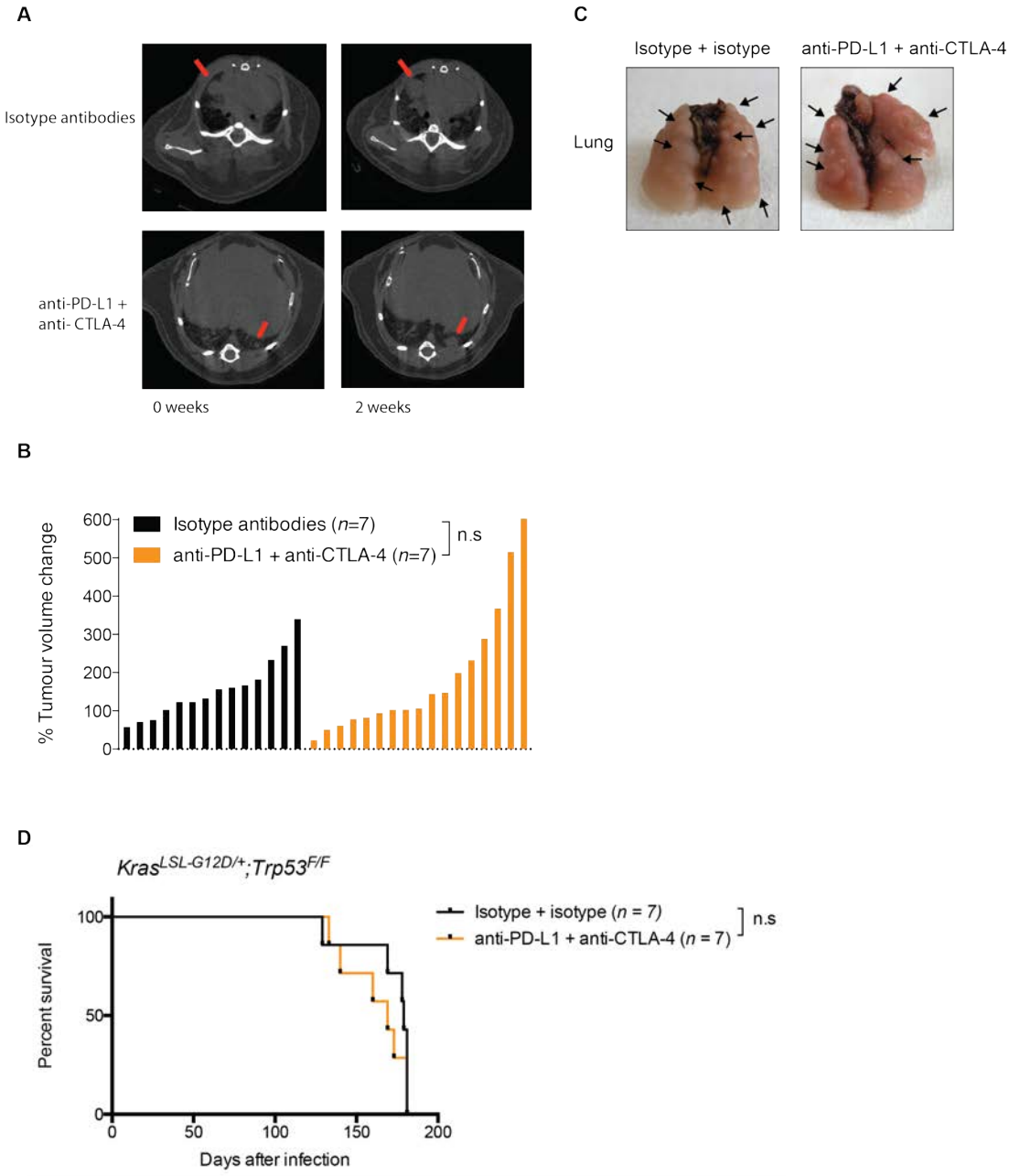

Figure 3.10 *KrasLSL-G12D/+; Trp53 F/F* mouse tumours are refractory to anti-PD-L1 + anti-CTLA4 combination immunotherapy

(**A**) Representative μCT scans of tumours (indicated by arrows) at time = 0 weeks and two weeks of treatment with anti-PD-L1 antibody (10F.9G2, 10 mg/kg) and anti-CTLA-4 antibody (9H10, 5 mg/kg) or isotype controls by i.p administration. Mice received three doses of combination therapy in total over a two-week course, with injections on day 0, 4 and 8.
(**B**) Waterfall plot of tumour volume change over a two-week treatment period, as described in (A). Unpaired, two-tailed Student's *t*-test; n.s, not significant. Each bar represents volume change of an individual tumour.
(**C**) Gross histological analysis of surface tumour burden (nodules are indicated by arrows) from mice treated as described in (A).

(**D**) Kaplan-Meier analysis of survival of mice treated as described in (A). Wilcoxen-rank test; n.s, not significant.

3.2.3 *KrasLSL-G12D/+; Trp53 F/F* mouse tumours are poorly immunogenic

In light of these negative data, we reasoned that the lack of response to immunotherapies might reflect the poor immunogenicity of *KP* tumours. Therefore, we set out to directly assess the immunogenicity of *KP* tumours, and the direct functional influence of the adaptive immune system on tumour progression.

As a first approach, we trialled antibody-mediated depletion of CD4+ and CD8+ T cells. We injected wild-type mice with monoclonal antibodies against CD8 and CD4 and then analysed the abundance of these cell populations by flow cytometry. We used a detection antibody raised against a distinct epitope to the depletion antibody to minimise the issue of lack of detection simply due to occlusion of the antigen. Three days after depletion antibody injection we noted significant reductions in CD45+ CD3+ cells (Figure 3.11A), and specifically, CD45+ CD3+ CD4+ T cells and CD45+ CD3+ CD8a+ T cells (Figure 3.11B). Secondly, we confirmed that our data represent *bona fide* depletion of T lymphocytes, rather than occlusion of the detection antigen by titrating depletion antibody against detection antibody in a splenocyte cell mixture *in vitro* (Figure 3.11C). As expected, higher concentrations of depletion antibody did not affect detection of CD4+ or CD8+ T cells.

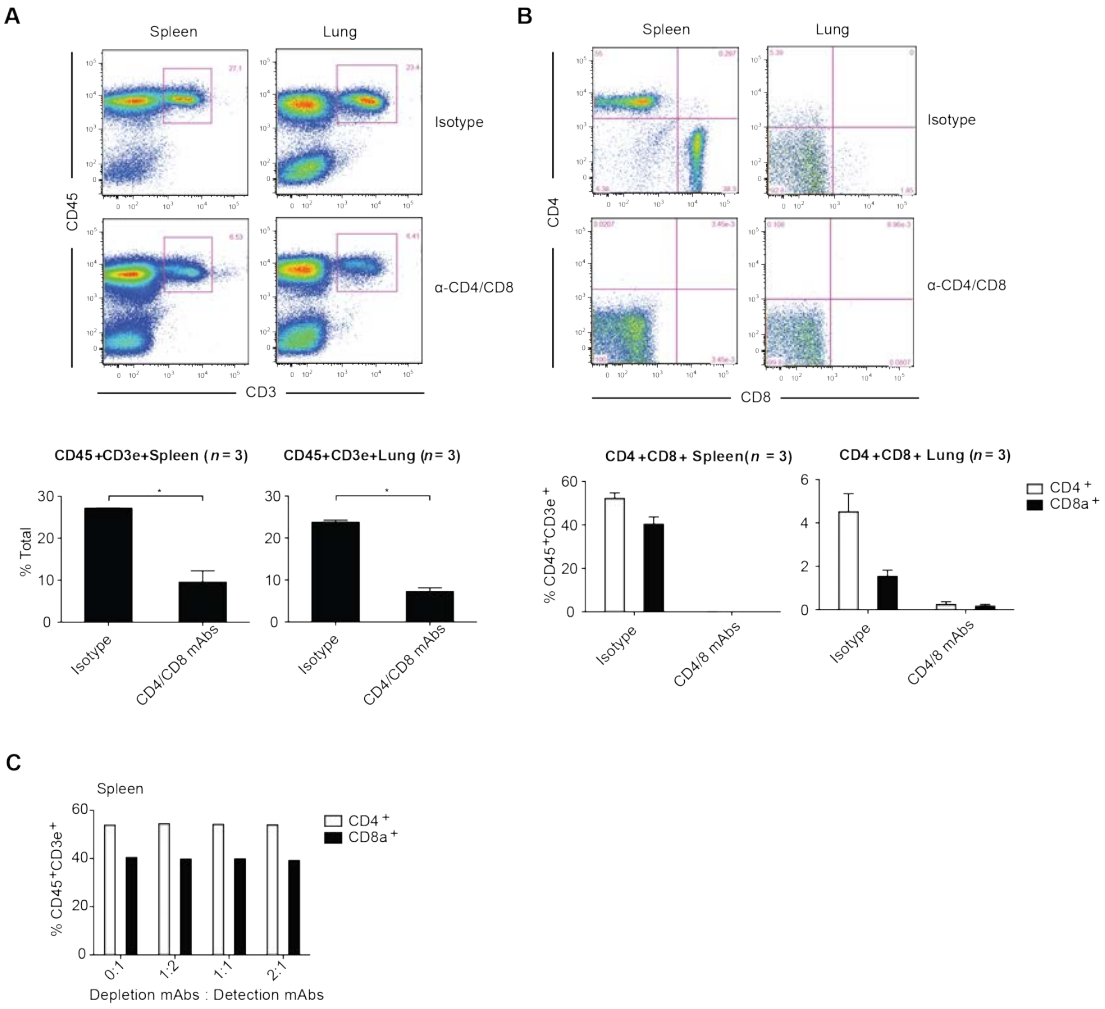

Figure 3.11 Strategy for the depletion of CD4 and CD8 T cells *in vivo*

(**A** and **B**) Flow cytometry analysis of mouse spleen (A) and lung tissue (B) freshly isolated from mice treated with anti-CD8 (2.43. IgG2b rat, 300 μg) and anti-CD4 (GK1. IgG2b rat, 300 μg) antibodies or isotype control antibodies by i.p administration 72 h before sacrifice. Data are representative of three mice per group. Detection antibodies used to detect CD4 and CD8 T cells were distinct from those used to deplete. *P <0.05, unpaired, two-tailed Student's *t*-test.
(**C**) Quantification of flow cytometry data from a competition assay between detection and depletion antibodies. Higher concentrations of depletion antibody cocktail were titrated into the cell mixture and the level of detection of CD4 and CD8 T cells by detection antibodies was quantified. Percentage total represents the percentage of viable cells.

We have shown that antibody depletion of CD4 and CD8 T cells can be technically effective in principle. However, the depletion is short-term, requiring repeat administration of expensive antibodies and may not

guarantee absolute depletion. Secondly, this approach will not give information regarding the functional effects of adaptive immunity before the depletion phase of the experiment. For these reasons, we adopted a genetic approach to completely abrogate T and B cell function from birth. We crossed the *KP* mouse onto *Rag2-/-* mice, which completely lack functional, mature T and B cells (Shinkai et al., 1992). Figure 3.12 shows the absence of T and B cells in the tumour microenvironment in *KP; Rag2-/-* mice. *KP; Rag2-/+* mice are normal with respect to adaptive immunity and can be generated as littermates with *KP; Rag2-/-* immunodeficient mice from crosses, and have been used as immunocompetent controls in subsequent experiments. Intriguingly, we noted CD3+ T cells, but very few B220+ B cells in the tumours of *KP; Rag2-/+* mice (Figure 3.12).

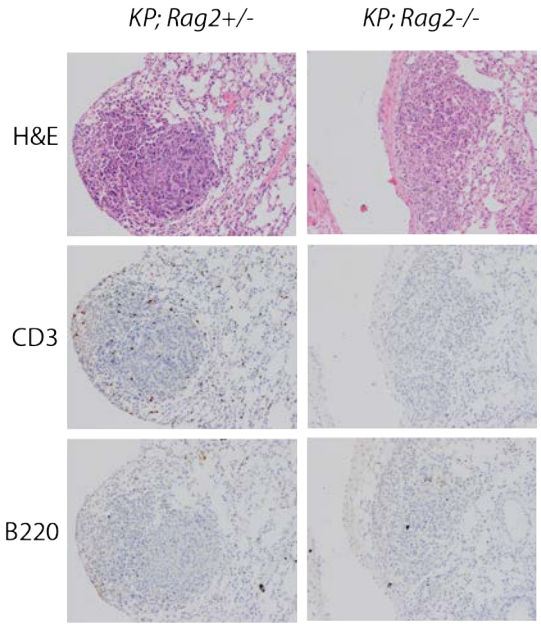

Figure 3.12 Characterisation of *KrasLSL-G12D/+; Trp53 F/F; Rag2 KO* mice

Histological analysis of lung tumours from *KP; Rag2 +/-* and *KP; Rag2 -/-* mice. CD3 staining and B220 immunostaining show T cell and B cell populations, respectively.

Using this GEMM, we monitored the latency, frequency and growth-rate of lung tumours in immunocompetent and immunocompromised settings.

Notably, we observed similar levels of total lung tumour burden as quantified by H & E staining and quantification of percentage tumour area (Figure 3.13A and Figure 3.13B). Similarly, using volumetric tracking of individual lesions by *μ*CT scanning, we found comparable growth rates for tumours in *KP; Rag+/-* and *KP; Rag-/-* mice (Figure 3.13C). Next, we compared the onset of tumorigenesis in *KP; Rag2-/-* and *KP; Rag2-/+* mice by measuring the number of tumours visible by H & E staining at the early time-point of nine weeks post-infection (Figure 3.13D). From this analysis we concluded that there is no significant difference in tumour onset between immunocompetent and immunocompromised mice. In sum, these data suggest that T cells and B cells do not significantly restrain tumour progression in the *KP* mouse model.

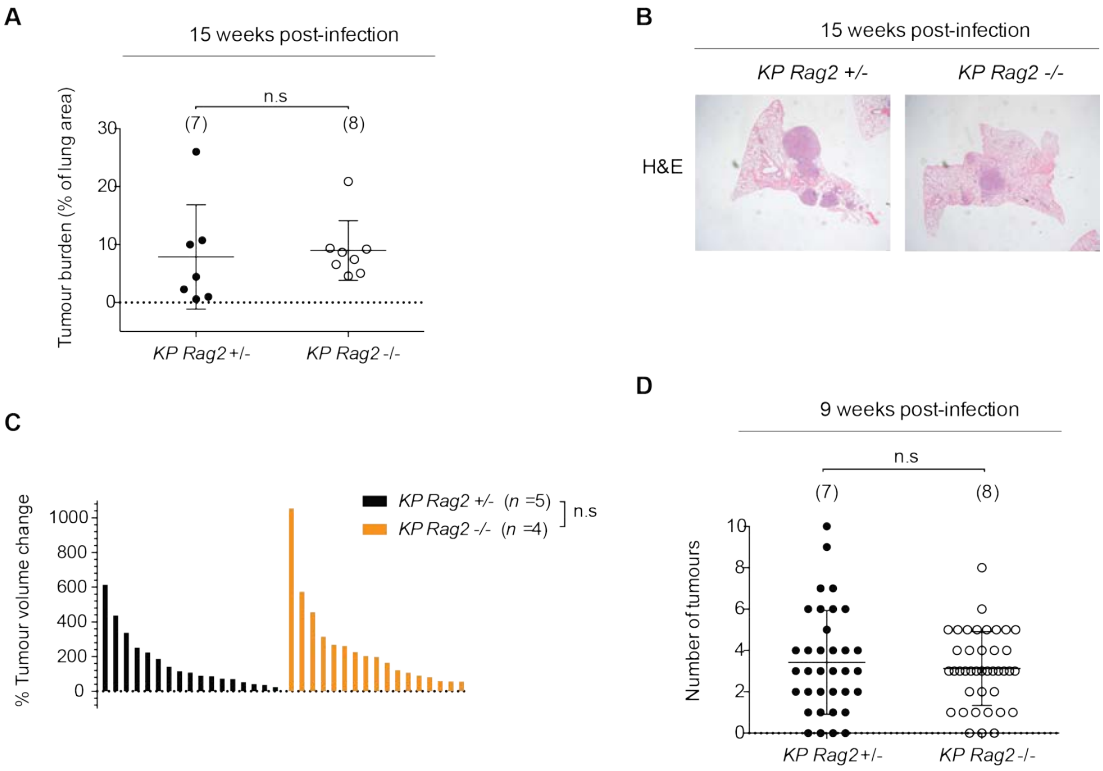

Figure 3.13 Adaptive immunity does not restain tumour progression or tumour initiation in *KrasLSL-G12D/+; Trp53 F/F* mice

(**A**) Tumour burden was quantified using a semi-automated software package (Ariol – Leica Biosystems) from H&E sections from *KP Rag-/-* and *KP Rag+/-*

mice 15 weeks after tumour initiation with Ad-Cre. Unpaired, two-tailed Student's *t*-test.
(**B**) Representative H&E staining of tumour-bearing lungs from *KP Rag-/-* and *KP Rag+/-* mice 15 weeks after tumour initiation with Ad-Cre.
(C) Waterfall plot showing tumour volume change over a two week period for *KP Rag-/-* and *KP Rag+/-* mice, as measured by *μ*CT scanning. Unpaired, two-tailed Student's *t*-test. Each bar represents volume change of an individual tumour.
(**D**) Tumour number was measured by microscopic inspection of 5 H&E slides per mouse taken at the early time-point of 9 weeks post-infection with Ad-Cre. Mann-Whitney *U* test.
Numbers of individual mice per group are indicated in parentheses. n.s, not significant.

Our results from previous sections have highlighted that PD-L1 blockade does not have therapeutic value in this mouse model, even when combined with anti-CTLA-4 treatment or cytotoxic agents. However, we wanted to directly examine whether therapeutic effects of anti-cancer compounds could have non-cell autonomous effects mediated by the adaptive immune system in this model. To this end, we treated *KP; Rag2-/-* and *KP; Rag2-/+* mice with trametinib (GSK1220212, or GSK) as before, but also combined with paclitaxel (taxol). Docetaxel and another MEK inhibitor, selumetinib, have shown significant promise in the *KP* model of lung cancer when combined (Chen et al., 2012). The docetaxel and selumetinib combination induces significant tumour cell apoptosis, with superior activity to either agent alone (Chen et al., 2012). Indeed, we observed significant reductions in tumour volume with GSK/Taxol therapy compared with vehicle-treated mice (Figure 3.14A). Although we did observe more complete regressions in the immunocompetent mice, the anti-tumour response was not significantly different between *KP; Rag2-/-* and *KP; Rag2-/+* mice. In addition, long-term tracking of the tumours off-treatment revealed similar growth dynamics in both cohorts of mice, with tumours growing back after the initial regressions (Figure 3.14B). Thus, there is no obvious adaptive immunity generated following these anti-tumour responses in *KP; Rag+/-* mice. Unfortunately, only a small number of tumours could be tracked at this late stage after therapy due to the fusing of individual nodules as the tumours grew, making

volumetric quantification of the single lesions impossible. Collectively, these data imply that there are no significant non-cell autonomous anti-tumour effects mediated by the adaptive immune system following GSK/Taxol therapy in *KP* mice.

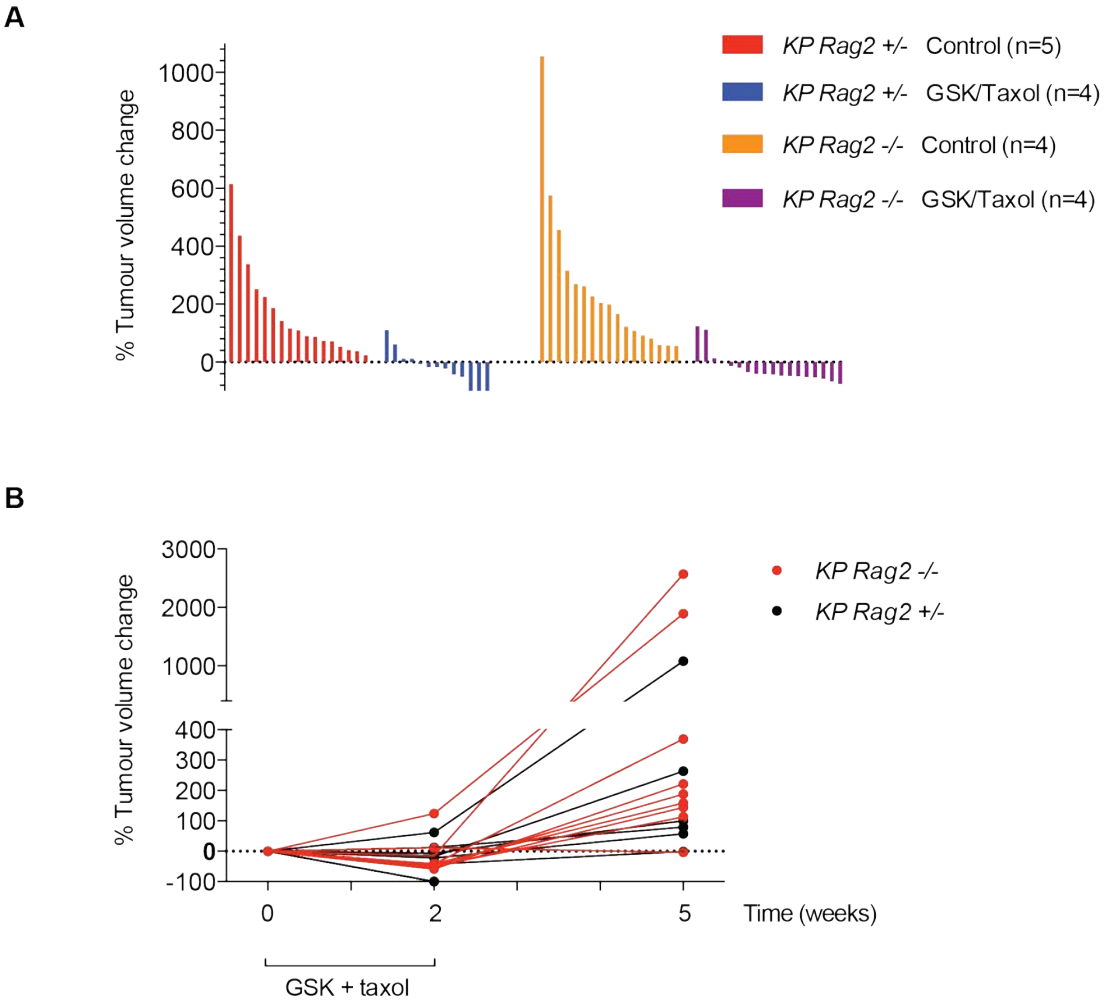

Figure 3.14 No significant contribution of adaptive immunity to therapy response in *KP* mouse lung cancer

(**A**) Waterfall plot of tumour volume change over a two-week treatment period as measured by μCT scanning. Each bar represents volume change of an individual tumour. Mice were treated with vehicle control or MEK inhibitor trametinib GSK1120212 (GSK) by daily oral gavage (3 mg/kg) and paclitaxel (taxol) by i.p administration once weekly (10 mg/kg) for two weeks.
(**B**) Tumours quantified in (A) were monitored by μCT scanning for an additional 3 weeks off-treatment. Tumours that fused into neighbouring structures and other tumours at later time points could no longer be quantified as single nodules and so have been omitted from this analysis.

KP tumours are ostensibly refractory to T and B cell attack and so are unlikely to be immunogenic under steady-state conditions. However, this may reflect profound immunosuppression or early immunoediting of potent antigens that renders the tumours capable of growing unabated. This would lead to a negligible negative impact on the overall tumour burden when measured long-term. To further investigate the possibility of immunoediting processes during tumour development in *KP* mice, we generated *KP; Rag1-/-* mice on a clean C57Bl/6 background (11 generations of backcrossing), which can be used for syngeneic transplantation experiments. Using *KP; Rag1-/-* or *KP; Rag1+/-* mice, we could directly assess if tumour immunoediting had occurred by comparing tumour progression in wild-type syngeneic hosts of lung tumour cell lines derived from the immunocompetent or immunodeficient strain. We established four independent lung tumour cell lines from a single *KP;Rag+/-* mouse and four lines from a *KP;Rag-/-* mouse. We injected the cell lines subcutaneously into C57Bl/6 syngeneic recipients or *Rag1-/-* C57Bl/6 recipients and followed tumour progression over time (Figure 3.15).

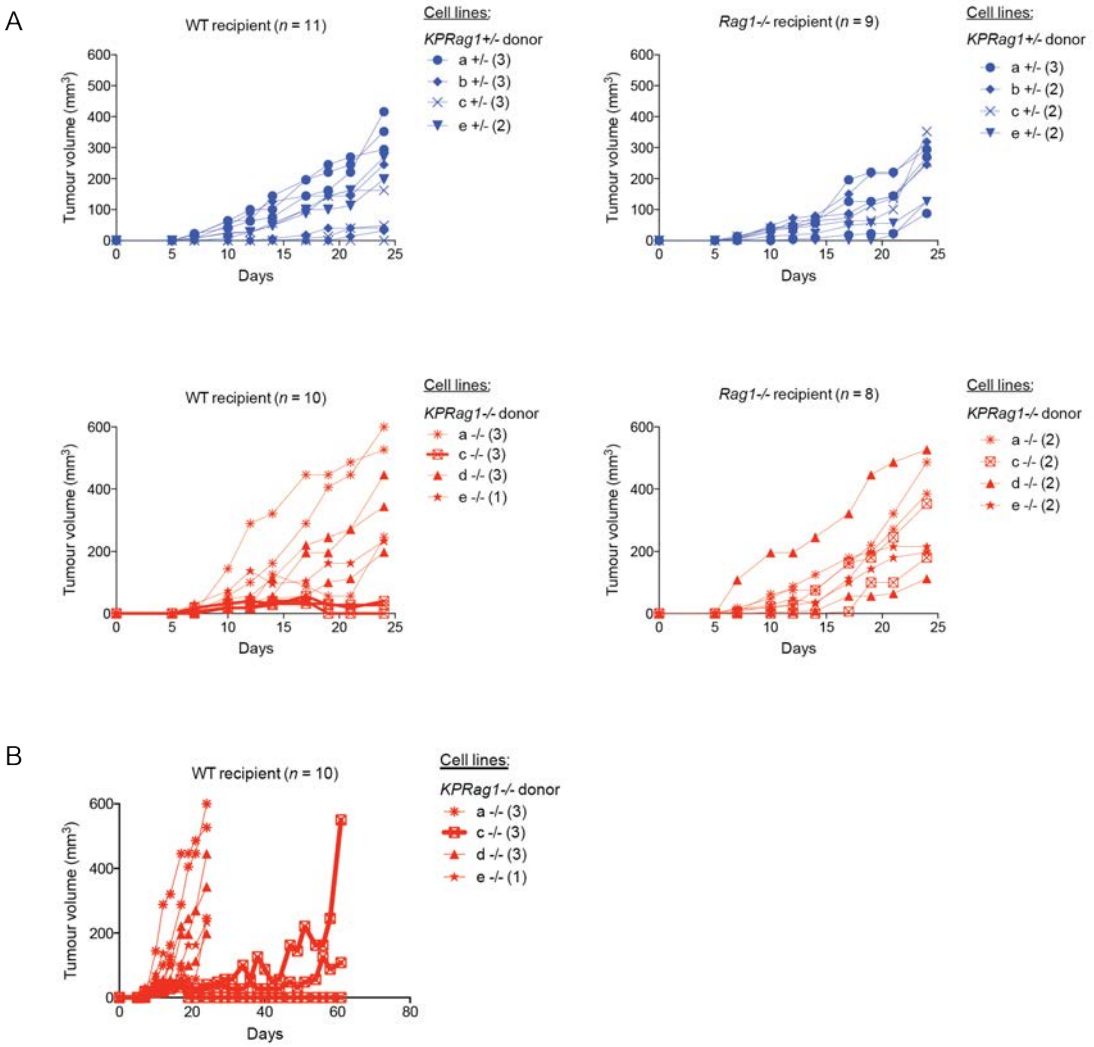

Figure 3.15 Examination of tumour immunoediting in *KrasLSL-G12D/+; Trp53 F/F* mice

(**A**) Four independent tumour cell lines were derived from different tumours from both *KP; Rag1-/-* and *KP; Rag1+/-* C57Bl/6J mice at 12 weeks post-infection with Adeno-Cre. Established cell lines were transplanted subcutaneously into syngeneic wild-type or *Rag1-/-* recipient mice as indicated (1.5 x10^5 cells in PBS into the left flank). Tumour growth was monitored with calipers.
(**B**) For the "*KPRag1-/-* c" cell line, tumours were monitored over an extended 60 day period.

Most cell lines from the *KP;Rag+/-* and *KP;Rag-/-* hosts grew comparably in immunodeficient and immunocompetent recipients, with progressive growth in both contexts, consistent with a similar degree of immunogenicity for all cell lines. However, there was one notable exception; the *KP; Rag1-/-* c cell

line, which reproducibly failed to grow progressively in the WT mice (3/3 cases), and moreover, this was the only cell line for which we observed a complete tumour regression (1/3 cases) (Figure 3.15A). Crucially, the c-/- cell line grew progressively in the *Rag1-/-* recipients, indicating an immune-mediated control mechanism. Long-term monitoring of the WT mice harbouring the c-/- line over a two-month period revealed sustained control and stable disease in 2/3 mice. The single mouse that had previously rejected the tumour remained disease-free over this extended period (Figure 3.15B). 1/3 of the WT mice with stable disease eventually experienced progressive tumour growth of the *KP;Rag1-/-* c line at 58-60 days post-injection, implying immune-escape (Figure 3.15B). We proceeded to repeat the experiment with the c-/- line to check the reproducibility of these effects (Figure 3.16). As expected, we observed the same trend, with the tumours growing progressively only in the *Rag1-/-* recipients.

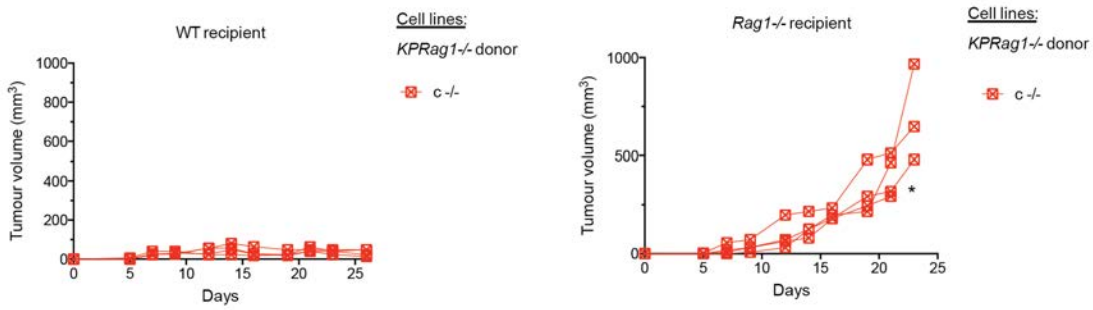

Figure 3.16 *KPRag1-/-* c lung cancer cell line is immunogenic

The *KP;Rag1-/-* c cell line was injected subcutaneously into either wild-type (WT) C57Bl/6 recipients, or immunocompromised *Rag1-/-* C57Bl/6 recipients (1.5 x10^5 cells in PBS into the left flank). Tumour growth was monitored using calipers. * denotes where a mouse was sacrificed prematurely due to ulceration or a skin condition. *n* = 4 mice per group.

The behaviour of the *KP;Rag1-/-* c cell line is suggestive of tumour cell immunogenicity. To confirm this, we rechallenged a WT mouse that had previously experienced a complete rejection of a tumour derived from the *KP;Rag1-/-* c cell line (Figure 3.17). Consistent with the existence of immunological memory and an anti-tumour immune response against this

cell line, the rechallenged mouse remained disease-free and did not develop a tumour at the site of injection, whereas naïve or *Rag1-/-* recipient control mice developed tumours as expected.

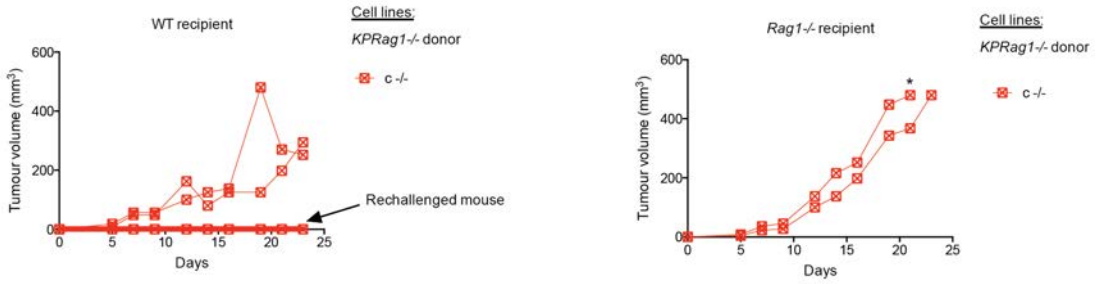

Figure 3.17 Immunological memory and rejection of the *KPRag1-/-* c lung cancer cell line

The *KP;Rag1-/-* c cell line was injected subcutaneously into either wild-type (WT) C57Bl/6 recipients, or immunocompromised *Rag1-/-* C57Bl/6 recipients (1.5 x10^5 cells in PBS). A mouse that had previously rejected a *KP;Rag1-/-* c tumour was rechallenged (as indicated) with a second cell injection into the contralateral flank. 2/3 WT mice and 3/3 of the *Rag-/-* mice were naïve recipients included as a control. Tumour growth was monitored using calipers. * denotes where a mouse was sacrificed prematurely due to ulceration or a skin condition. *n* = 2-3 mice per group.

In summary, these data provide evidence that some *KP* lung cancer cell clones can be immunogenic. The immunogenic cell line *KP;Rag1-/-* c was derived from an immunocompromised mouse, suggesting that immunoediting in WT mice may take place in the *KP* model. Whether the immunogenic determinant in this cell line is a rare neoantigen, or a tumour-associated antigen remains to be determined. We plan to investigate this further using RNA sequencing to determine mutations and gene expression differences between this cell line and others that are not rejected. If significant immunoediting does take place in this mouse model, it must only have minimal effect on the tumour burden and tumour onset, as described in our characterisation of the *KP;Rag2-/-* model. We speculate that immunogenic clones are destroyed rapidly, and very early in tumour development, therefore having minimal impact on tumour progression long-term.

We have shown that *KP* tumours are refractory to common immunotherapy treatments, but could potentially harbour uncommon immunogenic tumour cell clones that may be removed through immunoediting in an immunocompetent host. A determinant of immunotherapy response to PD-1 blocking agents is the engagement of the checkpoint pathway in the tumour microenvironment. Therefore, we questioned whether *KP* tumours were similar to human NSCLC tumours in expression and upregulation of immunosuppressive proteins such as PD-L1 (Topalian et al., 2012; Zitvogel and Kroemer, 2012b). Unexpectedly, we found high levels of tumour cell PD-L1 expression at the mRNA and protein level, with higher levels in the tumour relative to the adjacent healthy lung tissue (Figure 3.18A). Interestingly, Lastwika and colleagues recently showed that PD-L1 expression is upregulated in lung tumour tissue relative to normal lung in three independent mouse models of lung cancer: $KRAS^{LA2}$, $EGFR^{L85R}$ and NNK-driven mouse models (a carcinogen that introduces KRAS mutations) (Lastwika et al., 2016). In support of these data, an independent study showed that $EGFR^{L85R}$ mouse lung cancers overexpress PD-L1 relative to wild-type lung tissue by using a microarray based approach (Akbay et al., 2013). Genentech have also stated that most mouse tumour models constitutively express PD-L1, which does not reflect the more heterogeneous situation in human cancer (Herbst et al., 2014). Finally, cell lines derived from *KP* lung tumours that we have tested in our laboratory (e.g. KPB6 cell lines) express high levels of PD-L1 (data not shown). Collectively, these results may indicate that there may be profound immunosuppression in these lung tumours, thus protecting the tumour cells from the host adaptive immune system. Alternatively, these data might suggest that PD-L1 is expressed by *Kras*-driven tumours purely through a cell-intrinsic process, and this is not functionally important for tumour progression.

To help delineate between these possibilities, we checked *PD-L1* mRNA and PD-L1 protein expression in tumours from *KP; Rag2-/-* and *KP; Rag2-/+* mice

(Figure 3.18B). This analysis revealed similar levels of tumour cell *PD-L1* mRNA expression in tumours from both immunocompetent and immunocompromised mice, supporting the notion that upregulation of tumour cell PD-L1 expression in this mouse model is through cell intrinsic signalling mechanisms rather than through selection by the adaptive immune system. We verified that epithelial tumour cells were expressing high levels of PD-L1 in *KP* mouse tumours (rather than other cell types in the tumour) by analysing PD-L1 expression on CD45- CD31- DAPI- cells (thus excluding leukocytes, endothelial cell and dead cells) using FACS (Figure 3.18C). Consistently, we observed higher PD-L1 expression on these cells than matched normal lung.

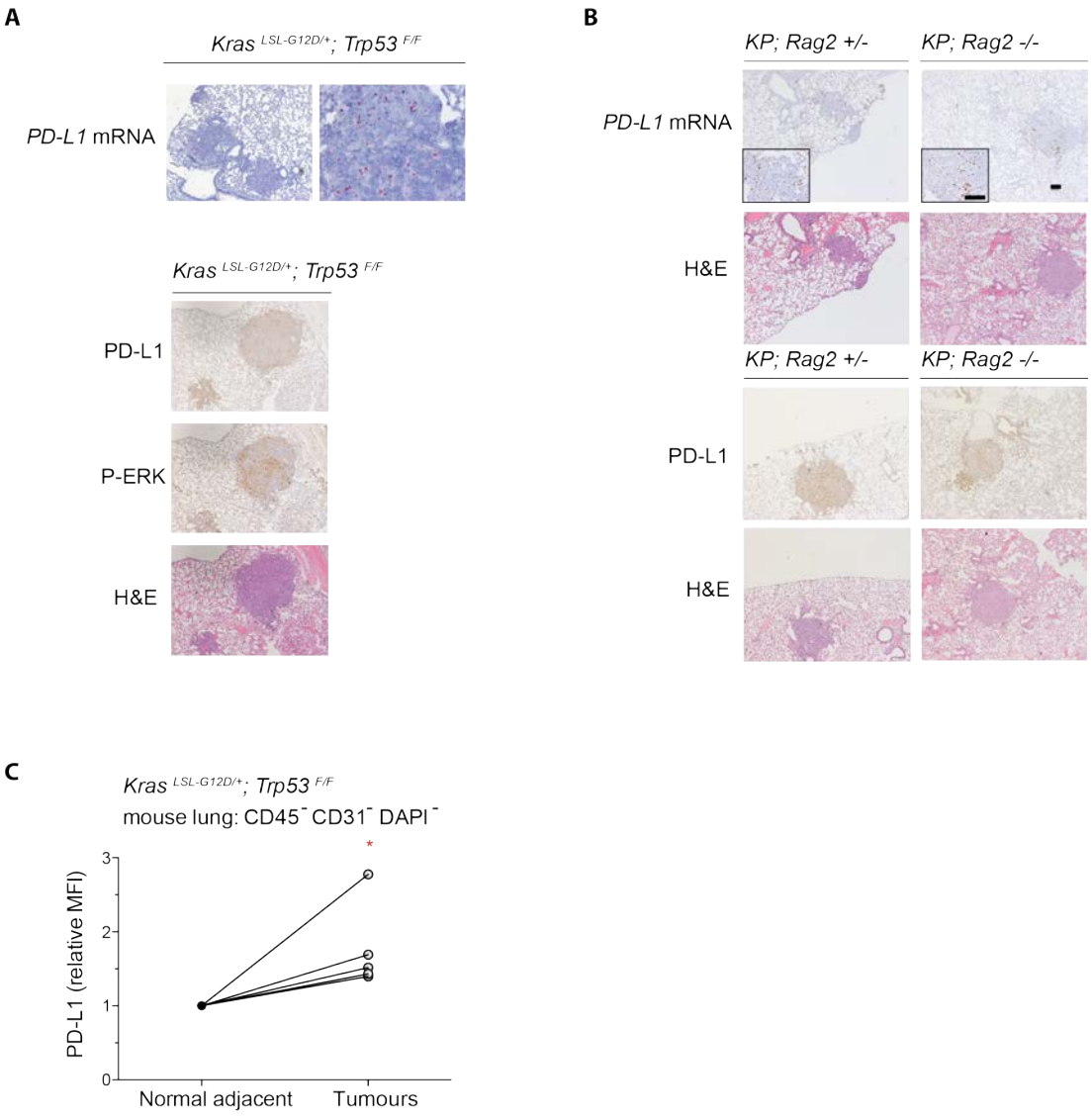

Figure 3.18 Kras-driven murine lung tumours express high levels of PD-L1 independently of adaptive immunity

(**A**) RNA-scope-based *in-situ* hybridisation for *PD-L1* mRNA and corresponding H & E staining of *KP* mouse lung tumours. *PD-L1* mRNA is in red.
(**B**) RNA-scope-based *in-situ* hybridisation for *PD-L1* mRNA, PD-L1 immunostaining and corresponding H & E staining of *KP; Rag1+/-* and *KP; Rag1-/-* mouse lung tumours.
(**C**) Flow cytometry analysis of surface PD-L1 protein expression in CD45-CD31-DAPI- cells freshly isolated from *KP* mouse tumours or matched, normal adjacent lung tissue. Data are normalised to normal tissue controls. Each paired data point represents an individual mouse. Data are pooled from two independent experiments.

Tuveson, Fearon and colleagues have shown that anti-tumour T cells are effectively excluded by cancer-associated fibroblasts in a mouse model of pancreatic cancer, and only when this barrier is overcome can T cells mediate an anti-tumour response (Feig et al., 2013). Hence, we directly tested the *in vitro* reactivity of T cells isolated from tumour-bearing *KP* mice against tumour cells freshly isolated from the same mouse. This approach eliminates any barriers between T cells and tumour cells, as they are co-cultured *in vitro*. T cell effector response is assessed by measurement of IFN- γ by ELISA.

Firstly, we isolated a purified population (approximately 96 % pure) of CD3+ CD8+ T cells from the spleens of tumour-bearing mice by a negative selection FAC-sorting strategy (Figure 3.19A). We also isolated CD45-CD31- tumour cells or normal lung epithelial cell populations by positive FAC-sorting. Co-culture with normal lung cells served as a negative control. PMA and ionomycin stimulation of unsorted splenocytes served as a technical positive control for IFN- γ detection. As a relevant biological positive control, we also included CD8 T cells isolated from wild-type mice vaccinated against the model antigen OVA. As targets, we included the EL4 lymphoma cell line engineered to express OVA constitutively (E.G7-Ova cells).

As expected, PMA and ionomycin treatment caused a massive release of IFN- γ (Figure 3.19B). CD8 T cells from OVA-vaccinated mice also released IFN- γ at detectable levels when presented with E.G7-Ova targets, but at much lower levels. As expected, CD8 T cells from naïve mice were not capable of reacting to E.G7-Ova targets, demonstrating the specificity of the assay.

Crucially, we were not able to detect CD8 T cell effector responses to purified lung tumour cells relative to normal lung cells. These results indicate that if any anti-tumour CD8 T cells exist in this GEMM, they are present at a low frequency, which is below the limit of detection of this assay (Figure 3.19B).

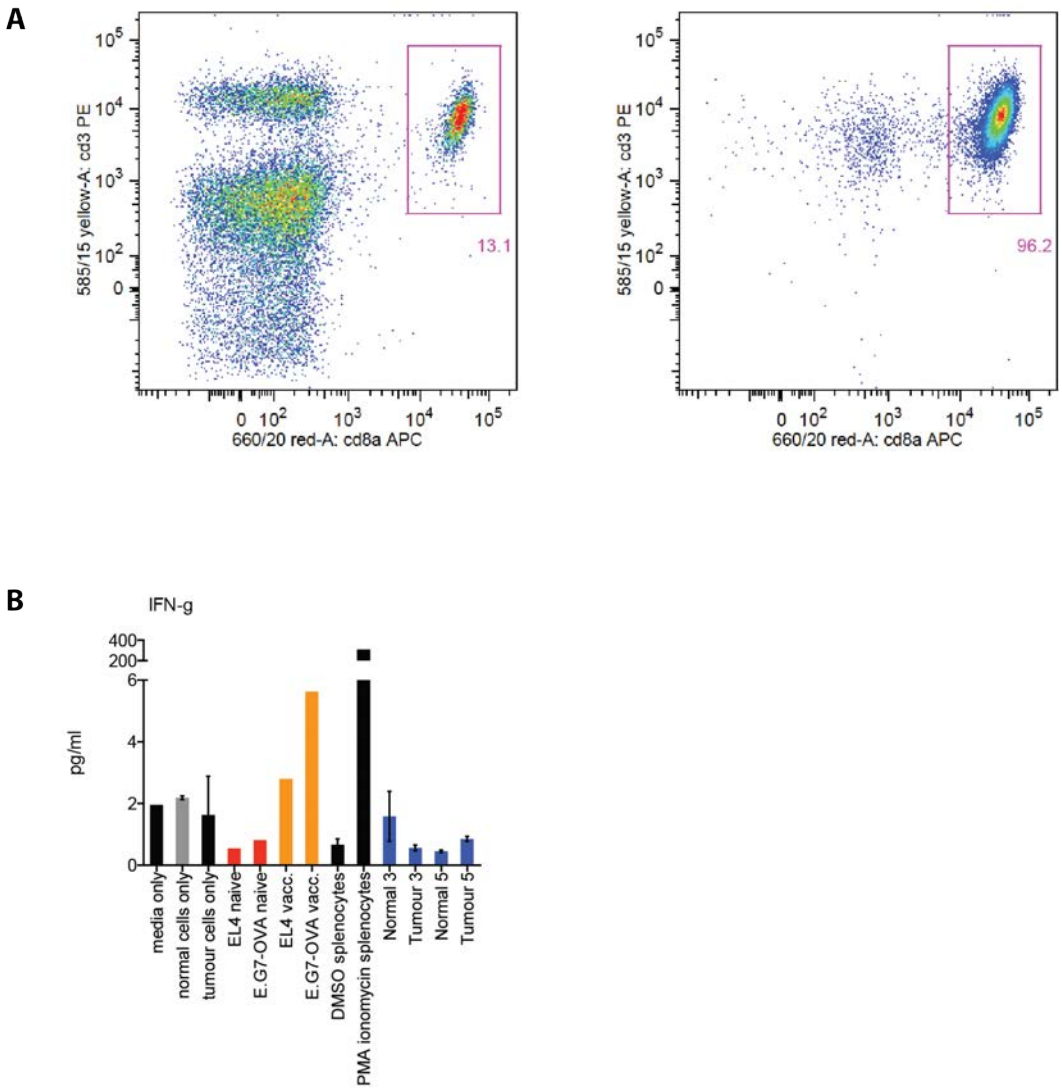

Figure 3.19 CD8 T cells from tumour-bearing *KP* mice do not express IFN-γ when presented with autologous lung tumour cells *in vitro*

(**A**) Flow cytometry analysis of unsorted mouse spleen (left) and the experimental, sorted CD8 T cell population isolated by a negative sorting strategy.
(**B**) ELISA detection of IFN-γ after 16 h of co-culture of effectors (CD8+ T cells) with target cells (CD45-CD31- cells). PMA and ionomycin treated splenocytes serve as a positive technical control. EG7-OVA target T lymphoma cells and CD8 T cells from mice vaccinated with ovalbumin serve as a positive biological control. $1x10^5$ CD8+ T effector cells were incubated with $5x10^3$ target tumour cells. Mean ± SEM of biological duplicates.

3.2.4 Suppression of mismatch repair to increase tumour immunogenicity

Next-generation sequencing of lung tumours from autochthonous GEMMs by our lab (data not shown) and others (McFadden et al., 2014b; Westcott et al., 2015a) have revealed very few non-synonymous somatic mutations. Since neo-antigen load contributes to immunogenicity of tumours and response to immune checkpoint blockade (Gubin et al., 2014), we reasoned that the low number of somatic mutations in *KP* lung tumours (especially in relation to human smoker's lung cancer) might contribute to the observed lack of tumour immunogenicity in the *KP* model.

A recent report has indicated that mismatch-repair (MMR)-deficient colorectal tumours are more likely to respond to PD-1 blockade with pembrolizumab than MMR-proficient colorectal tumours (Le et al., 2015). As expected, they found a greatly increased somatic mutational burden in the MMR-deficient tumours. Furthermore, tumour somatic mutational burden has recently been correlated with clinical response to PD-1 blockade in NSCLC (Rizvi et al., 2015b). Here, the authors identified mutations in *MSH2* (a key mismatch repair gene) in a lung tumour from a patient with a very high non-synonomous mutational burden and durable response to pembrolizumab.

Therefore, we attempted to increase the immunogenicity of *KP* tumours by genetically introducing MMR deficiency into the model. We reasoned that chronic, early-stage shRNA-mediated silencing of an essential component of the MMR machinery in tumour cells might contribute to an increased somatic mutation rate. We chose to silence Msh2 expression because (1) it is necessary for the formation of the Msh2: Msh6 complex that detects DNA mismatches at the first stage of the repair process (Acharya et al., 1996) and (2) it is commonly mutated in cancer with microsatellite instability and high somatic mutation frequency (de la Chapelle, 2004). For example, Lynch syndrome or hereditary non-polyposis colorectal cancer, is a condition with early-onset and a very high frequency of colorectal cancer as a result of loss of function mutations in one copy of *MSH2* (de la Chapelle, 2004).

Firstly we tested different pLKO.1 shRNA clones in KPB6 lung cancer cells to select the hairpin sequence that gave the greatest knock-down of *Msh2* gene expression. All shRNAs (5/5) knocked-down Msh2 at the protein level, but sh*Msh2.2* gave the most profound gene silencing, so we proceeded with this hairpin (henceforth referred to as sh*Msh2*) (Figure 3.20A). We then subcloned the shRNA sequence and associated promoter from pLKO.1 into a lentiviral vector expressing Cre recombinase from the Tyler Jacks laboratory (Figure 3.20B). The resulting plenti-Cre shRNA vector can be used to simultaneously initiate tumours in *KP* mice and achieve RNA interference in the nascent tumour as the construct is integrated into the genome following infection. As a control, we also generated the plenti-Cre sh*Scrambled* (sh*Scr*) construct, which is not predicted to target any known genes in the human or mouse genome. The only other modification we made to the original Jacks vector was the removal of the puromycin resistance gene, in order to prevent the expression of puromycin by tumour cells *in vivo*, which could potentially be immunogenic.

We verified the knock-down efficiency of the plenti-Cre shMsh2 construct in unselected KPB6 cells (as puromycin selection could no longer be

performed) (Figure 3.20C). We still observed substantial knock-down of Msh2 protein with this construct, considering that we did not expect to reach 100 % infection efficiency with the viral titre used. Next, we verified the Cre activity of the lentiviral constructs by infecting 3TZ reporter cells, which harbour a *LSL-LacZ* cassette under the control of a constitutively active promoter. X-gal staining can therefore be used as a readout for Cre activity. Importantly, both the plenti-Cre sh*Sc* and the plenti-Cre sh*Msh2* lentiviruses were able to initiate recombination of the LSL cassette and drive LacZ expression (Figure 3.20D). Based on these results, we proceeded to test these lentiviruses in *KP* mice by intratracheal delivery of lentivirus to the lung.

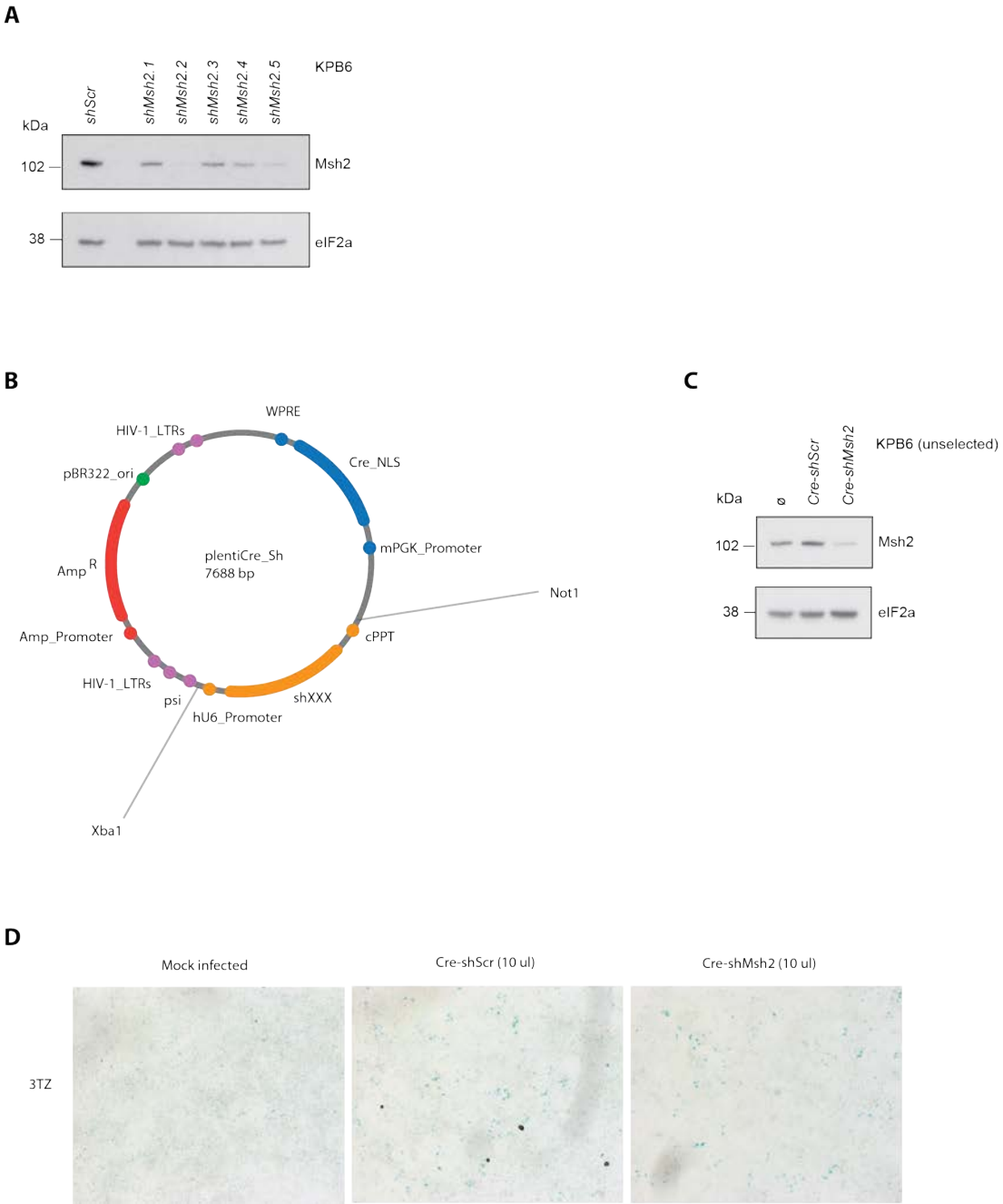

Figure 3.20 Generation of a plentiCre-shRNA contruct for *in vivo* silencing of mismatch repair machinery

(**A**) Western blotting analysis of Msh2 expression in KPB6 cells lines stably expressing the indicated pLKO.1 shRNA lentiviral constructs.
(**B**) Vector map of plentiCre-shRNA construct.
(**C**) Western blotting analysis of Msh2 expression in KPB6 cells 48 h after infection with the indicated lentivirus.
(**D**) β-galactosidase staining of 3TZ; LSL-β-galactosidase cells, 48 h after infection with the indicated lentivirus.

Both plenti-Cre sh*Sc* and plenti-Cre sh*Msh2* lentiviruses were able to initiate lung tumourigenesis *in vivo* in *KP* mice. We observed μCT-detectable tumours by 15 weeks post-infection (Figure 3.21A). Firstly, we checked knock-down of Msh2 in plenti-Cre sh*Msh2* tumours by two independent methods; (1) Western blotting (Figure 3.21B), and (2) immunohistochemistry (Figure 3.21C). Unfortunately, Msh2 levels were found to be comparable to the sh*Scr* control tumours by both methods. Notably, Msh2 protein levels were elevated in tumour tissue relative to normal adjacent lung.

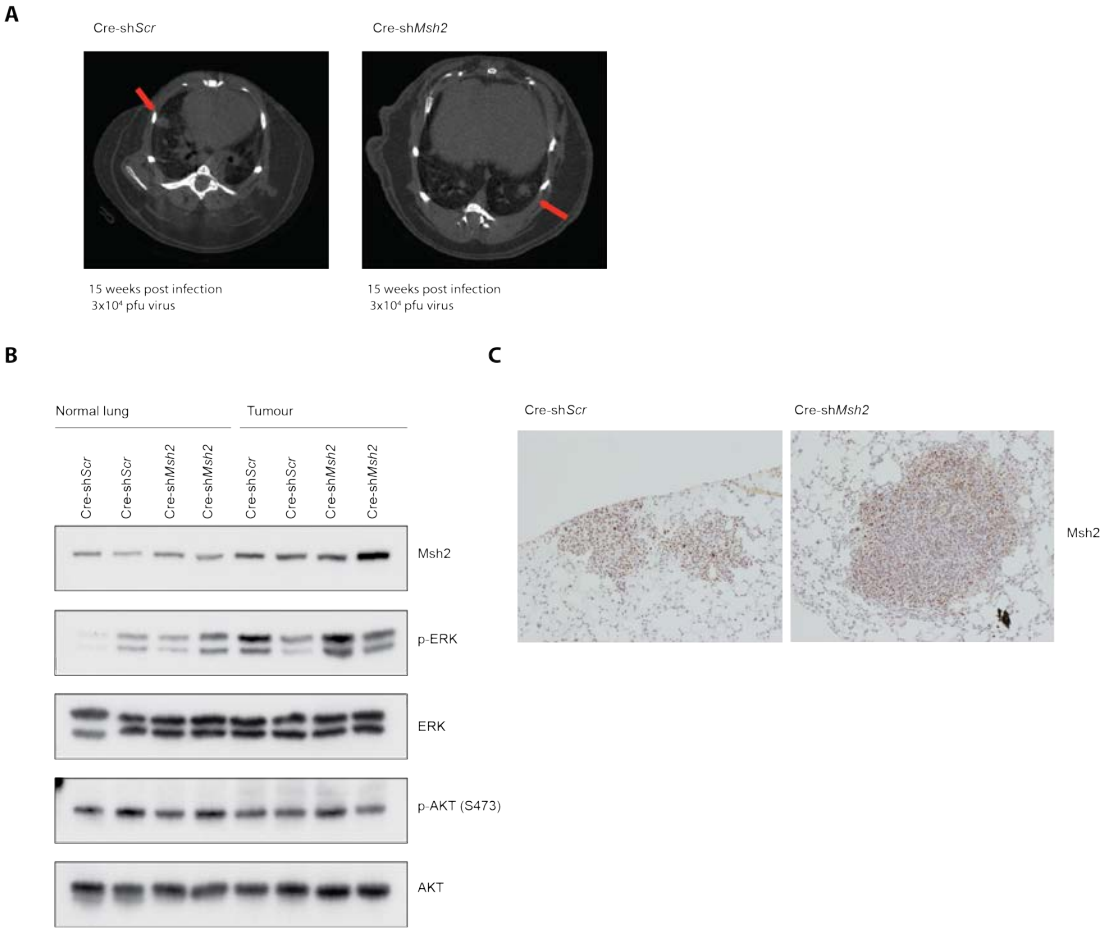

Figure 3.21 plenti Cre-shMsh2 initiates *KP* mouse lung tumourigenesis but fails to silence tumour Msh2 expression *in vivo*

(**A**) Representative μCT scans of *KP* mice 15 weeks after infection with plenti Cre-shScr and plenti Cre-shMsh2. Arrows indicate detectable lung tumours.

(**B**) Western blotting analysis of lung tumours and normal adjacent lung tissue from *KP* mice infected with the indicated lentivirus. Samples were derived from individual tumour nodules from two mice.
(**C**) Immunohistochemical analysis of Msh2 expression in tumour-bearing lungs from *KP* mice as in (A).

Taken together, these data suggest that there is selection against Msh2 silencing in lung tumours *in vivo*. We speculate that Msh2 silencing is detrimental for tumour cell survival, possibly through the deleterious accrual of somatic mutations. We speculate that the increase in Msh2 expression in lung tumour reflects the increased proliferation rate of the tumour cells and thus the increased rate of DNA replication and spontaneous mismatches arising. Indeed, we note that *MSH2* expression is increased in human lung tumours compared to matched normal lung tissue from a publically available dataset (Selamat et al., 2012) (Figure 3.22), suggesting that the tumour cell Msh2 expression from our mouse model may reflect the situation in the human disease.

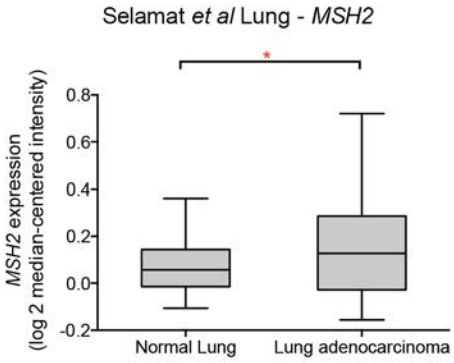

Figure 3.22 *MSH2* expression is increased in human lung tumours

Turkey box-and-whisker plot of *MSH2* mRNA expression in human, matched lung and lung adenocarcinoma samples from the Selamat *et al* dataset. Data are presented as log2-median-centered intensity. $n = 58$ per group. $^*P < 0.05$, Wilcoxen signed-rank test.

3.3 Conclusions

Our results from this chapter imply that the commonly used *KP* mouse model of lung cancer is poorly immunogenic. Most notably, our data from the *KP; Rag2-/-* model shows that adaptive immunity does not significantly restrain tumour growth in this model. Taken together with reports that the somatic mutation rate in similar GEMMs is very low, we conclude that neo-antigen burden is unlikely to be sufficient to confer sensitivity to immune checkpoint blockade. We cannot rule out that there are tumour-associated antigens in *KP* tumours that may facilitate an anti-tumour immune response. Similarly, our negative data cannot formerly exclude the possibility that there is profound immune-suppression in the *KP* model that cannot be eliminated with PD-L1 and CTLA-4 blockade alone, and is so efficient that *KP; Rag2+/-* and *KP; Rag2-/-* mice are ostensibly identical with respect to tumour progression. Hence, we aim to directly compare the *KP* model with a modified immunogenic GEMM (iGEMM). This is on going work in our laboratory. The attempted knock-down of mismatch repair enzyme Msh2 *in vivo* was unsuccessful, most likely due to strong counter-selection against Msh2 knock-down over the 15 week period usually required for tumours to become fully established. It will be interesting to test whether the same is true *in vitro*, or if the proposed counter-selection is at least partly non-cell autonomous. In future experiments, we would favour using irreversible knock-out of the target gene using CRISPR/Cas to prevent loss of gene silencing.

We were particularly interested in the observation that *KP* tumours express high levels of PD-L1 mRNA and protein, despite the apparent low immunogenicity of these tumours and the scarcity of tumour infiltrating T cells. We hypothesise that in this model, PD-L1 upregulation may be partly a tumour cell intrinsic phenomenon. The next chapter addresses the regulation of PD-L1 expression by RAS.

4 Chapter 4. Results 2. Regulation of PD-L1 by RAS and TTP *in vitro*

4.1 Introduction

The immunosuppressive molecule PD-L1 is upregulated in many cancers and contributes to evasion of the host immune system. The relative importance of the tumour microenvironment and cell-intrinsic signalling in the regulation of PD-L1 expression remains unclear. The inflammatory cytokine IFN-γ is the best-characterised stimulus for PD-L1 expression (Lee et al., 2005), however, several studies suggest cell-intrinsic oncogenic signalling can also promote PD-L1 expression in cancer cells, such as EGFR and AKT pathway activation (Akbay et al., 2013; Parsa et al., 2007). This raises the interesting concept of intrinsic tumour immunoresistance (Pardoll, 2012), in addition to adaptive evasion of the anti-tumour immune response (Schreiber et al., 2011). To date, RAS has not been directly linked to the regulation of PD-L1 expression. Studies performed on melanoma (Jiang et al., 2013) and acute myeloid leukaemia (Berthon et al., 2010) suggest that MEK signalling is implicated in the upregulation of PD-L1 in some tumour cell lines, but there are examples in melanoma where this relationship is less clear (Atefi et al., 2014), and the molecular basis of this regulation remains poorly defined.

In this chapter, I present images generated from histopathological analyses performed by Bradley Spencer-Dene and on my behalf.

4.2 Results

4.2.1 Cell-intrinsic Upregulation of PD-L1 through Oncogenic RAS Signalling

We tested the potential role of oncogenic RAS signalling itself to regulate tumour PD-L1 expression. To test whether oncogenic RAS signalling was sufficient to increase PD-L1 expression, we utilized ER-RAS^{G12V} fusion constructs, which allow for the rapid activation of oncogenic RAS signalling and downstream effectors such as MEK and PI3K with 4-hydroxytamoxifen (4-OHT). Firstly, we utilised the immortalised breast epithelial cell line MCF10A harbouring ER-HRAS^{G12V}, as this system allows for robust activation of RAS signalling (Figure 4.1A) (Molina-Arcas et al., 2013a). Initiation of oncogenic HRAS signalling led to a significant induction of *PD-L1* mRNA expression at six hours and at 24 hours (Figure 4.1B). Moreover, oncogenic RAS strongly induced PD-L1 surface protein expression in MCF10A cells, which normally only express very low levels of PD-L1 protein (Figure 4.1C).

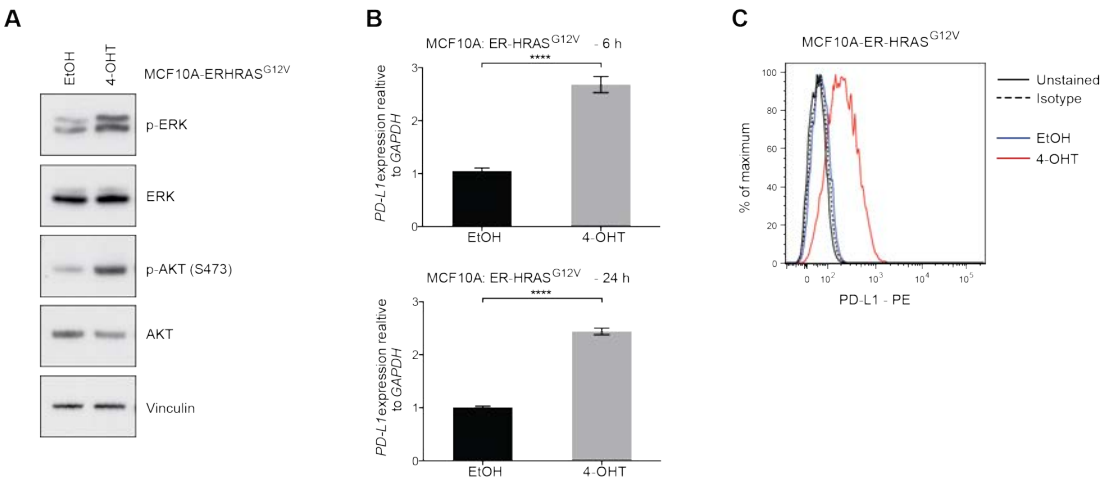

Figure 4.1 Oncogenic RAS signalling is sufficient to drive PD-L1 expression in breast epithelail cells

(**A**) Western blotting analysis of ER-HRAS^{G12V} MCF10A cells treated with 4-OHT or vehicle in starvation medium for 24 h.
(**B**) qPCR analysis of ER-HRAS^{G12V} MCF10A cells treated with 4-OHT or vehicle in starvation medium for 6 h or 24 h. Mean ± SEM of two independent experiments.
(**C**) Representative histogram from flow cytometry analysis of MCF10A-ER-HRAS^{G12V} cells treated with 4-OHT or vehicle in starvation medium for 24 h. Data are representative of two independent experiments.
4-OHT, 100 nM. ****P<0.0001, unpaired, two-tailed Student's *t*-test.

To extend our observations to a tissue type where *RAS* mutation is much more frequent, we investigated the significance of this finding in lung cells lines. Firstly, we tested *PD-L1* mRNA levels following short-term induction of KRASG12V activity in immortalised human type II pneumocytes. Downstream RAS effector signalling through ERK and PI3K was evident as early as 30 min after addition of 4-OHT (Figure 4.2A). Activation of oncogenic RAS signalling coincided with the rapid induction of *CCND1* and *c-MYC* mRNAs, as well as a strong induction of *PD-L1* mRNA expression (Figure 4.2B). At three hours post-induction, RAS signalling led to an increase of almost six fold in *PD-L1* mRNA, which was of the same order of magnitude following stimulation with IFN-γ under the same experimental conditions (~12 fold induction), indicating that the observed increase in *PD-L1* gene expression is likely to be physiologically relevant (Figure 4.2C). Finally, long-term activation of oncogenic RAS over four-days led to a profound increase in PD-L1 protein expression at the cell surface as measured by flow cytometry (Figure 4.2D). We observed a much higher basal level of PD-L1 protein expression in the immortalised lung cell lines used compared to MCF10A cells, but a significant further induction of PD-L1 expression was still achieved with the activation of KRAS G12V. Taken together with the data from MCF10A cells, these results suggest that the observed PD-L1 induction by RAS is not a RAS isoform-specific, or a tissue-specific phenomenon.

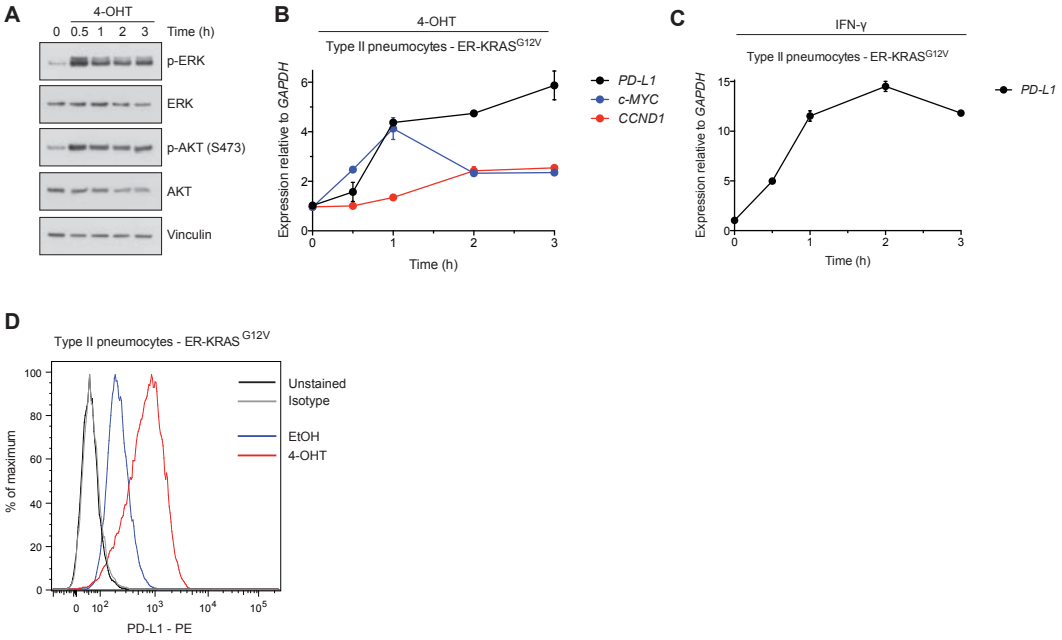

Figure 4.2 Oncogenic RAS signalling is sufficient to drive PD-L1 expression in lung cells

(**A**) Western blotting analysis of serum-starved type II pneumocyte cells harbouring an ER-KRAS^{G12V} construct, stimulated with 4-OHT for the indicated times.
(**B**) qPCR analysis of mRNA expression from the experiment described in (A). Data represent the mean ±SEM of duplicates.
(**C**) qPCR analysis of *PD-L1* mRNA expression in serum-starved type II pneumocyte cells harbouring an ER-KRAS^{G12V} construct, stimulated with IFN-γ for the indicated times. Data represent the mean ±SEM of duplicates.
(**D**) Flow cytometry analysis of PD-L1 protein surface expression in serum-starved type II pneumocyte cells harbouring an ER-KRAS^{G12V} construct, stimulated with 4-OHT or vehicle control for 4 d.
4-OHT, 100 nM. IFN-γ, 20 ng/ml.

Similarly, induction of oncogenic KRAS signalling (Figure 4.3A) increased PD-L1 surface protein expression in immortalised human type II pneumocyte and NL-20 lung cell lines at the shorter time-point of 24 h post-RAS induction (Figure 4.3A and Figure 4.3B). To dissect which downstream effectors of RAS are responsible for regulating PD-L1 expression, we used the specific inhibitors of MEK and pan type I PI3Ks, GSK1120212 (trametinib) and GDC-0941 (pictilisib), respectively. These inhibitors strongly reversed the

activation of ERK and AKT signalling, respectively, downstream of RAS (Figure 4.3A). Notably, the increased PD-L1 surface protein expression following activation of oncogenic KRAS signalling could be blocked by both the MEK and PI3K inhibitors, either alone, or in combination (Figure 4.3C). MEK inhibition also significantly reversed KRAS-mediated *PD-L1* upregulation at the mRNA level, however PI3K inhibition only reduced PD-L1 protein expression (Figure 4.3D). This effect is concordant with evidence for AKT signalling specifically increasing PD-L1 expression predominantly through activating translation of the transcript (Parsa et al., 2007).

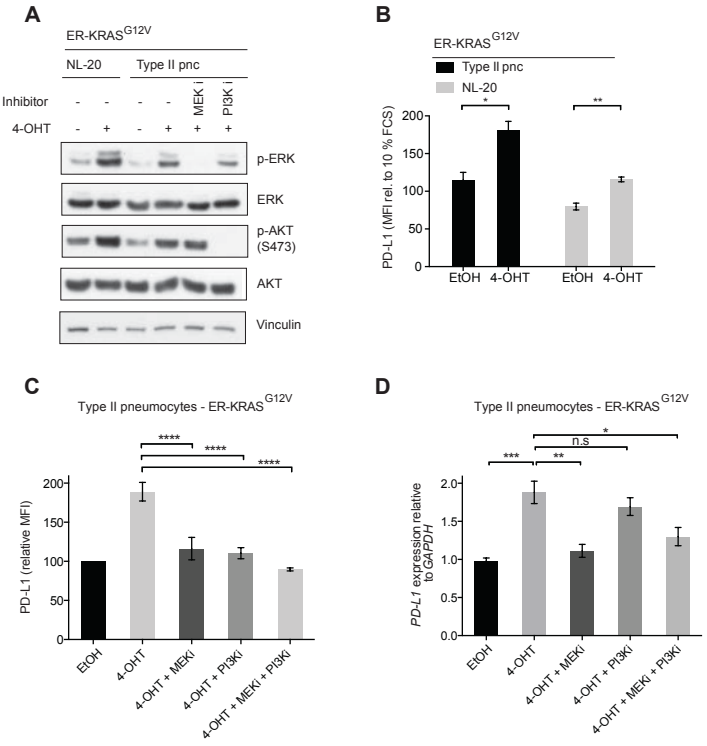

Figure 4.3 Oncogenic RAS signalling drives PD-L1 expression through MEK and PI3K pathways

(**A**) Western blotting analysis of ER-KRAS^{G12V} NL-20 cells and ER-KRAS^{G12V} type II pneumocytes treated with 4-OHT, MEK inhibitor or PI3K inhibitor in starvation medium for 24 h.
(**B**) Flow cytometry analysis of PD-L1 expression in ER-KRAS^{G12V} NL-20 cells and ER-KRAS^{G12V} type II pneumocytes treated with 4-OHT or vehicle in

starvation medium for 24 h. Data represent the mean ± SEM of three independent experiments and are relative to 10 % FCS medium controls.
(**C**) Flow cytometry analysis of ER-KRAS^{G12V} type II pneumocytes treated with 4-OHT, MEK inhibitor and PI3K inhibitor in starvation medium for 24 h. Mean ± SD of two independent experiments.
(**D**) qPCR analysis from the experiment described in (D). Mean ± SEM of biological triplicates.
MFI, Mean Fluorescence Intensity. 4-OHT, 100 nM. MEK inhibitor GSK1120212, 25 nM. PI3K inhibitor GDC-0941, 500 nM. ****P<0.0001, ***P<0.001, **P<0.01, *P<0.05, n.s; not significant. Unpaired, two-tailed Student's *t*-tests.

We verified that the induction of PD-L1 expression by 4-OHT treatment was attributable to the induction of RAS activity in the RAS-ER cell, rather than other effects including the activity of endogenous oestrogen receptor protein by treating parental MCF10A and type II pneumocyte cells with 4-OHT (Figure 4.4). As expected, there was no change in PD-L1 expression in the absence of expression of the RAS-ER constructs.

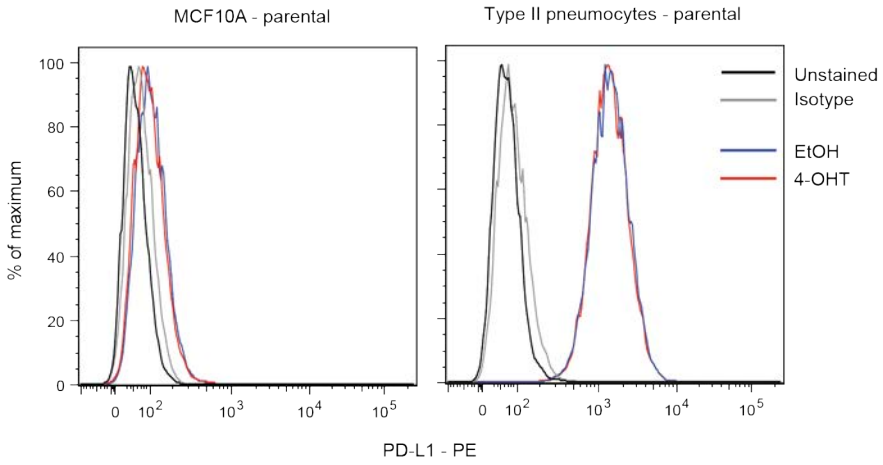

Figure 4.4 Parental MCF10A and type II pneumocyte cells do not respond to 4-OHT

Parental MCF10A and type II penumocytes were treated with 4-OHT (100 nM) or ethanol control for 24 h before FACS analysis of surface PD-L1 expression.

To test if PD-L1 induction was stimulated by general oncogenic stress, or if this was an effect specific to oncogenic RAS and RAS-effector signalling, we introduced a doxycycline-inducible *c-MYC* construct into immortalised NL-20

lung epithelial cells. However, overexpression of *c-MYC* expression was not able to increase *PD-L1* expression (Figure 4.5), despite massive upregulation of *c-MYC* in these cells. This suggests that the regulation of PD-L1 expression is not a general phenomenon associated with oncogene activation. However, our results are contrary to a recent report that oncogenic MYC upregulates PD-L1 expression in T cell acute lymphoblastic leukaemia, possibly reflecting tissue-specific differences (Casey et al., 2016b).

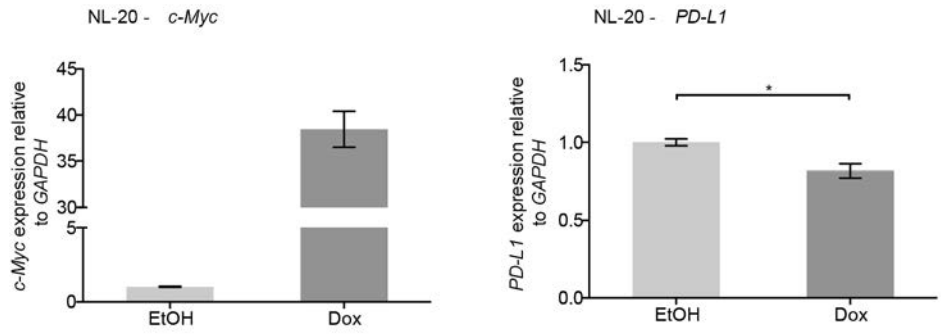

Figure 4.5 Oncogenic stress through forced MYC overexpression does not drive *PD-L1* expression

qPCR analysis of *c-MYC* and *PD-L1* expression in NL-20 cells harboring a doxycyline-inducible MYC construct (pSLIK MYC), 24 h after the addition of 1 *μ*g/ml doxycycline. Data represent the mean ± SD. **P*<0.05; unpaired, two-tailed Student's *t*-test.

Next, we wanted to assess if the regulation of PD-L1 expression by RAS was operating by a strictly cell-intrinsic mechanism, because we reasoned that activation of oncogenic RAS signalling has been linked to increased production of IL-6 (Ancrile et al., 2007), which may activate STAT signalling and thus PD-L1 expression. Hence, RAS might control PD-L1 expression via an autocrine loop. To test this hypothesis, we analysed the effect of adding conditioned medium from RAS-active type II pneumocyte cells to unstimulated cells. Firstly, we observed that activation of oncogenic RAS signalling in type II pneumocytes did not increase IL-6 mRNA levels (Figure 4.6A). Furthermore, conditioned medium from RAS-stimulated cells did not have significant effects on PD-L1 protein expression on parental type II

pneumocytes (Figure 4.6B), collectively implying that RAS controls PD-L1 expression independently of IL-6 and independently of other autocrine factors.

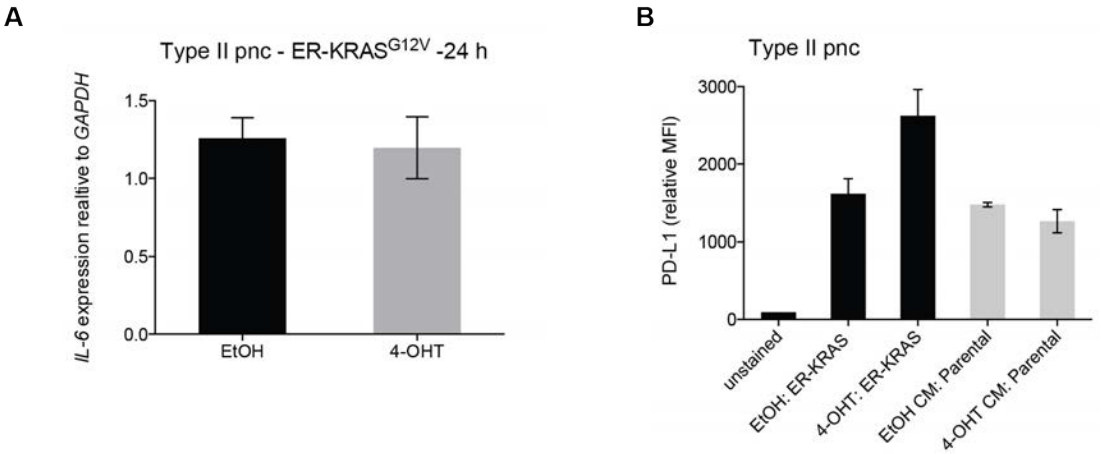

Figure 4.6 PD-L1 induction by RAS *in vitro* is not mediated by an autocrine-loop

(**A**) qPCR analysis of IL-6 expression in ER-KRASG12V type ii pneumocytes 24 h after the addition of 4-OHT. Mean ± SEM of biological triplicates.
(**B**) Flow cytometry analysis of surface PD-L1 protein expression in parental type ii pneumocytes after 24 h incubation with conditioned medium derived from ER-KRASG12V type ii pneumocytes activated with 4-OHT for 24 h. Mean ± SEM of biological triplicates.
4-OHT, 100 nM.

To assess whether more potent, acute activation of MEK signalling was also capable of inducing PD-L1 expression in a manner comparable to oncogenic RAS, we used the phorbol ester PMA, a potent chemical activator of MEK-ERK signalling (Rusanescu et al., 2001). We observed a dramatic and rapid increase in PD-L1 expression in H358 cells, an effect that was largely reversed with the inhibition of MEK (Figure 4.7A), functionally excluding other pathways that may be activated by phorbol ester treatment, such as protein kinase C. This result suggests that other pathways that may activate MEK signalling are potentially relevant in the regulation of PD-L1 in cancer.

Furthermore, MEK inhibition, but not PI3K inhibition, significantly reduced *PD-L1* mRNA expression in *KRAS*-mutant lung cancer cell line H358 (Figure 4.7B), suggesting that basal levels of oncogenic RAS signalling are important for driving PD-L1 upregulation. This result is also consistent with Figure 4.3C and Figure 4.3D, which indicates that PI3K signalling regulates PD-L1 at the protein but not the mRNA level.

More extensive analysis of PD-L1 surface expression on multiple human and mouse *KRAS*-mutant lung cancer cell lines revealed generally consistent PD-L1 downregulation following MEK and PI3K inhibition, suggesting this regulatory pathway is of broad significance (Figure 4.7C). PD-L1 expression on H1792 cells responded least to inhibition of RAS effector pathways, possibly reflecting that this cell line had low basal PD-L1 expression compared to H358 cells, for example, which expressed the highest levels of PD-L1 (data not shown). Taken together, these results suggest that oncogenic RAS signalling through MEK and PI3K is sufficient to drive PD-L1 expression.

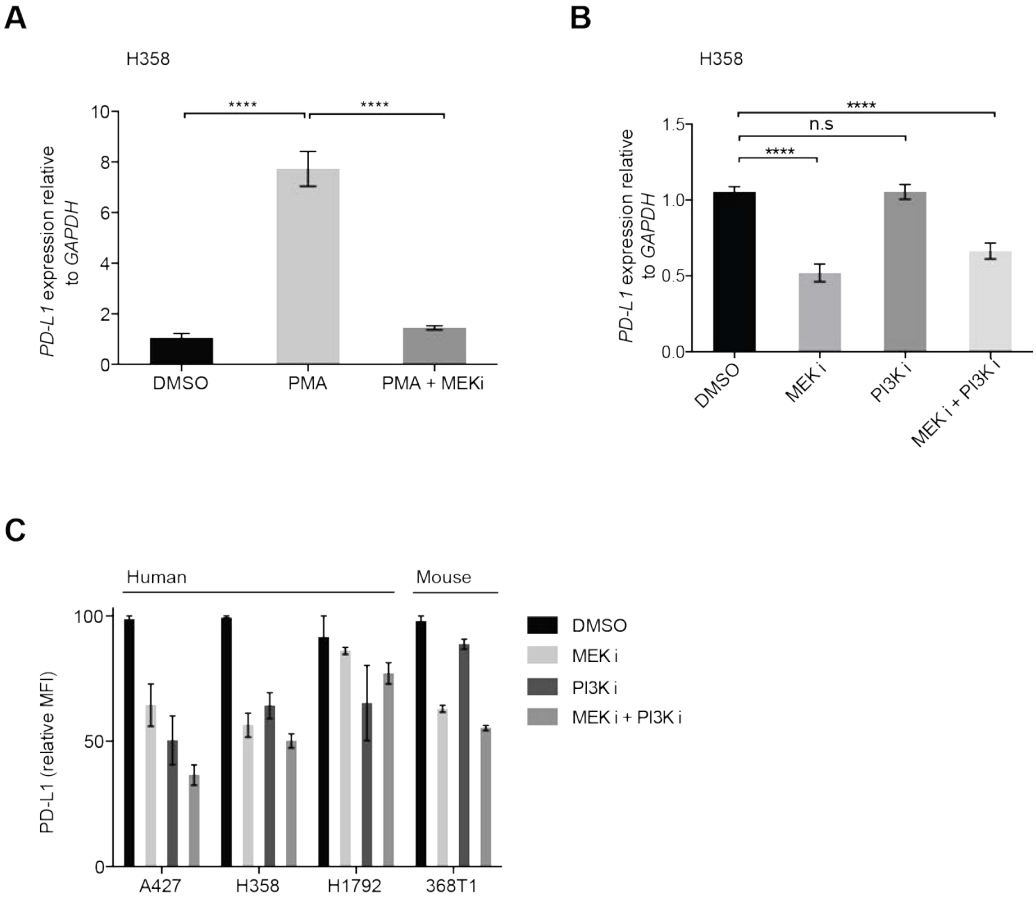

Figure 4.7 MEK and PI3K inhibition reduces RAS-driven PD-L1 expression

(**A**) qPCR analysis of H358 cells treated with PMA for 3 h following a 30 min pre-treatment with DMSO or MEK inhibitor. Mean ± SD of two independent experiments.
(**B**) qPCR analysis of H358 cells treated with MEK inhibitor and PI3K inhibitor for 24 h. Mean ± SEM of two independent experiments.
(**C**) Surface expression of PD-L1 was measured by flow cytometry. MFI values are adjusted for the isotype control in each condition. Data represent the mean ± SEM.
MFI, Mean Fluorescence Intensity. MEK inhibitor GSK1120212, 25 nM. PI3K inhibitor GDC-0941, 500 nM. PMA, 200 nM. ****P<0.0001, n.s; not significant. Unpaired, two-tailed Student's *t*-tests.

To extend our observations to a non-malignant setting, we considered the potential regulation of PD-L1 by wild-type RAS in T lymphocytes. PD-L1 is strongly upregulated in stimulated T cells following engagement of the T cell receptor. As signalling downstream of the T cell receptor relies on RAS signalling (Downward et al., 1990a), we tested to what extent PD-L1

induction was dependent on MEK activity in this system. To this end, we stimulated CD4 T cell lymphoma EL4 cells with anti-CD3 and anti-CD28 beads and measured stimulation and PD-L1 induction by flow cytometry. We used EL4 cells as a model system to obviate primary T cell isolation from animals in these preliminary experiments.

As expected, T cell receptor signalling in stimulated EL4 cells resulted in upregulation of the activation marker CD69 and coordinate upregulation of PD-L1 expression, although only modestly and only in a subset of cells, perhaps due to aberrant oncogenic signalling in these cancer cells and the high basal levels of PD-L1 (Figure 4.8). However, inhibition of MEK signalling completely reversed activation of both CD69 and PD-L1 expression, and even slightly decreased PD-L1 levels to below basal (unstimulated) levels (Figure 4.8), implying that this regulatory pathway may also have functional significance in T cell PD-L1 expression. This hypothesis will require further testing in untransformed T cells.

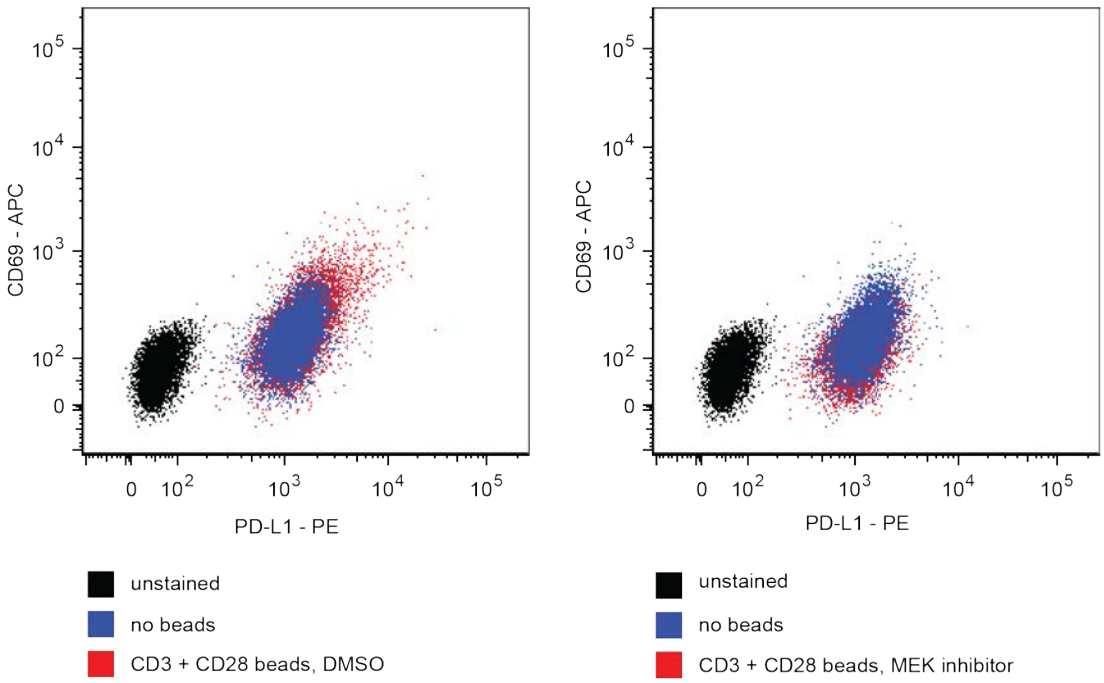

Figure 4.8 T cell receptor-dependent induction of PD-L1 is dependent on MEK activity

Flow cytometry analysis of surface protein PD-L1 and CD69 expression on unstimulated or CD3 + CD28 bead stimulated (24 h) with EL4 T cell lymphoma cells. Cells were co-treated with DMSO vehicle or MEK inhibitor GSK1120212, 25 nM.

4.2.2 RAS Signalling Increases *PD-L1* mRNA Stability through AU-rich Elements in the 3'UTR

To investigate how RAS-MEK signalling regulates PD-L1 expression mechanistically, we first asked whether RAS regulates PD-L1 via a transcriptional mechanism by inducing oncogenic KRAS signalling with 4-OHT in ER-KRAS^{G12V} type II pneumocytes and concomitantly blocking transcription with actinomycin D (Figure 4.9A). Surprisingly, we found human *PD-L1* mRNA to have a short half-life, which was significantly stabilised by the induction of oncogenic KRAS signalling (Figure 4.9A). Moreover, murine *PD-L1* mRNA also had a comparably short half-life, and the stability of the transcript could be reduced further still when MEK was inhibited (Figure 4.9B), implicating KRAS-MEK signalling in the stabilization of the labile *PD-L1* transcript. Inhibition of PI3K, however, did not result in altered *PD-L1* mRNA stability in KPB6 cancer cells (Figure 4.9C). This corroborates our data showing that PI3K pathway activity does not influence *PD-L1* mRNA expression in cancer cells, but rather PD-L1 protein levels.

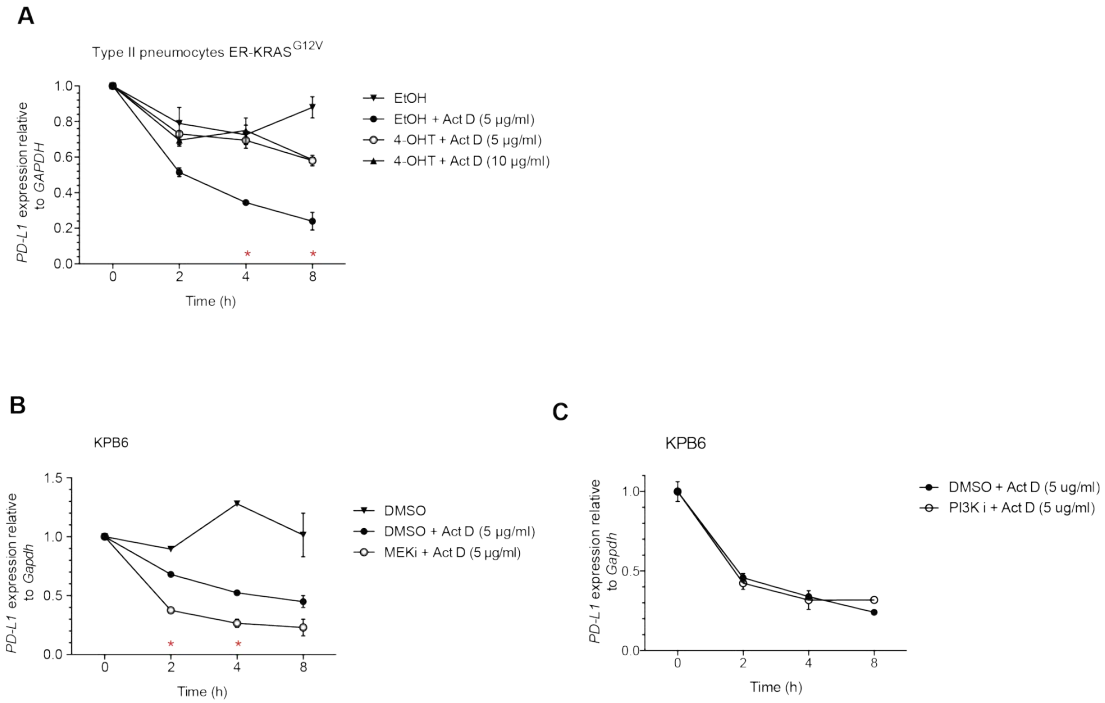

Figure 4.9 RAS-MEK signalling controls *PD-L1* mRNA stability

(**A**) Stability of human *PD-L1* mRNA measured by qPCR in ER-KRAS^{G12V} type II pneumocytes in starvation medium after the concomitant addition of actinomycin D (5 *µ*g/ml or 10 *µ*g/ml) and 4-OHT or vehicle. Values are normalized to the 0 h time point when actinomycin D was added. Mean ± SEM of two independent experiments. **P*<0.05; comparing 4 h and 8 h time-points of EtOH + 5 *µ*g/ml ActD, and 4-OHT + 5 *µ*g/ml ActD.
(**B**) Stability of murine *PD-L1* mRNA measured by qPCR after the addition of actinomycin D (5 *µ*g/ml) and DMSO or MEK inhibitor. KPB6 cells were pre-treated with DMSO or MEK inhibitor for 30 min before actinomycin D addition. Values are normalized to the 0 h time point when actinomycin D was added. Mean ± SEM of two independent experiments. **P*<0.05; comparing 2 h and 4 h time-points of DMSO + 5 *µ*g/ml ActD, and MEKi + 5 *µ*g/ml ActD.
(**C**) Stability of murine *PD-L1* mRNA measured by qPCR after the addition of actinomycin D (5 µg/ml) and DMSO or PI3K inhibitor GDC-0941 (500 nM). KPB6 cells were pre-treated with DMSO or PI3K inhibitor for 30 min before actinomycin D addition. Data represent the mean ± SEM and are normalized to the 0 h time point when actinomycin D was added, and are representative of two independent experiments.
4-OHT, 100 nM. MEK inhibitor GSK1120212, 25 nM. ****P*<0.0005, **P*<0.05, n.s; not significant. Unpaired, two-tailed Student's *t*-tests.

Common genetic elements conferring mRNA instability include miRNA binding sites and AU-rich elements (AREs) in the 3'UTR of the transcript (Garneau et al., 2007). The core motif for AREs is an ATTTA pentamer

sequence, however functional AREs are often found in an AU-rich context, conforming to the WWATTTAWW nonamer consensus (where W denotes an A or T) (Zubiaga et al., 1995) constituting the binding site for several AU-rich element binding proteins (AUBPs) (Brooks and Blackshear, 2013), which can subsequently recruit mRNA decay machinery (Lykke-Andersen and Wagner, 2005). Upon inspection of the 3'UTR of *PD-L1*, we noted a high number of ARE pentamers. Specifically, out of 14 ATTTA pentamer sequences in the human transcript and 11 in the murine transcript, there were three conserved AREs conforming to the nonamer consensus (Figure 4.10A and Figure 4.10B). Using standard nomenclature, this arrangement conforms to class I AREs.

Figure 4.10 *PD-L1 3'UTR* contains multiple conserved AU-rich elements

(**A**) DNA sequence of human and mouse *PD-L1 3'UTR* showing ATTTA pentamer sequences in red.
(**B**) Sequence alignment of murine and human *PD-L1* 3'UTR showing fragments containing the three most highly conserved ATTTA pentamer sequences in AU-rich context highlighted in red.
(**C**) Schematic representation of the murine and human *PD-L1* mRNA. AU-rich element ATTTA pentamer sequences are in orange, and highly conserved pentamers are in red.

To analyse the functional importance of these AREs, we constructed a luciferase reporter containing a fragment of the 3'UTR of human *PD-L1* containing the last six ATTTA pentamers, including the three conserved nonamer sequences (Figure 4.11C). It has been shown that mutation of functional ATTTA pentamers to ATGTA can increase the expression of the ARE-containing mRNA (Rajagopalan et al., 1995; Yang et al., 2004). Indeed, mutating the six ATTTA pentamer sequences to ATGTA increased expression of the *PD-L1 3'UTR* luciferase reporter in ER-HRAS^{G12V} MCF10A and H358 cells, suggesting these AREs are functionally relevant for controlling the expression of PD-L1 (Figure 4.11A and Figure 4.11B).

Crucially, stimulation with 4-OHT in ER-HRAS^{G12V} MCF10A cells, or PMA in H358 cells, increased expression of the wild-type reporter, whereas the ATGTA mutant reporter was insensitive to these treatments (Figure 4.11A and Figure 4.11B). In sum, these data suggest that AREs in the 3'UTR of *PD-L1* mRNA can mediate control of PD-L1 expression by RAS-MEK signalling.

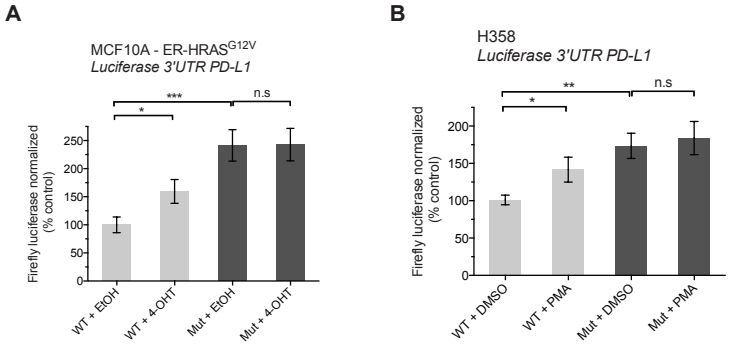

Figure 4.11 AU-rich elements control the expression of *PD-L1* mRNA downstream of RAS

(**A**) Luciferase reporter expression from a reporter containing a wild-type (ATTTA x 6) or mutant (ATGTA x 6) fragment of the human *PD-L1*-3'UTR after 4-OHT or vehicle treatment for 24 h in starvation medium. Data are normalized to a Renilla luciferase internal control and represent the mean ± SEM of three independent experiments.
(**B**) Luciferase expression from a reporter containing a wild-type (ATTTA x 6) or mutant (ATGTA x 6) fragment of the human *PD-L1* 3'UTR after DMSO or PMA (200 nM) treatment for 6 h. Data are normalized to a Renilla luciferase internal control and represent the mean ± SEM of three independent experiments.
4-OHT, 100 nM. ***P<0.0005, **P<0.005; *P<0.05; N.s; not significant; unpaired, two-tailed Student's *t*-test.

4.2.3 AU-rich element Binding Proteins TTP and KSRP are Negative Regulators of PD-L1 Expression

To assess which AU-rich element binding proteins (AUBPs) could mediate regulation of PD-L1 expression downstream of RAS signalling, we first performed a selected siRNA screen of likely candidate genes: *AUF1*, *KSRP*, *HuR* and *TTP* (also known as tristetraprolin or *ZFP36*), in three *RAS* mutant lung cancer cell lines (Figure 4.12A-C). Knockdown efficiency was verified in each case by qPCR (Figure 4.12D-F). siRNA-mediated knockdown of *KSRP* and *TTP* had the strongest and most consistent effects on *PD-L1* mRNA expression across the cell line panel. Knockdown of either *KSRP* or *TTP*

increased *PD-L1* expression, suggesting they are negative regulators of *PD-L1* expression.

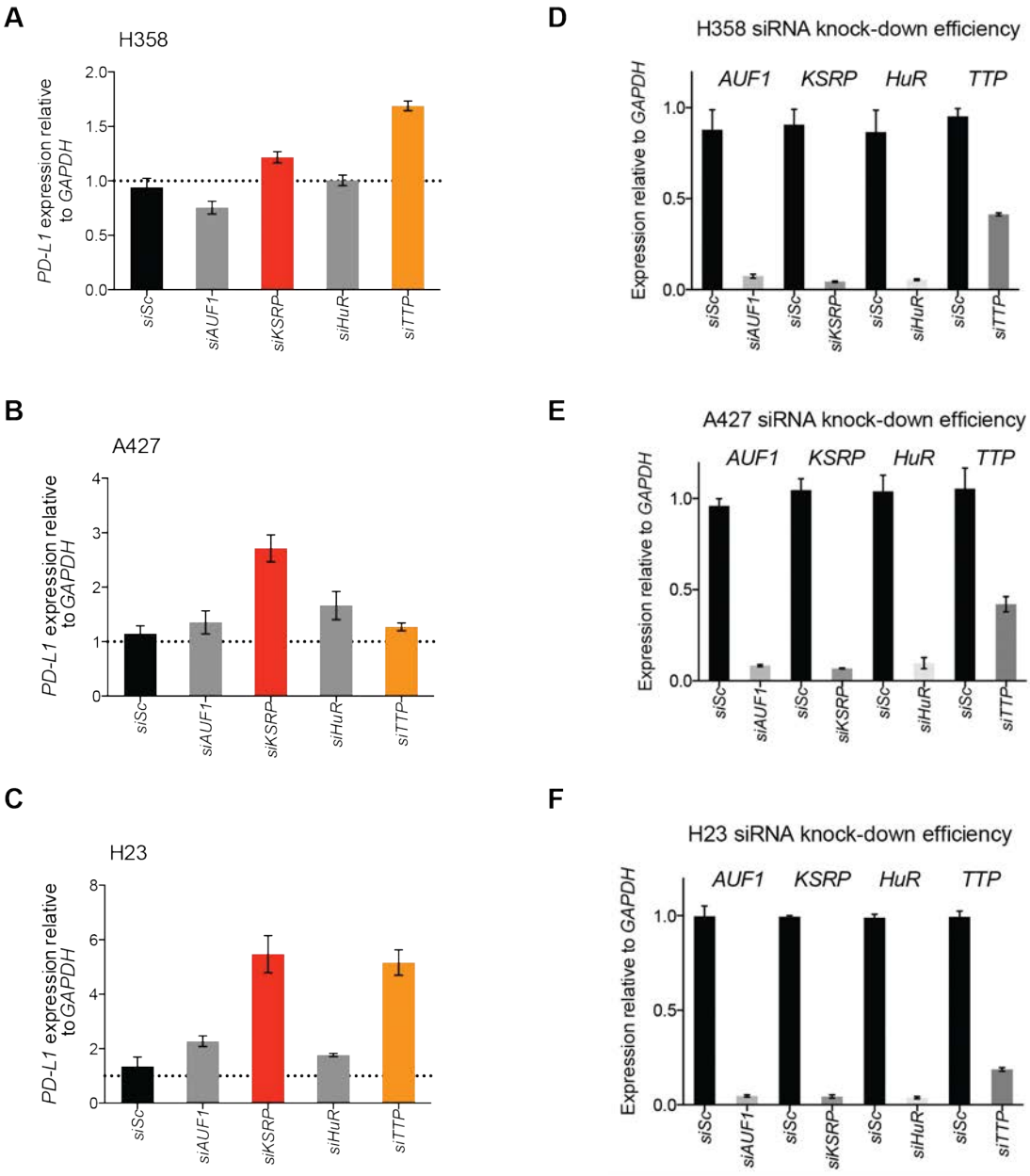

Figure 4.12 A selective siRNA-mediated screen of AU-rich element binding proteins reveals TTP and KSRP as novel negative regulators of *PD-L1* expression

(**A**-**C**) qPCR analysis of *PD-L1* expression and verification of knock-down (**D**-**E**), 48 h after transfection with siRNAs targeting AU-rich binding proteins (AU-BPs) in H358, A427 and H23 cells relative to siScrambled (siSc) control. Mean ± SD of biological triplicates.

TTP is a member of a small family of related protein, including ZFP36L1 (or BRF-1) and ZFP36-L2 (or BRF-2), which are less well-studied RNA-binding proteins with ostensibly similar roles in destabilising mRNA targets, but with limited overlap in mRNA targets (Adachi et al., 2014). Therefore we tested the potential functional contribution of BRF-1 and BRF-2 on PD-L1 regulation. However, siRNA-mediated knockdown of the expression of TTP family members BRF-1 and BRF-2 was incapable of increasing *PD-L1* expression to the extent achieved by silencing TTP expression (Figure 4.13A and Figure 4.13B), indicating a degree of mechanistic specificity for TTP itself in this pathway.

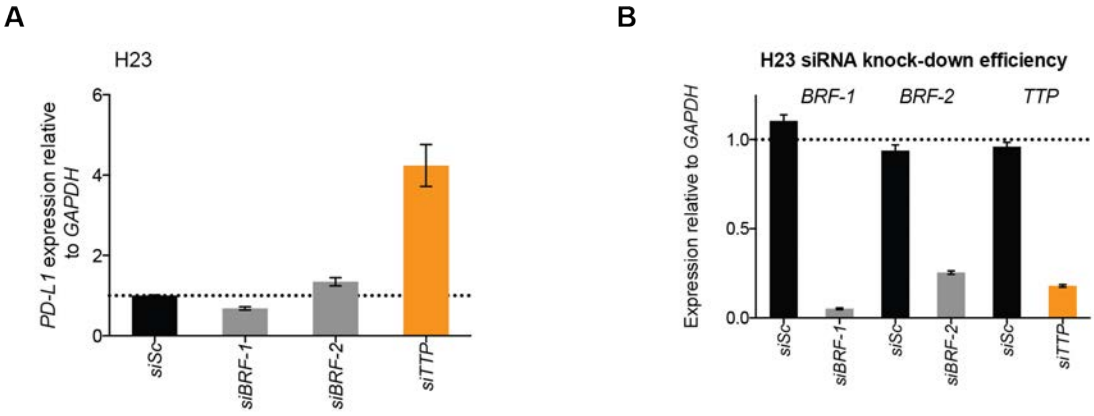

Figure 4.13 Knock-down of TTP family members BRF-1 and BRF-2 does not increase *PD-L1* expression

(**A**) qPCR analysis of *PD-L1* expression in H23 cells 48 h after transfection with siRNAs targeting AU-rich binding proteins (AU-BPs), relative to siScrambled (siSc) control. Data represent the mean ± SEM of two independent experiments.
(**B**) qPCR analysis of knock-down efficiency in H23 cells 48 h after siRNA transfections, relative to siScrambled control. Data represent the mean ± SEM of two independent experiments.

Overexpression of KSRP or TTP was sufficient to significantly decrease *PD-L1* expression (Figure 4.14A and Figure 4.14B) and *PD-L1 3'UTR* luciferase reporter expression in H358 cells (Figure 4.15A and Figure 4.15B), corroborating our results from the siRNA screen and confirming that KSRP and TTP impart their control on *PD-L1* expression through the 3'UTR of the

transcript. However, overexpression of KSRP and TTP together did not have a marked additive effect on the expression of *PD-L1* (Figure 4.14), or the *PD-L1 3'UTR* luciferase reporter (Figure 4.15). This may reflect a degree of redundancy in their role, or that they do not functionally cooperate to destabilise *PD-L1* mRNA.

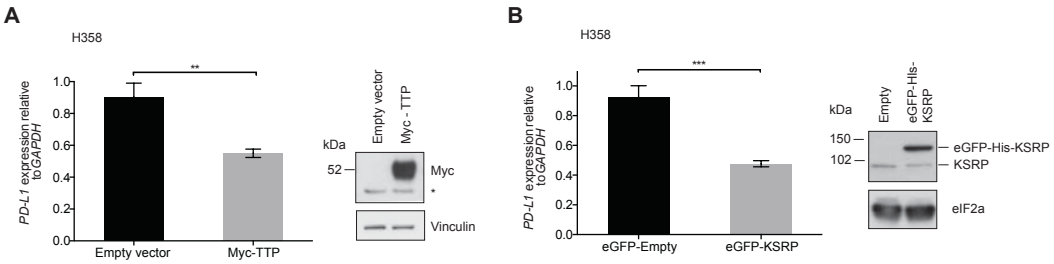

Figure 4.14 Overexpression of TTP and KSRP decreases *PD-L1* expression

(**A**) qPCR and Western blotting analysis of H358 cells 24 h after transfection with empty or Myc-TTP constructs. qPCR data represent the mean ± SD of biological triplicates and are representative of two independent experiments. *, non-specific band.
(**B**) qPCR and Western blotting analysis of H358 cells 24 h after transfection with empty or KSRP constructs. qPCR data represent the mean ± SD of biological triplicates and are representative of two independent experiments. ***P<0.001, **P<0.01. Unpaired, two-tailed Student's t-test.

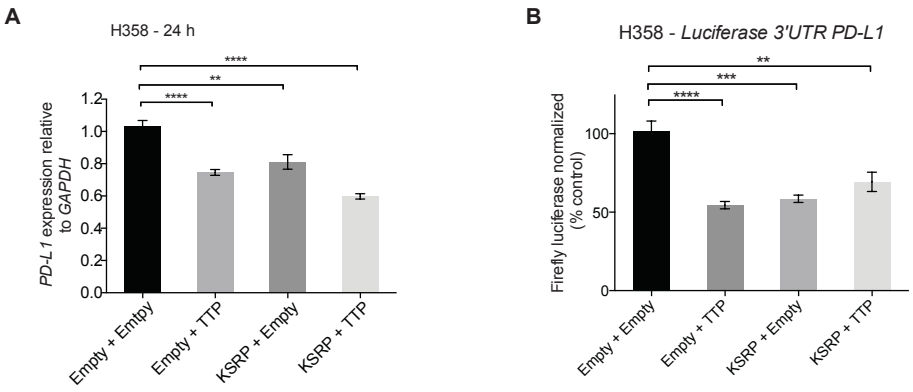

Figure 4.15 TTP and KSRP impart their negative control of *PD-L1* mRNA through the 3'UTR, but do not cooperate

(**A**) qPCR analysis of *PD-L1* expression 24 h after transfection with the indicated constructs. Data represent the mean ± SEM of two independent experiments.
(**B**) Luciferase expression from a reporter containing a fragment of the human, wild type *PD-L1*-3'UTR 24 h after co-transfection with the indicated constructs. Data are normalized to a Renilla luciferase internal control and represent the mean ± SEM of two independent experiments.
*****P*<0.0001, ****P*<0.001, ***P*<0.01; unpaired, two-tailed Student's *t*-test.

We further examined the regulation of *PD-L1* mRNA by TTP by using TTP WT and TTP KO MEFs. In the TTP KO MEFs, *TTP* mRNA is expressed but no functional TTP protein can be made due to the introduction of a premature stop codon at the endogenous locus (Lai et al., 2006; Taylor et al., 1996). As expected, the total absence of functional TTP protein in the TTP KO MEFs increased the half-life of *PD-L1* mRNA relative to TTP WT MEFs (Figure 4.16A). Moreover, acute activation of *TTP* expression with serum temporally coincided with a dramatic and transient decrease in *PD-L1* mRNA in TTP WT MEFs, but not in the TTP KO MEFs (Figure 4.16B), with *PD-L1* levels recovering to near baseline at 6 h after serum addition. In sum, these data provide evidence for the negative regulation of *PD-L1* mRNA expression by the AUBPs KSRP and TTP.

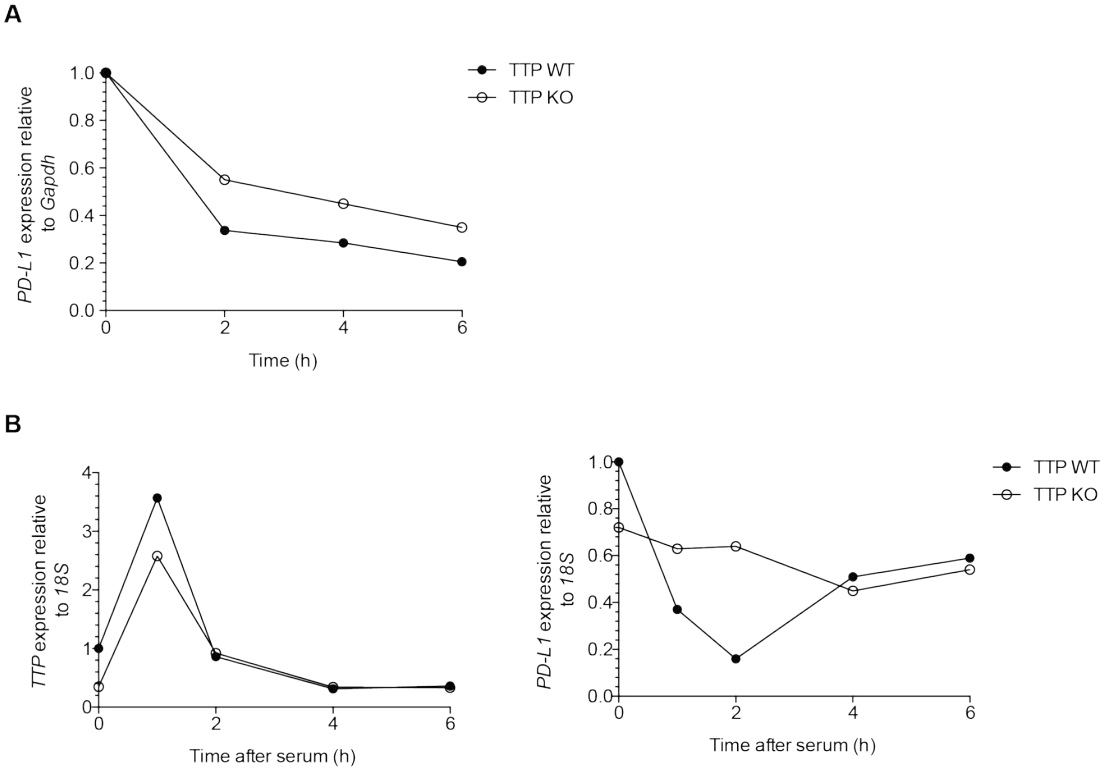

Figure 4.16 PD-L1 mRNA is stabilised in TTP KO MEFs

(**A**) Stability of murine *PD-L1* mRNA measured by qPCR after the addition of actinomycin D (5 µg/ml) in TTP WT or TTP KO MEFs. Values are normalized to the 0 h time point when actinomycin D was added and are representative of two independent experiments.
(**B**) qPCR analysis of *TTP* expression and *PD-L1* expression following serum stimulation in serum-starved TTP WT or TTP KO MEFs. Data are representative of two independent experiments.

4.2.4 RAS Regulates *PD-L1* Expression through TTP

To address how RAS signalling controls *PD-L1* mRNA stability and expression, we tested whether the RAS pathway regulates the activity of KSRP and/or TTP. Firstly, to test whether AUBP binding to the mRNA was subject to regulation by RAS-MEK signalling, we performed RNA immunoprecipitation with antibodies against KSRP or TTP in KPB6 mouse lung cancer cells treated with DMSO or MEK inhibitor. Notably, our trial experiments of RNA immunopreciptation using anti-TTP antibodies failed to show binding to *PD-L1* mRNA, however, it transpired that this was due to the

inclusion of EDTA in the immunoprecipitation buffers (not shown). TTP is a zinc-finger protein so chelation of zinc ions by EDTA renders the protein unable to bind RNA.

Using a revised protocol excluding EDTA from all buffers, we found that TTP and KSRP both significantly co-precipitated with *PD-L1* mRNA, implying they directly regulate PD-L1 expression through binding the transcript (Figure 4.17A and Figure 4.17B), however MEK inhibition did not significantly alter the occupancy of TTP or KSRP on *PD-L1* mRNA. Importantly, the high degree of enrichment for *PD-L1* mRNA in TTP and KSRP immunoprecipitates was not observed for a control mRNA (*Gapdh*) lacking AREs in the 3'UTR (Figure 4.17C and Figure 4.17D), verifying the relative specificity of the immunoprecipitation reactions. We observed a small degree of enrichment of *Gapdh* mRNA in the anti-KSRP RNA-IP control experiments, but this was approximately five-fold lower in terms of percentage input that *PD-L1* mRNA.

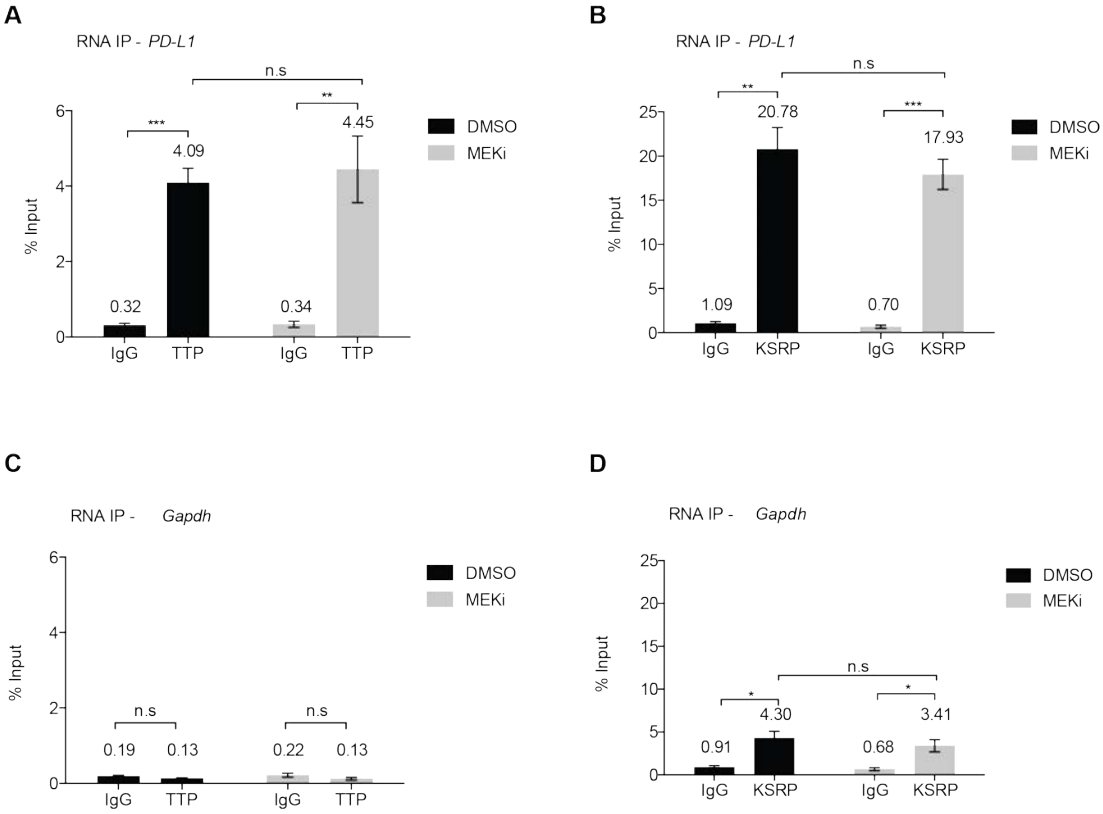

Figure 4.17 TTP and KSRP bind to *PD-L1* mRNA, but their occupancy is not affected by MEK activity

(**A** and **B**) qPCR analysis of *PD-L1* mRNA from RNA immunoprecipitates using IgG control or anti-TTP antibody, or in (B), anti-KSRP antibody, from KPB6 cells treated with DMSO or MEK inhibitor for 5.5 h. Mean ± SD of biological triplicate IPs.
(**C** and **D**) qPCR analysis of *Gapdh* control mRNA from RNA immunoprecipitates using IgG control or anti-TTP antibody, or in (B), anti-KSRP antibody, with lysate from KPB6 cells pre-treated with DMSO or MEK inhibitor GSK1120212 for 5.5 h (25 nM). Data represent the mean ± SD of biological triplicate IPs.
MEK inhibitor, GSK1120212, 25 nM. ****P<0.0001, ***P<0.001, **P<0.01, n.s; not significant; unpaired, two-tailed Student's *t*-test.

We also verified the binding of TTP to *PD-L1* mRNA in the human NSCLC cell line H358 (Figure 4.18). Although the relative levels of TTP binding to *PD-L1* mRNA was lower in this setting, we still observed significant binding o TTP to the transcript relative to the *GAPDH* control.

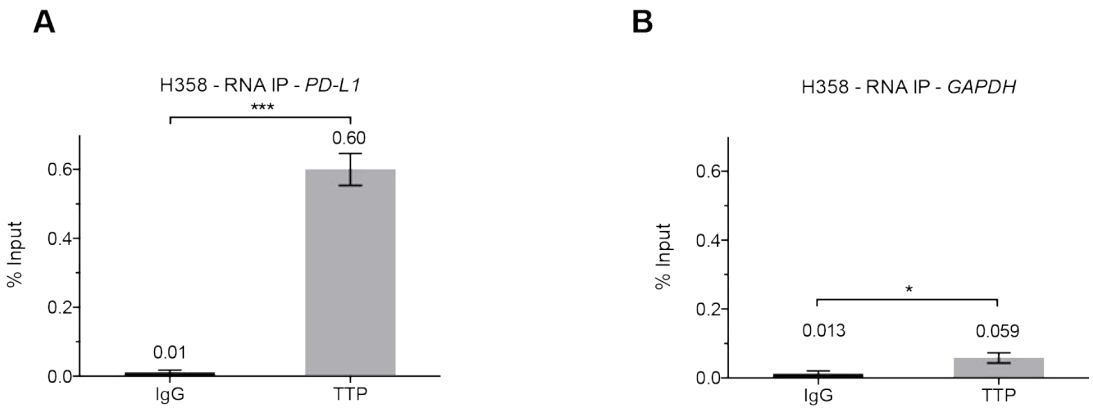

Figure 4.18 TTP binds to *PD-L1* mRNA

(**A**) qPCR analysis of *PD-L1* mRNA from RNA immunoprecipitates from H358 cells using IgG control or anti-TTP antibody.
(**B**) qPCR analysis of *GAPDH* mRNA from RNA immunoprecipitates from H358 cells using IgG control or anti-TTP antibody. This serves as a control mRNA to verify the specificity of the protein-mRNA interaction, as *GAPDH* mRNA does not contain AU-rich elements in the 3'UTR.
Data represent the mean ± SEM of triplicate RNA immunoprecipitation reactions.

Next, we asked whether MEK and AUBPs regulate *PD-L1* expression through the same pathway by using siRNA-mediated knockdown of TTP or KSRP in the context of MEK inhibition. Importantly, the knockdown of *TTP* was largely able to rescue the decrease in *PD-L1* expression caused by MEK inhibition (Figure 4.19A and Figure 4.19B), suggesting MEK and TTP regulate PD-L1 levels through a shared pathway. The knockdown of *KSRP*, however, could not rescue this phenotype, despite profound silencing of *KSRP* expression (Figure 4.19C and Figure 4.19D). Moreover, MEK inhibition significantly increased *TTP* mRNA expression (Figure 4.19B) and, concordantly, chronic activation of oncogenic KRAS signalling in ER-KRAS^{G12V} type II pneumocytes significantly decreased *TTP* mRNA expression (Figure 4.19E), implying that RAS-MEK activity controls TTP expression.

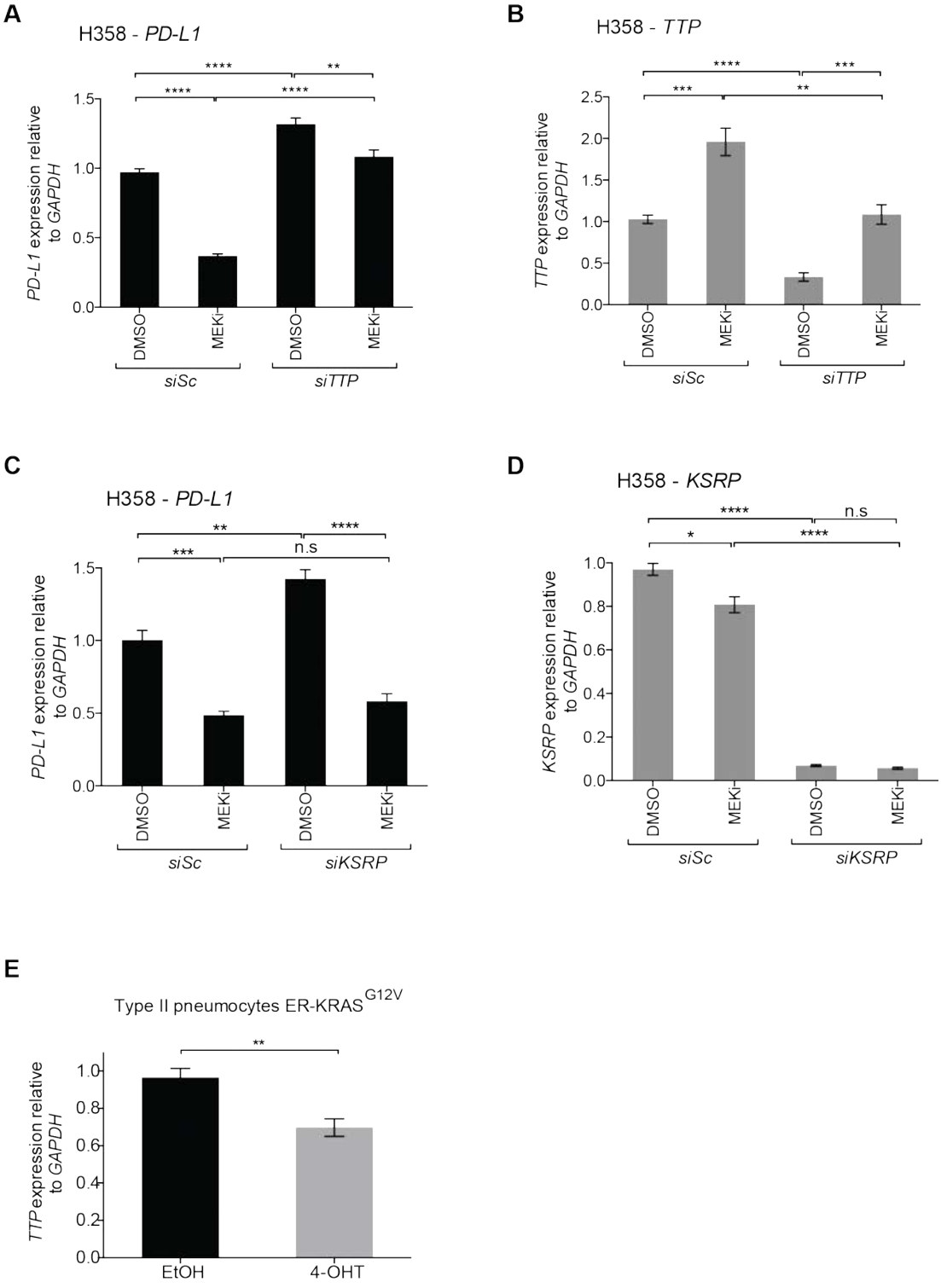

Figure 4.19 Regulation of PD-L1 by MEK is TTP-dependent

(**A** and **B**) qPCR analysis of H358 cells following siRNA-mediated knock-down of *TTP* (24 h) followed by MEK inhibition (24 h). Mean ± SEM of two independent experiments.

(**C** and **D**) qPCR analysis of H358 cells following siRNA mediated knock-down of *KSRP* (24 h) followed by MEK inhibition (24 h). Mean ± SEM of two independent experiments.
(**E**) qPCR analysis of ER-KRAS^{G12V} type II pneumocytes treated with 4-OHT for 24 h. Mean ± SEM of three independent experiments.
MEK inhibitor, GSK1120212, 25 nM. ****P<0.0001; ***P<0.001; **P<0.005; *P<0.05; N.s; not significant; unpaired, two-tailed Student's *t*-test.

The serine/threonine phosphatase PP2A has been implicated in positively regulating TTP function (Rahman et al., 2015; Sun et al., 2007). Therefore, we tested whether inhibition of PP2A with the inhibitor okadaic acid (OA) would increase PD-L1 expression. Indeed, OA significantly and rapidly increased *PD-L1* mRNA expression in TTP WT MEFs, but not TTP KO MEFs (Figure 4.20A), demonstrating that PP2A activity decreases PD-L1 expression specifically through modulating TTP activity.

Conversely, ERK has been shown to phosphorylate (Taylor et al., 1995) and negatively regulate TTP activity and expression (Bourcier et al., 2011; Deleault et al., 2008; Essafi-Benkhadir et al., 2007; Hardle et al., 2015). In addition, the downstream kinase RSK has been implicated in the negative regulation of TTP family members by the phosphorylation of a conserved motif, which is important in binding effector proteins for mRNA degradation (Adachi et al., 2014). Inhibition of MEK decreased phosphorylation of TTP at PXSP (ERK target-site consensus) and RXXS/T (RSK/AKT target-site consensus) motifs (Figure 4.20B and Figure 4.20C), confirming that TTP is regulated by phosphorylation downstream of MEK signalling in cancer cells. In line with these data, we observed a more potent decrease in *PD-L1* mRNA expression in H358 cells when inhibitors of MEK and RSK were combined (Figure 4.20D). Mutation of two of the highest confidence predicted ERK-target residues on human TTP, S218 and S228, abrogated detection of TTP with the phospho-PXSP motif-specific antibody (Figure 4.20B). The reduction of the phospho-TTP signal with MEK inhibitor suggested that these residues might be functionally relevant, but the S218A 228A double-mutant TTP did not show enhanced activity in reducing *PD-L1* mRNA expression compared to wild-type TTP when overexpressed in H358 cells (data not shown),

implying the involvement of other target residues that are not readily detected with this antibody. Furthermore, although AKT signalling has been shown to regulate KSRP activity through phosphorylation of S193 (Diaz-Moreno et al., 2009), a KSRP S193A phospho-mutant did not show enhanced activity in reducing *PD-L1* mRNA expression compared to wild-type KSRP when overexpressed in H358 cells (Figure 4.20E).

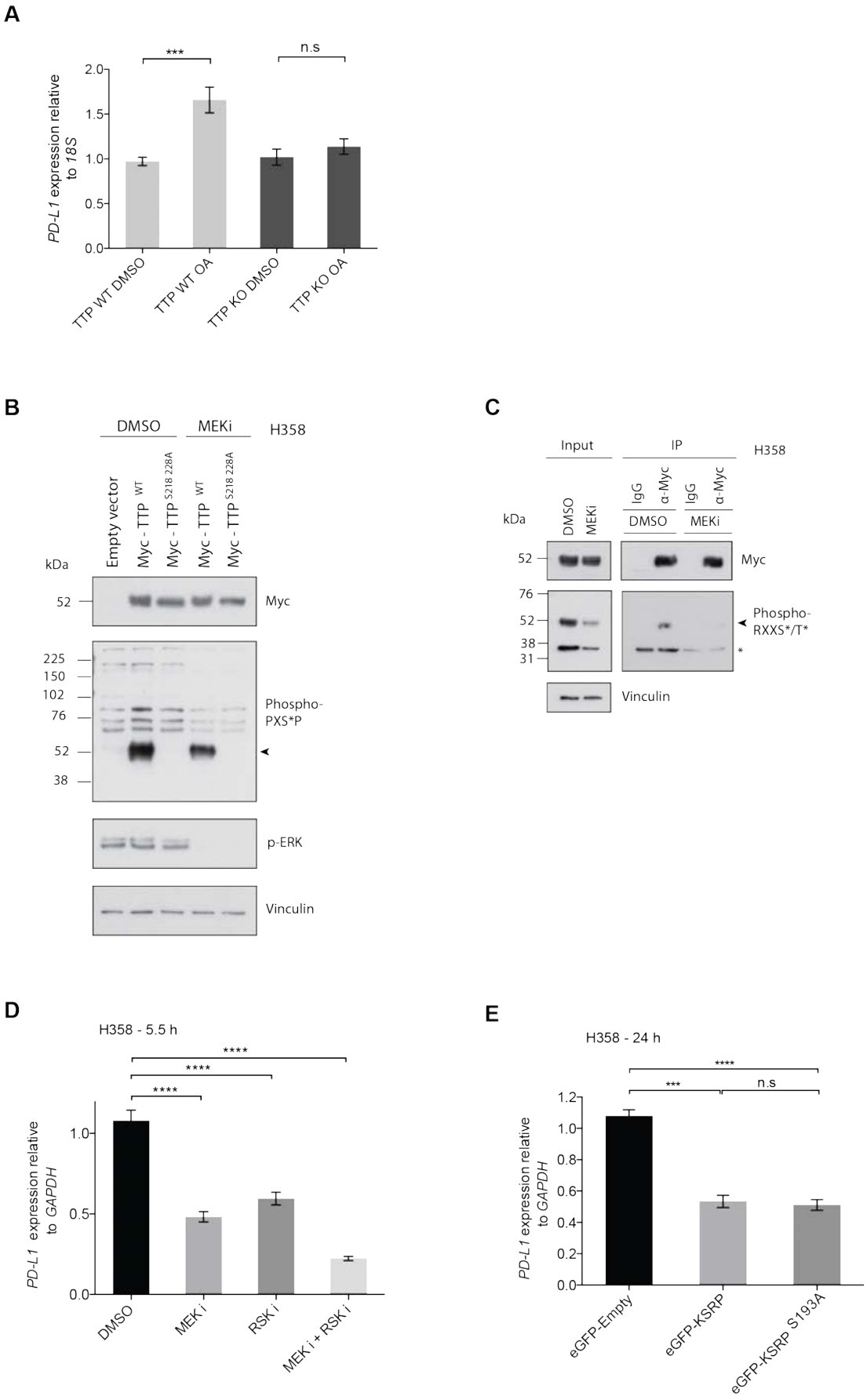
A
***
n.s
PD-L1 expression relative to 18S
2.0
1.5
1.0
0.5
0.0
TTP WT DMSO
TTP WT OA
TTP KO DMSO
TTP KO OA
B
DMSO
MEKi
H358
Empty vector
Myc - TTP WT
Myc - TTP S218 228A
Myc - TTP WT
Myc - TTP S218 228A
kDa
52
Myc
225
150
102
76
52
38
Phospho-PXS*P
p-ERK
Vinculin
C
Input
IP
H358
IgG
α-Myc
IgG
α-Myc
kDa
DMSO
MEKi
DMSO
MEKi
52
Myc
76
52
38
31
Phospho-RXXS*/T*
*
Vinculin
D
H358 - 5.5 h
****
****
****
PD-L1 expression relative to GAPDH
1.0
0.5
0.0
DMSO
MEK i
RSK i
MEK i + RSK i
E
H358 - 24 h
****
***
n.s
PD-L1 expression relative to GAPDH
1.2
1.0
0.8
0.6
0.4
0.2
0.0
eGFP-Empty
eGFP-KSRP
eGFP-KSRP S193A

Figure 4.20 TTP is controlled by phosphorylation downstream of MEK

(**A**) qPCR analysis of TTP WT or TTP KO MEFs treated with okadaic acid or DMSO for 2 h. Mean ± SEM of two independent experiments.
(**B**) Western blotting analysis of H358 cells expressing the indicated constructs. 6.5 h post-transfection, cells were treated with DMSO or MEK inhibitor for an additional 16 h. Arrow indicates Myc-TTP.
(**C**) Western blotting analysis of immunoprecipitations from H358 cells transfected with wild type Myc-TTP. 6.5 h post-transfection, cells were treated with DMSO or MEK inhibitor for an additional 16 h. Arrow indicates Myc-TTP; * indicates co-precipitating protein.
(**D**) qPCR analysis of *PD-L1* expression in H358 cells treated for 5.5 h with the indicated inhibitors. MEK inhibitor, GSK1120212 (25 nM); RSK inhibitor, BI-D1870 (10 μM). Data represent the mean ± SD of two independent experiments. ****P<0.0001.
(**E**) qPCR analysis of *PD-L1* expression in H358 cells 24 after transfection with empty, wild-type KSRP or phospho-mutant KSRP^{S193A} constructs. Data represent the mean ± SEM of two independent experiments.
****P<0.0001, ***P<0.001, **P<0.01, n.s, not significant; unpaired, two-tailed Student's *t*-test.

4.2.5 RAS-ROS-p38 Signalling Controls TTP Activity

To further explore the potential regulation of TTP activity by RAS-MEK signalling, we performed mass spectrometry on immunoprecipitated Myc-TTP after PMA, MEK inhibitor, or PMA and MEK inhibitor treatment in CT26 colon carcinoma cells (Table 5). We selected the CT26 cell line due to its immunogenicity and *Kras* mutant status. We proceed to use this cell line further in *in vivo* studies in Chapter 5.

The mass spectrometry analysis revealed MEK-dependent phosphorylation of S52 and S178; PMA significantly enhanced phosphorylation of these residues and this effect was reversed with MEK inhibition. Moreover, MEK inhibition alone was sufficient to reduce phosphorylation of these residues (Figure 4.21).

PEP	Score	Position	Modified sequence	Phospho (STY) Probabilities	Number of Phospho (STY)
0.011674	100	52	_STS(ph)LVEGR_	STS(1)LVEGR	1
1.41E-10	70	80	_PGPELS(ph)PSPT(ph)SPTATPTTSSR_	PGPELS(0.998)PS(0.006)PT(0.477)S(0.43)PT(0.068)AT(0.011)PT(0.002)T(0.002)S(0.002)S(0.003)R	2
1.41E-10	69	82	_PGPELSPS(ph)PTSPTATPTTSSR_	PGPELS(0.036)PS(0.911)PT(0.04)S(0.009)PT(0.002)AT(0.001)PTTSSR	1
1.07E-52	186	85	_PGPELSPSPTS(ph)PTATPTTSSR_	PGPELSPSPT(0.128)S(0.857)PT(0.013)ATPTTSSR	1
0.040396	74	105	_TYS(ph)ESGRCR_	TYS(1)ESGRCR	1
6.90E-08	130	178	_QSIS(ph)FSGLPSGR_	QSIS(1)FSGLPSGR	1
1.50E-22	96	189	_RSS(ph)PPPPGFS(ph)GPSLSSCSFSPSSSPPPPGDLPLSPSAFSAAPGTPVTR_	RS(0.17)S(0.767)PPPPGFS(0.195)GPS(0.146)LS(0.131)S(0.124)CS(0.111)FS(0.1)PS(0.09)S(0.085)S(0.081)PPPPGDLPLSPSAFSAAPGTPVTR	2
1.50E-22	96	196	_RSSPPPPGFS(ph)GPS(ph)LSSCSFSPSSSPPPPGDLPLSPSAFSAAPGTPVTR_	RS(0.051)S(0.25)PPPPGFS(0.367)GPS(0.173)LS(0.169)S(0.167)CS(0.166)FS(0.165)PS(0.165)S(0.164)S(0.164)PPPPGDLPLSPSAFSAAPGTPVTR	2
1.50E-22	96	199	_RSS(ph)PPPPGFS(ph)GPS(ph)LSSCSFSPSSSPPPPGDLPLSPSAFSAAPGTPVTR_	RS(0.072)S(0.368)PPPPGFS(0.279)GPS(0.303)LS(0.3)S(0.297)CS(0.29)FS(0.282)PS(0.274)S(0.27)S(0.265)PPPPGDLPLSPSAFSAAPGTPVTR	2
9.68E-15	69	201	_RSSPPPPGFS(ph)GPS(ph)LSSCSFSPSSSPPPPGDLPLSPSAFSAAPGTPVTR_	RS(0.013)S(0.177)PPPPGFS(0.202)GPS(0.201)LS(0.201)S(0.201)CS(0.201)FS(0.201)PS(0.201)S(0.201)S(0.201)PPPPGDLPLSPSAFSAAPGTPVTR	2
9.68E-15	69	202	_RSSPPPPGFS(ph)GPS(ph)LSSCSFSPSSSPPPPGDLPLSPSAFSAAPGTPVTR_	RS(0.013)S(0.177)PPPPGFS(0.202)GPS(0.201)LS(0.201)S(0.201)CS(0.201)FS(0.201)PS(0.201)S(0.201)S(0.201)PPPPGDLPLSPSAFSAAPGTPVTR	2
9.68E-15	69	204	_RSSPPPPGFS(ph)GPS(ph)LSSCSFSPSSSPPPPGDLPLSPSAFSAAPGTPVTR_	RS(0.013)S(0.177)PPPPGFS(0.202)GPS(0.201)LS(0.201)S(0.201)CS(0.201)FS(0.201)PS(0.201)S(0.201)S(0.201)PPPPGDLPLSPSAFSAAPGTPVTR	2
9.68E-15	69	206	_RSSPPPPGFS(ph)GPS(ph)LSSCSFSPSSSPPPPGDLPLSPSAFSAAPGTPVTR_	RS(0.013)S(0.177)PPPPGFS(0.202)GPS(0.201)LS(0.201)S(0.201)CS(0.201)FS(0.201)PS(0.201)S(0.201)S(0.201)PPPPGDLPLSPSAFSAAPGTPVTR	2
9.68E-15	69	208	_RSSPPPPGFS(ph)GPS(ph)LSSCSFSPSSSPPPPGDLPLSPSAFSAAPGTPVTR_	RS(0.013)S(0.177)PPPPGFS(0.202)GPS(0.201)LS(0.201)S(0.201)CS(0.201)FS(0.201)PS(0.201)S(0.201)S(0.201)PPPPGDLPLSPSAFSAAPGTPVTR	2
9.68E-15	69	209	_RSSPPPPGFS(ph)GPS(ph)LSSCSFSPSSSPPPPGDLPLSPSAFSAAPGTPVTR_	RS(0.013)S(0.177)PPPPGFS(0.202)GPS(0.201)LS(0.201)S(0.201)CS(0.201)FS(0.201)PS(0.201)S(0.201)S(0.201)PPPPGDLPLSPSAFSAAPGTPVTR	2
9.68E-15	69	210	_RSSPPPPGFS(ph)GPS(ph)LSSCSFSPSSSPPPPGDLPLSPSAFSAAPGTPVTR_	RS(0.013)S(0.177)PPPPGFS(0.202)GPS(0.201)LS(0.201)S(0.201)CS(0.201)FS(0.201)PS(0.201)S(0.201)S(0.201)PPPPGDLPLSPSAFSAAPGTPVTR	2
0.007218	63	248	_S(ph)TTPSTIWGPLGGLAR_	S(0.333)T(0.333)T(0.333)PSTIWGPLGGLAR	1
0.007218	63	249	_S(ph)TTPSTIWGPLGGLAR_	S(0.333)T(0.333)T(0.333)PSTIWGPLGGLAR	1
1.93E-20	158	250	_STT(ph)PSTIWGPLGGLAR_	ST(0.003)T(0.997)PSTIWGPLGGLAR	1
6.07E-19	89	264	_S(ph)PSAHSLGSDPDDYASSGSSLGGGSDSPVFEAGVFGPPQTPAPPR_	S(0.446)PS(0.412)AHS(0.087)LGS(0.022)DPDDY(0.004)AS(0.005)S(0.005)GS(0.005)S(0.005)LGGS(0.005)DS(0.005)PVFEAGVFGPPQTPAPPR	1
6.07E-19	89	266	_S(ph)PSAHSLGSDPDDYASSGSSLGGGSDSPVFEAGVFGPPQTPAPPR_	S(0.41)PS(0.41)AHS(0.165)LGS(0.006)DPDDY(0.001)AS(0.001)S(0.001)GS(0.001)S(0.001)LGGS(0.001)DS(0.001)PVFEAGVFGPPQTPAPPR	1
5.37E-14	83	269	_SPSAHSLGSDPDDYASSGSSLGGGSDSPVFEAGVFGPPQTPAPPR_	S(0.272)PS(0.272)AHS(0.447)LGS(0.004)DPDDY(0.001)AS(0.001)S(0.001)GS(0.001)S(0.001)LGGS(0.001)DS(0.001)PVFEAGVFGPPQTPAPPR	1
1.50E-07	59	272	_SPSAHSLGS(ph)DPDDYASSGSSLGGGSDSPVFEAGVFGPPQTPAPPR_	S(0.019)PS(0.019)AHS(0.078)LGS(0.343)DPDDY(0.073)AS(0.078)S(0.078)GS(0.078)S(0.078)LGGS(0.078)DS(0.078)PVFEAGVFGPPQTPAPPR	1
0.001495	41	279	_SPSAHSLGS(ph)DPDDYASSGSSLGGGSDSPVFEAGVFGPPQTPAPPR_	S(0.044)PS(0.044)AHS(0.044)LGS(0.109)DPDDY(0.103)AS(0.109)S(0.109)GS(0.109)S(0.109)LGGS(0.109)DS(0.109)PVFEAGVFGPPQTPAPPR	1
0.001495	41	280	_SPSAHSLGS(ph)DPDDYASSGSSLGGGSDSPVFEAGVFGPPQTPAPPR_	S(0.044)PS(0.044)AHS(0.044)LGS(0.109)DPDDY(0.103)AS(0.109)S(0.109)GS(0.109)S(0.109)LGGS(0.109)DS(0.109)PVFEAGVFGPPQTPAPPR	1
0.001495	41	282	_SPSAHSLGS(ph)DPDDYASSGSSLGGGSDSPVFEAGVFGPPQTPAPPR_	S(0.044)PS(0.044)AHS(0.044)LGS(0.109)DPDDY(0.103)AS(0.109)S(0.109)GS(0.109)S(0.109)LGGS(0.109)DS(0.109)PVFEAGVFGPPQTPAPPR	1
0.001495	41	283	_SPSAHSLGS(ph)DPDDYASSGSSLGGGSDSPVFEAGVFGPPQTPAPPR_	S(0.044)PS(0.044)AHS(0.044)LGS(0.109)DPDDY(0.103)AS(0.109)S(0.109)GS(0.109)S(0.109)LGGS(0.109)DS(0.109)PVFEAGVFGPPQTPAPPR	1
0.001495	41	287	_SPSAHSLGS(ph)DPDDYASSGSSLGGGSDSPVFEAGVFGPPQTPAPPR_	S(0.044)PS(0.044)AHS(0.044)LGS(0.109)DPDDY(0.103)AS(0.109)S(0.109)GS(0.109)S(0.109)LGGS(0.109)DS(0.109)PVFEAGVFGPPQTPAPPR	1
0.001495	41	289	_SPSAHSLGS(ph)DPDDYASSGSSLGGGSDSPVFEAGVFGPPQTPAPPR_	S(0.044)PS(0.044)AHS(0.044)LGS(0.109)DPDDY(0.103)AS(0.109)S(0.109)GS(0.109)S(0.109)LGGS(0.109)DS(0.109)PVFEAGVFGPPQTPAPPR	1

Table 5. Mass spectrometry analysis reveals MEK-dependent TTP phosphorylation events

Table of identified mouse TTP phosphopeptides from MS analyses pooled from two independent biological experiments. Identifications are 1 % FDR controlled. PEP indicates the probability that the identification is incorrect. Phosphosite assignment probabilities are indicated in parenthesis.

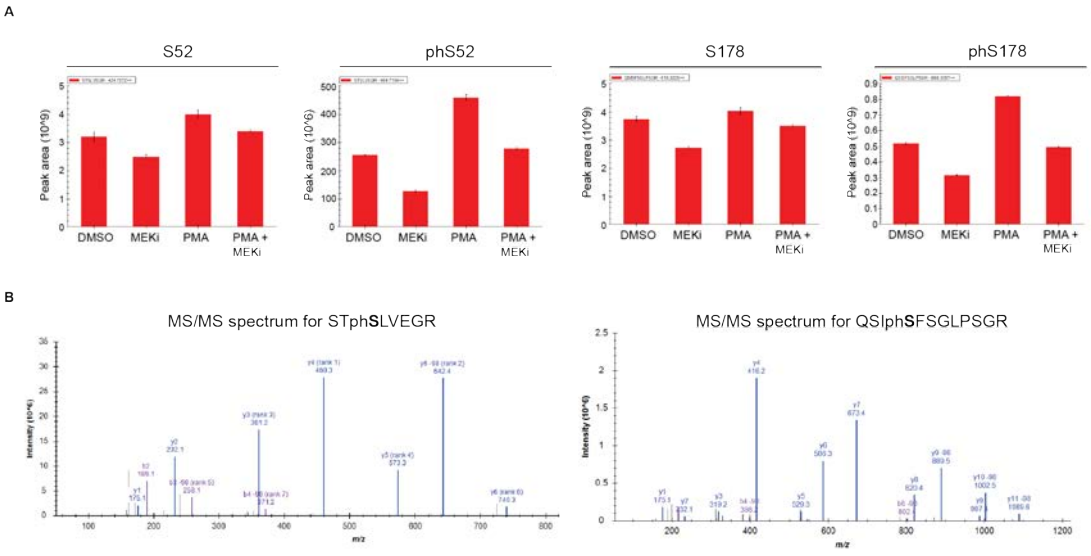

Figure 4.21 S52 and S178 of mouse TTP are phosphorylated in response to MEK signalling

(**A**) Semi-quantitative analysis of non-phosphorylated and phosphorylated peptides corresponding to S52 and S178 phosphosites of mouse TTP, generated in Skyline. Myc-TTP was immunoprecipitated from CT26 cells

stably expressing a doxycycline inducible Myc-TTP construct, 1 h after treatment with DMSO vehicle, PMA (200 nM), MEK inhibitor GSK1120212 (25 nM) or PMA and MEK inhibitor together. Data represent the mean ± SD of technical triplicates and are representative of two independent biological experiments.
(**B**) MS/MS mass spectra for phosphopeptides STphSLVEGR (S52) and QSIphSFSGLPSGR (S178). -98 indicates the loss of H_3PO_4.

TTP is tightly regulated by p38 signalling through phosphorylation by the downstream kinase MK2 (also known as MAPKAPK2), resulting in decreased TTP activity and increased target mRNA stability (Mahtani et al., 2001; Stoecklin et al., 2004). In parallel, phosphorylation of S52 and S178 stabilizes TTP protein (Brook et al., 2006), which is consistent with the increased abundance of total TTP peptides detected in the PMA versus the MEK inhibitor-treated condition observed in our mass spectrometry analysis (Figure 4.21).

Since oncogenic RAS can stimulate p38 activity through promoting the accumulation of reactive oxygen species (ROS) downstream of MEK-ERK activation (Nicke et al., 2005), we reasoned that p38 signalling might contribute to TTP inactivation downstream of RAS. Indeed, oncogenic RAS signalling dramatically increased intracellular ROS in MCF10A cells, and ROS levels were distinctly correlated with the extent of PD-L1 induction (Figure 4.22). Moreover, the addition of the potent anti-oxidant N-acetyl-L-cysteine (NAC) largely reversed the induction of PD-L1 protein by RAS (Figure 4.22), collectively suggesting that ROS induction by oncogenic RAS is functionally important in driving PD-L1 expression.

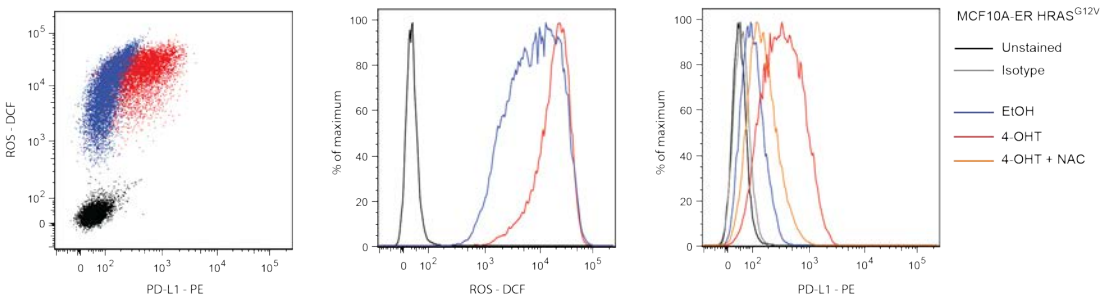

Figure 4.22 ROS accumulation is critical for RAS-induced PD-L1 upregulation

Flow cytometry analysis of PD-L1 surface protein, and intracellular ROS measured by staining with H_2DCFDA, in MCF10A ER-HRASG12V cells treated with 4-OHT or vehicle ± NAC for 24 h. Data are representative of two independent experiments.
4-OHT, 100 nM. NAC, 10 mM.

Chronic endogenous mutant RAS expression has been shown to select for a compensatory state of lower ROS levels, achieved by the activation of an Nrf2 transcriptional programme (DeNicola et al., 2011). Therefore, we tested whether chronic activation of oncogenic RAS signalling would result in comparable PD-L1 expression to acute activation of RAS. Surprisingly, we found that PD-L1 expression was further increased after four days of stimulation, suggesting that potential compensatory transcriptional mechanisms are unlikely to reverse PD-L1 induction at these time-points (Figure 4.23).

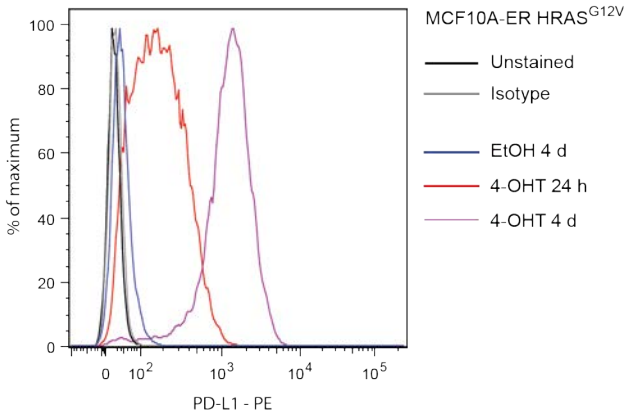

Figure 4.23 Long-term RAS activation leads to augmented PD-L1 expression

Representative histograms from flow cytometry analysis of surface PD-L1 protein expression on MCF10A ERHRASG12V cells 24 h or 4 days (d) after treatment with vehicle or 4-OHT (100 nM). Data are representative of two independent experiments.

Strikingly, specific activation of the p38 pathway using an inducible version of the upstream kinase MEKK3 (ΔMEKK3-ER; Figure 4.24B) (Garner et al.,

2002) was sufficient to activate PD-L1 protein expression, albeit to a lesser extent than that achieved by RAS itself (Figure 4.24A). Importantly, co-treatment with NAC was considerably less effective in reversing PD-L1 induction in this context, implying ROS operates upstream of p38 signalling in this pathway.

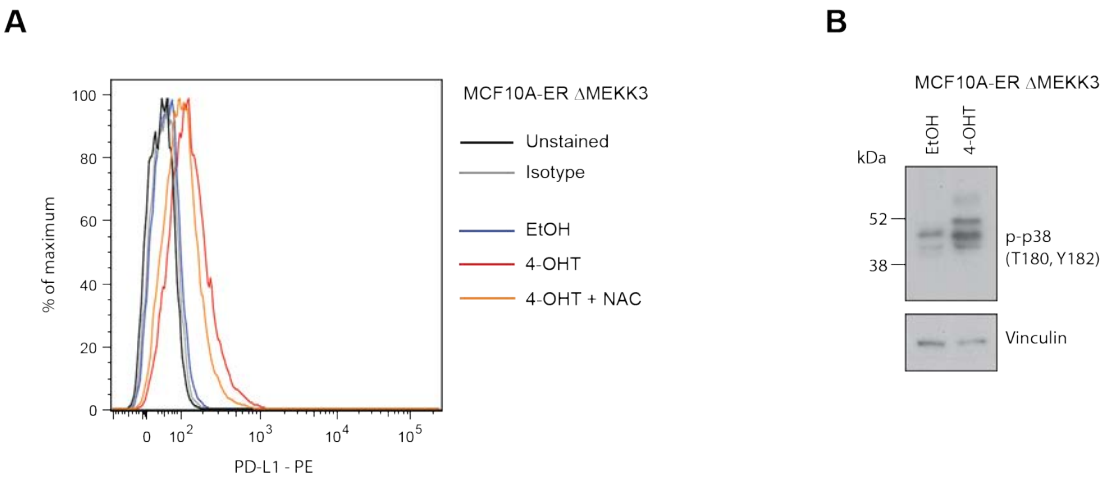

Figure 4.24 p38 signalling is sufficient to drive PD-L1 induction downstream of ROS

(**A**) Flow cytometry analysis of PD-L1 surface protein in MCF10A ER-ΔMEKK3 cells treated with 4-OHT or vehicle ± NAC for 24 h. Data are representative of three independent experiments.
(**B**) Western blotting analysis of MCF10A cells harboring an inducible version of the kinase domain of MEKK3 (ER-ΔMEKK3), 24 h after the addition of 4-OHT or vehicle.
4-OHT, 100 nM. NAC, 10 mM.

Downstream of p38 activation, MK2 phosphorylates TTP at two conserved serine residues involved in binding to 14-3-3 proteins; S52 and S178 of the mouse protein, of which S52 conforms to the RXXS/T phosphosite motif (Chrestensen et al., 2004). We therefore analysed the potential role MK2 activity downstream of RAS in the induction of PD-L1 expression. Two independent, specific, ATP-competitive inhibitors of MK2 strongly reversed RAS-dependent PD-L1 induction in MCF10A cells (Figure 4.25).

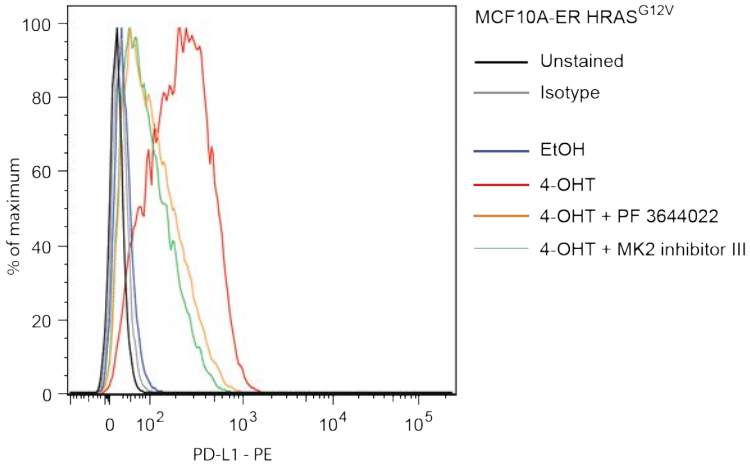

Figure 4.25 MK2 activity is required for optimal PD-L1 induction by RAS

Representative histograms from flow cytometry analysis of surface PD-L1 protein expression on MCF10A ERHRASG12V cells 24 h after treatment with vehicle, 4-OHT (100 nM) or 4-OHT and MK2 inhibitor PF 3644022 (1 μM) or MK2 inhibitor III (1 μM). Data are representative of two independent experiments.

Since p38 operates upstream of MK2, we also tested the efficacy of p38 inhibitor SB203580 on PD-L1 expression in H358 cancer cells. Unexpectedly, p38 inhibition increased PD-L1 expression in this system, although only modestly (Figure 4.26A). We confirmed p38 was inhibited effectively by Western blotting for the phosphorylated form of the downstream substrate CREB (Figure 4.26B). However, we also noted that ERK activity was dramatically stimulated upon addition of the p38 inhibitor (Figure 4.26B). ERK pathway activation following treatment with SB203580 and other p38 inhibitors has been reported by others (Hall and Davis, 2002). This effect may account for the lack of p38 inhibitor activity against PD-L1 expression. Indeed, this is consistent with MEK inhibition reversing the activation of PD-L1 expression by p38 inhibition (Figure 4.26A).

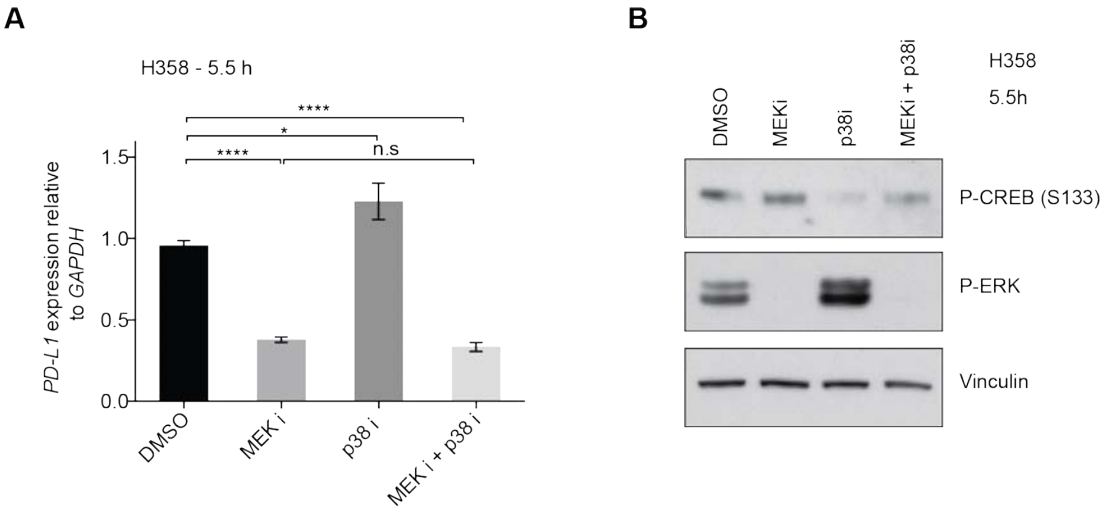

Figure 4.26 p38 inhibitor SB203580 paradoxically increases PD-L1 expression

(**A**) qPCR analysis of *PD-L1* expression in H358 cells treated for 5.5 h with the indicated inhibitors. MEK inhibitor, GSK1120212 (25 nM); p38 inhibitor, SB203580 (10 μM). Data represent the mean ± SEM of two independent experiments. ****P<0.0001; *P<0.05; NS, not significant; unpaired, two-tailed Student's t-test.
(**B**) Western blotting analysis of H358 cells treated with the indicated inhibitors for 5.5 h. Phospho-CREB (S133) signal serves as an indicator of p38 MAPK pathway activity.
MEK inhibitor, GSK1120212 (25 nM); p38 inhibitor, SB203580 (10 μM).

To analyse the functional significance of these MK2 target residues downstream of RAS-MEK pathway activation, we generated TTP KO CT26 colon carcinoma cell lines using CRISPR/Cas in order to obviate functional contributions from endogenous TTP. Western blotting confirmed lack of TTP protein expression in KO clone #1 (Figure 4.27A), and this was further validated by TOPO-TA cloning of the endogenous *Zfp36* locus followed by sequencing to confirm total allele disruption (Figure 4.27B). All colonies sequenced for clone KO clone #1 carried missense mutations (Figure 4.27C).

Interestingly, the total number and frequency of unique mutations suggested that the CT26 cell line is tetraploid for this region of chromosome seven.
We then reconstituted TTP KO CT26 cells with either a wild-type (WT) or phosphosite-mutant (S52A S178A), tetracycline-inducible TTP transgene.

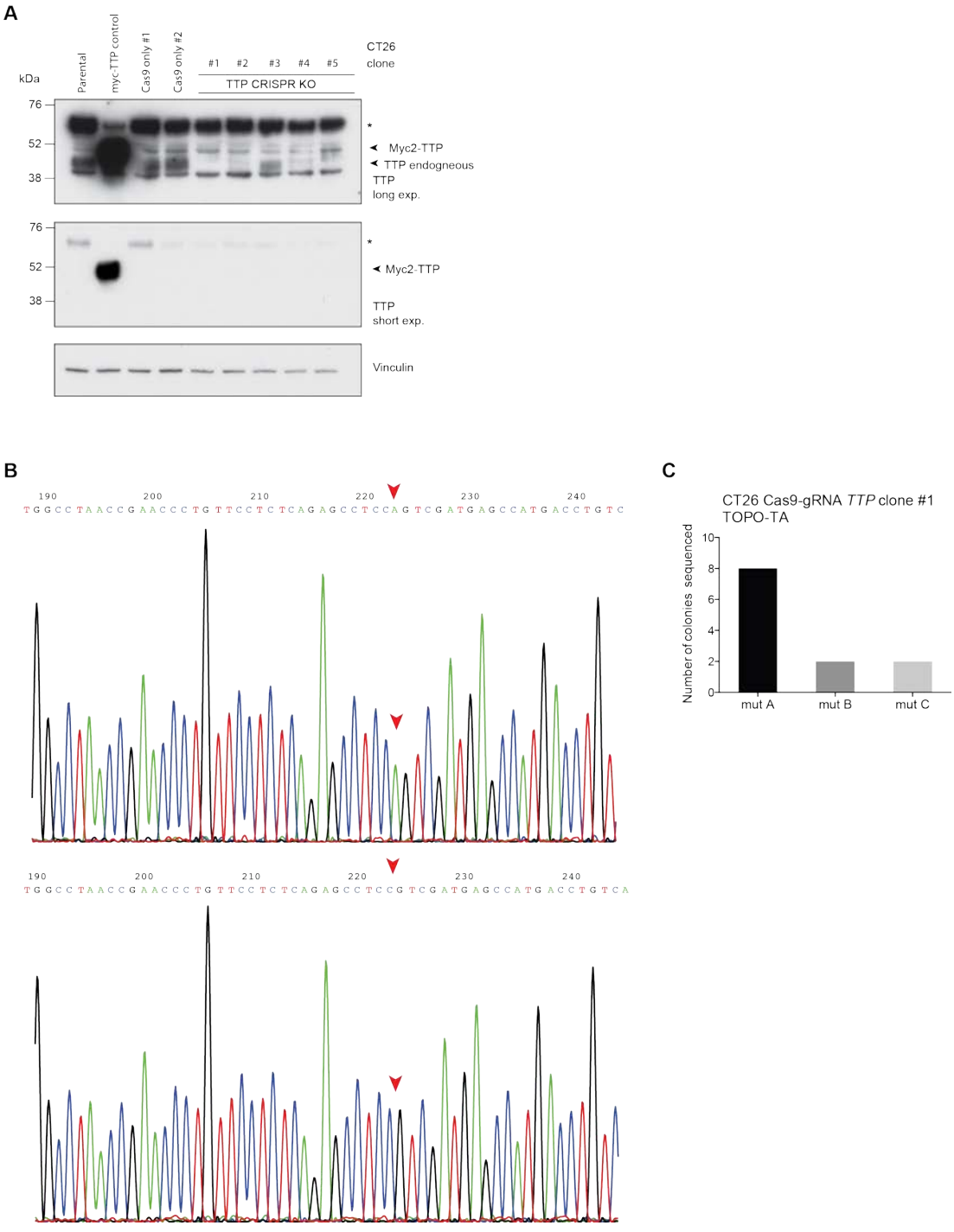

Figure 4.27 CRISPR/Cas-mediated disruption of *Zfp36*

(**A**) Western blotting analysis of CT26 cell clones following genome editing by CRISPR/Cas. *TTP* KO clone #1 was selected for use in subsequent experiments in the main text. Parental clones, Cas9-transfected clones and the overexpression of Myc-TTP transgene serve as controls.

(**B**) Complete *Zfp36* allele disruption was confirmed by TOPO-TA cloning and sequencing. Shown are representative sequencing histograms showing a common nonsense mutation ("mutA") proximal to the gRNA binding site. (**C**) Quantification of the number of different nonsense mutations found in clone #1, found by TOPO-TA cloning and sequencing.

Immunoprecipitation of Myc-tagged TTP following acute MAPK activation with PMA revealed phosphorylation of WT TTP, but not of the S52A S178A mutant protein at RXXS/T sites (Figure 4.28B). Moreover, the S52A S178A mutant TTP had enhanced activity in reducing *PD-L1* mRNA expression relative to WT TTP (Figure 4.28C and Figure 4.28D). We also noted increased protein stability of WT TTP following PMA stimulation in the input. In concordance with our results from mass spectrometry analysis, the TTP S178A 52A double mutant TTP input did not change in response to PMA treatment, reflecting abrogation of the phosphorylation-dependent change in protein stability. In sum, these results suggest that a RAS-ROS-p38 signalling axis contributes to PD-L1 upregulation through phosphorylation and inactivation of TTP.

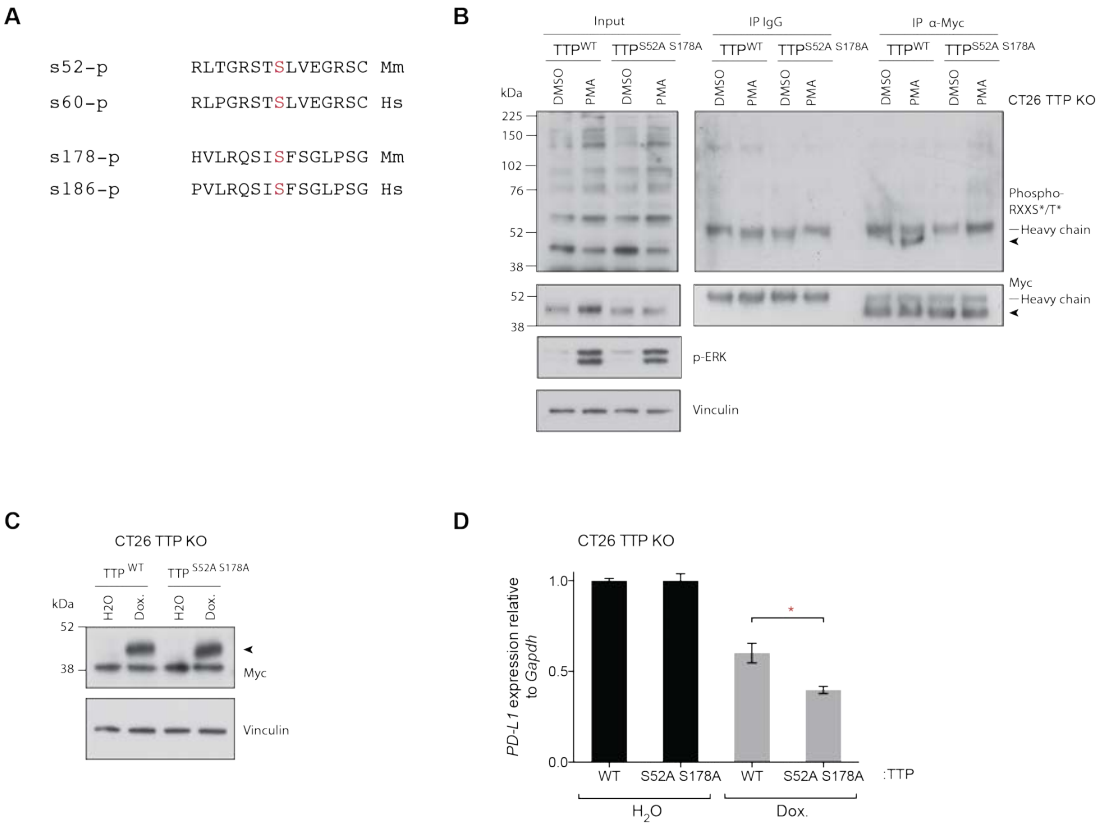

Figure 4.28 RAS-induced p38 activity decreases TTP activity

(**A**) Sequence alignments of the conserved phosphosites targeted by MK2 in the mouse (*Mm*) and human (*Hs*) TTP protein. The phosphorylated serines are highlighted in red.
(**B**) Western blotting of immunoprecipitation reactions from CT26 TTP KO cells harboring doxycycline-inducible WT or phospho-mutant Myc-TTP constructs, treated with doxycycline for 24 h before the addition of PMA or vehicle for an additional 1 h. Arrow indicates Myc-TTP.
(**C**) Western blotting analysis of Myc-TTP expression 24 h after the addition of doxycycline or vehicle. Arrow indicates Myc-TTP.
(**D**) qPCR analysis of CT26 TTP KO cells harboring doxycycline-inducible WT or phospho-mutant Myc-TTP constructs, treated with doxycycline or vehicle for 48 h. Mean ± SEM of two independent experiments.
*$P < 0.05$; unpaired, two-tailed Student's *t*-test. PMA, 200 nM. Dox., doxycycline, 1 μg/ml.

4.3 Conclusions

In this chapter, we demonstrate that oncogenic RAS signaling can increase tumor cell-intrinsic PD-L1 expression, implying that RAS can directly contribute to evading immune destruction in lung cancer. The use of tumor PD-L1 expression in stratifying patients for cancer immunotherapy may be confounded by antigen-independent processes including the cell-intrinsic signaling mechanisms controlling tumor PD-L1 expression outlined here. Our observations indicate a role for mutant RAS in contributing to the uncoupling of tumor PD-L1 expression from the immunogenicity of the tumor.

We reveal that RAS-MEK signaling controls expression of PD-L1, at least in part, by modulating the stability of the transcript. We show that the mouse and human *PD-L1* mRNAs are labile transcripts containing multiple AREs in the 3'UTR that are functionally important for controlling PD-L1 expression. Moreover, we demonstrate that AREs permit the regulation of PD-L1 expression downstream of RAS. miRNAs such as miR-200 and miR-513 have also been implicated in regulating the stability of the *PD-L1* transcript (Chen et al., 2014; Gong et al., 2009). However, we show that mutation of

AREs in the 3'UTR of *PD-L1* is sufficient to abrogate sensitivity of the 3'UTR reporter to RAS-MEK activity, implying that miRNAs that do not target these sites are unlikely to be pertinent in this pathway downstream of RAS.

We identify TTP as a principle AUBP responsible for negatively regulating PD-L1 expression. Our data are consistent with a previous report identifying *PD-L1* mRNA as a TTP target in an RNA-immunoprecipitation, microarray-based screen in mouse macrophages (Stoecklin et al., 2008). Using an RNA interference approach, we also identify KSRP as an additional AUBP capable of negatively regulating PD-L1 expression in cancer cells. As our selective screening of candidate AUBPs was non-exhaustive, it is plausible that other AUBPs may be involved in coordinately regulating PD-L1 expression in lung cancer. Indeed, differential expression of TTP, KSRP and other AUBPs may account for the disparities in the extent of PD-L1 upregulation following knockdown of *TTP* or *KSRP* between the cancer cell lines analysed in this study.

Mechanistically, MEK inhibition reduced *PD-L1* mRNA stability, coinciding with an increase in TTP expression and reduction in phosphorylation of TTP at ERK and RSK/AKT consensus motifs. Conversely, activation of MAPK and the associated ROS accumulation led to enhanced TTP phosphorylation, notably by MK2 at key inhibitory sites. Intriguingly, p38 inhibition has been shown to significantly decrease PD-L1 expression in lymphoma (Yamamoto et al., 2009). Our results offer a possible mechanistic explanation for these findings and imply that p38 and MK2 inhibitors may be effective in reducing PD-L1 expression in other malignancies. Collectively, our data support the finding that chronic RAS activity leads to a concerted reduction in TTP function.

5 Chapter 5. Results 3. Regulation of PD-L1 by RAS and TTP *in vivo*

5.1 Introduction

Thus far, we have investigated the molecular detail of how RAS regulates *PD-L1* mRNA stability through the ARE-element binding protein TTP. Here, we aim to investigate the relevance of this regulatory pathway *in vivo*. We investigate the regulation of PD-L1 expression in human lung cancer using publically available datasets and bioinformatics analysis. In addition, we establish an experimental mouse model to directly test the functional importance of TTP expression in tumour immunoresistance and progression.

In this chapter, I present bioinformatics analyses that were conducted by Phil East and Sophie de Carne on my behalf. This includes the GSEA and the associated interpretation of TCGA datasets. I also present images generated from histopathological analyses performed by Bradley Spencer-Dene on my behalf.

5.2 Results

5.2.1 RAS Pathway Activation is Associated with PD-L1 Upregulation in Human Lung Cancer

To further evaluate the role of oncogenic RAS signalling in regulating PD-L1 expression in human lung cancer, we analysed TCGA gene expression data from patient-derived lung adenocarcinoma (LUAD) samples. To account for the effects of alternative oncogenes that can activate downstream RAS effector pathways such as EGFR, BRAF and ALK, we used two published RAS activation gene expression signatures (Loboda et al., 2010; Sweet-

Cordero et al., 2005) to classify samples regarding their RAS pathway activity. The Loboda-Watters signature was derived from a meta-analysis of RAS mutant lung, colon and breast tumour samples and cell lines and consists of 105 upregulated genes associated with RAS activation. The Sweet-Cordero-Jacks signature constitutes gene expression data from lung tumours from the KRAS LA2 mouse model of NSCLC, compared to human RAS-mutant lung cancers, consisting of 89 upregulated genes. Both signatures have been biologically validated in their respective studies, and the use of both of them in parallel increases the robustness of our analytical approach. The overlap between the gene signature sets is only three genes out of a total of 194 genes, implying they provide truly distinct approaches for sample segregation.

Using these independently generated gene expression signatures, we were able to segregate patient LUAD samples into “high” and “low” RAS pathway activity based on gene expression. Encouragingly, annotation of *KRAS* mutation status revealed a strong enrichment for *KRAS* mutant samples in the high RAS activity cohorts in both signatures, although this was weaker in the Loboda-Watters signature (Figure 5.1). As expected, the majority of the KRAS mutations annotated were in the G12 position, as denoted by a red block next to the patient sample row (Figure 5.1).

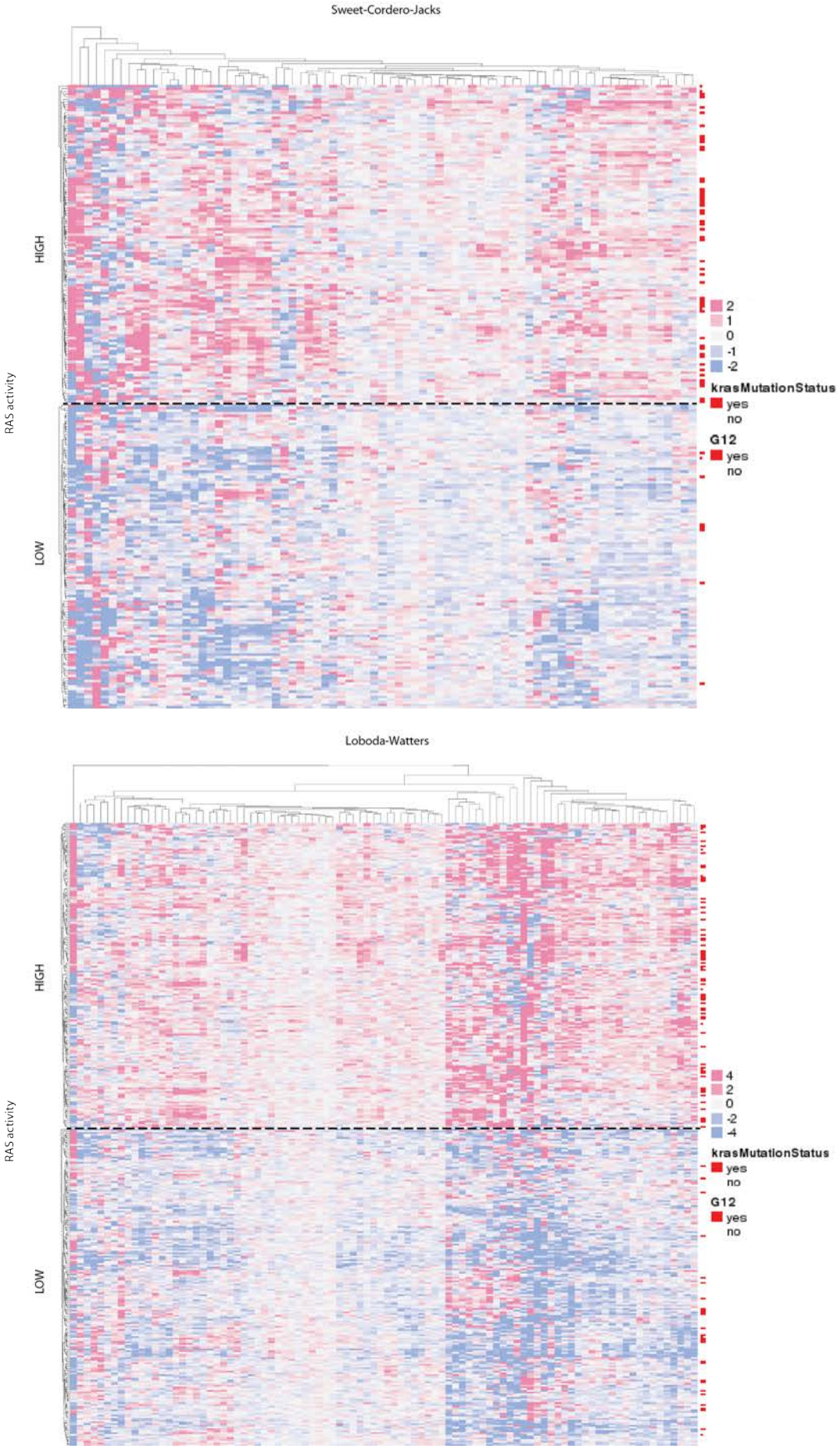
Sweet-Cordero-Jacks
RAS activity
HIGH
LOW
2
1
0
-1
-2
krasMutationStatus
yes
no
G12
yes
no
Loboda-Watters
RAS activity
HIGH
LOW
4
2
0
-2
-4
krasMutationStatus
yes
no
G12
yes
no

Figure 5.1 Clustering of TCGA LUAD samples into high and low RAS pathway activity using GSEA

Heat maps showing human lung adenocarcinoma samples from the TCGA dataset clustered into RAS high or low pathway activity groups using RNA sequencing expression data and published RAS activity gene expression signatures (Loboda et al., 2010; Sweet-Cordero et al., 2005). *KRAS* mutation status, and specifically *KRAS* codon 12 mutation status, are shown for each sample.

Next, we compared the expression of T cell function related genes between high and low RAS activity cohorts. We found *CD274* (*PD-L1*) expression to be significantly increased in the high RAS pathway activity samples in both the Sweet-Cordero-Jacks and the Loboda-Watters signatures (2.65 and 2.71 fold change, respectively) (Figure 5.2A and Figure 5.2B). However, the expression of the pan-leukocyte marker *PTPRC* (coding for CD45) and lymphocyte marker *CD3E* were only modestly increased in the high RAS pathway activity cohort (*PTPRC* 1.26 and 1.21, *CD3E* 1.36 and 1.04 fold change) indicating that the differential in *PD-L1* expression is not likely to be solely attributable to a higher degree of leukocyte infiltration and inflammation in the tumour microenvironment. Notably, when comparing high and low RAS pathway activity samples we did not find concordant differences in *TTP* expression between the two signatures; it was only significantly changed in the Loboda-Watters signature (1.9 fold change).

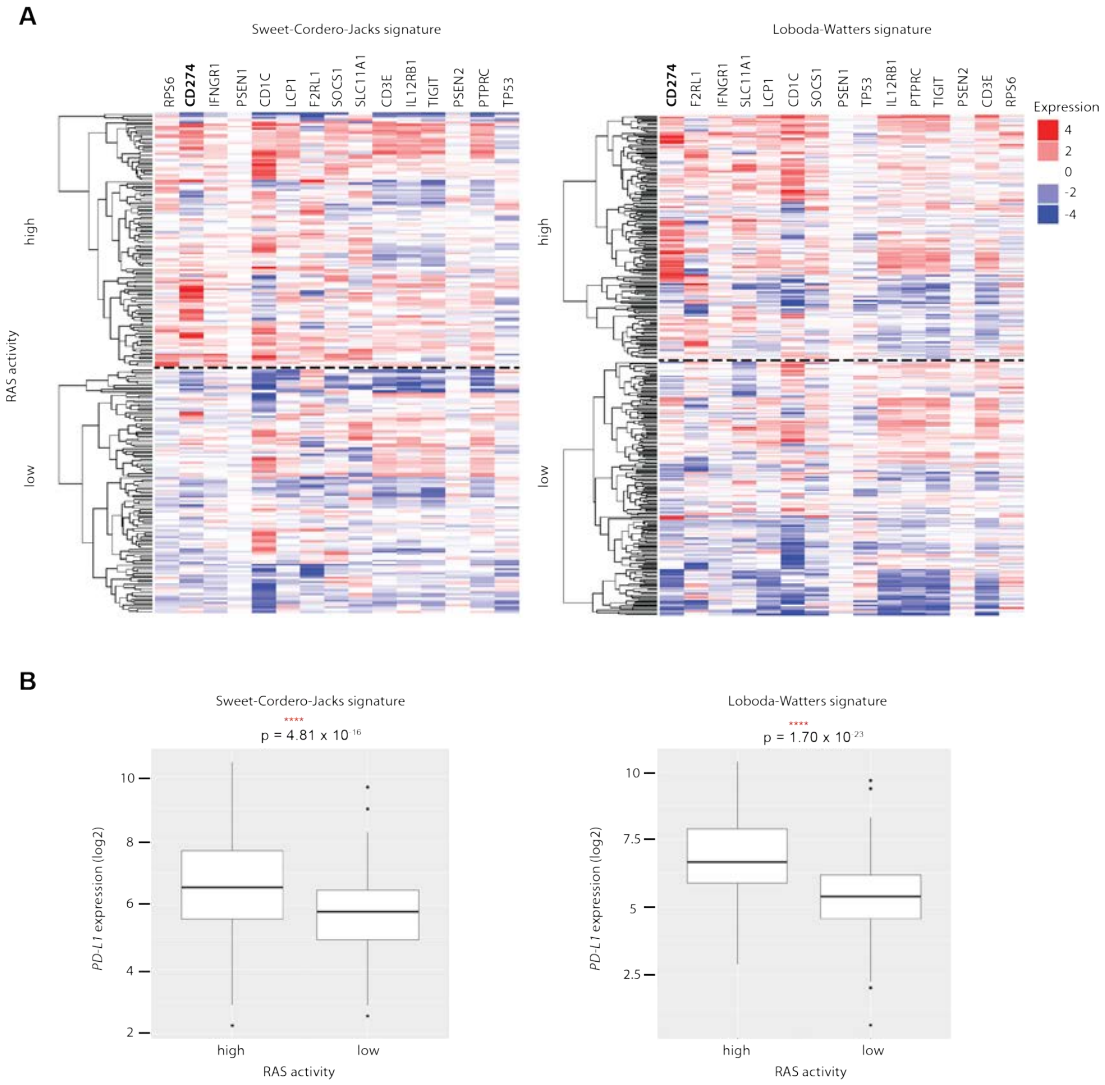

Figure 5.2 High RAS pathway activity in human lung tumours is associated with high PD-L1 expression

(**A**) Heat-maps showing fold change in expression of T cell function related genes between high and low RAS pathway activity TCGA lung adenocarcinoma (LUAD) cohorts using two independent RAS gene expression signatures. Genes are ranked in order of significance from left to right. Wald test with Benjamini-Hochberg correction.
(**B**) Box-and-whisker plots showing *PD-L1* expression represented as log2 normalized count in RAS high versus low pathway activity TCGA LUAD cohorts using two independent RAS gene expression signatures. Wald test with Benjamini-Hochberg correction.

To further explore the *in vivo* relevance of TTP regulation in lung cancer, we compared *TTP* expression in FACS-sorted epithelial cells isolated from normal lung or matched tumour tissue from KP mice (*Kras*$^{LSL\text{-}G12D/+}$; *Trp53*$^{F/F}$

mice where tumour formation was initiated by local introduction of a Cre-expressing adenovirus to the lung) (Figure 5.3A), and found that *TTP* expression was downregulated in lung tumour tissue (Figure 5.3B). *PD-L1* mRNA expression was generally higher in tumour tissue than in normal lung but not significantly increased. However, PD-L1 protein expression was significantly elevated on tumour tissue relative to normal adjacent lung, hence we speculate that AKT pathway activation downstream of KRAS may contribute to increasing PD-L1 protein expression *in vivo* (Figure 5.4).

A

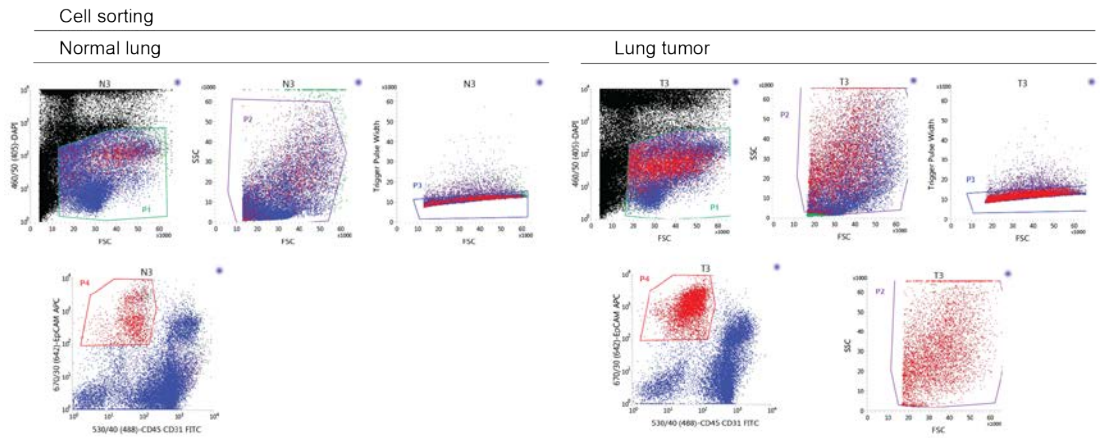

B

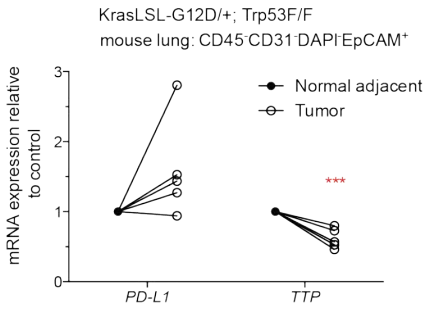

Figure 5.3 TTP is reduced in murine, Kras-driven lung cancer

(**A**) FACS sorting strategy to isolate CD45-CD31-DAPI-EpCAM+ cells from macroscopically dissected lung tumours or normal adjacent lung tissue from *Kras*$^{LSL\text{-}G12D/+}$; *Trp53*$^{F/F}$ mice.
(**B**) qPCR analysis of *PD-L1* and *TTP* expression in FACS purified CD45^{-} CD31^{-}DAPI^{-}EpCAM^{+} cells derived from lung tumours or matched normal adjacent lung tissue from *Kras*$^{LSL\text{-}G12D/+}$; *Trp53*$^{F/F}$ mice. Each point represents

data from an individual mouse and is normalized to the matched normal lung tissue. ***P<0.0005; unpaired, two-tailed Student's t-tests.

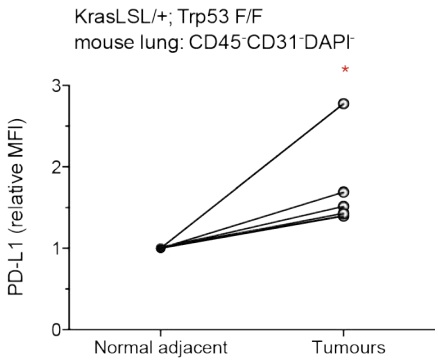

Figure 5.4 PD-L1 protein expression is upregulated on Kras-driven lung tumour cells *in vivo*

Flow cytometry analysis of PD-L1 expression on CD45-CD31-DAPI- cells derived from macroscopically dissected lung tumours or normal adjacent lung tissue from $Kras^{LSL\text{-}G12D/+}$; $Trp53^{F/F}$ mice. Each point represents data from an individual mouse and is normalized to the matched normal lung tissue. Data are pooled from two independent experiments. MFI; Mean Fluorescence Intensity. *P<0.05; unpaired, two-tailed Student's t-test.

Consistent with our results from the KP mouse model of NSCLC, we found that *TTP* was strikingly downregulated in human tumour samples (0.21 fold change) from a publically available dataset comparing mRNA expression in matched normal lung and lung adenocarcinoma tissue (Selamat et al., 2012), confirming that aberrant regulation of *TTP* expression is indeed relevant in the human disease, but may not be a trait specific to tumours with high RAS activity (Figure 5.5A). Rather, our data suggests that remaining tumour TTP activity is suppressed at the level of post-translational modification by RAS signalling. *KRAS* mutation status alone did not strongly segregate with higher *PD-L1* expression in this smaller dataset of lung cancer samples, perhaps indicating that other common drivers of RAS effectors do indeed need to be considered to reliably reflect the regulation of PD-L1 by RAS pathway activity *in vivo* (Figure 5.5B). Unexpectedly, *PD-L1* expression was not significantly increased in the lung tumours versus normal lung tissue in this dataset, despite significant TTP suppression. This may reflects the complex combination of antigen-dependent cell-extrinsic, and antigen independent cell

intrinsic combinatorial effects that influence PD-L1 expression in lung cancer. TTP suppression was not significantly correlated with the KRAS mutational status in this lung cancer dataset (Figure 5.5B), in line with our TCGA data analysis. Interestingly, in breast cancer, a malignancy where RAS deregulation and mutation is uncommon, we observed a strong inverse correlation between *TTP* expression and *PD-L1* expression (Figure 5.5C). TTP was suppressed and PD-L1 was upregulated in breast cancer compared to normal breast tissue. Notably, somatic mutational load is dramatically lower in breast versus lung carcinoma on average (Cancer Genome Atlas, 2012; Cancer Genome Atlas Research, 2014). Therefore this scenario more likely reflects cell-intrinsic and antigen independent control of PD-L1 expression (for example, when considering infiltration by T cells due to recognition of tumour neo-antigens). This pattern of TTP regulation may be more reflective of Myc transcriptional repression of TTP expression in lung and breast, as has been previously reported for lymphoma (Rounbehler et al., 2012).

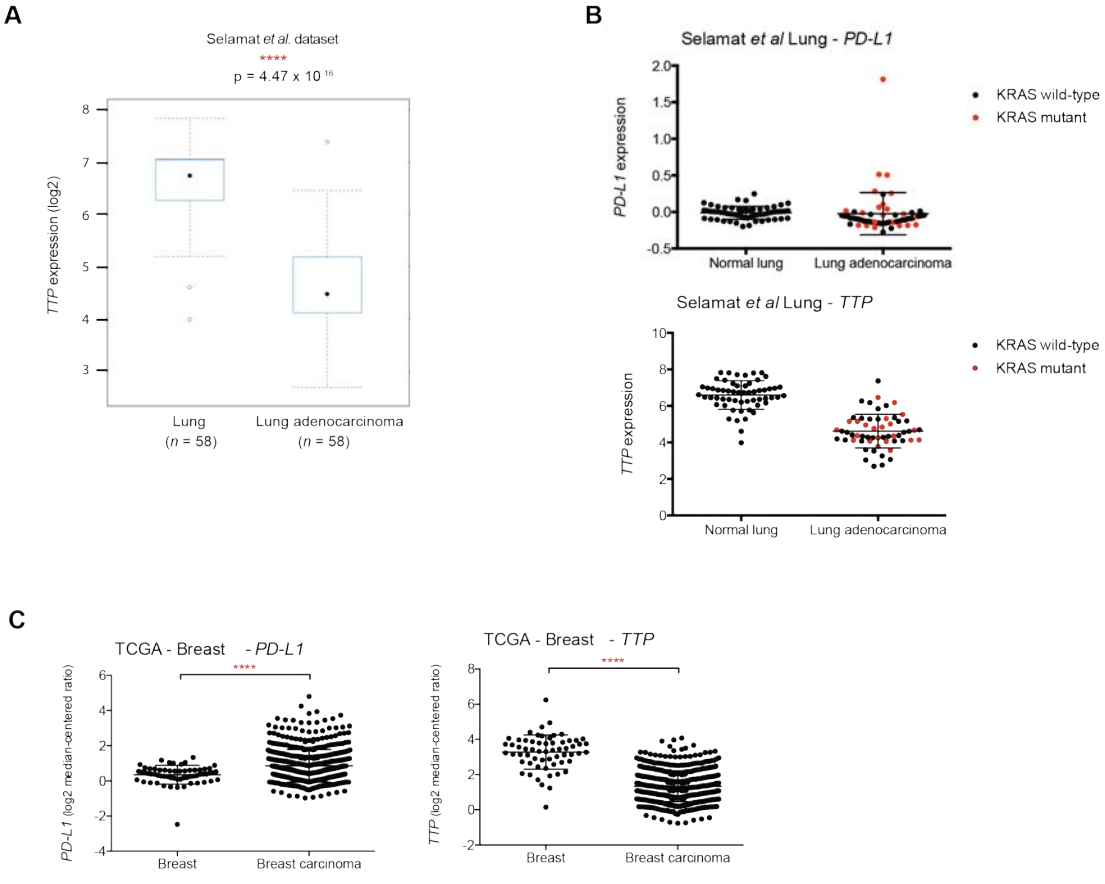

Figure 5.5 TTP is reduced in human lung cancer and breast cancer

(**A**) *TTP* mRNA expression in matched patient lung and LUAD samples. Expression is represented as log2 median-centered intensity. Wilcoxon signed-rank test.
(**B**) *PD-L1* and *TTP* mRNA expression from the Selamat *et al* cohort as in (A), but with dot-plot representation where KRAS mutant samples are highlighted in red. Expression is represented as log2 median-centered intensity.
(**C**) *PD-L1* and *TTP* mRNA expression in matched patient breast and breast carcinoma samples. Expression is represented as log2 median-centered intensity. Wilcoxon signed-rank test.

Using "KM-plotter" software, we found lower tumour *TTP* expression to be significantly correlated with shorter time to progression following surgery in lung adenocarcinoma patients (Figure 5.6). Similar results were obtained when patients were segregated based on either lower quartile or upper quartile *TTP* expression thresholds. These data imply that TTP function may delay lung tumour progression *in vivo*.

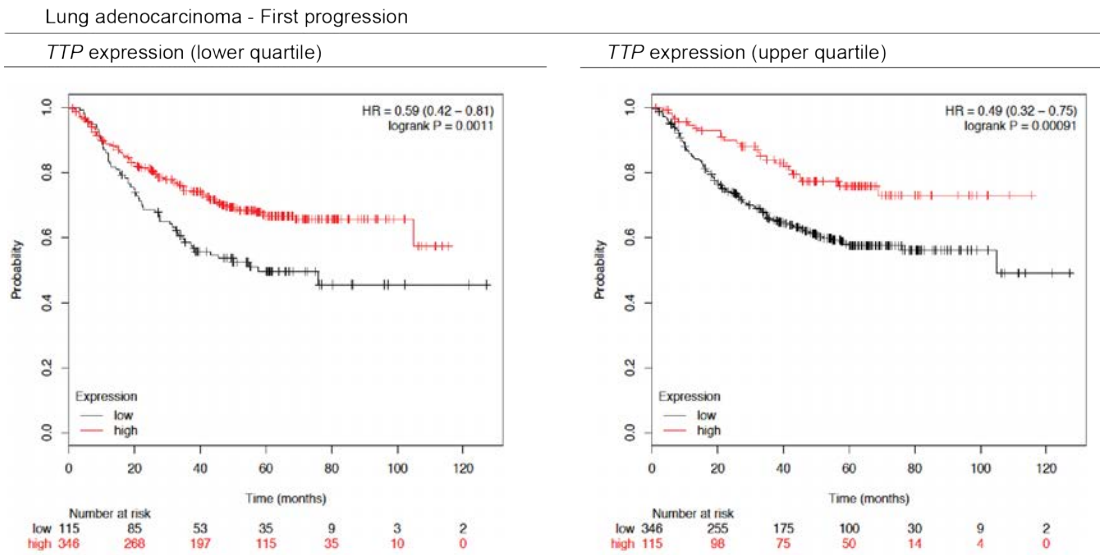

Figure 5.6 Low TTP tumour expression is associated with shorter time to progression in human lung cancer

Kaplan-Meier plots showing time until first progression, generated using "KM-plotter" for lung adenocarcinoma patients (Gyorffy et al., 2013). Samples were segregated into low or high *TTP* expression groups using lower quartile (left panel) or upper quartile (right panel) *TTP* expression thresholds.

To further explore the functional relevance of the control of PD-L1 expression by RAS in lung cancer, we analysed *PD-L1* mRNA and phosphorylated ERK (pERK) levels and localisation in human patient lung adenocarcinoma samples. We analysed *PD-L1* mRNA (by a proprietary *in situ* hybridisation technique, RNAscope) rather than protein because PD-L1 antibodies commercially available at this time did not give satisfactory results on human tissue in our hands. In addition, it is particularly pertinent to measure *PD-L1* mRNA given the regulatory mechanism we describe in Chapter 4.

Although these data are only preliminary given that we only had material from two patients, we observed localised regions of high pERK levels (especially near the periphery of the tumour) that were associated with areas of high *PD-L1* mRNA detection (Figure 5.7). These findings will need to be verified by analysing additional cases, but are generally consistent with our findings from TCGA data analysis (Figure 5.2).

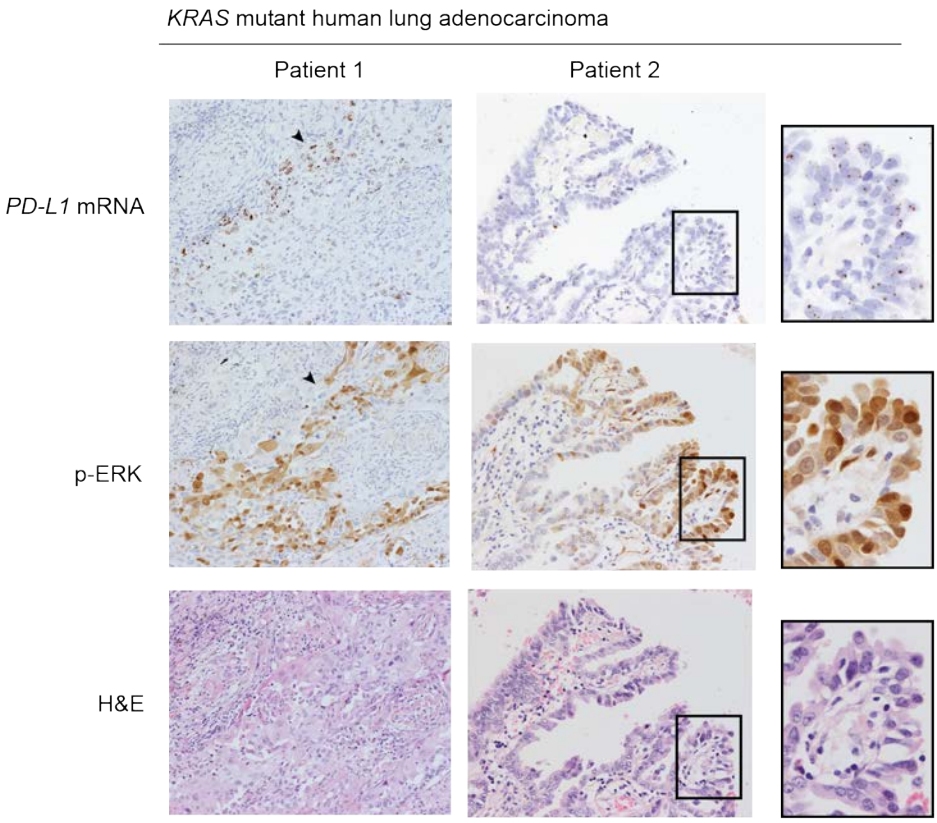

Figure 5.7 Localised RAS activity is assocaited with regions of high *PD-L1* mRNA expression in human lung tumours

Histological analysis of *KRAS* mutant lung adenocarcinoma samples from two different patients. *PD-L1* mRNA was detected by RNAscope. Regions of high pERK activity are also shown at higher magnification (20X).

5.2.2 Restoration of Tumour Cell TTP Expression Enhances Anti-tumour Immunity

Next, we set out to directly assess the functional importance of the regulation of PD-L1 expression by TTP and RAS in tumour progression. To this end, we tested several different syngeneic tumour transplant models for sensitivity to PD-L1 antibody treatment. Firstly, we tested KPB6 cells, as they are *Kras*-mutant lung cancer cells from a C57Bl/6 background and therefore can be transplanted into C57Bl/6 immunocompetent hosts (unpublished). However,

based on our observations in Chapter 3, we reasoned that these cancer cells might lack potent neoantigens as they are derived from an autochthonous GEMM. Therefore, we engineered KPB6 cells that express a modified, non-secreted form of the model antigen ovalbumin, fused to the fluorescent protein cherry (ΔOVA-Cherry). We then subcutaneously injected parental KPB6 cells, and in parallel, injected the OVA-derivative cells into the contralateral flank. We then treated tumour-bearing mice with MEK inhibitor, PD-L1 monoclonal antibody, the combination therapy, or vehicle and isotype control antibodies and measured tumour growth over time (Figure 5.8A). This treatment schedule was generally well tolerated, with little or no weight loss throughout the drug treatment course in female or male mice (Figure 5.8B).

Although the KPB6 parental line responded to MEK inhibitor, there was no significant effect of anti-PD-L1 antibody therapy, perhaps reflecting the lack of antigens expressed by this cell line. The KPB6-OVA cells were spontaneously rejected after approximately nine days post-engraftment. Temporally, this indicates that this rejection was linked to a spontaneous adaptive immune response against the tumour. Unfortunately, these results preclude this system from testing ways to increase anti-tumour immunity, as any functional modulation of PD-L1 expression will likely be masked by this strong spontaneous response.

Secondly, we tested the same treatment schedule on the Lewis lung carcinoma cell line LLC1 from C57Bl/6 strain background (Figure 5.8C). We chose to test this lung cancer cell line because there are reports that show LLC1 tumours are responsive to modulation of tumour-cell PD-L1 expression (Chen et al., 2014). Conversely, we did not find that anti-PD-L1 antibody treatment significantly controlled tumour progression; only MEK inhibitor reduced tumour growth and, moreover, PD-L1 did not combine strongly with MEK inhibitor (Figure 5.8C).

Next, we used the *Kras*-mutant, mouse colon carcinoma cell line CT26, based on its immunogenicity and sensitivity to anti-PD-L1 antibody therapy (Duraiswamy et al., 2013). For this cell line, we engineered CT26 cells to overexpress PD-L1 cDNA, and analysed the growth of several concentrations of parental or PD-L1-high derivative CT26 cells in syngeneic BALB/c mice (Figure 5.8D). In this preliminary experiment, we observed that PD-L1-high cells generally grew faster than parental cells engrafted at the same concentration, suggesting that this model may be amenable to test the functional role of the regulation of PD-L1 expression by TTP *in vivo*.

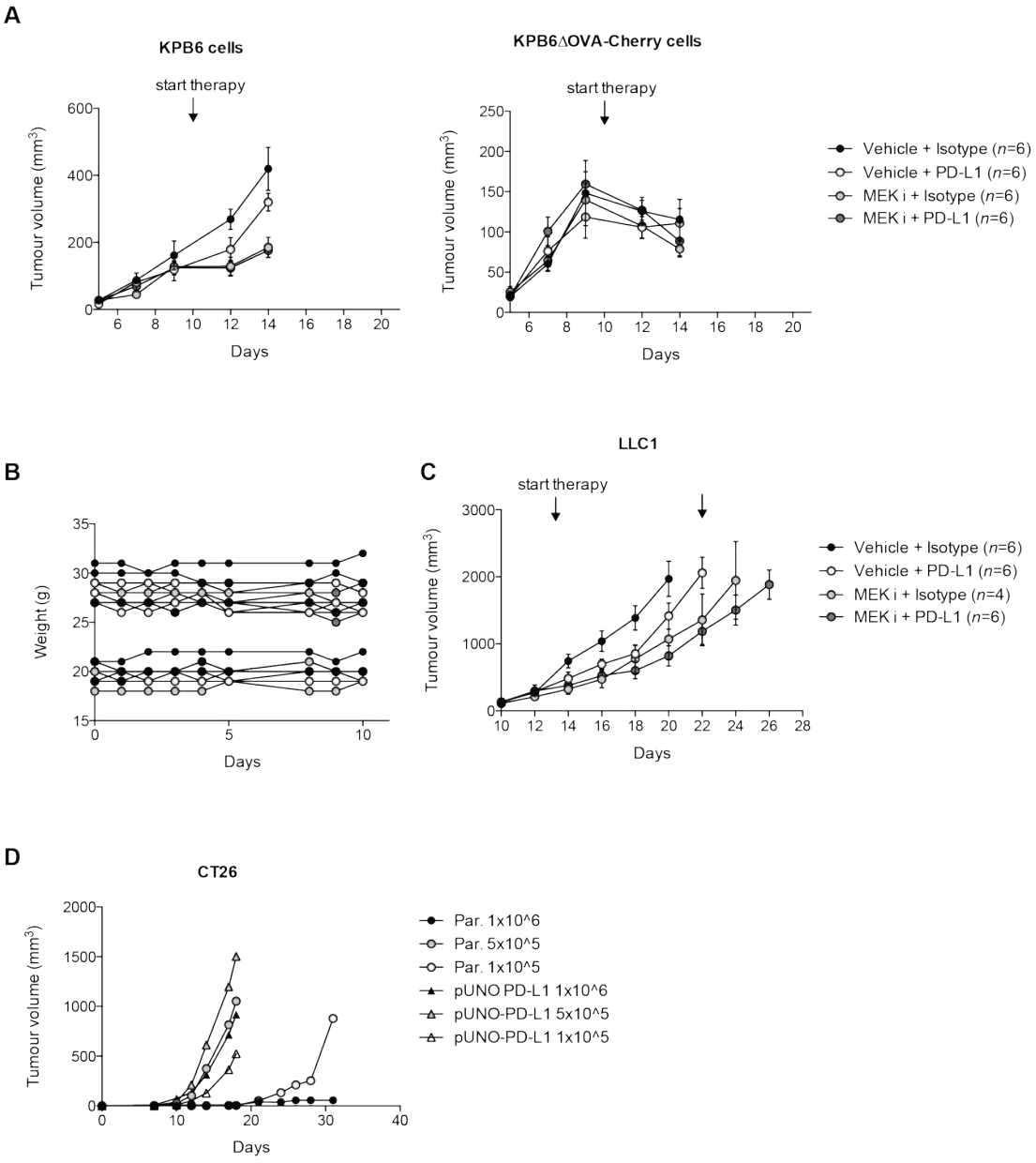

Figure 5.8 Surveying immunogenicity and PD-L1-dependence of syngeneic tumour models

(**A**) Tumour growth curves following subcutaneous injection with 5 x10^5 KPB6, and with 5 x10^5 KPB6ΔOVA-Cherry lung cancer cells in the contralateral flank.
(**B**) Weight of mice over treatment period. Mice with weights ranging from 17-22 g are female, and from 25-33 are male.
(**C**) Tumour growth curves following subcutaneous injection with 1 x10^5 LLC1 lung cancer cells.
(**D**) Tumour growth curves following subcutaneous injection with different concentrations of parental (Par.) and PD-L1Δ3'UTR overexpressing CT26 colon carcinoma cells.
The start of therapy is indicated with arrows. MEK inhibitor GSK1120212 was given by oral gavage daily (3 mg/kg). Tumour dimensions were monitored with calipers. Anti-PD-L1 antibodies or isotype control antibodies were given i.p once weekly (10 mg/kg).

We tested several approaches to experimentally manipulate TTP expression levels before tumour cell engraftment. Firstly, we used shRNAs against TTP. In conjunction, we also targeted PD-L1 with shRNAs in an attempt to reverse functional effects of PD-L1 upregulation following *TTP* knock-down. However, *TTP* knock-down levels were very poor for all of the shRNA sequences tested from the pLKO.1 clone collection (Figure 5.9A). Only shTTP#2 significantly reduced *TTP* expression in 368T1 mouse lung cancer cells, and this was associated with a small but significant increase in *PD-L1* expression. Similar results were obtained in CT26 cells for shTTP#2 and the best shRNA for PD-L1 in this system from the pLKO.1 set, but effects on target gene expression were still modest and there was an unanticipated upregulation of TTP expression with the shRNA against *PD-L1* (Figure 5.9A). Attempts to knock-down *TTP* and *PD-L1* with next-generation back-bone shRNA constructs from Transomics also failed (data not shown). Given these results, we attempted to overexpress TTP protein as an alternative approach.

To this end, we constructed constitutive TTP expression vectors in pCDNA and pBABE backbones and introduced them stably into CT26 cells. However, we found that long-term selection of these cells failed to result in cells

expressing TTP at detectable levels, despite complete resistance to selection antibiotics (Figure 5.9B). We speculate that this effect may be due to the long-term negative effects of high levels of TTP overexpression, since TTP has been implicated in cell-autonomous tumour-suppressive roles (Rounbehler et al., 2012).

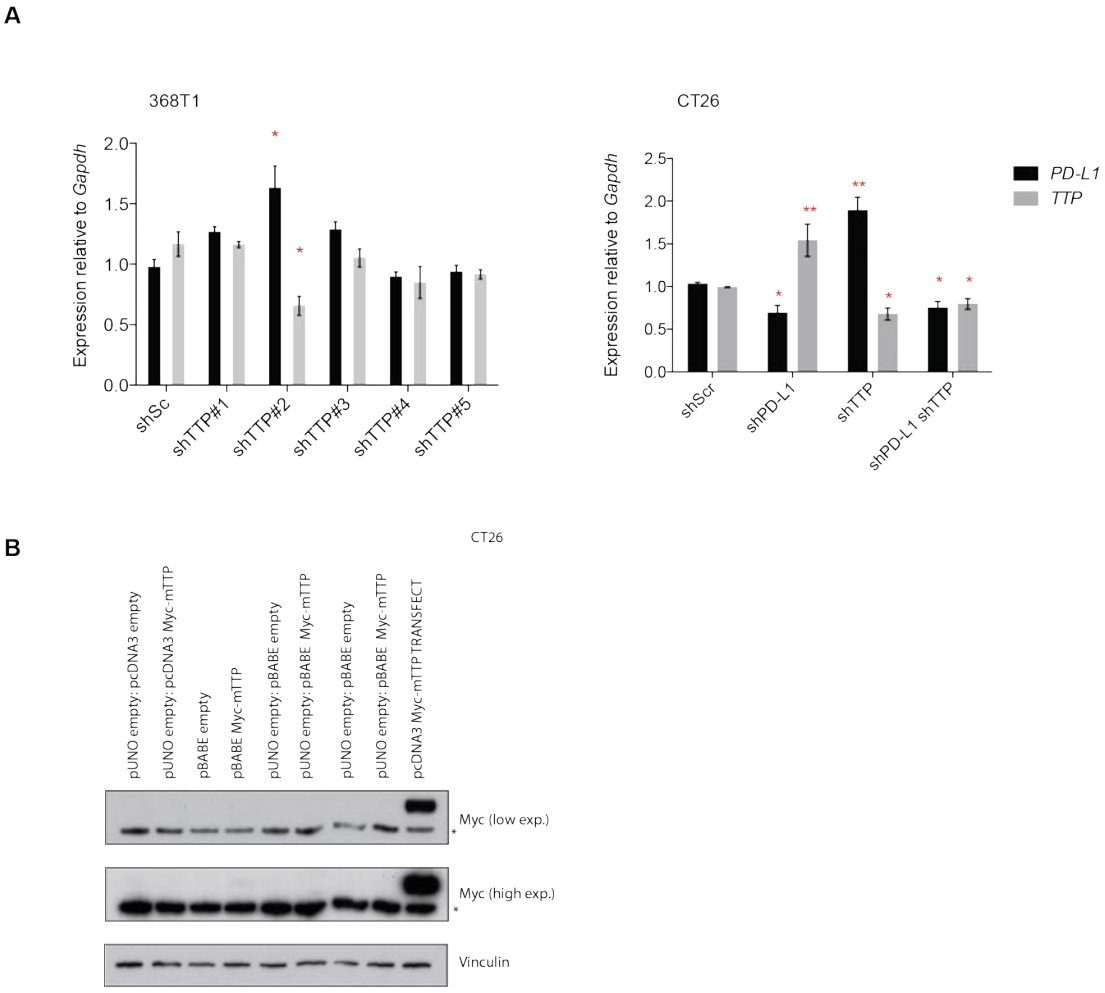

Figure 5.9 Optimisation of the experimental modulation of TTP expression

(**A**) qPCR analysis of *PD-L1* and *TTP* expression in 368T1 and CT26 mouse cancer cells stably expressing the indicated shRNAs. Data are mean ± SEM from biological triplicates.
(**B**) Western blotting analysis of Myc2-mTTP transgene expression in multiple CT26-derivative cell lines harbouring the indicated constructs. Transfection of pCDNA3 Myc-mTTP serves as a positive control. mTTP, mouse TTP.

To overcome the issues regarding long-term constitutive expression of TTP, we next generated a series of stable CT26 cell lines expressing Myc-tagged, mouse TTP under a tetracycline-inducible promoter (TTP tet-ON). TTP expression was induced upon addition of doxycycline in a dose-dependent manner (Figure 5.10A), resulting in decreased PD-L1 protein expression at the cell surface (Figure 5.10B). In addition, we engineered these CT26 cells to constitutively express either empty vector as a control (Empty), or mouse *PD-L1* cDNA lacking the 3'UTR (PD-L1 Δ3'UTR). Overexpression of PD-L1 Δ3'UTR rendered total PD-L1 levels effectively insensitive to TTP induction (Figure 5.10B).

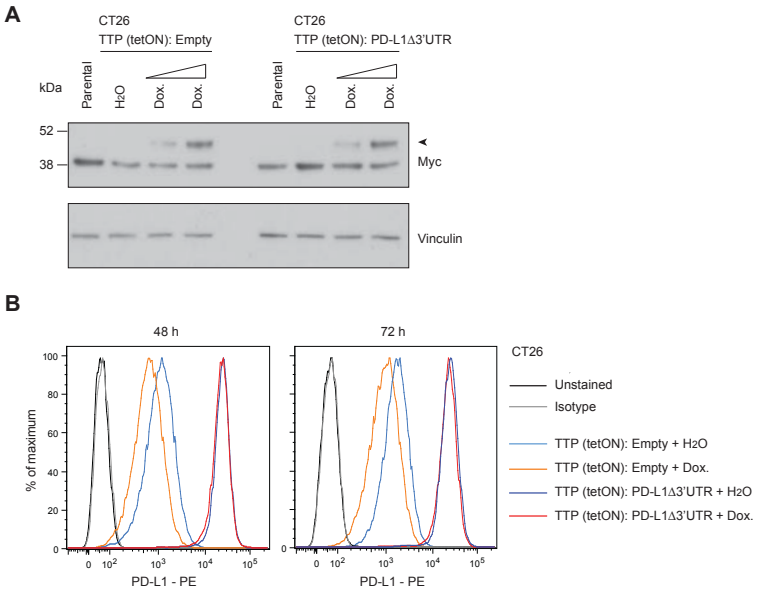

Figure 5.10 3'UTR-dependent suppression of PD-L1 by TTP transgene induction

(**A**) Western blotting analysis of stable CT26 cell lines expressing Myc-tagged, mouse TTP under a tetracycline-inducible promoter (TTP tet-ON), and expressing either empty vector (Empty) or mouse *PD-L1* cDNA lacking the 3'UTR (PD-L1 Δ3'UTR). Cells were treated with doxycycline (Dox., 0.1 μg/ml or 1 μg/ml) or vehicle for 24 h before analysis. Arrow indicates Myc-TTP.
(**B**) Representative histograms from flow cytometry analysis of PD-L1 surface expression in CT26 stable cells lines in (A) after treatment with doxycycline

(Dox., 1 μg/ml) or vehicle for 48 h or 72 h. Data are representative of three independent experiments.

Furthermore, we further verified the functional repression of PD-L1 expression by also engineering CT26 cells expressing the full length PD-L1 cDNA including the 3'UTR. As expected, these cells expressed lower levels of PD-L1 than the PD-L1Δ3'UTR expressing cells (Figure 5.11).

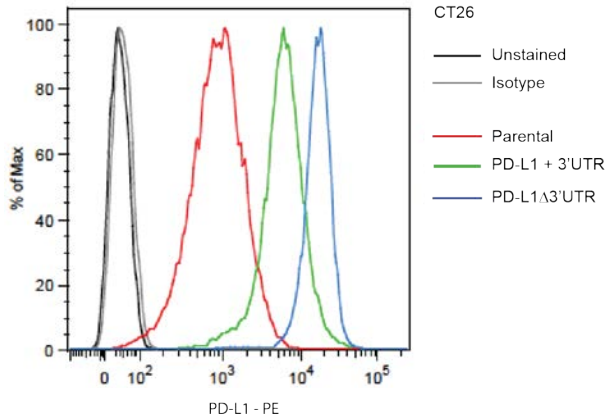

Figure 5.11 The endogenous 3'UTR of PD-L1 decreases expression of a PD-L1 transgene

Representative histograms of flow cytometry analysis of PD-L1 expression in stable CT26 cell lines harbouring the indicated PD-L1 expression constructs.

As expected, TTP transgene expression with doxycycline was associated with a decrease in *PD-L1* mRNA stability, which was comparable to that mediated by MEK inhibition in this system (Figure 5.12A). Crucially, the growth rates of the stable cell lines *in vitro* did not significantly differ with the overexpression of PD-L1 Δ3'UTR cDNA (Figure 5.12B), or the induction of TTP transgene expression with doxycycline (Figure 5.12C).

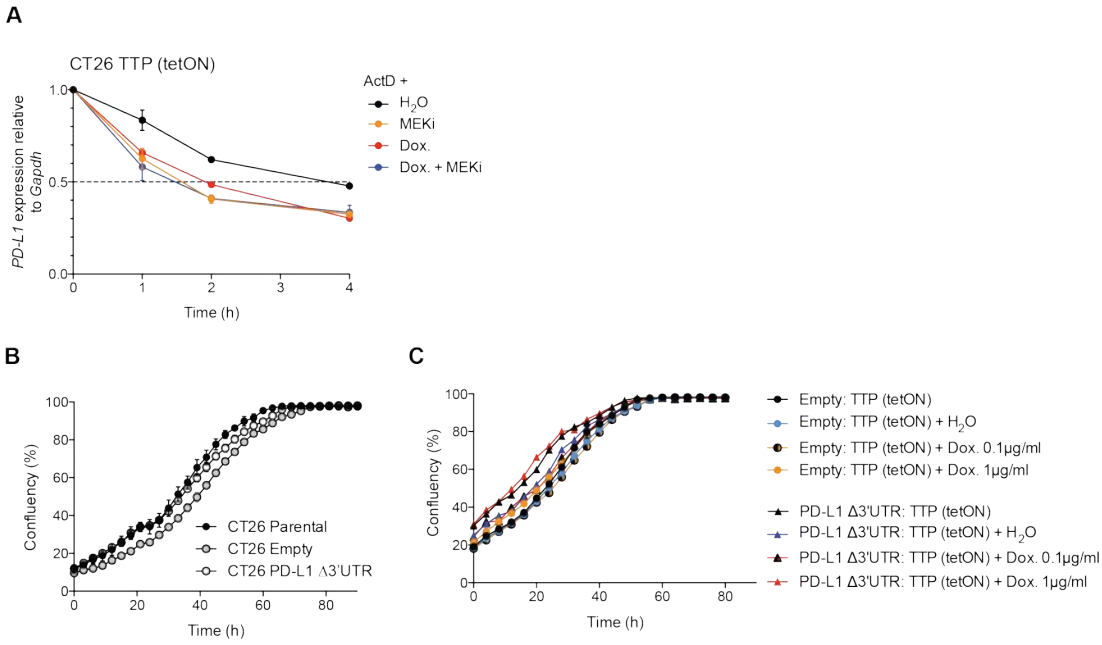

Figure 5.12 TTP transgene induction reduces *PD-L1* mRNA stability but does not reduce cell proliferation *in vitro*

(**A**) Stability of murine *PD-L1* mRNA measured by qPCR analysis. CT26 TTP (tetON) cells were pretreated with doxycycline (Dox.; 1 µg/ml) or vehicle for 16 h and then MEK inhibitor (GSK1120212, trametinib; 25 nM) for an additional 30 min before actinomycin D (ActD; 10 µg/ml) was added. Data are normalized to time 0 h when ActD was added and represent the mean ± SEM of two independent experiments.
(**B**) Confluency was measured using IncuCyte for CT26 parental and stable derivative cell lines. Data represent the mean ± SD of biological triplicates.
(**C**) Confluency was measured using IncuCyte for CT26 stable derivative cell lines treated with the indicated concentrations of doxycycline or vehicle at t = 0 h. Data represent the mean ± SD of biological triplicates and are representative of two independent experiments.

Using these engineered CT26 cell lines, we performed subcutaneous transplantation experiments in mice and monitored tumour progression. *In vivo*, doxycycline treatment significantly reduced tumour growth in immune competent, syngeneic BALB/c mice (Figure 5.13A). Strikingly, the anti-tumour effects mediated by doxycycline treatment were absent in immunocompromised *nu/nu* mice, implying an essential contribution from the adaptive immune system to this anti-tumour response (Figure 5.13A).

Tumour cells overexpressing PD-L1 Δ3'UTR grew significantly faster than the empty vector cells in BALB/c mice, but had no growth advantage in *nu/nu* mice. Moreover, expression of PD-L1 Δ3'UTR was able to rescue the growth inhibition mediated by doxycycline treatment in BALB/c mice, suggesting that suppression of tumour cell PD-L1 expression is an essential component of the anti-tumour effects mediated by TTP transgene induction. Consistently, tumours derived from mice treated with doxycycline had a greater degree of CD3+ lymphocyte infiltration than tumours from mice treated with vehicle, and this corresponding infiltration was abrogated in tumours derived from cells overexpressing PD-L1 Δ3'UTR (Figure 5.13B and Figure 5.13C).

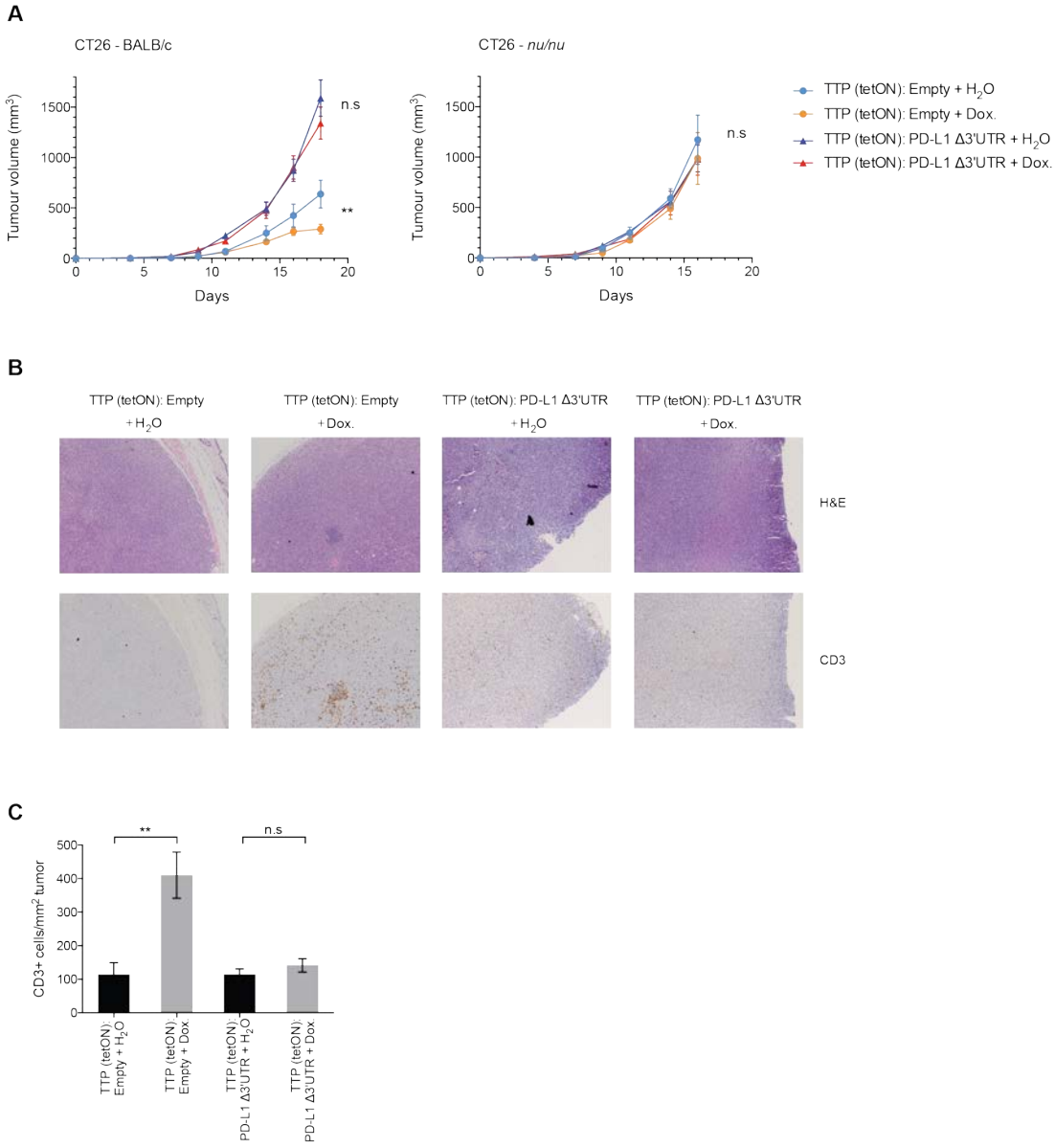

Figure 5.13 Restoration of tumour cell TTP enhances anti-tumour immunity

(**A**) Tumour growth curves for the indicated CT26-derived cell lines subcutaneously transplanted into BALB/c mice (left panel, $n = 8$ per group) or *nu/nu* mice (right panel, $n = 6$ per group). Treatment with vehicle or doxycycline (Dox., 50 mg/kg) by oral gavage commenced from day three after tumour cell injection. Mean ± SEM. $^{**}P=0.0072$, n.s., not significant; two-way ANOVA.
(**B**) Histological analysis of subcutaneous tumours at the end-point from the experiment described in (A). Magnification is 4X.
(**C**) Semi-automated quantification of CD3+ cell in the CT26 tumours as in (B) using NIS elements software. Five fields of view were quantified per mouse, with 5-6 mice per group. $^{**}P > 0.01$.

Collectively, these data highlight the functional importance of the regulation of PD-L1 expression by TTP in tumour progression, and demonstrate that this novel regulatory pathway may be exploited for the treatment of *Ras*-mutant cancers. These findings support a model where tumour-specific suppression of TTP can foster PD-L1 upregulation, and ultimately, tumour immunoresistance.

5.3 Conclusions

In this chapter, we have verified the *in vivo* relevance of our findings on the regulation of PD-L1 expression in cancer by TTP and RAS. We have found that human lung tumours with high RAS pathway activity express increased levels of PD-L1 compared to low RAS activity tumours. It is the subject of on going work in our laboratory to further characterise the immune profile of RAS active lung tumours using bioinformatics approaches.

We found that TTP expression is strikingly reduced in lung cancer versus normal lung tissue. We also confirmed that this downregulation of tumour TTP expression is evident in the *KP* mouse model. However, we did not find that TTP is significantly downregulated in human RAS active tumours

compared to RAS low activity tumours. This may be partly influenced by the complication of TTP's ability to autoregulate expression of its own transcript through AREs in the 3'UTR of TTP (Tchen et al., 2004). Regardless, we speculate that remaining TTP protein in tumours is further suppressed by phosphorylation and inactivation in RAS active tumours.

We note that acute activation of TTP expression can be achieved by growth factor stimulation of serum-starved cells; however, acute serum stimulation resulted in only a rapid and transient increase followed by a prolonged reduction in TTP expression. Concordantly, *TTP* expression was significantly suppressed in lung tumours from a genetically engineered mouse model of *Kras*-driven lung cancer, and in human patient lung adenocarcinoma samples relative to normal lung tissue. This is consistent with a tumour-suppressive role for TTP *in vivo* (Rounbehler et al., 2012). We also noted an increase in time to first progression from surgery in lung adenocarcinoma patients with high TTP expression levels. Indeed, this may reflect suppression of immune evasion in these tumours.

We reveal that TTP transgene expression can restrain tumour growth in an experimental CT26 tumour model, and demonstrate that this anti-tumour effect is predominantly non-cell autonomous, dependent on the adaptive immune system and suppression of tumour cell PD-L1 expression. We noted only minor reductions in tumour growth rates following TTP transgene induction in cells overexpressing PD-L1 Δ3'UTR, although these differences were not significant. TTP has been reported to have cell-autonomous tumour suppressive roles (Rounbehler et al., 2012) and other non-cell autonomous anti-tumour effects mediated by targeting VEGF and COX-2 mRNAs (Cha et al., 2011; Essafi-Benkhadir et al., 2007), which may contribute to some of these ostensibly PD-L1-independent effects, the magnitude of which are likely to be determined by the level of TTP overexpression in each system.

We also provide further evidence that targeting RAS effectors such as MEK and PI3K may elicit non-cell autonomous, anti-tumour effects in *RAS*-mutant tumours. Recently, the MEK inhibitor trametinib (used in this study) and PD-1 blockade were shown to combine strongly *in vivo* in a syngeneic tumour model of *Ras*-mutant colon carcinoma (Liu et al., 2015). Therefore, our findings may inform the development of rational and effective combination therapies with immune checkpoint blockade in cancer.

6 Chapter 6. Discussion

6.1 Immunogenicity of autochthonous GEMMs

We reason that the *Kras*$^{LSL\text{-}G12D/+}$; *Trp53*$^{F/F}$ mouse failed to recapitulate the positive clinical responses observed for anti-PD-L1 immunotherapy (Brahmer et al., 2012) due to the relatively poor immunogenicity of these murine tumours for the following reasons: (1) we administered the maximum dose of anti-PD-L1 antibody successfully used in patients in clinical trials (10 mg/kg; (Brahmer et al., 2012), (2) we confirmed that the therapeutic antibody was binding to the target lung tissue, and (3) we observed no significant difference in tumour growth dynamics in immunocompromised *Kras*$^{LSL\text{-}G12D/+}$; *Trp53*$^{F/F}$; *Rag2*$^{-/-}$ mice compared to their immunocompetent counterparts, suggesting that adaptive immunity plays little role in controlling tumour growth in *Kras*$^{LSL\text{-}G12D/+}$; *Trp53*$^{F/F}$ mice. Concordantly, several recent studies demonstrate that, in the absence of carcinogens from cigarette smoke, lung tumours from GEMMs have a dramatically lower rate of point mutations in their genome than a smoker's lung adenocarcinoma (McFadden et al., 2014b); (Westcott et al., 2015a); (Rizvi et al., 2015a); Julian Downward's laboratory, unpublished data). However, we cannot exclude possible immunosuppressive mechanisms from contributing to primary anti-PD-L1/anti-CTLA-4 antibody resistance. Still, our findings together with published reports on the tumour somatic mutation rate in GEMMs of lung cancer indicate that there is a need for GEMMs that more closely mimic the mutation rate, and thus immunogenicity, of human NSCLC.

Contrary to our results, other mouse models of *KP*-driven cancer have been shown to respond to immunotherapies. For example the *LSL-KrasG12D/+; LSL-Trp53 R172H/+; Pdx1-Cre* (*KPC*) model of pancreatic cancer has been shown to respond to a p110δ inhibitor, affecting Treg function (Ali et al., 2014). However, the authors do not report on decreases in tumour volume

and we note that there are now concerns about the authenticity of this data (Ali et al., 2016). In addition, the *KPC* model has been demonstrated to respond to anti-PD-1 antibody treatment, but only in combination with a CXCR4 inhibitor, which promotes T cell infiltration into the pancreatic tumour (Feig et al., 2013). This inhibitor of the CXCR4 chemokine receptor partially reverses immunosuppression mediated by tumour-associated fibroblasts in the stroma of pancreatic cancers in this model. Also, Vonderheide and colleagues showed that *KPC* mouse tumours that were normally refractory to anti-PD-1 and anti-CTLA-4 combination therapy were rendered sensitive only when ICB antibodies were combined as a five-drug combination, with nab-paclitaxel, gemcitabine and an agonistic anti-CD40 antibody (Winograd et al., 2015). In line with our data, the authors report high levels of PD-L1 upregulation on pancreatic tumour cells, a phenomenon that is not influenced by T cell depletion; this implies a degree of cell-intrinsic PD-L1 upregulation in RAS-mutant pancreatic tumour cells. Furthermore, CXCR2 inhibition has been shown to sensitise *KPC* pancreatic tumours to anti-PD-1 therapy by reversing immunosuppression by neutrophils and myeloid-derived suppressor cells in the tumour microenvironment and increasing T cell infiltration into tumours (Steele et al., 2016). Strikingly, inhibition of CXCR2 signalling alone with the small molecule inhibitor AZ13381758 was sufficient to reduce the incidence of metastasis in the *KPC* model. Finally, the *KP* – OVA lung cancer model ostensibly responded to anti-PD-1 and CTLA-4 ICB, but only when combined with the ICD-inducer oxaliplatin and the Treg-depleting chemotherapy cyclophosphamide (Pfirschke et al., 2016). However, we note that the anti-tumour effects reported by Pfirschke *et al* mediated by the combination of oxaliplatin, cyclophosphamide and ICB are modest and only slightly better than chemotherapy alone. In addition, many of their analyses of anti-tumour responses were based on measurement of lung weight, which is a crude read-out of tumour-burden and easily confounded by immune infiltrates and other issues relating to the dynamic cellularity of the diseased lung. Moreover, this method does not give information on the behaviour of single tumour lesions over time.

In a study using a mouse cell line derived from a GEMM of melanoma, syngeneically engrafted tumours were essentially resistant to anti-PD-1 therapy and grew similarly in immunodeficient mice (Zelenay et al., 2015). However, when COX-mediated production of immunosuppressive prostaglandins was disrupted in tumour cells, these tumours responded to PD-1 antibody therapy. This cell line is unlikely to harbour many potent neo-antigens, although there are examples of tumours with lower mutational burden responding to ICB (Hugo et al., 2016). Finally, in a mouse model of BRAF-driven melanoma, tumours were resistant to PD-L1 ICB until CD103+ DC recruitment and expansion was initiated with FLT3L and poly(I:C) treatment (Salmon et al., 2016b).

There is clearly a recurrent theme in the reports outlined above: RAS/RAF-driven GEMMs of cancer have primary resistance to ICB treatments in isolation, and require additional therapies to remodel the tumour-microenvironment in order to be efficacious. Although our data points towards unrealistically low levels of lung tumour immunogenicity, it remains possible that tumour-associated antigens are present that could facilitate tumour rejection if the immune-suppressive microenvironment is perturbed. One potentially important difference in the *KPC* mouse model is the expression of the mutant form of *Trp53* (in contrast to *Trp53* deletion, in our *KP* lung model), which could potentially act as a tumour neo-antigen. One might argue that these poorly immunogenic models could be used to model tumours lacking strong neo-antigens found in the clinic.

By generating lung tumour cell lines from immunocompetent *Rag1+/-* or immunodeficient *Rag1-/-* hosts, we were able to show that most cell lines were not classically “immunoeditied” *in vivo,* that is, they grew comparably well when transplanted into wild-type or *Rag1-/-* recipient mice. However, we did identify one cell line that behaved as if it elicited a strong anti-tumour immune response. Mice that rejected this *KPRag1-/- c* cell line developed

immunological memory and could reject these tumour cells upon re-challenge. Although further investigation is required to determine the nature of the tumour-rejection antigen, these are the first data to suggest that there are immunogenic clones in the tumours from this mouse model that could be selected against by the adaptive immune system. Theoretically, very few neo-antigens are actually necessary to evoke an immune response; regarding tumour neo-antigens, successful anti-tumour immunity seems to be more reliant on quality than quantity. For example, Ribas, Lo and colleagues found that tumour mutational burden alone could not reliably predict response to PD-1 therapy in melanoma patients, as several tumours with low mutational burden still responded (Hugo et al., 2016). Importantly, the comparable tumour progression we observed in *KP;Rag2+/-* and *KP;Rag2-/-* mice suggests that any immunoediting in this model is likely to be infrequent and has minimal impact on long-term tumour burden and latency of the disease.

Several groups have introduced foreign antigens into GEMMs of cancer to more easily study host-tumour interactions, notably OVA (DuPage and Jacks, 2013). The development of tetramer reagents to follow antigen specific T cell responses to tumours with known model antigens is a powerful advantage of this approach. Such studies have elucidated interesting, tissue-specific modes of immunosuppression *in vivo*. For example, the Tyler Jacks laboratory recently showed that Tregs play a significant role in supressing anti-tumour immune responses against a modified *KP* model, where tumour cells express OVA antigens (Joshi et al., 2015b). As mentioned in the Introduction, the evolution of a polyclonal tumour is likely to differ significantly from this monoclonal tumour model expressing potent foreign antigens.

Using a spontaneous GEMM of NSCLC without the expression of exogenous tumour antigens, we found that numbers of APCs were significantly elevated in tumour-bearing lungs, but not healthy lungs, of mice treated with Carb/Tax chemotherapy. To delineate whether the increase in APC numbers is due to

local expansion of resident APCs or influx from neighbouring lymphoid structures, one could perform an adoptive transfer experiment using labelled APCs before treatment. Although increases in APC numbers in the lung did not lead to a detectable anti-tumour adaptive immune response, it would be interesting to examine the consequence of these effects in a more immunogenic mouse tumour model. Our laboratory is currently developing ways to increase tumour mutation rate and thus neo-antigen burden, for example, by introducing carcinogens. Urethane is a carcinogen found in tobacco smoke and can initiate lung tumours harbouring driving mutations in *Kras* as well as an average of 185 single nucleotide polymorphisms (SNVs) (Westcott et al., 2015a). Lung tumours from the *KrasLA2* GEMM on the other hand (where the latent oncogenic *Kras* allele is spontaneously activated by recombination), only carried an average of 47 SNVs. We predict that mouse models of lung cancer initiated with urethane or MNU will be more immunogenic, although this remains to be demonstrated. Importantly, the carcinogen mouse models will overcome the requirement for tumour initiation by lentiviruses or adenoviruses. Viral infection and transient expression of the bacterial Cre-recombinase at the pre-neoplastic stage may have profound implications on anti-tumour immunity, and is unrepresentative of virus-independent tumorigenesis in humans. A disadvantage of both tumour models (and perhaps a critique of mouse models of cancer in general) is that tumour progression is very rapid and occurs within months. This does not recapitulate tumour development in humans. In fact, there is evidence that lung cancer progression can take decades before becoming clinically overt (de Bruin et al., 2014). The accrual of other important genetic changes, and the co-evolution of host and tumour over this time-scale is not feasible in mouse models of cancer.

6.2 Regulation of PD-L1 expression by TTP and RAS

In this report, we uncover an oncogenic KRAS-driven signalling network capable of driving cell intrinsic tumour PD-L1 expression, implying that this oncogenic program may uncouple tumour PD-L1 expression and the immunogenicity of the tumour. RAS controls *PD-L1* mRNA expression partly through an unanticipated post-transcriptional mechanism, mediated by the AU-rich element binding protein TTP (Figure 6.1).

We discovered that PD-L1 is encoded by an unstable transcript, from which gene expression can be controlled through functional AU-rich elements in the 3'UTR of the mRNA. Immunomodulatory molecules such as cytokines are among the most frequently controlled genes by ARE-mediated decay, as their expression often requires rapid and dynamic regulation (Anderson, 2008). For example, CD28 ligation on T cells results in the stabilisation of several ARE-containing cytokine mRNAs (Lindstein et al., 1989). Since PD-L1 is upregulated on T cells following CD28/CD3 ligation and MAPK activation (Yamazaki et al., 2002), our results suggest that PD-L1 may also be upregulated through mRNA stabilisation in activated T cells.

We show that endogenous levels of TTP and KSRP bind to the unstable *PD-L1* transcript. There are reports that these ARE-BPs work together to destabilise target transcripts (Linker et al., 2005), but we did not observe obvious signs of cooperation when we over-expressed TTP and KSRP together. However, there are limitations to experiments involving overexpression; for example, the maximum repression of *PD-L1* mRNA or *PD-L1 3'UTR* luciferase reporter expression might have already been reached with the overexpression of TTP or KSRP alone, essentially leading to saturation of the mRNA degradation machinery.

Our finding that TTP binds to the 3'UTR of *PD-L1* potentially explains why the 3'UTR of *PD-L1* is recurrently lost in cancer, including NSCLC (Kataoka et al., 2016). Here, we show that complete loss of *PD-L1* 3'UTR increases PD-L1 expression (as in (Kataoka et al., 2016)) and furthermore, mutation of AREs increases expression of a *PD-L1* 3'UTR luciferase reporter. Kataoka and colleagues reveal that *PD-L1* 3'UTR loss is found in many different cancers, perhaps supporting the functional relevance of our findings across multiple tissue types and malignancies. We speculate that aberrant regulation of TTP is a more common mechanism of *PD-L1* dysregulation, although presumably complete loss of the 3'UTR would lead to a more profound increase in *PD-L1* expression, as miRNA-mediated regulation is also lost. Modulating TTP function using small molecule inhibitors of the appropriate pathways may be a therapeutic option in the majority of immunogenic cancers that have intact *PD-L1* 3'UTRs (Figure 6.1).

Recently, several studies using RNA individual-nucleotide resolution crosslinking and immunoprecipitation (iCLIP) approaches have provided useful insights into the mRNA targets and binding sites of TTP and TTP family-members. In a comprehensive analysis of TTP binding partners in LPS-stimulated mouse macrophages, TTP was found to bind to *PD-L1* mRNA at AREs in the 3'UTR (Sedlyarov et al., 2016). Using genome-wide RNA sequencing, Sedlyarov and colleagues revealed that *PD-L1* mRNA was more stable and more potently induced in response to LPS in TTP KO macrophages compared with wild-type macrophages. Using a similar approach, work on ARE-BP involvement in mouse B-cell development revealed that *PD-L1* mRNA was among the many target transcripts of Zfp36l1, and moreover, *PD-L1* mRNA expression was elevated in *Zfp36l1* and *Zfp36l2* double-knockout B-cells (Hodson et al., 2010). These data imply a degree of redundancy within the TTP family. In lung cancer cells, we showed that siRNA-mediated knock-down of *ZFP36L1* or *ZFP36L2* did not significantly increase *PD-L1* expression, perhaps reflecting tissue-specific

differences, and the obvious limitations of gene silencing by RNAi as compared with full genetic deletion.

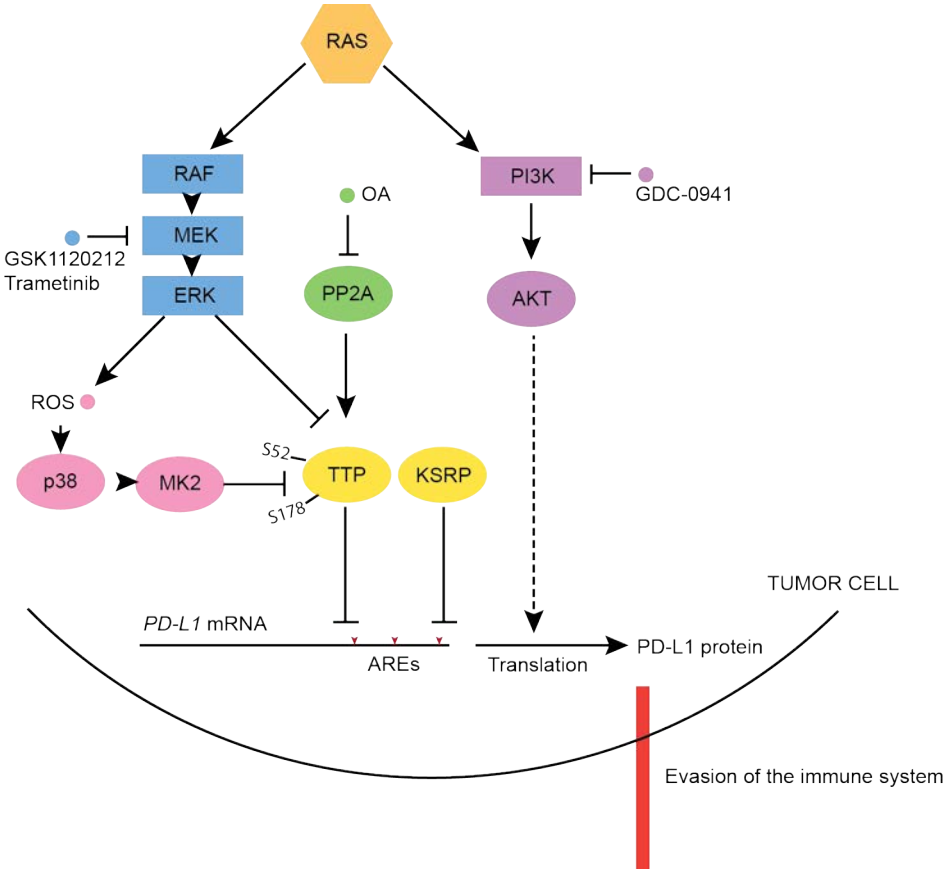

Figure 6.1 Regulation of *PD-L1* mRNA stability through RAS and TTP signaling networks

Proposed molecular model. RAS-mediated upregulation of PD-L1 is dependent on both MEK and PI3K effector pathways. MEK signalling stabilises the labile transcript, and PI3K-AKT signalling predominantly acts via upregulating translation of the mRNA (Parsa et al., 2007). *PD-L1* mRNA is targeted by AUBPs including TTP and KSRP via AREs in the 3'UTR. Chronic oncogenic RAS-MEK signalling downregulates TTP activity, resulting in increased expression of PD-L1 in tumour cells. Signalling nodes are highlighted that may be targeted with drugs to modulate anti-tumour immunity. S52 and S178 represent MK2 target sites and numbering corresponds to mouse TTP. OA, Okadaic acid.

Mechanistically, TTP expression is suppressed in human and mouse lung cancer. Remaining TTP function in *RAS*-mutant cancer cells is further downregulated by phosphorylation (Figure 6.2). TTP is phosphorylated by

ERK activation (Taylor et al., 1995) and, importantly, by MK2, at key inhibitory sites. Although mutation of ERK-consensus sites had no discernable effect on TTP function alone, it is possible that MK2 and ERK function together to strongly suppress TTP activity (Brook et al., 2006). In addition, RSK downstream of ERK may play a significant role in reducing TTP binding to deadenylase machinery, as this has been demonstrated for ZFP36L1 and ZFP36L2 (Adachi et al., 2014). This is concordant with our data showing that the RSK inhibitor BI-D1870 reduced *PD-L1* mRNA expression in lung cancer cells. *In vitro* kinase assays initially demonstrated that S52 and S178 MK2 consensus sites are phosphorylated by active MK2 protein (Chrestensen et al., 2004). Since these *in vitro* kinases assays do not formerly exclude the involvement of other regulators, it is possible that S52 and S178 are also phosphorylated by other kinases activated downstream of RAS. Indeed, RSK has a similar phosphorylation consensus motif, requiring an arginine residue at the -3 position and -5 position (Cargnello and Roux, 2012). Indeed, there are instances where AGC kinases such as AKT, S6K and RSK share phosphosite specificity (for example, glycogen synthase kinase 3) (Pearce et al., 2010). Nonetheless, our data strongly implicate a ROS-p38-MK2 signalling cascade in the inactivation of TTP because: (1) ROS promoted PD-L1 expression downstream of RAS, (2) ΔMEKK3-ER activity specifically elevated PD-L1 levels, and (3) MK2 inhibitors substantially reverse PD-L1 induction by RAS.

Signalling nodes that regulate TTP activity that could be potential therapeutic targets to treat cancer are highlighted in Figure 6.1. Although p38 and MK2 inhibitors are being developed for the treatment of inflammatory disorders such as arthritis, the use of these drugs in oncology is questionable, as the p38 pathway has predominantly been associated with growth arrest and tumour suppression (Xu et al., 2014b). There are some reports that p38 can promote tumour progression, but this seems to be context-dependent (Yoshizuka et al., 2012). Specifically, p38 activation by oncogenic signalling has been suggested to be initially tumour-suppressive by initiating growth

arrest, but once this stage has been overcome by the acquisition of additional oncogenic or epigenetic changes, p38 signalling can have a tumour-promoting role in epithelial tumours by promoting angiogenesis (Yoshizuka et al., 2012). Pharmacological targeting of kinases or phosphatases regulating TTP in order to increase TTP activity may also affect the senescence associated secretory phenotype (SASP). SASP induced by chronic RAS activation was shown to depend on MK2-mediated phosphorylation and inactivation of ZFP36L1, which targets several SASP mRNAs under steady-state conditions (Herranz et al., 2015). Thus, the regulatory pathway we describe in this thesis may also be pertinent to the biology of ageing in mammals.

MEK inhibition may be a suitable alternative to directly inhibiting p38 or MK2 signalling. MEK inhibitors have been shown to have clinical activity in NSCLC as monotherapies, but have also been used in preclinical studies in mice to augment anti-PD-1 responses (Ebert et al., 2016; Liu et al., 2015). Initially, there were concerns that inhibition of RAS effector pathways may profoundly compromise T cell activity as RAS is involved signalling through the TCR (Downward et al., 1990a). Crucially, MEK or RAF inhibition only transiently decreased T cell proliferation capacity *in vitro* (Liu et al., 2015). Moreover, *in vivo*, the specific MEK inhibitor trametinib was shown to combine with anti-PD-1 antibody in a CT26 syngeneic tumour model, and this effect was associated with increased lymphocyte infiltration into regressing tumours (Liu et al., 2015). Mechanistically, although MEK inhibition reduces the efficiency of T cell priming, it spares chronically activated anti-tumour T cells from TCR activation-induced apoptosis, thus preserving a larger pool of anti-tumour T cells that can be subsequently activated with anti-PD-1 therapy (Ebert et al., 2016). Our data also support the use of MEK inhibitors with PD-1 blockade in NSCLC. MEK inhibition is likely to induce tumour-cell death, which will help activate DCs and prime T cell responses. Secondly, assuming incomplete PD-1/PD-L1 pathway inhibition, decreases in tumour-cell PD-L1 expression

by inhibition of MEK will likely cause more profound activation of anti-tumour immunity.

Comprehensive RNA sequencing analysis of melanoma patients receiving PD-1 ICB therapy revealed that intrinsic resistance to pembrolizumab or nivolumab was associated with a transcriptional programme analogous to that observed for melanomas following MAPK inhibitor treatment (Hugo et al., 2016). Although, *PD-L1* expression did not significantly correlate with anti-PD-1 therapy response in this study, Hugo and colleagues' PD-1 resistance signature has several corollaries regarding RAS regulation of PD-L1 in ICB response: firstly, it provides further evidence that tumours with highly active RAS signalling (i.e. the opposite of a MAPK inhibitor signature) may be more susceptible to PD-1 blockade. Secondly, since resistance to PD-1 is closely associated with a MAPK inhibitor-treated gene expression signature, it implies that dual resistance to both of these therapeutic agents may be easily achievable. Little is currently known about clinical resistance to immunotherapies, but Hugo et al. provide an important cautionary note for the clinical trials combining PD-1 and MEK inhibitors that are currently underway.

One ambiguity in the mechanism described in this thesis relates to how PD-L1 expression responds to MEK inhibition. Although it is clear from our data that RAS increases PD-L1 expression, and this process is expressly dependent on MEK activity, we have discovered that the level of PD-L1 expression in response to MEK inhibition is more nuanced in some KRAS-mutant cell lines. For example, in CT26 cells, *PD-L1* mRNA expression initially falls rapidly following MEK inhibition at 2 h, and then recovers to baseline levels after 24 h (data not shown), suggesting that there is a compensatory signalling mechanism that leads to eventual recovery of PD-L1 expression. In addition, from a panel of KRAS mutant human colon cancer cell lines, only 2/6 cell lines had reduced PD-L1 protein expression following 24 of trametinib treatment, whereas others had unchanged levels of PD-L1 or

increased PD-L1 expression at 48 h. Moreover, a recent publication showed that prolonged exposure to trametinib at high doses could lead to increased PD-L1 expression in breast cancer cells (Loi et al., 2016). These data suggest that there may be some tissue specific and cell line specific differences governing the response of PD-L1 expression to MEK inhibitors. We speculate that chronic exposure to MEK inhibition in MEK-dependent cancer cells may trigger the activation of stress signalling, such as p38 MAPK pathway stimulation and other pathways relating to apoptosis (Berra et al., 1998), especially at later time-points. Moreover, several MEK inhibitors, including trametinib, have been shown to increase STAT3 phosphorylation in cancer cells (Lee et al., 2014; Zhao et al., 2015), which would then lead to potent transcriptional upregulation of PD-L1. This mechanism would also explain the biphasic response of PD-L1 expression in CT26 cells treated with trametinib. Although the mechanism responsible for STAT3 activation following MEK inhibition is unclear at this time, it is likely that it involves compensatory feedback to receptor tyrosine kinases and c-Src activation (Girotti et al., 2013), the activation of JAK-STAT signalling through autocrine signalling (Lee et al., 2014), or a combination of these pathways. We are currently testing whether combining inhibitors of STAT pathway activation with MEK inhibitors can profoundly reduce PD-L1 expression in cell lines that do not response to MEK inhibition alone. Further understanding of the molecular mechanisms behind the susceptibility to MEK inhibitors and immunotherapies should lead to insights into how these inhibitors can be successfully scheduled to maximise response and minimise drug resistance in lung and colon cancers.

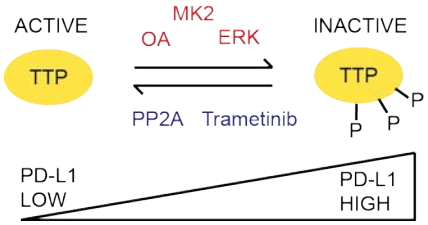

Figure 6.2 Post-translational regulation of TTP activity in cancer

Proposed molecular model. Oncogenic RAS activity leads to hyperphosphorylation, whereas PP2A activity promotes hypophosphorylation of TTP (Bourcier et al., 2011; Deleault et al., 2008; Essafi-Benkhadir et al., 2007; Hardle et al., 2015; Rahman et al., 2015; Sun et al., 2007), constituting a rapid switch controlling TTP activity. Low TTP expression and activity in tumour cells represents a permissive context for PD-L1 expression and immune evasion.

Using bioinformatics analysis, we discovered that PD-L1 expression was significantly higher in lung tumours with gene expression characteristics indicative of high RAS activity. This was not solely attributable to preferential T cell infiltration or an inflammatory phenotype as indicated by only modest changes in mRNA expression of CD3 or IFN-γ in RAS pathway active tumours. Therefore, RAS active human tumours may evade immune destruction partly by upregulating PD-L1. This poses the question: do patients with RAS mutant/active lung cancer have improved response rates to anti-PD-L1 or anti-PD-1 therapy? Although further large-scale trials of PD-1 pathway-directed immunotherapies in lung cancer are required to definitively answer this question, there are early indications that KRAS-mutant NSCLC patients respond better than KRAS-wild-type patients to nivolumab (Borghaei et al., 2015). It is worth noting that KRAS-mutant cancers are often associated with a history of smoking, and can therefore harbour hundreds of non-synonymous mutations (de Bruin et al., 2014; Matsushita et al., 2012). We must also consider the scenario where cell-intrinsic KRAS signalling drives tumour PD-L1 expression in the absence of anti-tumour antigen expression. As immunotherapy success depends on tumour antigens (Gubin et al., 2014), ICB will fail in this setting.

We discovered that restoration of TTP expression could promote anti-tumour immunity and stall tumour growth *in vivo*. Although most of our work focussed on lung cancer we chose the CT26 colon carcinoma cell line as it is highly immunogenic and responds to PD-L1 antibody therapy and PD-L1 expression modulation. There are very few cell lines available that are amenable to syngeneic cell transplantation experiments to test anti-tumour immune responses. The most common publically available cell lines used in publications pertaining to cancer immunology are MC38 and CT26 for modelling colon carcinoma, the EL4 and E.G7-OVA lymphoma cell line pair, 4T1 and EMT-6 for breast cancer, the mildly immunogenic B16 melanoma cell line and the LLC1 Lewis lung carcinoma line for lung. However, we found that LLC1 did not show significant responses to anti-PD-L1 antibody therapy *in vivo*, and KPB6 tumour cells engineered to express the model antigen OVA proved too immunogenic in untreated mice. Therefore, once fully characterised, the immunogenic *KPR* c-/- cell line that we have generated, and the paired escape variant that has been passaged through an immunocompetent host, may serve as useful tools for the study anti-tumour immune responses in lung cancer. A possible advantage of using an immunogenic cell line derived from the *KP* GEMM rather than a carcinogen-induced tumour is that the genetic driving events in this cell line are already well defined.

Our *in vivo* experiments in Chapter 5 suggest that activation of TTP activity in tumour cells may have therapeutic potential in tumours wild-type for *PD-L1 3'UTR*. This is supported by the observation that TTP expression is massively suppressed in many tumour types, especially in cancers with Myc involvement (Rounbehler et al., 2012). Interestingly, withdrawal of Myc expression from tumours addicted to oncogenic Myc has been associated with tumour microenvironment remodelling and tumour regression involving poorly defined immune cell involvement (Casey et al., 2016a)(Gerard Evan, unpublished). Although Myc has been involved in directly promoting *PD-L1*

transcription (Casey et al., 2016a), we speculate that this effect may also rely on de-repression of TTP expression and PD-L1 downregulation through decreasing *PD-L1* mRNA stability. This would constitute a novel, non-cell autonomous mechanism of oncogene cooperation between RAS and Myc. However, our results from overexpressing c-Myc in NL-20 lung cells did not indicate Myc-driven expression of *PD-L1* mRNA.

6.3 Concluding remarks

Immune checkpoint blockade already holds great promise for curing some cancers, but their maximum therapeutic potential is only just starting to be explored. Notably, approaches focussed on activating anti-tumour immune responses to clonal, non-essential passenger mutations may require further personalised peptide or RNA vaccines to achieve complete regressions (Schumacher and Schreiber, 2015). Tantalisingly, the unexpected discovery of tumour-infiltrating T cells specific for KrasG12D in a patient with gastrointestinal cancer suggests that common oncogenes can be immunogenic (Tran et al., 2015). Re-invigorating immune responses against essential driver mutations is likely to lead to more profound and durable tumour regressions, and even cures. Deeper understanding of how oncogenes such as RAS can manipulate the tumour-microenvironment, and how to reverse such signalling will undoubtedly play a central role in improving immunotherapies and patient stratification.

Although mouse models of cancer are often key to understanding therapy responses, we show that the *KP* GEMM of lung cancer is refractory to ICB therapies targeting PD-L1 and CTLA-4. The intrinsically low tumour somatic mutation rate in GEMMs of cancer make them inappropriate for modelling smoker's lung cancer, but perhaps well suited to model cancers with low somatic mutation rates such as glioblastoma and pancreatic cancer (Alexandrov et al., 2013); cancers that are yet to show clinical responses to ICB. Cancer immunologists may be forced to step back in time and revisit

early carcinogen induced models and move away from sophisticated conditional genetic animal models in order to account for the mutational complexity and heterogeneity observed in some human cancers.

Inevitably, personalised and combinatorial treatment approaches including targeted therapies will have to be adopted for patients with poorly immunogenic tumours. In this thesis, we show that RAS can drive immunoresistance through PD-L1 upregulation, involving the modulation of TTP activity and increased *PD-L1* mRNA stability. We hope that the mechanism of PD-L1 regulation described will inform the interpretation of PD-L1 expression as a biomarker for treatment response in lung cancer, and eventually aid therapeutic advances against RAS-driven cancers.

7 References

Acharya, S., Wilson, T., Gradia, S., Kane, M. F., Guerrette, S., Marsischky, G. T., Kolodner, R., and Fishel, R. (1996). hMSH2 forms specific mispair-binding complexes with hMSH3 and hMSH6. Proceedings of the National Academy of Sciences of the United States of America *93*, 13629-13634.
Adachi, S., Homoto, M., Tanaka, R., Hioki, Y., Murakami, H., Suga, H., Matsumoto, M., Nakayama, K. I., Hatta, T., Iemura, S., and Natsume, T. (2014). ZFP36L1 and ZFP36L2 control LDLR mRNA stability via the ERK-RSK pathway. Nucleic acids research *42*, 10037-10049.
Akbay, E. A., Koyama, S., Carretero, J., Altabef, A., Tchaicha, J. H., Christensen, C. L., Mikse, O. R., Cherniack, A. D., Beauchamp, E. M., Pugh, T. J.*, et al.* (2013). Activation of the PD-1 Pathway Contributes to Immune Escape in EGFR-Driven Lung Tumors. Cancer Discov *3*, 1355-1363.
Albert, M. L., and Darnell, R. B. (2004). Paraneoplastic neurological degenerations: Keys to tumour immunity. Nature Reviews Cancer *4*, 36-44.
Alexandrov, L. B., Nik-Zainal, S., Wedge, D. C., Aparicio, S. A., Behjati, S., Biankin, A. V., Bignell, G. R., Bolli, N., Borg, A., Borresen-Dale, A. L.*, et al.* (2013). Signatures of mutational processes in human cancer. Nature *500*, 415-421.
Ali, K., Soond, D. R., Pineiro, R., Hagemann, T., Pearce, W., Lim, E. L., Bouabe, H., Scudamore, C. L., Hancox, T., Maecker, H.*, et al.* (2014). Inactivation of PI(3)K p110delta breaks regulatory T-cell-mediated immune tolerance to cancer. Nature *510*, 407-411.
Ali, K., Soond, D. R., Pineiro, R., Hagemann, T., Pearce, W., Lim, E. L., Bouabe, H., Scudamore, C. L., Hancox, T., Maecker, H.*, et al.* (2016). Corrigendum: Inactivation of PI(3)K p110delta breaks regulatory T-cell-mediated immune tolerance to cancer. Nature.
Ancrile, B., Lim, K. H., and Counter, C. M. (2007). Oncogenic Ras-induced secretion of IL6 is required for tumorigenesis. Genes & development *21*, 1714-1719.
Anderson, P. (2008). Post-transcriptional control of cytokine production. Nature immunology *9*, 353-359.
Apetoh, L., Ghiringhelli, F., Tesniere, A., Obeid, M., Ortiz, C., Criollo, A., Mignot, G., Maiuri, M. C., Ullrich, E., Saulnier, P.*, et al.* (2007). Toll-like receptor 4-dependent contribution of the immune system to anticancer chemotherapy and radiotherapy. Nature medicine *13*, 1050-1059.
Atefi, M., Avramis, E., Lassen, A., Wong, D. J., Robert, L., Foulad, D., Cerniglia, M., Titz, B., Chodon, T., Graeber, T. G.*, et al.* (2014). Effects of MAPK and PI3K pathways on PD-L1 expression in melanoma. Clinical cancer research : an official journal of the American Association for Cancer Research *20*, 3446-3457.
Bakheet, T., Williams, B. R. G., and Khabar, K. S. A. (2006). ARED 3.0: the large and diverse AU-rich transcriptome. Nucleic acids research *34*, D111-D114.

Balmain, A., and Pragnell, I. B. (1983). Mouse Skin Carcinomas Induced Invivo by Chemical Carcinogens Have a Transforming Harvey-Ras Oncogene. Nature *303*, 72-74.
Barber, D. L., Wherry, E. J., Masopust, D., Zhu, B., Allison, J. P., Sharpe, A. H., Freeman, G. J., and Ahmed, R. (2006). Restoring function in exhausted CD8 T cells during chronic viral infection. Nature *439*, 682-687.
Barreau, C., Paillard, L., and Osborne, H. B. (2005). AU-rich elements and associated factors: are there unifying principles? Nucleic acids research *33*, 7138-7150.
Beatty, G. L., Chiorean, E. G., Fishman, M. P., Saboury, B., Teitelbaum, U. R., Sun, W. J., Huhn, R. D., Song, W. R., Li, D. G., Sharp, L. L.*, et al.* (2011). CD40 Agonists Alter Tumor Stroma and Show Efficacy Against Pancreatic Carcinoma in Mice and Humans. Science *331*, 1612-1616.
Berra, E., Diaz-Meco, M. T., and Moscat, J. (1998). The activation of p38 and apoptosis by the inhibition of Erk is antagonized by the phosphoinositide 3-kinase Akt pathway (vol 273, pg 10792, 1998). Journal of Biological Chemistry *273*, 16630-16630.
Berthon, C., Driss, V., Liu, J. Z., Kuranda, K., Leleu, X., Jouy, N., Hetuin, D., and Quesnel, B. (2010). In acute myeloid leukemia, B7-H1 (PD-L1) protection of blasts from cytotoxic T cells is induced by TLR ligands and interferon-gamma and can be reversed using MEK inhibitors. Cancer Immunol Immun *59*, 1839-1849.
Blackshear, P. J., Phillips, R. S., Ghosh, S., Ramos, S. B., Richfield, E. K., and Lai, W. S. (2005). Zfp36l3, a rodent X chromosome gene encoding a placenta-specific member of the Tristetraprolin family of CCCH tandem zinc finger proteins. Biol Reprod *73*, 297-307.
Blank, C., Brown, I., Peterson, A. C., Spiotto, M., Iwai, Y., Honjo, T., and Gajewski, T. F. (2004). PD-L1/B7H-1 inhibits the effector phase of tumor rejection by T cell receptor (TCR) transgenic CD8+ T cells. Cancer Res *64*, 1140-1145.
Borghaei, H., Paz-Ares, L., Horn, L., Spigel, D. R., Steins, M., Ready, N. E., Chow, L. Q., Vokes, E. E., Felip, E., Holgado, E.*, et al.* (2015). Nivolumab versus Docetaxel in Advanced Nonsquamous Non-Small-Cell Lung Cancer. N Engl J Med.
Bourcier, C., Griseri, P., Grepin, R., Bertolotto, C., Mazure, N., and Pages, G. (2011). Constitutive ERK activity induces downregulation of tristetraprolin, a major protein controlling interleukin8/CXCL8 mRNA stability in melanoma cells. American journal of physiology Cell physiology *301*, C609-618.
Brahmer, J., Reckamp, K. L., Baas, P., Crino, L., Eberhardt, W. E., Poddubskaya, E., Antonia, S., Pluzanski, A., Vokes, E. E., Holgado, E.*, et al.* (2015). Nivolumab versus Docetaxel in Advanced Squamous-Cell Non-Small-Cell Lung Cancer. N Engl J Med *373*, 123-135.
Brahmer, J. R., Tykodi, S. S., Chow, L. Q., Hwu, W. J., Topalian, S. L., Hwu, P., Drake, C. G., Camacho, L. H., Kauh, J., Odunsi, K.*, et al.* (2012). Safety and activity of anti-PD-L1 antibody in patients with advanced cancer. N Engl J Med *366*, 2455-2465.
Brennan, S. E., Kuwano, Y., Alkharouf, N., Blackshear, P. J., Gorospe, M., and Wilson, G. M. (2009). The mRNA-Destabilizing Protein Tristetraprolin Is

Suppressed in Many Cancers, Altering Tumorigenic Phenotypes and Patient Prognosis. Cancer Research *69*, 5168-5176.
Brook, M., Tchen, C. R., Santalucia, T., McIlrath, J., Arthur, J. S., Saklatvala, J., and Clark, A. R. (2006). Posttranslational regulation of tristetraprolin subcellular localization and protein stability by p38 mitogen-activated protein kinase and extracellular signal-regulated kinase pathways. Mol Cell Biol *26*, 2408-2418.
Brooks, S. A., and Blackshear, P. J. (2013). Tristetraprolin (TTP): interactions with mRNA and proteins, and current thoughts on mechanisms of action. Biochimica et biophysica acta *1829*, 666-679.
Burnet, M. (1957). Cancer; a biological approach. I. The processes of control. Br Med J *1*, 779-786.
Butte, M. J., Keir, M. E., Phamduy, T. B., Sharpe, A. H., and Freeman, G. J. (2007). Programmed death-1 ligand 1 interacts specifically with the B7-1 costimulatory molecule to inhibit T cell responses. Immunity *27*, 111-122.
Cancer Genome Atlas, N. (2012). Comprehensive molecular portraits of human breast tumours. Nature *490*, 61-70.
Cancer Genome Atlas Research, N. (2014). Comprehensive molecular profiling of lung adenocarcinoma. Nature *511*, 543-550.
Cao, H. P., Dzineku, F., and Blackshear, P. J. (2003). Expression and purification of recombinant tristetraprolin that can bind to tumor necrosis factor-alpha mRNA and serve as a substrate for mitogen-activated protein kinases. Arch Biochem Biophys *412*, 106-120.
Caput, D., Beutler, B., Hartog, K., Thayer, R., Brown-Shimer, S., and Cerami, A. (1986). Identification of a common nucleotide sequence in the 3'-untranslated region of mRNA molecules specifying inflammatory mediators. Proceedings of the National Academy of Sciences of the United States of America *83*, 1670-1674.
Carballo, E., Lai, W. S., and Blackshear, P. J. (1998). Feedback inhibition of macrophage tumor necrosis factor-alpha production by tristetraprolin. Science *281*, 1001-1005.
Cargnello, M., and Roux, P. P. (2012). Activation and Function of the MAPKs and Their Substrates, the MAPK-Activated Protein Kinases (vol 75, pg 50, 2011). Microbiol Mol Biol R *76*, 496-496.
Casey, S. C., Tong, L., Li, Y., Do, R., Walz, S., Fitzgerald, K. N., Gouw, A. M., Baylot, V., Gutgemann, I., Eilers, M., and Felsher, D. W. (2016a). MYC regulates the antitumor immune response through CD47 and PD-L1. Science *352*, 227-231.
Casey, S. C., Tong, L., Li, Y. L., Do, R., Walz, S., Fitzgerald, K. N., Gouw, A. M., Baylot, V., Gutgemann, I., Eilers, M., and Felsher, D. W. (2016b). MYC regulates the antitumor immune response through CD47 and PD-L1. Science *352*, 227-231.
Castellano, E., Sheridan, C., Thin, M. Z., Nye, E., Spencer-Dene, B., Diefenbacher, M. E., Moore, C., Kumar, M. S., Murillo, M. M., Gronroos, E.*, et al.* (2013). Requirement for interaction of PI3-kinase p110alpha with RAS in lung tumor maintenance. Cancer cell *24*, 617-630.
Cha, H. J., Lee, H. H., Chae, S. W., Cho, W. J., Kim, Y. M., Choi, H. J., Choi, D. H., Jung, S. W., Min, Y. J., Lee, B. J.*, et al.* (2011). Tristetraprolin

downregulates the expression of both VEGF and COX-2 in human colon cancer. Hepatogastroenterology *58*, 790-795.
Chemnitz, J. M., Parry, R. V., Nichols, K. E., June, C. H., and Riley, J. L. (2004). SHP-1 and SHP-2 associate with immunoreceptor tyrosine-based switch motif of programmed death 1 upon primary human T cell stimulation, but only receptor ligation prevents T cell activation. Journal of Immunology *173*, 945-954.
Chen, C. Y., and Shyu, A. B. (1995). AU-rich elements: characterization and importance in mRNA degradation. Trends Biochem Sci *20*, 465-470.
Chen, L., Gibbons, D. L., Goswami, S., Cortez, M. A., Ahn, Y. H., Byers, L. A., Zhang, X., Yi, X., Dwyer, D., Lin, W.*, et al.* (2014). Metastasis is regulated via microRNA-200/ZEB1 axis control of tumour cell PD-L1 expression and intratumoral immunosuppression. Nature communications *5*, 5241.
Chen, Z., Cheng, K., Walton, Z., Wang, Y., Ebi, H., Shimamura, T., Liu, Y., Tupper, T., Ouyang, J., Li, J.*, et al.* (2012). A murine lung cancer co-clinical trial identifies genetic modifiers of therapeutic response. Nature *483*, 613-617.
Chrestensen, C. A., Schroeder, M. J., Shabanowitz, J., Hunt, D. F., Pelo, J. W., Worthington, M. T., and Sturgill, T. W. (2004). MAPKAP kinase 2 phosphorylates tristetraprolin on in vivo sites including Ser178, a site required for 14-3-3 binding. J Biol Chem *279*, 10176-10184.
Chuang, E., Fisher, T. S., Morgan, R. W., Robbins, M. D., Duerr, J. M., Vander Heiden, M. G., Gardner, J. P., Hambor, J. E., Neveu, M. J., and Thompson, C. B. (2000). The CD28 and CTLA-4 receptors associate with the serine/threonine phosphatase PP2A. Immunity *13*, 313-322.
Ciampricotti, M., Hau, C. S., Doornebal, C. W., Jonkers, J., and de Visser, K. E. (2012). Chemotherapy response of spontaneous mammary tumors is independent of the adaptive immune system. Nature medicine *18*, 344-346.
Clement, S. L., Scheckel, C., Stoecklin, G., and Lykke-Andersen, J. (2011). Phosphorylation of Tristetraprolin by MK2 Impairs AU-Rich Element mRNA Decay by Preventing Deadenylase Recruitment. Molecular and Cellular Biology *31*, 256-266.
Cortez, M. A., Ivan, C., Valdecanas, D., Wang, X., Peltier, H. J., Ye, Y., Araujo, L., Carbone, D. P., Shilo, K., Giri, D. K.*, et al.* (2016). PDL1 Regulation by p53 via miR-34. J Natl Cancer Inst *108*.
D'Incecco, A., Andreozzi, M., Ludovini, V., Rossi, E., Capodanno, A., Landi, L., Tibaldi, C., Minuti, G., Salvini, J., Coppi, E.*, et al.* (2015). PD-1 and PD-L1 expression in molecularly selected non-small-cell lung cancer patients. Br J Cancer *112*, 95-102.
de Bruin, E. C., McGranahan, N., Mitter, R., Salm, M., Wedge, D. C., Yates, L., Jamal-Hanjani, M., Shafi, S., Murugaesu, N., Rowan, A. J.*, et al.* (2014). Spatial and temporal diversity in genomic instability processes defines lung cancer evolution. Science *346*, 251-256.
de la Chapelle, A. (2004). Genetic predisposition to colorectal cancer. Nature Reviews Cancer *4*, 769-780.
Deleault, K. M., Skinner, S. J., and Brooks, S. A. (2008). Tristetraprolin regulates TNF TNF-alpha mRNA stability via a proteasome dependent

mechanism involving the combined action of the ERK and p38 pathways. Molecular immunology *45*, 13-24.
DeNicola, G. M., Karreth, F. A., Humpton, T. J., Gopinathan, A., Wei, C., Frese, K., Mangal, D., Yu, K. H., Yeo, C. J., Calhoun, E. S.*, et al.* (2011). Oncogene-induced Nrf2 transcription promotes ROS detoxification and tumorigenesis. Nature *475*, 106-109.
Denkert (2010). Tumor-Associated Lymphocytes As an Independent Predictor of Response to Neoadjuvant Chemotherapy in Breast Cancer (vol 28, pg 105, 2010). Journal of Clinical Oncology *28*, 708-708.
Diaz-Moreno, I., Hollingworth, D., Frenkiel, T. A., Kelly, G., Martin, S., Howell, S., Garcia-Mayoral, M., Gherzi, R., Briata, P., and Ramos, A. (2009). Phosphorylation-mediated unfolding of a KH domain regulates KSRP localization via 14-3-3 binding. Nat Struct Mol Biol *16*, 238-246.
Dolado, I., Swat, A., Ajenjo, N., De Vita, G., Cuadrado, A., and Nebreda, A. R. (2007). p38 alpha MAP kinase as a sensor of reactive oxygen species in tumorigenesis. Cancer cell *11*, 191-205.
Dong, H., Strome, S. E., Salomao, D. R., Tamura, H., Hirano, F., Flies, D. B., Roche, P. C., Lu, J., Zhu, G., Tamada, K.*, et al.* (2002). Tumor-associated B7-H1 promotes T-cell apoptosis: a potential mechanism of immune evasion. Nature medicine *8*, 793-800.
Downward, J. (2003). Targeting ras signalling pathways in cancer therapy. Nature Reviews Cancer *3*, 11-22.
Downward, J., Graves, J. D., Warne, P. H., Rayter, S., and Cantrell, D. A. (1990a). Stimulation of P21ras Upon T-Cell Activation. Nature *346*, 719-723.
Downward, J., Riehl, R., Wu, L., and Weinberg, R. A. (1990b). Identification of a Nucleotide Exchange-Promoting Activity for P21ras. Proceedings of the National Academy of Sciences of the United States of America *87*, 5998-6002.
Dunn, G. P., Bruce, A. T., Ikeda, H., Old, L. J., and Schreiber, R. D. (2002). Cancer immunoediting: from immunosurveillance to tumor escape. Nature immunology *3*, 991-998.
DuPage, M., Cheung, A. F., Mazumdar, C., Winslow, M. M., Bronson, R., Schmidt, L. M., Crowley, D., Chen, J. Z., and Jacks, T. (2011). Endogenous T Cell Responses to Antigens Expressed in Lung Adenocarcinomas Delay Malignant Tumor Progression. Cancer cell *19*, 72-85.
DuPage, M., Dooley, A. L., and Jacks, T. (2009a). Conditional mouse lung cancer models using adenoviral or lentiviral delivery of Cre recombinase. Nature protocols *4*, 1064-1072.
DuPage, M., Dooley, A. L., and Jacks, T. (2009b). Conditional mouse lung cancer models using adenoviral or lentiviral delivery of Cre recombinase. Nature protocols *4*, 1064-1072.
DuPage, M., and Jacks, T. (2013). Genetically engineered mouse models of cancer reveal new insights about the antitumor immune response. Current opinion in immunology *25*, 192-199.
DuPage, M., Mazumdar, C., Schmidt, L. M., Cheung, A. F., and Jacks, T. (2012). Expression of tumour-specific antigens underlies cancer immunoediting. Nature *482*, 405-U1512.

Duraiswamy, J., Kaluza, K. M., Freeman, G. J., and Coukos, G. (2013). Dual blockade of PD-1 and CTLA-4 combined with tumor vaccine effectively restores T-cell rejection function in tumors. Cancer Res *73*, 3591-3603.
Ebert, P. J., Cheung, J., Yang, Y., McNamara, E., Hong, R., Moskalenko, M., Gould, S. E., Maecker, H., Irving, B. A., Kim, J. M.*, et al.* (2016). MAP Kinase Inhibition Promotes T Cell and Anti-tumor Activity in Combination with PD-L1 Checkpoint Blockade. Immunity *44*, 609-621.
Essafi-Benkhadir, K., Onesto, C., Stebe, E., Moroni, C., and Pages, G. (2007). Tristetraprolin inhibits Ras-dependent tumor vascularization by inducing vascular endothelial growth factor mRNA degradation. Molecular biology of the cell *18*, 4648-4658.
Fabian, M. R., Frank, F., Rouya, C., Siddiqui, N., Lai, W. S., Karetnikov, A., Blackshear, P. J., Nagar, B., and Sonenberg, N. (2013). Structural basis for the recruitment of the human CCR4-NOT deadenylase complex by tristetraprolin. Nat Struct Mol Biol *20*, 735-739.
Feig, C., Jones, J. O., Kraman, M., Wells, R. J., Deonarine, A., Chan, D. S., Connell, C. M., Roberts, E. W., Zhao, Q., Caballero, O. L.*, et al.* (2013). Targeting CXCL12 from FAP-expressing carcinoma-associated fibroblasts synergizes with anti-PD-L1 immunotherapy in pancreatic cancer. Proceedings of the National Academy of Sciences of the United States of America *110*, 20212-20217.
Francisco, L. M., Salinas, V. H., Brown, K. E., Vanguri, V. K., Freeman, G. J., Kuchroo, V. K., and Sharpe, A. H. (2009). PD-L1 regulates the development, maintenance, and function of induced regulatory T cells. The Journal of experimental medicine *206*, 3015-3029.
Franks, T. M., and Lykke-Andersen, J. (2007). TTP and BRF proteins nucleate processing body formation to silence mRNAs with AU-rich elements. Genes & development *21*, 719-735.
Freeman, G. J., Long, A. J., Iwai, Y., Bourque, K., Chernova, T., Nishimura, H., Fitz, L. J., Malenkovich, N., Okazaki, T., Byrne, M. C.*, et al.* (2000). Engagement of the PD-1 immunoinhibitory receptor by a novel B7 family member leads to negative regulation of lymphocyte activation. The Journal of experimental medicine *192*, 1027-1034.
Frese, K. K., and Tuveson, D. A. (2007). Maximizing mouse cancer models. Nature Reviews Cancer *7*, 645-658.
Fritsch, R., de Krijger, I., Fritsch, K., George, R., Reason, B., Kumar, M. S., Diefenbacher, M., Stamp, G., and Downward, J. (2013). RAS and RHO families of GTPases directly regulate distinct phosphoinositide 3-kinase isoforms. Cell *153*, 1050-1063.
Fu, R., Olsen, M. T., Webb, K., Bennett, E. J., and Lykke-Andersen, J. (2016). Recruitment of the 4EHP-GYF2 cap-binding complex to tetraproline motifs of tristetraprolin promotes repression and degradation of mRNAs with AU-rich elements. Rna *22*, 373-382.
Galluzzi, L., Buque, A., Kepp, O., Zitvogel, L., and Kroemer, G. (2015). Immunological Effects of Conventional Chemotherapy and Targeted Anticancer Agents. Cancer cell *28*, 690-714.
Galluzzi, L., Vitale, I., Abrams, J. M., Alnemri, E. S., Baehrecke, E. H., Blagosklonny, M. V., Dawson, T. M., Dawson, V. L., El-Deiry, W. S., Fulda,

S.*, et al.* (2012). Molecular definitions of cell death subroutines: recommendations of the Nomenclature Committee on Cell Death 2012. Cell Death Differ *19*, 107-120.
Galon, J., Costes, A., Sanchez-Cabo, F., Kirilovsky, A., Mlecnik, B., Lagorce-Pages, C., Tosolini, M., Camus, M., Berger, A., Wind, P.*, et al.* (2006). Type, density, and location of immune cells within human colorectal tumors predict clinical outcome. Science *313*, 1960-1964.
Garg, A. D., Krysko, D. V., Verfaillie, T., Kaczmarek, A., Ferreira, G. B., Marysael, T., Rubio, N., Firczuk, M., Mathieu, C., Roebroek, A. J.*, et al.* (2012). A novel pathway combining calreticulin exposure and ATP secretion in immunogenic cancer cell death. EMBO J *31*, 1062-1079.
Garneau, N. L., Wilusz, J., and Wilusz, C. J. (2007). The highways and byways of mRNA decay. Nature reviews Molecular cell biology *8*, 113-126.
Garner, A. P., Weston, C. R., Todd, D. E., Balmanno, K., and Cook, S. J. (2002). Delta MEKK3:ER* activation induces a p38 alpha/beta 2-dependent cell cycle arrest at the G2 checkpoint. Oncogene *21*, 8089-8104.
Garon, E. B., Rizvi, N. A., Hui, R., Leighl, N., Balmanoukian, A. S., Eder, J. P., Patnaik, A., Aggarwal, C., Gubens, M., Horn, L.*, et al.* (2015). Pembrolizumab for the treatment of non-small-cell lung cancer. N Engl J Med *372*, 2018-2028.
Gerlinger, M., Rowan, A. J., Horswell, S., Larkin, J., Endesfelder, D., Gronroos, E., Martinez, P., Matthews, N., Stewart, A., Tarpey, P.*, et al.* (2012). Intratumor heterogeneity and branched evolution revealed by multiregion sequencing. N Engl J Med *366*, 883-892.
Ghiringhelli, F., Apetoh, L., Tesniere, A., Aymeric, L., Ma, Y., Ortiz, C., Vermaelen, K., Panaretakis, T., Mignot, G., Ullrich, E.*, et al.* (2009). Activation of the NLRP3 inflammasome in dendritic cells induces IL-1beta-dependent adaptive immunity against tumors. Nature medicine *15*, 1170-1178.
Girotti, M. R., Pedersen, M., Sanchez-Laorden, B., Viros, A., Turajlic, S., Niculescu-Duvaz, D., Zambon, A., Sinclair, J., Hayes, A., Gore, M.*, et al.* (2013). Inhibiting EGF receptor or SRC family kinase signaling overcomes BRAF inhibitor resistance in melanoma. Cancer Discov *3*, 158-167.
Goldberg, M. V., Maris, C. H., Hipkiss, E. L., Flies, A. S., Zhen, L. J., Tuder, R. M., Grosso, J. F., Harris, T. J., Getnet, D., Whartenby, K. A.*, et al.* (2007). Role of PD-1 and its ligand, B7-H1, in early fate decisions of CD8 T cells. Blood *110*, 186-192.
Gong, A. Y., Zhou, R., Hu, G., Li, X., Splinter, P. L., O'Hara, S. P., LaRusso, N. F., Soukup, G. A., Dong, H., and Chen, X. M. (2009). MicroRNA-513 regulates B7-H1 translation and is involved in IFN-gamma-induced B7-H1 expression in cholangiocytes. J Immunol *182*, 1325-1333.
Green, M. R., Monti, S., Rodig, S. J., Juszczynski, P., Currie, T., O'Donnell, E., Chapuy, B., Takeyama, K., Neuberg, D., Golub, T. R.*, et al.* (2010). Integrative analysis reveals selective 9p24.1 amplification, increased PD-1 ligand expression, and further induction via JAK2 in nodular sclerosing Hodgkin lymphoma and primary mediastinal large B-cell lymphoma. Blood *116*, 3268-3277.

Gubin, M. M., Zhang, X., Schuster, H., Caron, E., Ward, J. P., Noguchi, T., Ivanova, Y., Hundal, J., Arthur, C. D., Krebber, W. J.*, et al.* (2014). Checkpoint blockade cancer immunotherapy targets tumour-specific mutant antigens. Nature *515*, 577-581.
Gyorffy, B., Surowiak, P., Budczies, J., and Lanczky, A. (2013). Online survival analysis software to assess the prognostic value of biomarkers using transcriptomic data in non-small-cell lung cancer. PLoS One *8*, e82241.
Halama, N., Michel, S., Kloor, M., Zoernig, I., Benner, A., Spille, A., Pommerencke, T., Doeberitz, M. V., Folprecht, G., Luber, B.*, et al.* (2011). Localization and Density of Immune Cells in the Invasive Margin of Human Colorectal Cancer Liver Metastases Are Prognostic for Response to Chemotherapy. Cancer Research *71*, 5670-5677.
Hall, J. P., and Davis, R. J. (2002). Inhibition of the p38 pathway upregulates macrophage JNK and ERK activities, and the ERK, JNK, and p38 MAP kinase pathways are reprogrammed during differentiation of the murine myeloid M1 cell line. J Cell Biochem *86*, 1-11.
Hall, M. P., Huang, S., and Black, D. L. (2004). Differentiation-induced colocalization of the KH-type splicing regulatory protein with polypyrimidine tract binding protein and the c-src pre-mRNA. Molecular biology of the cell *15*, 774-786.
Hanahan, D., and Weinberg, R. A. (2011). Hallmarks of cancer: the next generation. Cell *144*, 646-674.
Hardle, L., Bachmann, M., Bollmann, F., Pautz, A., Schmid, T., Eberhardt, W., Kleinert, H., Pfeilschifter, J., and Muhl, H. (2015). Tristetraprolin regulation of interleukin-22 production. Sci Rep *5*, 15112.
Herbst, R. S., Soria, J. C., Kowanetz, M., Fine, G. D., Hamid, O., Gordon, M. S., Sosman, J. A., McDermott, D. F., Powderly, J. D., Gettinger, S. N.*, et al.* (2014). Predictive correlates of response to the anti-PD-L1 antibody MPDL3280A in cancer patients. Nature *515*, 563-567.
Herr, H. W., Schwalb, D. M., Zhang, Z. F., Sogani, P. C., Fair, W. R., Whitmore, W. F., Jr., and Oettgen, H. F. (1995). Intravesical bacillus Calmette-Guerin therapy prevents tumor progression and death from superficial bladder cancer: ten-year follow-up of a prospective randomized trial. J Clin Oncol *13*, 1404-1408.
Herranz, N., Gallage, S., Mellone, M., Wuestefeld, T., Klotz, S., Hanley, C. J., Raguz, S., Acosta, J. C., Innes, A. J., Banito, A.*, et al.* (2015). mTOR regulates MAPKAPK2 translation to control the senescence-associated secretory phenotype. Nat Cell Biol *17*, 1205-1217.
Hiraoka, K., Miyamoto, M., Cho, Y., Suzuoki, M., Oshikiri, T., Nakakubo, Y., Itoh, T., Ohbuchi, T., Kondo, S., and Katoh, H. (2006). Concurrent infiltration by CD8(+) T cells and CD4(+) T cells is a favourable prognostic factor in non-small-cell lung carcinoma. Brit J Cancer *94*, 275-280.
Hitti, E., Iakovleva, T., Brook, M., Deppenmeier, S., Gruber, A. D., Radzioch, D., Clark, A. R., Blackshear, P. J., Kotlyarov, A., and Gaestel, M. (2006). Mitogen-activated protein kinase-activated protein kinase 2 regulates tumor necrosis factor mRNA stability and translation mainly by altering tristetraprolin expression, stability, and binding to adenine/uridine-rich element. Molecular and Cellular Biology *26*, 2399-2407.

Hodi, F. S., O'Day, S. J., McDermott, D. F., Weber, R. W., Sosman, J. A., Haanen, J. B., Gonzalez, R., Robert, C., Schadendorf, D., Hassel, J. C.*, et al.* (2010). Improved Survival with Ipilimumab in Patients with Metastatic Melanoma. New Engl J Med *363*, 711-723.
Hodson, D. J., Janas, M. L., Galloway, A., Bell, S. E., Andrews, S., Li, C. M., Pannell, R., Siebel, C. W., MacDonald, H. R., De Keersmaecker, K.*, et al.* (2010). Deletion of the RNA-binding proteins ZFP36L1 and ZFP36L2 leads to perturbed thymic development and T lymphoblastic leukemia (vol 11, pg 717, 2010). Nature immunology *11*, 969-969.
Hugo, W., Zaretsky, J. M., Sun, L., Song, C. Y., Moreno, B. H., Hu-Lieskovan, S., Berent-Maoz, B., Pang, J., Chmielowski, B., Cherry, G.*, et al.* (2016). Genomic and Transcriptomic Features of Response to Anti-PD-1 Therapy in Metastatic Melanoma. Cell *165*, 35-44.
Ishida, Y., Agata, Y., Shibahara, K., and Honjo, T. (1992). Induced expression of PD-1, a novel member of the immunoglobulin gene superfamily, upon programmed cell death. EMBO J *11*, 3887-3895.
Janne, P. A., Shaw, A. T., Pereira, J. R., Jeannin, G., Vansteenkiste, J., Barrios, C., Franke, F. A., Grinsted, L., Zazulina, V., Smith, P.*, et al.* (2013). Selumetinib plus docetaxel for KRAS-mutant advanced non-small-cell lung cancer: a randomised, multicentre, placebo-controlled, phase 2 study. Lancet Oncol *14*, 38-47.
Jenkins, M. K., Ashwell, J. D., and Schwartz, R. H. (1988). Allogeneic Non-T Spleen-Cells Restore the Responsiveness of Normal T-Cell Clones Stimulated with Antigen and Chemically Modified Antigen-Presenting Cells. Journal of Immunology *140*, 3324-3330.
Jenkins, M. K., Taylor, P. S., Norton, S. D., and Urdahl, K. B. (1991). Cd28 Delivers a Costimulatory Signal Involved in Antigen-Specific Il-2 Production by Human T-Cells. Journal of Immunology *147*, 2461-2466.
Jiang, X., Zhou, J., Giobbie-Hurder, A., Wargo, J., and Hodi, F. S. (2013). The activation of MAPK in melanoma cells resistant to BRAF inhibition promotes PD-L1 expression that is reversible by MEK and PI3K inhibition. Clinical cancer research : an official journal of the American Association for Cancer Research *19*, 598-609.
Jing, Q., Huang, S., Guth, S., Zarubin, T., Motoyama, A., Chen, J. M., Di Padova, F., Lin, S. C., Gram, H., and Han, J. H. (2005). Involvement of MicroRNA in AU-rich element-mediated mRNA instability. Cell *120*, 623-634.
Johnson, L., Mercer, K., Greenbaum, D., Bronson, R. T., Crowley, D., Tuveson, D. A., and Jacks, T. (2001). Somatic activation of the K-ras oncogene causes early onset lung cancer in mice. Nature *410*, 1111-1116.
Joshi, N. S., Akama-Garren, E. H., Lu, Y., Lee, D. Y., Chang, G. P., Li, A., DuPage, M., Tammela, T., Kerper, N. R., Farago, A. F.*, et al.* (2015a). Regulatory T Cells in Tumor-Associated Tertiary Lymphoid Structures Suppress Anti-tumor T Cell Responses. Immunity *43*, 579-590.
Joshi, N. S., Akama-Garren, E. H., Lu, Y. S., Lee, D. Y., Chang, G. P., Li, A., DuPage, M., Tammela, T., Kerper, N. R., Farago, A. F.*, et al.* (2015b). Regulatory T Cells in Tumor-Associated Tertiary Lymphoid Structures Suppress Anti-tumor T Cell Responses. Immunity *43*, 579-590.

Kantoff, P. W., Higano, C. S., Shore, N. D., Berger, E. R., Small, E. J., Penson, D. F., Redfern, C. H., Ferrari, A. C., Dreicer, R., Sims, R. B.*, et al.* (2010). Sipuleucel-T Immunotherapy for Castration-Resistant Prostate Cancer. New Engl J Med *363*, 411-422.
Kataoka, K., Shiraishi, Y., Takeda, Y., Sakata, S., Matsumoto, M., Nagano, S., Maeda, T., Nagata, Y., Kitanaka, A., Mizuno, S.*, et al.* (2016). Aberrant PD-L1 expression through 3'-UTR disruption in multiple cancers. Nature.
Keir, M. E., Butte, M. J., Freeman, G. J., and Sharpe, A. H. (2008). PD-1 and its ligands in tolerance and immunity. Annual review of immunology *26*, 677-704.
Keir, M. E., Freeman, G. J., and Sharpe, A. H. (2007). PD-1 regulates self-reactive CD8+ T cell responses to antigen in lymph nodes and tissues. J Immunol *179*, 5064-5070.
Kleffel, S., Posch, C., Barthel, S. R., Mueller, H., Schlapbach, C., Guenova, E., Elco, C. P., Lee, N., Juneja, V. R., Zhan, Q.*, et al.* (2015). Melanoma Cell-Intrinsic PD-1 Receptor Functions Promote Tumor Growth. Cell *162*, 1242-1256.
Kohl, N. E., Omer, C. A., Conner, M. W., Anthony, N. J., Davide, J. P., deSolms, S. J., Giuliani, E. A., Gomez, R. P., Graham, S. L., Hamilton, K., and et al. (1995). Inhibition of farnesyltransferase induces regression of mammary and salivary carcinomas in ras transgenic mice. Nature medicine *1*, 792-797.
Koyama, S., Akbay, E. A., Li, Y. Y., Aref, A. R., Skoulidis, F., Herter-Sprie, G. S., Buczkowski, K. A., Liu, Y., Awad, M. M., Denning, W. L.*, et al.* (2016). STK11/LKB1 Deficiency Promotes Neutrophil Recruitment and Proinflammatory Cytokine Production to Suppress T-cell Activity in the Lung Tumor Microenvironment. Cancer Research *76*, 999-1008.
Kumar, M. S., Hancock, D. C., Molina-Arcas, M., Steckel, M., East, P., Diefenbacher, M., Armenteros-Monterroso, E., Lassailly, F., Matthews, N., Nye, E.*, et al.* (2012). The GATA2 transcriptional network is requisite for RAS oncogene-driven non-small cell lung cancer. Cell *149*, 642-655.
Kwong, J., Chen, M., Lv, D., Luo, N., Su, W., Xiang, R., and Sun, P. (2013). Induction of p38delta expression plays an essential role in oncogenic ras-induced senescence. Mol Cell Biol *33*, 3780-3794.
Kwong, J., Hong, L. X., Liao, R., Deng, Q. D., Han, J. H., and Sun, P. Q. (2009). p38 alpha and p38 gamma Mediate Oncogenic ras-induced Senescence through Differential Mechanisms. Journal of Biological Chemistry *284*, 11237-11246.
Lai, W. S., Kennington, E. A., and Blackshear, P. J. (2003). Tristetraprolin and its family members can promote the cell-free deadenylation of AU-rich element-containing mRNAs by poly(A) ribonuclease. Molecular and Cellular Biology *23*, 3798-3812.
Lai, W. S., Parker, J. S., Grissom, S. F., Stumpo, D. J., and Blackshear, P. J. (2006). Novel mRNA targets for tristetraprolin (TTP) identified by global analysis of stabilized transcripts in TTP-deficient fibroblasts. Mol Cell Biol *26*, 9196-9208.

Lai, W. S., Stumpo, D. J., and Blackshear, P. J. (1990). Rapid insulin-stimulated accumulation of an mRNA encoding a proline-rich protein. J Biol Chem *265*, 16556-16563.
Langer, C. J., Leighton, J. C., Comis, R. L., O'Dwyer, P. J., McAleer, C. A., Bonjo, C. A., Engstrom, P. F., Litwin, S., and Ozols, R. F. (1995). Paclitaxel and carboplatin in combination in the treatment of advanced non-small-cell lung cancer: a phase II toxicity, response, and survival analysis. J Clin Oncol *13*, 1860-1870.
Larkin, J., Chiarion-Sileni, V., Gonzalez, R., Grob, J. J., Cowey, C. L., Lao, C. D., Schadendorf, D., Dummer, R., Smylie, M., Rutkowski, P.*, et al.* (2015a). Combined Nivolumab and Ipilimumab or Monotherapy in Untreated Melanoma. N Engl J Med *373*, 23-34.
Larkin, J., Hodi, F. S., and Wolchok, J. D. (2015b). Combined Nivolumab and Ipilimumab or Monotherapy in Untreated Melanoma. N Engl J Med *373*, 1270-1271.
Lastwika, K. J., Wilson, W., Li, Q. K., Norris, J., Xu, H. Y., Ghazarian, S. R., Kitagawa, H., Kawabata, S., Taube, J. M., Yao, S.*, et al.* (2016). Control of PD-L1 Expression by Oncogenic Activation of the AKT-mTOR Pathway in Non-Small Cell Lung Cancer. Cancer Research *76*, 227-238.
Latchman, Y., Wood, C. R., Chernova, T., Chaudhary, D., Borde, M., Chernova, I., Iwai, Y., Long, A. J., Brown, J. A., Nunes, R.*, et al.* (2001). PD-L2 is a second ligand for PD-1 and inhibits T cell activation. Nature immunology *2*, 261-268.
Latchman, Y. E., Liang, S. C., Wu, Y., Chernova, T., Sobel, R. A., Klemm, M., Kuchroo, V. K., Freeman, G. J., and Sharpe, A. H. (2004). PD-L1-deficient mice show that PD-L1 on T cells, antigen-presenting cells, and host tissues negatively regulates T cells. Proceedings of the National Academy of Sciences of the United States of America *101*, 10691-10696.
Le, D. T., Uram, J. N., Wang, H., Bartlett, B. R., Kemberling, H., Eyring, A. D., Skora, A. D., Luber, B. S., Azad, N. S., Laheru, D.*, et al.* (2015). PD-1 Blockade in Tumors with Mismatch-Repair Deficiency. N Engl J Med *372*, 2509-2520.
Leach, D. R., Krummel, M. F., and Allison, J. P. (1996). Enhancement of antitumor immunity by CTLA-4 blockade. Science *271*, 1734-1736.
Lee, H. H., Son, Y. J., Lee, W. H., Park, Y. W., Chae, S. W., Cho, W. J., Kim, Y. M., Choi, H. J., Choi, D. H., Jung, S. W.*, et al.* (2010). Tristetraprolin regulates expression of VEGF and tumorigenesis in human colon cancer. Int J Cancer *126*, 1817-1827.
Lee, H. J., Zhuang, G. L., Cao, Y., Du, P., Kim, H. J., and Settleman, J. (2014). Drug resistance via feedback activation of Stat3 in oncogene-addicted cancer cells. Cancer Research *74*.
Lee, S. J., Jang, B. C., Lee, S. W., Yang, Y. I., Suh, S. I., Park, Y. M., Oh, S., Shin, J. G., Yao, S., Chen, L. P., and Choi, I. H. (2006). Interferon regulatory factor-1 is prerequisite to the constitutive expression and IFN-gamma-induced upregulation of B7-H1 (CD274). FEBS letters *580*, 755-762.
Lee, S. K., Seo, S. H., Kim, B. S., Kim, C. D., Lee, J. H., Kang, J. S., Maeng, P. J., and Lim, J. S. (2005). IFN-gamma regulates the expression of B7-H1 in dermal fibroblast cells. Journal of dermatological science *40*, 95-103.

Leevers, S. J., Paterson, H. F., and Marshall, C. J. (1994). Requirement for Ras in Raf Activation Is Overcome by Targeting Raf to the Plasma-Membrane. Nature *369*, 411-414.
Lindstein, T., June, C. H., Ledbetter, J. A., Stella, G., and Thompson, C. B. (1989). Regulation of lymphokine messenger RNA stability by a surface-mediated T cell activation pathway. Science *244*, 339-343.
Linker, K., Pautz, A., Fechir, M., Hubrich, T., Greeve, J., and Kleinert, H. (2005). Involvement of KSRP in the post-transcriptional regulation of human iNOS expression-complex interplay of KSRP with TTP and HuR. Nucleic acids research *33*, 4813-4827.
Linnemann, C., van Buuren, M. M., Bies, L., Verdegaal, E. M. E., Schotte, R., Calis, J. J. A., Behjati, S., Velds, A., Hilkmann, H., el Atmioui, D*., et al.* (2015). High-throughput epitope discovery reveals frequent recognition of neo-antigens by CD4(+) T cells in human melanoma. Nature medicine *21*, 81-85.
Linsley (1995). Human B7-1 (Cd80) and B7-2 (Cd86) Bind with Similar Avidities but Distinct Kinetics to Cd28 and Ctla-4 Receptors (Vol 1, Pg 793, 1994). Immunity *2*, U7-U7.
Liu, J. Z., Hamrouni, A., Wolowiec, D., Coiteux, V., Kuliczkowski, K., Hetuin, D., Saudemont, A., and Quesnel, B. (2007). Plasma cells from multiple myeloma patients express B7-H1 (PD-L1) and increase expression after stimulation with IFN-gamma and TLR ligands via a MyD88-, TRAF6-, and MEK-dependent pathway. Blood *110*, 296-304.
Liu, L., Mayes, P. A., Eastman, S., Shi, H., Yadavilli, S., Zhang, T., Yang, J., Seestaller-Wehr, L., Zhang, S. Y., Hopson, C*., et al.* (2015). The BRAF and MEK Inhibitors Dabrafenib and Trametinib: Effects on Immune Function and in Combination with Immunomodulatory Antibodies Targeting PD1, PD-L1 and CTLA-4. Clinical cancer research : an official journal of the American Association for Cancer Research.
Liu, Y. W., Carlsson, R., Comabella, M., Wang, J. Y., Kosicki, M., Carrion, B., Hasan, M., Wu, X. D., Montalban, X., Dziegiel, M. H*., et al.* (2014). FoxA1 directs the lineage and immunosuppressive properties of a novel regulatory T cell population in EAE and MS. Nature medicine *20*, 272-282.
Loboda, A., Nebozhyn, M., Klinghoffer, R., Frazier, J., Chastain, M., Arthur, W., Roberts, B., Zhang, T., Chenard, M., Haines, B*., et al.* (2010). A gene expression signature of RAS pathway dependence predicts response to PI3K and RAS pathway inhibitors and expands the population of RAS pathway activated tumors. BMC Med Genomics *3*, 26.
Loi, S., Dushyanthen, S., Beavis, P. A., Salgado, R., Denkert, C., Savas, P., Combs, S., Rimm, D. L., Giltnane, J. M., Estrada, M. V*., et al.* (2016). RAS/MAPK Activation Is Associated with Reduced Tumor-Infiltrating Lymphocytes in Triple-Negative Breast Cancer: Therapeutic Cooperation Between MEK and PD-1/PD-L1 Immune Checkpoint Inhibitors. Clinical cancer research : an official journal of the American Association for Cancer Research *22*, 1499-1509.
Lujambio, A., Akkari, L., Simon, J., Grace, D., Tschaharganeh, D. F., Bolden, J. E., Zhao, Z., Thapar, V., Joyce, J. A., Krizhanovsky, V., and Lowe, S. W.

(2013). Non-Cell-Autonomous Tumor Suppression by p53. Cell *153*, 449-460.
Lykke-Andersen, J., and Wagner, E. (2005). Recruitment and activation of mRNA decay enzymes by two ARE-mediated decay activation domains in the proteins TTP and BRF-1. Genes & development *19*, 351-361.
Ma, Y., Adjemian, S., Mattarollo, S. R., Yamazaki, T., Aymeric, L., Yang, H., Catani, J. P. P., Hannani, D., Duret, H., Steegh, K.*, et al.* (2013). Anticancer Chemotherapy-Induced Intratumoral Recruitment and Differentiation of Antigen-Presenting Cells. Immunity *38*, 729-741.
MacCorkle, R. A., and Tan, T. H. (2004). Inhibition of JNK2 disrupts anaphase and produces aneuploidy in mammalian cells. J Biol Chem *279*, 40112-40121.
Mahtani, K. R., Brook, M., Dean, J. L., Sully, G., Saklatvala, J., and Clark, A. R. (2001). Mitogen-activated protein kinase p38 controls the expression and posttranslational modification of tristetraprolin, a regulator of tumor necrosis factor alpha mRNA stability. Mol Cell Biol *21*, 6461-6469.
Malumbres, M., and Barbacid, M. (2003). RAS oncogenes: the first 30 years. Nature reviews Cancer *3*, 459-465.
Marchese, F. P., Aubareda, A., Tudor, C., Saklatvala, J., Clark, A. R., and Dean, J. L. (2010). MAPKAP kinase 2 blocks tristetraprolin-directed mRNA decay by inhibiting CAF1 deadenylase recruitment. J Biol Chem *285*, 27590-27600.
Marengere, L. E. M. (1997). Regulation of T cell receptor signaling by tyrosine phosphatase SYP association with CTLA-4 (vol 272, pg 1170, 1996). Science *276*, 21-21.
Marzec, M., Zhang, Q., Goradia, A., Raghunath, P. N., Liu, X. B., Paessler, M., Wang, H. Y., Wysocka, M., Cheng, M. G., Ruggeri, B. A., and Wasik, M. A. (2008). Oncogenic kinase NPM/ALK induces through STAT3 expression of immunosuppressive protein CD274 (PD-L1, B7-H1). Proceedings of the National Academy of Sciences of the United States of America *105*, 20852-20857.
Matsushita, H., Vesely, M. D., Koboldt, D. C., Rickert, C. G., Uppaluri, R., Magrini, V. J., Arthur, C. D., White, J. M., Chen, Y. S., Shea, L. K.*, et al.* (2012). Cancer exome analysis reveals a T-cell-dependent mechanism of cancer immunoediting. Nature *482*, 400-U149.
Matsuzawa, A., Saegusa, K., Noguchi, T., Sadamitsu, C., Nishitoh, H., Nagai, S., Koyasu, S., Matsumoto, K., Takeda, K., and Ichijo, H. (2005). ROS-dependent activation of the TRAF6-ASK1-p38 pathway is selectively required for TLR4-mediated innate immunity. Nature immunology *6*, 587-592.
Mayr, C., and Bartel, D. P. (2009). Widespread shortening of 3'UTRs by alternative cleavage and polyadenylation activates oncogenes in cancer cells. Cell *138*, 673-684.
McFadden, D. G., Papagiannakopoulos, T., Taylor-Weiner, A., Stewart, C., Carter, S. L., Cibulskis, K., Bhutkar, A., McKenna, A., Dooley, A., Vernon, A.*, et al.* (2014a). Genetic and Clonal Dissection of Murine Small Cell Lung Carcinoma Progression by Genome Sequencing. Cell *156*, 1298-1311.
McFadden, D. G., Papagiannakopoulos, T., Taylor-Weiner, A., Stewart, C., Carter, S. L., Cibulskis, K., Bhutkar, A., McKenna, A., Dooley, A., Vernon, A.,

et al. (2014b). Genetic and clonal dissection of murine small cell lung carcinoma progression by genome sequencing. Cell *156*, 1298-1311.
McGranahan, N., Furness, A. J. S., Rosenthal, R., Ramskov, S., Lyngaa, R., Saini, S. K., Jamal-Hanjani, M., Wilson, G. A., Birkbak, N. J., Hiley, C. T.*, et al.* (2016). Clonal neoantigens elicit T cell immunoreactivity and sensitivity to immune checkpoint blockade. Science *351*, 1463-1469.
Meuwissen, R., and Berns, A. (2005). Mouse models for human lung cancer. Genes & development *19*, 643-664.
Michaud, M., Martins, I., Sukkurwala, A. Q., Adjemian, S., Ma, Y., Pellegatti, P., Shen, S., Kepp, O., Scoazec, M., Mignot, G.*, et al.* (2011). Autophagy-dependent anticancer immune responses induced by chemotherapeutic agents in mice. Science *334*, 1573-1577.
Molina-Arcas, M., Hancock, D. C., Sheridan, C., Kumar, M. S., and Downward, J. (2013a). Coordinate Direct Input of Both KRAS and IGF1 Receptor to Activation of PI3 Kinase in KRAS-Mutant Lung Cancer. Cancer Discov *3*, 548-563.
Molina-Arcas, M., Hancock, D. C., Sheridan, C., Kumar, M. S., and Downward, J. (2013b). Coordinate direct input of both KRAS and IGF1 receptor to activation of PI3 kinase in KRAS-mutant lung cancer. Cancer discovery *3*, 548-563.
Moodie, S. A., Willumsen, B. M., Weber, M. J., and Wolfman, A. (1993). Complexes of Ras.GTP with Raf-1 and mitogen-activated protein kinase kinase. Science *260*, 1658-1661.
Murali-Krishna, K., Altman, J. D., Suresh, M., Sourdive, D. J. D., Zajac, A. J., Miller, J. D., Slansky, J., and Ahmed, R. (1998). Counting antigen-specific CD8 T cells: A reevaluation of bystander activation during viral infection. Immunity *8*, 177-187.
Nauts, H. C., Fowler, G. A., and Bogatko, F. H. (1953). A review of the influence of bacterial infection and of bacterial products (Coley's toxins) on malignant tumors in man; a critical analysis of 30 inoperable cases treated by Coley's mixed toxins, in which diagnosis was confirmed by microscopic examination selected for special study. Acta Med Scand Suppl *276*, 1-103.
Nicke, B., Bastien, J., Khanna, S. J., Warne, P. H., Cowling, V., Cook, S. J., Peters, G., Delpuech, O., Schulze, A., Berns, K.*, et al.* (2005). Involvement of MINK, a Ste20 family kinase, in Ras oncogene-induced growth arrest in human ovarian surface epithelial cells. Mol Cell *20*, 673-685.
Nishimura, H., Minato, N., Nakano, T., and Honjo, T. (1998). Immunological studies on PD-1-deficient mice: implication of PD-1 as a negative regulator for B cell responses. International Immunology *10*, 1563-1572.
Nishimura, H., Nose, M., Hiai, H., Minato, N., and Honjo, T. (1999). Development of lupus-like autoimmune diseases by disruption of the PD-1 gene encoding an ITIM motif-carrying immunoreceptor. Immunity *11*, 141-151.
Noman, M. Z., Desantis, G., Janji, B., Hasmim, M., Karray, S., Dessen, P., Bronte, V., and Chouaib, S. (2014). PD-L1 is a novel direct target of HIF-1 alpha., and its blockade under hypoxia enhanced MDSC-mediated T cell activation. Journal of Experimental Medicine *211*, 781-790.

Obeid, M., Tesniere, A., Ghiringhelli, F., Fimia, G. M., Apetoh, L., Perfettini, J. L., Castedo, M., Mignot, G., Panaretakis, T., Casares, N.*, et al.* (2007). Calreticulin exposure dictates the immunogenicity of cancer cell death. Nature medicine *13*, 54-61.
Ostrem, J. M., Peters, U., Sos, M. L., Wells, J. A., and Shokat, K. M. (2013). K-Ras(G12C) inhibitors allosterically control GTP affinity and effector interactions. Nature *503*, 548-551.
Ota, K., Azuma, K., Iwama, E., Harada, T., Matsumoto, K., Takamori, S., Kage, M., Hoshino, T., Nakanishi, Y., and Okamoto, I. (2015). Induction of PD-L1 expression by the EML4-ALK oncoprotein and downstream signaling pathways in non-small cell lung cancer. Ann Oncol *26*, 104-105.
Pardoll, D. M. (2012). The blockade of immune checkpoints in cancer immunotherapy. Nature reviews Cancer *12*, 252-264.
Parry, R. V., Chemnitz, J. M., Frauwirth, K. A., Lanfranco, A. R., Braunstein, I., Kobayashi, S. V., Linsley, P. S., Thompson, C. B., and Riley, J. L. (2005). CTLA-4 and PD-1 receptors inhibit T-cell activation by distinct mechanisms. Molecular and Cellular Biology *25*, 9543-9553.
Parsa, A. T., Waldron, J. S., Panner, A., Crane, C. A., Parney, I. F., Barry, J. J., Cachola, K. E., Murray, J. C., Tihan, T., Jensen, M. C.*, et al.* (2007). Loss of tumor suppressor PTEN function increases B7-H1 expression and immunoresistance in glioma. Nature medicine *13*, 84-88.
Pearce, L. R., Komander, D., and Alessi, D. R. (2010). The nuts and bolts of AGC protein kinases. Nat Rev Mol Cell Bio *11*, 9-22.
Pfirschke, C., Engblom, C., Rickelt, S., Cortez-Retamozo, V., Garris, C., Pucci, F., Yamazaki, T., Poirier-Colame, V., Newton, A., Redouane, Y.*, et al.* (2016). Immunogenic Chemotherapy Sensitizes Tumors to Checkpoint Blockade Therapy. Immunity *44*, 343-354.
Phan, G. Q., Yang, J. C., Sherry, R. M., Hwu, P., Topalian, S. L., Schwartzentruber, D. J., Restifo, N. P., Haworth, L. R., Seipp, C. A., Freezer, L. J.*, et al.* (2003). Cancer regression and autoimmunity induced by cytotoxic T lymphocyte-associated antigen 4 blockade in patients with metastatic melanoma. Proceedings of the National Academy of Sciences of the United States of America *100*, 8372-8377.
Plaza-Menacho, I., Barnouin, K., Goodman, K., Martinez-Torres, R. J., Borg, A., Murray-Rust, J., Mouilleron, S., Knowles, P., and McDonald, N. Q. (2014). Oncogenic RET kinase domain mutations perturb the autophosphorylation trajectory by enhancing substrate presentation in trans. Mol Cell *53*, 738-751.
Postow, M. A., Callahan, M. K., Barker, C. A., Yamada, Y., Yuan, J. D., Kitano, S., Mu, Z. Y., Rasalan, T., Adamow, M., Ritter, E.*, et al.* (2012). Immunologic Correlates of the Abscopal Effect in a Patient with Melanoma. New Engl J Med *366*, 925-931.
Postow, M. A., Chesney, J., Pavlick, A. C., Robert, C., Grossmann, K., McDermott, D., Linette, G. P., Meyer, N., Giguere, J. K., Agarwala, S. S.*, et al.* (2015). Nivolumab and ipilimumab versus ipilimumab in untreated melanoma. N Engl J Med *372*, 2006-2017.
Powles, T., Eder, J. P., Fine, G. D., Braiteh, F. S., Loriot, Y., Cruz, C., Bellmunt, J., Burris, H. A., Petrylak, D. P., Teng, S. L.*, et al.* (2014).

MPDL3280A (anti-PD-L1) treatment leads to clinical activity in metastatic bladder cancer. Nature *515*, 558-562.
Rahman, M. M., Rumzhum, N. N., Morris, J. C., Clark, A. R., Verrills, N. M., and Ammit, A. J. (2015). Basal protein phosphatase 2A activity restrains cytokine expression: role for MAPKs and tristetraprolin. Sci Rep *5*, 10063.
Rajagopalan, L. E., Burkholder, J. K., Turner, J., Culp, J., Yang, N. S., and Malter, J. S. (1995). Granulocyte-macrophage colony-stimulating factor mRNA stabilization enhances transgenic expression in normal cells and tissues. Blood *86*, 2551-2558.
Rizvi, N. A., Hellmann, M. D., Snyder, A., Kvistborg, P., Makarov, V., Havel, J. J., Lee, W., Yuan, J., Wong, P., Ho, T. S.*, et al.* (2015a). Cancer immunology. Mutational landscape determines sensitivity to PD-1 blockade in non-small cell lung cancer. Science *348*, 124-128.
Rizvi, N. A., Hellmann, M. D., Snyder, A., Kvistborg, P., Makarov, V., Havel, J. J., Lee, W., Yuan, J. D., Wong, P., Ho, T. S.*, et al.* (2015b). Mutational landscape determines sensitivity to PD-1 blockade in non-small cell lung cancer. Science *348*, 124-128.
Rodriguezviciana, P., Warne, P. H., Dhand, R., Vanhaesebroeck, B., Gout, I., Fry, M. J., Waterfield, M. D., and Downward, J. (1994). Phosphatidylinositol-3-Oh Kinase as a Direct Target of Ras. Nature *370*, 527-532.
Rosenberg, S. A. (2014). IL-2: The First Effective Immunotherapy for Human Cancer. Journal of Immunology *192*, 5451-5458.
Rosenberg, S. A., Lotze, M. T., Muul, L. M., Leitman, S., Chang, A. E., Ettinghausen, S. E., Matory, Y. L., Skibber, J. M., Shiloni, E., Vetto, J. T.*, et al.* (1985). Observations on the Systemic Administration of Autologous Lymphokine-Activated Killer Cells and Recombinant Interleukin-2 to Patients with Metastatic Cancer. New Engl J Med *313*, 1485-1492.
Rosenberg, S. A., and Restifo, N. P. (2015). Adoptive cell transfer as personalized immunotherapy for human cancer. Science *348*, 62-68.
Rounbehler, R. J., Fallahi, M., Yang, C., Steeves, M. A., Li, W., Doherty, J. R., Schaub, F. X., Sanduja, S., Dixon, D. A., Blackshear, P. J., and Cleveland, J. L. (2012). Tristetraprolin impairs myc-induced lymphoma and abolishes the malignant state. Cell *150*, 563-574.
Rusanescu, G., Gotoh, T., Tian, X., and Feig, L. A. (2001). Regulation of Ras signaling specificity by protein kinase C. Mol Cell Biol *21*, 2650-2658.
Saitoh, M., Nishitoh, H., Fujii, M., Takeda, K., Tobiume, K., Sawada, Y., Kawabata, M., Miyazono, K., and Ichijo, H. (1998). Mammalian thioredoxin is a direct inhibitor of apoptosis signal-regulating kinase (ASK) 1. Embo Journal *17*, 2596-2606.
Salmon, H., Idoyaga, J., Rahman, A., Leboeuf, M., Remark, R., Jordan, S., Casanova-Acebes, M., Khudoynazarova, M., Agudo, J., Tung, N.*, et al.* (2016a). Expansion and Activation of CD103(+) Dendritic Cell Progenitors at the Tumor Site Enhances Tumor Responses to Therapeutic PD-L1 and BRAF Inhibition. Immunity *44*, 924-938.
Salmon, H., Idoyaga, J., Rahman, A., Leboeuf, M., Remark, R., Jordan, S., Casanova-Acebes, M., Khudoynazarova, M., Agudo, J., Tung, N.*, et al.* (2016b). Expansion and Activation of CD103(+) Dendritic Cell Progenitors at

the Tumor Site Enhances Tumor Responses to Therapeutic PD-L1 and BRAF Inhibition. Immunity *44*, 924-938.
Schott, J., Reitter, S., Philipp, J., Haneke, K., Schafer, H., and Stoecklin, G. (2014). Translational Regulation of Specific mRNAs Controls Feedback Inhibition and Survival during Macrophage Activation. Plos Genet *10*.
Schreiber, R. D., Old, L. J., and Smyth, M. J. (2011). Cancer immunoediting: integrating immunity's roles in cancer suppression and promotion. Science *331*, 1565-1570.
Schumacher, T. N., and Schreiber, R. D. (2015). Neoantigens in cancer immunotherapy. Science *348*, 69-74.
Sedlyarov, V., Fallmann, J., Ebner, F., Huemer, J., Sneezum, L., Ivin, M., Kreiner, K., Tanzer, A., Vogl, C., Hofacker, I., and Kovarik, P. (2016). Tristetraprolin binding site atlas in the macrophage transcriptome reveals a switch for inflammation resolution. Mol Syst Biol *12*.
Selamat, S. A., Chung, B. S., Girard, L., Zhang, W., Zhang, Y., Campan, M., Siegmund, K. D., Koss, M. N., Hagen, J. A., Lam, W. L.*, et al.* (2012). Genome-scale analysis of DNA methylation in lung adenocarcinoma and integration with mRNA expression. Genome research *22*, 1197-1211.
Senovilla, L., Vitale, I., Martins, I., Tailler, M., Pailleret, C., Michaud, M., Galluzzi, L., Adjemian, S., Kepp, O., Niso-Santano, M.*, et al.* (2012). An immunosurveillance mechanism controls cancer cell ploidy. Science *337*, 1678-1684.
Shankaran, V., Ikeda, H., Bruce, A. T., White, J. M., Swanson, P. E., Old, L. J., and Schreiber, R. D. (2001). IFNgamma and lymphocytes prevent primary tumour development and shape tumour immunogenicity. Nature *410*, 1107-1111.
Sharma, P., and Allison, J. P. (2015). Immune Checkpoint Targeting in Cancer Therapy: Toward Combination Strategies with Curative Potential. Cell *161*, 205-214.
Shinkai, Y., Rathbun, G., Lam, K. P., Oltz, E. M., Stewart, V., Mendelsohn, M., Charron, J., Datta, M., Young, F., Stall, A. M., and et al. (1992). RAG-2-deficient mice lack mature lymphocytes owing to inability to initiate V(D)J rearrangement. Cell *68*, 855-867.
Slebos, R. J. C., Kibbelaar, R. E., Dalesio, O., Kooistra, A., Stam, J., Meijer, C. J. L. M., Wagenaar, S. S., Vanderschueren, R. G. J. R. A., Vanzandwijk, N., Mooi, W. J.*, et al.* (1990). K-Ras Oncogene Activation as a Prognostic Marker in Adenocarcinoma of the Lung. New Engl J Med *323*, 561-565.
Smith, J. L., Jr., and Stehlin, J. S., Jr. (1965). Spontaneous regression of primary malignant melanomas with regional metastases. Cancer *18*, 1399-1415.
Snyder, A., Makarov, V., Merghoub, T., Yuan, J., Zaretsky, J. M., Desrichard, A., Walsh, L. A., Postow, M. A., Wong, P., Ho, T. S.*, et al.* (2014). Genetic basis for clinical response to CTLA-4 blockade in melanoma. N Engl J Med *371*, 2189-2199.
Steele, C. W., Karim, S. A., Leach, J. D., Bailey, P., Upstill-Goddard, R., Rishi, L., Foth, M., Bryson, S., McDaid, K., Wilson, Z.*, et al.* (2016). CXCR2 Inhibition Profoundly Suppresses Metastases and Augments Immunotherapy in Pancreatic Ductal Adenocarcinoma. Cancer cell.

Steidl, C., Shah, S. P., Woolcock, B. W., Rui, L. X., Kawahara, M., Farinha, P., Johnson, N. A., Zhao, Y. J., Telenius, A., Ben Neriah, S.*, et al.* (2011). MHC class II transactivator CIITA is a recurrent gene fusion partner in lymphoid cancers. Nature *471*, 377-+.
Stoecklin, G., Gross, B., Ming, X. F., and Moroni, C. (2003). A novel mechanism of tumor suppression by destabilizing AU-rich growth factor mRNA. Oncogene *22*, 3554-3561.
Stoecklin, G., Stubbs, T., Kedersha, N., Wax, S., Rigby, W. F., Blackwell, T. K., and Anderson, P. (2004). MK2-induced tristetraprolin:14-3-3 complexes prevent stress granule association and ARE-mRNA decay. EMBO J *23*, 1313-1324.
Stoecklin, G., Tenenbaum, S. A., Mayo, T., Chittur, S. V., George, A. D., Baroni, T. E., Blackshear, P. J., and Anderson, P. (2008). Genome-wide analysis identifies interleukin-10 mRNA as target of tristetraprolin. J Biol Chem *283*, 11689-11699.
Strauss, D. C., and Thomas, J. M. (2010). Transmission of donor melanoma by organ transplantation. Lancet Oncology *11*, 790-796.
Stutman, O. (1974). Tumor Development after 3-Methylcholanthrene in Immunologically Deficient Athymic Nude Mice. Science *183*, 534-536.
Sun, L., Stoecklin, G., Van Way, S., Hinkovska-Galcheva, V., Guo, R. F., Anderson, P., and Shanley, T. P. (2007). Tristetraprolin (TTP)-14-3-3 complex formation protects TTP from dephosphorylation by protein phosphatase 2a and stabilizes tumor necrosis factor-alpha mRNA. J Biol Chem *282*, 3766-3777.
Swanton, C., and Govindan, R. (2016). Clinical Implications of Genomic Discoveries in Lung Cancer. New Engl J Med *374*, 1864-1873.
Sweet-Cordero, A., Mukherjee, S., Subramanian, A., You, H., Roix, J. J., Ladd-Acosta, C., Mesirov, J., Golub, T. R., and Jacks, T. (2005). An oncogenic KRAS2 expression signature identified by cross-species gene-expression analysis. Nat Genet *37*, 48-55.
Taylor, G. A., Carballo, E., Lee, D. M., Lai, W. S., Thompson, M. J., Patel, D. D., Schenkman, D. I., Gilkeson, G. S., Broxmeyer, H. E., Haynes, B. F., and Blackshear, P. J. (1996). A pathogenetic role for TNF alpha In the syndrome of cachexia, arthritis, and autoimmunity resulting from tristetraprolin (TTP) deficiency. Immunity *4*, 445-454.
Taylor, G. A., Thompson, M. J., Lai, W. S., and Blackshear, P. J. (1995). Phosphorylation of tristetraprolin, a potential zinc finger transcription factor, by mitogen stimulation in intact cells and by mitogen-activated protein kinase in vitro. J Biol Chem *270*, 13341-13347.
Tchen, C. R., Brook, M., Saklatvala, J., and Clark, A. R. (2004). The stability of tristetraprolin mRNA is regulated by mitogen-activated protein kinase p38 and by tristetraprolin itself. Journal of Biological Chemistry *279*, 32393-32400.
Tiedje, C., Ronkina, N., Tehrani, M., Dhamija, S., Laass, K., Holtmann, H., Kotlyarov, A., and Gaestel, M. (2012). The p38/MK2-Driven Exchange between Tristetraprolin and HuR Regulates AU-Rich Element-Dependent Translation. Plos Genet *8*.

Tivol, E. A., Borriello, F., Schweitzer, A. N., Lynch, W. P., Bluestone, J. A., and Sharpe, A. H. (1995). Loss of CTLA-4 leads to massive lymphoproliferation and fatal multiorgan tissue destruction, revealing a critical negative regulatory role of CTLA-4. Immunity *3*, 541-547.
Topalian, S. L., Drake, C. G., and Pardoll, D. M. (2015). Immune Checkpoint Blockade: A Common Denominator Approach to Cancer Therapy. Cancer cell *27*, 450-461.
Topalian, S. L., Hodi, F. S., Brahmer, J. R., Gettinger, S. N., Smith, D. C., McDermott, D. F., Powderly, J. D., Carvajal, R. D., Sosman, J. A., Atkins, M. B.*, et al.* (2012). Safety, activity, and immune correlates of anti-PD-1 antibody in cancer. N Engl J Med *366*, 2443-2454.
Topalian, S. L., Sznol, M., McDermott, D. F., Kluger, H. M., Carvajal, R. D., Sharfman, W. H., Brahmer, J. R., Lawrence, D. P., Atkins, M. B., Powderly, J. D.*, et al.* (2014). Survival, durable tumor remission, and long-term safety in patients with advanced melanoma receiving nivolumab. J Clin Oncol *32*, 1020-1030.
Trahey, M., and Mccormick, F. (1987). A Cytoplasmic Protein Stimulates Normal N-Ras P21 Gtpase, but Does Not Affect Oncogenic Mutants. Science *238*, 542-545.
Tran, E., Ahmadzadeh, M., Lu, Y. C., Gros, A., Turcotte, S., Robbins, P. F., Gartner, J. J., Zheng, Z. L., Li, Y. F., Ray, S.*, et al.* (2015). Immunogenicity of somatic mutations in human gastrointestinal cancers. Science *350*, 1387-1390.
Tran, E., Turcotte, S., Gros, A., Robbins, P. F., Lu, Y. C., Dudley, M. E., Wunderlich, J. R., Somerville, R. P., Hogan, K., Hinrichs, C. S.*, et al.* (2014). Cancer Immunotherapy Based on Mutation-Specific CD4+T Cells in a Patient with Epithelial Cancer. Science *344*, 641-645.
Tumeh, P. C., Harview, C. L., Yearley, J. H., Shintaku, I. P., Taylor, E. J., Robert, L., Chmielowski, B., Spasic, M., Henry, G., Ciobanu, V.*, et al.* (2014). PD-1 blockade induces responses by inhibiting adaptive immune resistance. Nature *515*, 568-571.
Tuveson, D. A., Shaw, A. T., Willis, N. A., Silver, D. P., Jackson, E. L., Chang, S., Mercer, K. L., Grochow, R., Hock, H., Crowley, D.*, et al.* (2004). Endogenous oncogenic K-ras(G12D) stimulates proliferation and widespread neoplastic and developmental defects. Cancer cell *5*, 375-387.
vanderMerwe, P. A., Bodian, D. L., Daenke, S., Linsley, P., and Davis, S. J. (1997). CD80 (B7-1) binds both CD28 and CTLA-4 with a low affinity and very fast kinetics. Journal of Experimental Medicine *185*, 393-403.
Vanhaesebroeck, B., Guillermet-Guibert, J., Graupera, M., and Bilanges, B. (2010). The emerging mechanisms of isoform-specific PI3K signalling. Nat Rev Mol Cell Bio *11*, 329-341.
Ventura, J. J., Tenbaum, S., Perdiguero, E., Huth, M., Guerra, C., Barbacid, M., Pasparakis, M., and Nebreda, A. R. (2007). p38 alpha MAP kinase is essential in lung stem and progenitor cell proliferation and differentiation. Nature Genetics *39*, 750-758.
Vojtek, A. B., Hollenberg, S. M., and Cooper, J. A. (1993). Mammalian Ras interacts directly with the serine/threonine kinase Raf. Cell *74*, 205-214.

Walunas, T. L., Lenschow, D. J., Bakker, C. Y., Linsley, P. S., Freeman, G. J., Green, J. M., Thompson, C. B., and Bluestone, J. A. (1994). Ctla-4 Can Function as a Negative Regulator of T-Cell Activation. Immunity *1*, 405-413.
Wang, W., Li, F., Mao, Y., Zhou, H., Sun, J., Li, R., Liu, C., Chen, W., Hua, D., and Zhang, X. (2013). A miR-570 binding site polymorphism in the B7-H1 gene is associated with the risk of gastric adenocarcinoma. Hum Genet *132*, 641-648.
Wang, W. P., Chen, J. X., Liao, R., Deng, Q. D., Zhou, J. J., Huang, S., and Sun, P. Q. (2002). Sequential activation of the MEK-extracellular signal-regulated kinase and MKK3/6-p38 mitogen-activated protein kinase pathways mediates oncogenic ras-induced premature senescence. Molecular and Cellular Biology *22*, 3389-3403.
Wang, W. P., Sun, J., Li, F., Li, R., Gu, Y. P., Liu, C. P., Yang, P., Zhu, M., Chen, L. J., Tian, W. Y.*, et al.* (2012). A frequent somatic mutation in CD274 3'-UTR leads to protein over-expression in gastric cancer by disrupting miR-570 binding. Hum Mutat *33*, 480-484.
Warne, P. H., Viciana, P. R., and Downward, J. (1993). Direct interaction of Ras and the amino-terminal region of Raf-1 in vitro. Nature *364*, 352-355.
Waterhouse, P., Penninger, J. M., Timms, E., Wakeham, A., Shahinian, A., Lee, K. P., Thompson, C. B., Griesser, H., and Mak, T. W. (1995). Lymphoproliferative disorders with early lethality in mice deficient in Ctla-4. Science *270*, 985-988.
Webster, R. M., and Mentzer, S. E. (2014). The malignant melanoma landscape. Nat Rev Drug Discov *13*, 491-492.
Westcott, P. M., Halliwill, K. D., To, M. D., Rashid, M., Rust, A. G., Keane, T. M., Delrosario, R., Jen, K. Y., Gurley, K. E., Kemp, C. J.*, et al.* (2015a). The mutational landscapes of genetic and chemical models of Kras-driven lung cancer. Nature *517*, 489-492.
Westcott, P. M. K., Halliwill, K. D., To, M. D., Rashid, M., Rust, A. G., Keane, T. M., Delrosario, R., Jen, K. Y., Gurley, K. E., Kemp, C. J.*, et al.* (2015b). The mutational landscapes of genetic and chemical models of Kras-driven lung cancer. Nature *517*, 489-+.
Willimsky, G., and Blankenstein, T. (2005). Sporadic immunogenic tumours avoid destruction by inducing T-cell tolerance. Nature *437*, 141-146.
Winograd, R., Byrne, K. T., Evans, R. A., Odorizzi, P. M., Meyer, A. R. L., Bajor, D. L., Clendenin, C., Stanger, B. Z., Furth, E. E., Wherry, E. J., and Vonderheide, R. H. (2015). Induction of T-cell Immunity Overcomes Complete Resistance to PD-1 and CTLA-4 Blockade and Improves Survival in Pancreatic Carcinoma. Cancer Immunol Res *3*, 399-411.
Wolfle, S. J., Strebovsky, J., Bartz, H., Sahr, A., Arnold, C., Kaiser, C., Dalpke, A. H., and Heeg, K. (2011). PD-L1 expression on tolerogenic APCs is controlled by STAT-3. Eur J Immunol *41*, 413-424.
Wolfman, A., and Macara, I. G. (1990). A Cytosolic Protein Catalyzes the Release of Gdp from P21ras. Science *248*, 67-69.
Xu, C., Fillmore, C. M., Koyama, S., Wu, H., Zhao, Y., Chen, Z., Herter-Sprie, G. S., Akbay, E. A., Tchaicha, J. H., Altabef, A.*, et al.* (2014a). Loss of Lkb1 and Pten leads to lung squamous cell carcinoma with elevated PD-L1 expression. Cancer cell *25*, 590-604.

Xu, Y. X., Li, N., Xiang, R., and Sun, P. Q. (2014b). Emerging roles of the p38 MAPK and PI3K/AKT/mTOR pathways in oncogene-induced senescence. Trends Biochem Sci *39*, 268-276.
Xue, W., Meylan, E., Oliver, T. G., Feldser, D. M., Winslow, M. M., Bronson, R., and Jacks, T. (2011). Response and resistance to NF-kappaB inhibitors in mouse models of lung adenocarcinoma. Cancer Discov *1*, 236-247.
Yadav, M., Jhunjhunwala, S., Phung, Q. T., Lupardus, P., Tanguay, J., Bumbaca, S., Franci, C., Cheung, T. K., Fritsche, J., Weinschenk, T.*, et al.* (2014). Predicting immunogenic tumour mutations by combining mass spectrometry and exome sequencing. Nature *515*, 572-576.
Yamamoto, R., Nishikori, M., Tashima, M., Sakai, T., Ichinohe, T., Takaori-Kondo, A., Ohmori, K., and Uchiyama, T. (2009). B7-H1 expression is regulated by MEK/ERK signaling pathway in anaplastic large cell lymphoma and Hodgkin lymphoma. Cancer Sci *100*, 2093-2100.
Yamazaki, T., Akiba, H., Iwai, H., Matsuda, H., Aoki, M., Tanno, Y., Shin, T., Tsuchiya, H., Pardoll, D. M., Okumura, K.*, et al.* (2002). Expression of programmed death 1 ligands by murine T cells and APC. J Immunol *169*, 5538-5545.
Yang, J. C., Hughes, H., Kammula, U., Royal, R., Sherry, R. M., Topalian, S. L., Suri, K. B., Levy, C., Allen, T., Mavroukakis, S.*, et al.* (2007). Ipilimumab (anti-CTLA4 antibody) causes regression of metastatic renal cell cancer associated with enteritis and hypophysitis. J Immunother *30*, 825-830.
Yang, N. S., Wang, J. H., and Turner, J. (2004). Molecular strategies for improving cytokine transgene expression in normal and malignant tissues. Gene therapy *11*, 100-108.
Yoon, K. W., Byun, S., Kwon, E., Hwang, S. Y., Chu, K., Hiraki, M., Jo, S. H., Weins, A., Hakroush, S., Cebulla, A.*, et al.* (2015). Control of signaling-mediated clearance of apoptotic cells by the tumor suppressor p53. Science *349*, 1261669.
Yoshizuka, N., Chen, R. M., Xu, Z., Liao, R., Hong, L. X., Hu, W. Y., Yu, G. L., Han, J. H., Chen, L. C., and Sun, P. Q. (2012). A Novel Function of p38-Regulated/Activated Kinase in Endothelial Cell Migration and Tumor Angiogenesis. Molecular and Cellular Biology *32*, 606-618.
Zelenay, S., van der Veen, A. G., Bottcher, J. P., Snelgrove, K. J., Rogers, N., Acton, S. E., Chakravarty, P., Girotti, M. R., Marais, R., Quezada, S. A.*, et al.* (2015). Cyclooxygenase-Dependent Tumor Growth through Evasion of Immunity. Cell *162*, 1257-1270.
Zhao, C., Xiao, H., Wu, X., Li, C., Liang, G., Yang, S., and Lin, J. (2015). Rational combination of MEK inhibitor and the STAT3 pathway modulator for the therapy in K-Ras mutated pancreatic and colon cancer cells. Oncotarget *6*, 14472-14487.
Zitvogel, L., and Kroemer, G. (2012a). Chemotherapy response of spontaneous mammary tumors is independent of the adaptive immune system reply. Nature medicine *18*, 346-346.
Zitvogel, L., and Kroemer, G. (2012b). Targeting PD-1/PD-L1 interactions for cancer immunotherapy. Oncoimmunology *1*, 1223-1225.

Zubiaga, A. M., Belasco, J. G., and Greenberg, M. E. (1995). The nonamer UUAUUUAUU is the key AU-rich sequence motif that mediates mRNA degradation. Mol Cell Biol *15*, 2219-2230.